Regulation of Muscle Stem Cell Function by the Transcription Factor Pax7

Alessandra Pasut

Thesis submitted to the
Faculty of Graduate and Postdoctoral Studies
in partial fulfillment of the requirements
for the Doctorate in Philosophy degree in Cellular and Molecular Medicine

Department of Cellular and Molecular Medicine

Faculty of Medicine

University of Ottawa

...above all don’t fear difficult moments, the best comes out from them.

[Rita Levi Montalcini-Nobel laureate, 1909-2012]

Abstract

Pax7 is a paired box transcription factor expressed by all satellite cells which are critically required for muscle regeneration and growth. The absolute requirements of *Pax7* in the maintenance of the satellite cell pool are widely acknowledged. However the mechanisms by which *Pax7* executes muscle regeneration or contributes to satellite cell homeostasis remain elusive.

We performed cell and molecular analysis of *Pax7* null satellite cells to investigate muscle stem cell function. Through genome wide studies, we found that genes involved in cell-cell interactions, regulation of migration, control of lipid metabolism and inhibition of myogenic differentiation were significantly perturbed in *Pax7* null satellite cells. Analysis of satellite cells in vitro showed that *Pax7* null satellite cells undergo precocious myogenic differentiation and have perturbed expression of genes involved in the Notch signaling pathway.

We showed that *Notch 1* is a novel Pax7 target gene and by using a genetic approach we demonstrate that ectopic expression of the constitutively active intracellular domain of *Notch1* (NICD1) in *Pax7* null satellite cells is sufficient to maintain the satellite cell pool as well as to restore their proliferation. Instead of differentiating into myogenic cells and in the absence of a myogenic cue, NICD1 Pax7 *null* satellite cells become a source of ectopic brown fat within muscles and give rise to brown adipocytes both in vivo and in vitro.

In conclusion we showed that Notch 1 partially rescues Pax7 deficient satellite cells loss and proliferation. Additionally we provide the first evidence that Notch signalling contributes to satellite cell fate by inhibiting terminal myogenic differentiation and inducing brown adipogenesis.

Aknowledgements

My first BIG thank you goes to my supervisor. Michael, you inspire me to be creative and fearless. Your leadership showed me what it takes to be at the forefront of innovation and research and I hope the skills I've learned in your lab and under your guidance will be the foundation for reaching even bigger achievements. *Ad majora semper.*

A SINCERE thank you goes to my lab mates, past and present. Too many to mention here. You know who you are. A SPECIAL thank you goes to Jennifer Ritchie, Hong Ming and Fan Xiao. Your help has been invaluable throughout these years.

During my PhD I had the pleasure to work for and collaborate with excellent scientists both within OHRI and outside. I'd like to thank my PhD advisory committee members Dr Valerie Wallace, Dr Alan Mears, Dr Lynn Megeney and Dr Jeff Dilworth for their guidance as well as Dr Vittorio Sartorelli for being a long distant but precious advisor.

A WARM and affectionate thank you goes to my dearest Canadian friends, Sarah, Mari, Alex , the 977 Shefford girls Tammy and Laura, Erika, Andrea, Paul and Sandy. A SUPER thank you goes to those people that have known me forever and still haven't gotten tired of me: Vane and Le Sacilesi, grazie per essermi state vicino anche se lontane; Elena e Piera abbiamo iniziato e finito i rispettivi dottorati in tre paesi diversi e ne abbiamo condiviso gioie e dolori!

My final and MOST IMPORTANT thank you goes to my family. Thank you for giving me this incredible opportunity. I hope I made you proud. Grazie per avermi supportato e sopportato in questi anni, spero di avervi resi orgogliosi. A special thank you goes to my grandma, your b-day cards and Christmas messages sent over the ocean and across thousands miles made me feel closer to home. La tua forza e la tua dolcezza sono un esempio di vita che rimarra' con me per sempre.

Contributions of co-authors

All experimental work was performed by the thesis author unless otherwise specified. The writing and preparation of the manuscript in Chapter 2 were carried out by the author, with help from Dr Michael Rudnicki and Paul Oleynik for FACS analysis and interpretation of results. The writing and preparation of the manuscript in Chapter 3 were carried out by the author with help from Michael Rudnicki. RNA-seq data presented in Figure 1C and Supplementary Figure 2 of Chapter 3 were carried out by Chris Porter. Data presented in Figure 4A and C of Chapter 3were provided by Hong Ming. Dr Vahab Soleimani helped with the analysis of ChIP-seq data and provided all cell lines used to perform experiments in Figure 4A. Dr Robin Parks provided adenovirus constructs used in Figure 7 and Supplementary Figure 7. Dr Melanie Lacaria performed cardiotoxin injury and provided technical help with experiments shown in Figure 8. Jennifer Ritchie contributed to the maintenance of all mouse lines used throughout this thesis.

Contents

List of Figures

Chapter 1- General Introduction

Chapter 2- Isolation of Muscle Stem Cells by Fluorescence Activated Cell Sorting Cytometry

Chapter 3- Notch1 rescues Pax7-deficient satellite cell survival and induces brown adipogenesis

List of Tables

Chapter 3- Notch1 Rescues Pax7-deficient Satellite Cell Loss and Induces Brown Adipogenesis

List of Abbreviations

ATP	adenosine triphosphate
b HLH	basic helix loop helix
bFGF	basic fibroblast growth factor
BMP	bone morphogenetic protein
CTX	cardiotoxin
ChIP	chromatin immunoprecipitation
ChIPseq	high throughput ChIP sequencing
DAPI	4',6-diamidino 2-phosphate
DNA	deoxyribonucleic acid
E	embryonic day
ECM	extracellular matrix
EDL	extensor digitorum longus
EMT	epithelial to mesenchymal transition
ER	estrogen receptor
FACS	Fluorescent activated cell sorting
FBS	fetal bovine serum
FKHR	foxO1
FPKM	fragments per kilobase of exon per millions fragments mapped
GAPDH	glyceraldyde-3-phosphate dehydrogenase
GFP	green fluorescent protein
GO	gene ontology
GSK-3β	glycogen synthase kinase 3β
GTP	guanosine triphosphate
Hbox	homeobox
HDAC	histone deacetylase
Hes	hairy and enhancer of split

Hey	hes related with YRPW motif
HS	horse serum
Kb	kilobase
Lin	Lineage
MEF	myocyte enhancer factor
MRF	myogenic regulatory factor
mRNA	messanger ribonucleic acid
NADH	nicotinamide adenine dinucleotide -hydrogen
NICD	Notch intracellular domain
OE	over expression
PBS	phosphate buffered saline
PCR	polymerase chain reaction
PFA	paraformaldehyde
Ppia	peptidylprolyl isomerase A
Prd	paired domain
q-RT	quantitative reverse transcription
RDA	representational difference analysis
RFP	red fluorescent protein
RMS	rhabdomyosarcoma
RNA	ribonucleic acid
RT	reverse transcription
Shh	sonic hedgehog
SP	side population
TA	tibialis anterior
TF	transcription factor
Tmx	tamoxifen
TSS	transcription start site
UTR	untranslated region
YFP	yellow fluorescent protein

Chapter 1- General Introduction

Introduction

The primary functions of the skeletal muscle tissue are to allow locomotion, provide postural support and to sustain breathing. The skeletal muscle apparatus receive, integrate and transduce signals from all organs. Given its vital roles and complex dynamics, understanding the molecular mechanisms by which muscle is formed and repaired is of fundamental importance to both improve muscle performance as well as to restore its functionality in the context of a pathological state or disease.

1.1. The anatomy and mechanics of the adult skeletal muscle tissue

Each muscle is formed by hundreds of fibers organized into bundles and surrounded by the perimysium, a thin membrane of connective tissue which separates muscles from adjacent blood vessels, nerves and skin. Connections to the bones are mediated by fibrous structure called tendons though the myo-tendinous junctions (Gray H. 20th ed. 2000).

The arrangement of fibers, parallel, oblique or convergent, their caliber and their structural compositions vary from muscle to muscle and it ultimately determines their functions (Charge and Rudnicki, 2000). For examples, muscles with long and parallel fibers have great range of movement but low power while muscles with short and convergent fibers have low range of movement but high power. Slow twitching fibers are highly vascularised and primarily use oxygen to produce energy (oxidative fibers). They are resistant to fatigues and can contract for large amount of time. On the other hand, fast twitching fibers (glycolitic fibers) excel at producing short but powerful bursts of energy

by using anaerobic metabolism and are rich in glycogen content (Charge and Rudnicki, 2000; Yin et al., 2014).

The main force generating components of the myofiber are the structural protein actin and myosin (Hopkins, 2006). The regular arrangement of thick (myosin) and thin (actin) filaments defined the sarcomere, the contractile unit of a muscle fiber. Biochemical studies have demonstrated that the mechanism responsible for muscle contraction is based on the “sliding filaments” or “cross bridge” model whereby myosin filaments can form cross bridge with actin filaments. Contractile force is produced by the “grab, twist and slide” movements of myosin over actin in an ATP-dependent manner (Hopkins, 2006; Goldman, 1987).

The process of muscle contraction is triggered by the release of acetylcolin from motor neurons whose axons project from the spinal cord to the neuromuscular junction on each muscle fiber (Van De Graaff; 2002)

1.2 The embryogenesis of the skeletal muscle tissue

Our current knowledge of adult myogenesis relies upon studies performed on embryonic muscles (Figure 1.2) (Buckingham et al., 2003; Bentzinger et al., 2014). The development of skeletal muscle tissue from the mesoderm starts around embryonic day 8 (E8) in mice and occurs around the 25^{th} day post fertilization in humans and it is marked by the appearance of the first pair of somites (Gray H; 20^{th} ed, 2000). Somites are transient mesodermal structures formed in a pair-wise pattern. The process of somite segmentation follows an anterior-posterior direction from head to toes. Each pair of somites is formed at precise intervals (~90min) from one another, a process known as clock segmentation (Gibbs et al., 2010). Morphogenic gradients of Wnt and FGF

molecules as well as cyclic oscillations in genes of the Notch signaling pathway synergistically establish the spatiotemporal regulation of somitogenesis (Hirsinger et al., 1997; Zhao and Hofmann, 2004; Hofmann, 2004).

In the paraxial mesoderm, the mesoderm that flanks the neural tube, the specification of each somite into different cell types is regulated by the establishment of a dorso-ventral axis. Cells of the somites will give rise to the vertebrae, ribs, dermis and skeletal muscle of the back, trunk and limbs (Kaufman, 1992; Kablar et al., 1997) (Figure 1.2). In the ventral domain, cells of the sclerotome will aggregate and later form the vertebral disks and ribs as well as cartilage. In the dorsal region of the somites, cells of the dermomyotome will instead give rise to the dermis as well as trunk, back and limb muscles. These founder cells are marked by the expression of the paired box transcription factors *Pax3* and *Pax7* (Figure 1.2) (Buckingham et al., 2003 and 2007; Goulding et al., 1994; Kassar-Duchossoy et al., 2005).

The first muscle to be formed at E8.5 is the myotome right underneath the dermomyotome by differentiation of Pax3+/Pax7+ cells into muscle cells through the sequential up-regulation of *Myf5* and *MyoD* and *MRF4* and *Myogenin* later (Figure 1.2) (Kassar-Duchossoy et al., 2005; Ott et al., 1991; Tajbakhsh et al., 1997; Sassoon et al., 1989). The hypaxial domain of the demormyotome will generate trunk muscles while the epaxial domain will generate deep back muscles (Maroto et al., 1997; Buckingham, 2001). Genetic studies using a *Pax3* mutant allele have shown that *Myf5* is downstream of *Pax3* and that *Pax3* activates *Myf5* expression by binding to a -57.5kb region upstream of the *Myf5* promoter (Bajard et al., 2006). *Eya* and *Six* genes synergistically maintain

Pax3 expression and cooperate with Pax3 to drive the expression of *Myf5* (Grifone et al., 2007; Ridgeway et al., 2000).

Extrinsic signalling from surrounding tissues contributes to the process of muscle development. Specifically, the maintenance of undifferentiated progenitors' pool is regulated by BMP signaling, mainly through BMP4, which restricts *Myf5* and *MyoD* expression while maintaining *Pax3* expression (Porquie et al., 1996; Reshef et al., 1998). Conversely, Sonic Hedgehog (Shh) and Wnt signaling increase *Myf5* and *MyoD* expression and therefore are thought to promote muscle differentiation (Ridgeway and Skerjanc 2001; Borello et al., 2006, Brunelli et al., 2007, Zhang et al., 2001; Munsterberg et al., 1995).

Limb muscles are generated through a secondary wave of myogenesis occurring at distal sites in the body (Buckingham et al., 2003). This process starts around E10.5 with the delamination and migration of cells in the central region of the dermomyotome (Tremblay et al., 1998). This event requires an Epithelial to Mesenchymal Transition (EMT) which is triggered by the up-regulation of *c-Met* and *Lbx1* by Pax3+cells in response to FGF signaling (Schafer et al., 1999; Lagha et al., 2008; Goulding et al., 1994, Daston et al., 1996; Epstein et al., 1996). The commitment to myogenic differentiation starts only after Pax3+ cells have reached their final destination (Buckingham et al., 2003; Yin et al., 2013).

Towards the end of the third gestational semester, the developing embryo contains a mix population of both differentiating as well as premature muscle precursors. While myogenic differentiation is reinforced by the up-regulation of *Myf5* and *MyoD*, the expression of *Pax3* and *Pax7* remain confined to muscle progenitors (Daston et al., 1996;

Relaix et al., 2004 and 2005). Most of these cells progenitors will continue to proliferate and differentiate throughout fetal myogenesis. A portion of Pax3+/Pax7+ cells will later become a source of muscle stem cells in the adult and the primary executioner of post natal muscle growth and regeneration (Yin et al., 2013; Tajbakhsh, 2009).

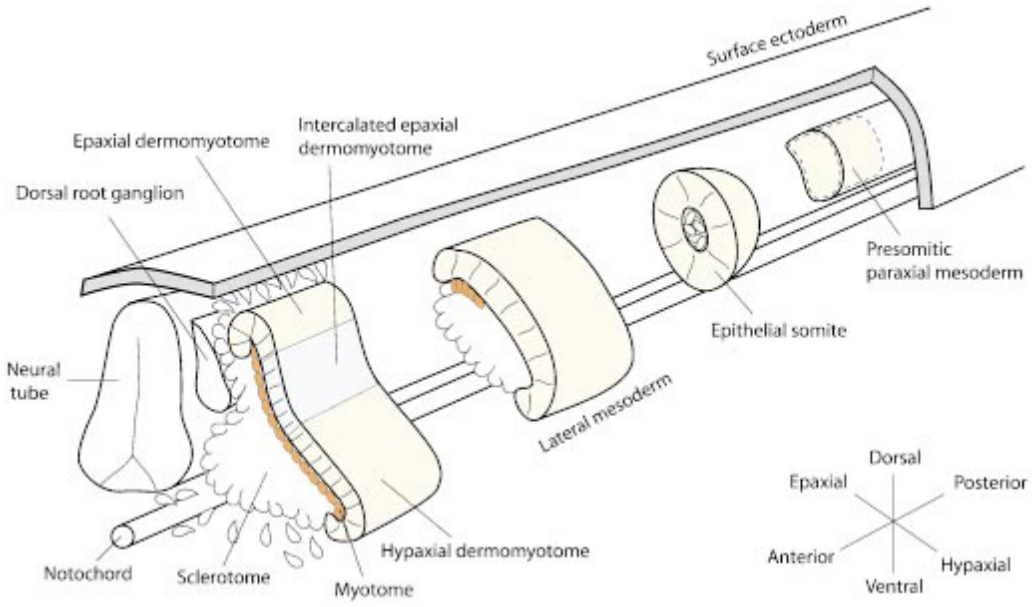

Figure 1.2. Embyonic development of the skeletal muscle tissue. The pairwise segmentation of the paraxial mesoderm (1) along the body midline results in the formation of transient structures called somites (2). Each somite specifies into two distinct domains: the ventral domain and the dorsal domain (3). The ventral domain (sclerotome) will give rise to ribs, vertebrae and cartilage. The central region of the dorsal domain (dermomyotome) will give rise to all muscles of the body (4). Specifically the hypaxial domain will generate trunk muscles while the epaxial domain will give rise to deep muscles. Migrating Pax3+/Lbx1+/c-Met + progenitors from the collapsing dermomyotome will then reach distal sites of myogenesis and sequentially upregulate Myf5/MyoD/MRF4 and Myogenin to generate all limb muscles. Undifferentiated Pax3+/Pax7+ progenitors will remain as a source of muscle stem cells. [Buckingham et al., 2003].

1.3 Molecular determinants of muscle differentiation

The process of muscle formation (myogenesis) is hierarchically controlled by distinct transcriptional gene networks each under the precise control of a "master" regulator (Buckingham and Rigby, 2014). While *Pax3* and *Pax7* mark myogenic ancestors, the induction of *Myf5* and *MyoD* expression is required to direct the specification into the myogenic lineage (Daston et al., 1996; Tajbakhsh et al., 1997; Relaix et al., 2005; Kassar Duchossoy et al., 2005). *Myf5* and *MyoD* together with *Myogenin* and *MRF4* belong to the family of Myogenic Regulatory Factors (MRFs) (Rudnicki and Jaenish, 1995; Berkes and Tapscott, 2005).

The generation of transgenic knock-out mouse models for these genes was instrumental to identify their role in myogenesis and to understand how they regulate each other expression. These studies have shown that *MyoD* and *Myf5* compensate for each other loss since single *MyoD* or *Myf5* mutant mice do not display major muscle defects (Braun et al., 1992 and 1994; Rudnicki et al., 1992). However, rib abnormalities in *Myf5* mutant mice suggest that *Myf5* is critically required for the specification of the epaxial dermomyotome (Braun et al., 1992). Double *MyoD/Myf5* transgenic knock-out mice completely lack all skeletal muscle tissues unequivocally establishing their function as lineage determinators upstream of the MRFs cascade (Rudnicki et al., 1992 and 1993). Compared to Myf5, MyoD was shown to be a stronger inducer of terminal myogenic differentiation (Thayer et al., 1989; Megeney et al., 1995; Sabourin et al., 1999; Ishibashi et al., 2005). Notably, *MyoD* was also the first reprogramming factor capable to convert different cell lines, from 10T1/2 fibroblasts to retinal epithelial cells, into fully competent myoblasts (Davis et al., 1987; Choi et al., 1990; Miner et al.,1992).

The observation that *Myogenin* and *MRF4* knock-out mice do not show gross abnormalities in muscle development but showed a delayed in muscle differentiation and fusion (Rhodes et al., 1989; Hasty et al., 1993; Nabeshima et al., 1993; Rawls et al., 1998) points to a model in which *Myogenin* and *MRF4* are downstream of *Myf5* and *MyoD* and are not required for lineage commitment (Wright et al., 1994; Zhang et al., 1994). However in the absence of *Myf5* and *MyoD*, *MRF4* has been suggested to act as a potential lineage initiator rather than executioner of differentiation (Kassar-Duchossoy et al., 2005). It remains unproven that *MRF4* performs this function in the presence of *Myf5* and *MyoD*.

Together with MRFs, the family of the Myocyte Enhancer Factor 2 (MEF2) transcription factors drive terminal myogenic differentiation (Molkentin et al.,1996; Sandmann et al., 2006). Chromatin immunoprecipitation (ChIP) experiments coupled with gene expression studies have shown that *MyoD* and *MEF2* synergistically control the up-regulation of late differentiation genes as exemplified by the regulation of the *Myogenin* locus (Weintraub et al., 1991; Puri and Sartorelli, 2000; Faralli and Dilworth, 2012; Fong and Tapscott 2013;).

The transcriptional activity of MRFs and MEFs is regulated at multiple levels, from tissue specific splicing events (Sebastian et al., 2013), to post transcriptional modifications such as phoshorylation (Gillespie et al., 2009), methylation (Ling et al., 2012) or acetylation (Di Padova et al., 2007) or other co-factors (Caretti et al., 2006). Additionally, competitive DNA binding of MyoD and Snail to E-boxes (CANNTG) sites on common target genes has been shown to prevent the transcription of late differentiation muscle genes in primary myoblasts (Soleimani et al., 2012).

The ability of MRF or MEFs to initiate and maintain gene transcription in muscle cells relies on the recruitment of epigenetic modifiers (Dilworth and Blais, 2011). These co-factors act upon histones and by altering its chemical composition they induce structural changes that allow the dynamic binding of the transcription apparatus. The class of HDAC (histone deacelyases) inhibitors Sirtuins 1 and 2 has also been shown to inhibit MyoD and MEF2 transcriptional activity by promoting the de-acetylation of histones on muscle specific gene enhancers and the repression of the myogenic gene program in a NADH-dependent manner (Fulco et al., 2003 and 2008; Pardo and Boriek, 2011). A remarkable example of the absolute requirement of chromatin modifiers was recently reported by Albini et al. In this study, the authors showed that while MyoD was not able to directly convert human embryonic stem cells (hESCs) into functional myospheres, the presence of the BAF60 subunit of the SWI/SNF chromatin remodeling complex allowed the direct conversion of hESCs into competent myogenic cells (Albini et al., 2013).

1.4 Satellite cells regulate muscle regeneration and post natal growth

The differentiation of muscle progenitors into muscle fibers is an irreversible process and mature fibers are post-mitotic cells incapable of regeneration. Muscle regeneration and post natal growth rely on the existence of an undifferentiated population of stem cells called satellite cells (Bischoff 1994; Charge and Rudnicki, 2004; Yin et al., 2013; Bentzinger et al., 2012).

The search for a muscle stem cell source received an unexpected twist when a serendipity electron microscopy study performed on frogs legs led to the peculiar discovery of a population of cells intimately associated with the muscle fibers `whose

investigation, as suggested by the author himself, “may be inherent to the vexing problem of muscle regeneration” (Katz, 1961; Mauro, 1961). Those cells were named satellite cells because of their “wedged” position along the muscle fiber (Figure 1.4)

After more than 50 years of research into the mechanisms of adult myogenesis we now know that satellite cells are the driving engine of the regeneration, hypertrophy and postnatal growth of skeletal muscle.

While initially satellite cells were labeled as muscle progenitors, the identification of satellite cell specific markers coupled with lineage tracing experiments have indeed unequivocally demonstrated that satellite cells are able to give rise to new muscle fibers as well as to self-renew and maintain their pool through asymmetric divisions (Sacco et al., 2008; Collins et al., 2005; Seale et al., 2000; Kuang et al., 2006; Montarras et al., 2005).

Likewise other somatic stem cells, adult satellite cells can differentiate into multiple lineages (Asakura et al., 2001; Aguiari et al., 2008; Rossi et al., 2007). Lineage tracing experiments have shown that Pax7 derived satellite cells can give rise to brown adipocytes and that the myogenic indentity of satellite cells is regulated by the muscle specific microRNA *miR-133* (Yin et al., 2013; Lepper et al., 2010; Seale et al., 2008).

In resting muscle satellite cells are normally quiescent as shown by different label retaining techniques including thymidin-H (Moss et al., 1970), BrdU (Schultz et al., 1978) and PyroninA labeling (Fukada et al., 2007). However, upon regeneration caused by an injury, satellite cells exit the cell cycle activate and repopulate the damaged fibers by progressively up regulating MRFs expression, partially recapitulating embryonic myogenesis (Rudnicki et al., 2008).

The embryonic origin of adult satellite cells has been long debated with disputes between a somitic and an endothelial origin. However, labeling of Pax3+ muscle progenitors in chick and mouse embryos have clearly demonstrated that most if not all satellite cells found in adult muscles derived from somatic progenitors of the dermomyotome (Gros et al., 2005; Schienda et al., 2006).

Figure 1.4

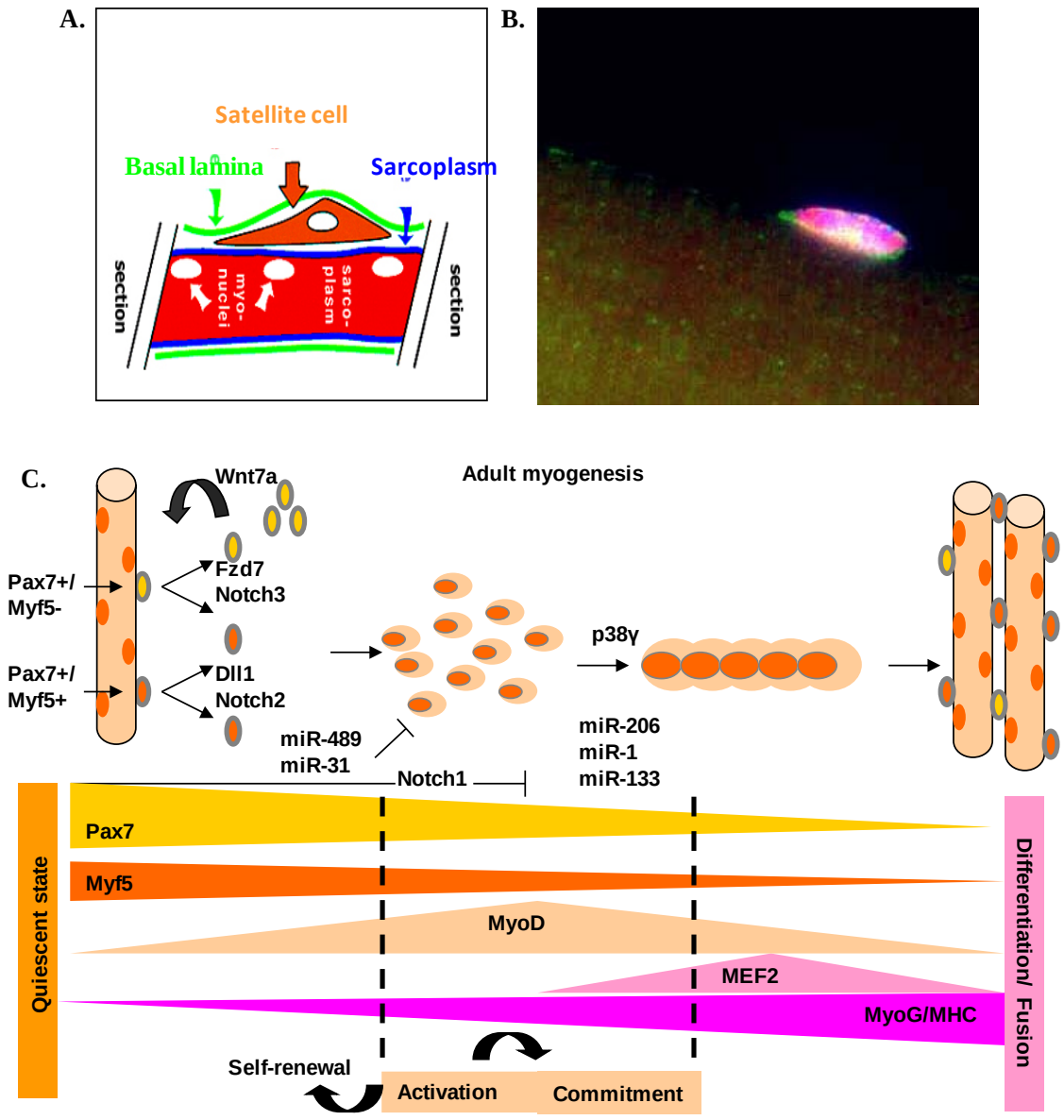

Figure 1.4. Satellite cells in adult myogenesis. **A**. Schematic of the anatomical position of satellite cells on adult fibers between the sarcolemma and the basal lamina. **B**. shown is a quiescent Pax7+ (red), α7Integrin + (green) satellite cell on a single EDL fiber. **C**. Adult myogenesis is orchestrated by the temporal regulation of Pax7, MRFs and MEF proteins whose temporal patterns of expression distinguish the 3 phases of muscle regeneration (ie exit from quiescence, activation and differentiation). Wnt and Notch have been proposed to regulate the self renewal and the expansion of satellite "stem" cells by inhibiting MyoD and myogenic commitment. The p38 signaling pathway and microRNAs miR-206, miR-1 and miR-133 have been shown to maintain and drive terminal muscle differentiation.

1.5. Heterogeneity of satellite cells

Satellite cells are not a homogenous population of stem cells and they express a plethora of surface markers including the cell surface receptor α7Integrin (Blanco-Bose et al., 2001); the cluster of differentiation CD34 (Alfaro et al., 2011; Beauchamp et al., 2000); the vascular cell-adhesion molecule 1 VCAM-1 (Fukada et al., 2004); the transmembrane proteoglycans Syndecan 3 and 4 (Cornelison et al., 2001); the multiple EGF-like domain protein 10 Megf10 (Holterman et al., 2007). Additional markers include the cell adhesion protein m-cadherin; the tyrosin receptor kinase c-Met; the chemokine receptor 4 CXCR4 (reviewed in Yin et al., 2013). This intrinsic heterogeneity for most part does not translate into a difference in their function; rather it reflects the stochastic nature of fluctuations in gene expression.

One such exception is the differential expression of *Myf5* (Kuang et al., 2007). The use of a *Myf5-Cre Rosa26YFP* reporter mouse line has shown that most satellite cells (~90%) had at some point in their development expressed the *Myf5Cre* allele and were thus identified as Pax7+/Myf5+expressing cells. However a smaller fraction of satellite cells (approximately 10%) had never turned on *Myf5* expression and were thus labeled as Pax7+/Myf5- expressing cells (Kuang et al., 2007). *In vivo* transplantation experiments of these two populations showed that Pax7+/Myf5- cells have a higher ability to self-renew and contribute long term to the replenishment of the stem cell pool. Conversely Pax7+/Myf5+ cells represent a pool of cells readily accessible to engage in muscle differentiation but do not self-renew. These findings led to reframe the definition of satellite cells by functionally clustering Pax7+/Myf5- satellite cells as satellite " stem"

cells and Pax7+/Myf5+ satellite cells as satellite “committed” cells (Kuang et al., 2007; Chang et al., 2014).

Importantly Kuang et al., showed that Pax7+/Myf5- cells are hierarchically upstream and give rise to either two identical Myf5- cells (symmetric division) or to one Myf5+ and one Myf5- cell (asymmetric division). Pax7+/Myf5+ cells can only divide symmetrically. Live imaging experiments of satellite cell divisions on muscle fibers have shown that symmetric divisions are more likely to occur in the same plane of the muscle fiber while asymmetric divisions are more likely to occur perpendicular to the fiber plane (apical/basal divisions) (Kuang et al., 2007).

The mechanisms driving the symmetric or asymmetric expansion of satellite cells remain to be elucidated. Segregation of cytoplasmic factors (Conboy and Rando, 2002) as well as the geometry and distribution of extra cellular matrix components (ECM) (Yennek et al., 2014) have been shown to impact satellite cell asymmetric divisions. For instance, the secreted Wnt7a molecule and its obligated membrane bound receptor Frizzled 7 (Fzd7) have been shown to drive satellite stem cell expansion. Work from Le Grand et al has shown that *Fzd7* is enriched in Pax7+/Myf5- satellite stem cells and it becomes asymmetrically distributed during cell division. The binding of Wnt7a to Fzd7 promotes symmetric divisions of Pax7+/Myf5- cells through the Planar Cell Polarity (PCP) pathway as well as direct their migration resulting in more efficient muscle regeneration (Le Grand et al., 2009; Bentzinger et al., 2013).

1.6. Regulation of satellite cells quiescence

Stem cell differentiation is an essential requirement of tissue regeneration. However, the maintenance of quiescence allows stem cells to engage and respond to

repetitive waves of injuries. The quiescent state is defined as a state of reversible dormancy (G0 phase of the cell cycle) in which adult stem cells can be found for extensive period of time but from which they can exit in response to external stimuli. (Cheung and Rando, 2013). Dis-regulation and/or loss of the quiescent state lead to decrease number of stem cells over time and impaired tissue regeneration (Shea et al., 2010; Abou-Khalil et al., 2010).

Recent studies have challenged the traditional definition of quiescence and have shown that not all satellite cells are equally quiescent (Chakkalakal et al., 2012; Rodgers et al., 2014). The use of lineage tracing coupled with labeling retention technique led to the identification of two functionally distinct populations of quiescent satellite cells that were named label retaining cells (LRC) and non label retaining cells (non-LRC). Importantly non-LRC cells were shown to primarily contribute to muscle turnover and to divide at a higher rate than LRC cells. Conversely LRC cells are hierarchically upstream and are called to "action" upon major trauma as in the case of a muscle injury (Chakkalakal et al., 2012 and 2014). Maintenance of high level of the cell cycle CDK inhibitor p27/Kip1 expression in LRC cells protect them from engaging in excessive round of divisions (Chakkalakal et al., 2014).

An elegant study from Rodgers and colleagues have shown that satellite cells can transition between two distinct quiescent states named G0 and G0 alert. Satellite cells in G0 alert are primed to more rapidly respond to injury compared to cells arrested in a G0 state. Finally, the transition between G0 to G0 alert is facilitated by components of the mTOR signaling pathway (Rodgers et al., 2014).

Comparison of microarray data sets of different types of stem cells have highlighted the existence of common genetic requirements of quiescence including cell cycle regulators, DNA replication and RNA processing enzymes, chromatin modifiers, regulators of mitochondrial activities, inhibitors of differentiation and genes involved in the regulation of metabolism (Fukada et al., 2007; Gnocchi V et al., 2009; Cornelison and Wold, 1997; Palafacchina et al., 2010; Forsberg et al., 2010; reviewed in Cheung and Rando, 2013).

These studies have shown that rather than being a default state, the quiescent state is actively maintained by stem cells to preserve their genome integrity from DNA damage or other environmental stressors (Cheung and Rando, 2013).

Together with protein coding genes, microRNAs (miRs) have also been shown to affect satellite cell quiescence by either preventing cell cycle entry (Cheung et al., 2012) , or inhibiting the expression of differentiation genes such as *Myf5* (Crist et al., 2012 and 2009a; Bartel, 2004).

Additionally, the epigenetic modifiers such as the Polycomb group of proteins Ezh2 and Ezh1maitain and safeguard quiescence in multiple stem cells including satellite cells and support the theory of a poised quiescent state in which genes that are required for stem cell activation are marked by specific epigenetic marks (Kamminga et al., 2006; Juan et al., 2011).

1.7 *Pax7* is an absolute requirement of satellite cells in adult myogenesis

A landmark in the study of satellite cells and muscle regeneration was the discovery of *Pax7* as a universal satellite cell marker (Seale et al., 2000). *Pax7*, similarly to its paralogue *Pax3*, belongs to a family of conserved paired box transcription factors

implicated in the development of different tissues and organs (Mansouri et al., 1994; Buckingham and Relaix, 2007).

The uniqueness of *Pax7* in the context of adult myogenesis resides in two main findings: first *Pax7* is the only Pax gene that is unequivocally expressed by all satellite cells. Indeed while *Pax3* can also be used to label satellite cells (Buckingham and Relaix 2007; Relaix et al., 2004), not all satellite cells express *Pax3* (Kuang et al., 2006; Boutet et al., 2012; Crist et al., 2009b). The finding that *Pax7* is a universal marker of satellite cells has led to the generation of several *Pax7* transgenic reporter mouse strains which have been used to study the spatial and temporal kinetics of satellite cells at different embryonic and post natal stages (Lepper et al., 2010; Lepper et al., 2009; Nishijo et al., 2009, Bosnakovski et al., 2008).

Among many, the most extensive and comprehensive lineage tracing study of satellite cells was performed by Lepper et al., in 2010 (Lepper et al., 2010). By using a tamoxifen inducible *Pax7Cre* reporter mouse line and by administering tamoxifen at different stages throughout embryonic development, Lepper et al., showed that *Pax7* positive cells at E9.5 differentiate into both muscle fibers as well as contribute to dermis and brown fat depots while by E12.5 they become restricted to the myogenic lineage and in post natal muscles *Pax7* expression is restricted to satellite cells. Secondarily *Pax7* is critical for satellite cell maintenance in adult myogenesis and loss of *Pax7* is intimately associated with a satellite cell phenotype. Numerous evidences have shown that *Pax7* is expressed in quiescent and activated satellite cells and maintained in self-renewing but not differentiating cells (Seale et al., 2000; Kuang et al., 2006; Zammit et al., 2004 and 2006; Olguin and Olwin, 2004).

Regenerative studies performed on *Pax7* null mutant mice have shown that genetic inactivation of *Pax7* results in decrease satellite cell number after birth and severe regeneration deficit (Seale et al., 2000; Kuang et al., 2006; Sambasivan et al., 2011).

Initial experiments using conditional inactivation of *Pax7* via a Cre/LoxP system allegedly showed that *Pax7* requirements are restricted to juvenile satellite cells and dispensable for adult myogenesis as inactivation of *Pax7* after post-natal day 21 (P21) does not compromise satellite cell function and neither muscle regeneration (Lepper et al., 2009). However, follow up experiments by the same authors disproved their initial findings as Gunther et al., reported that inactivation of the *Pax7* gene in adult (2 month old) mice results in extensive regenerative deficits due to loss of satellite cells (Gunther et al., 2013). Studies from our laboratory demonstrate that *Pax7* deletion in adult satellite cells results in dramatic regeneration deficit recapitulating the same phenotype observed following genetic inactivation of *Pax7* (von Maltzahn et al., 2013)

1.8. Pax7 transcriptional network

Gene expression coupled with genome wide chromatin immunoprecipitation (ChIP) studies of Pax7 and Pax3 have shown that Pax7 plays a dominant role in adult myogenesis (Punch et al., 2009; Soleimani et al., 2013; Collins et al., 2009; White et al., 2008; Horst et al., 2006). These studies have shown that while both transcription factors recognized the same DNA motifs, Pax7 has a higher affinity than Pax3 to the DNA homeodomain (Soleimani et al., 2013). These intrinsic differences in DNA binding properties result in the regulation of distinct genetic programs by Pax3 and Pax7. While Pax3 binds a subset of Pax7 genes mainly involved in the regulation of embryonic functions and maintenance of an undifferentiated phenotype, Pax7 specifically activates

genes involved in the maintenance of adult satellite cell phenotype from regulation of proliferation to inhibition of differentiation (Soleimani et al., 2013; White et al., 2008; Collins et al., 2009; Horst et al., 2006).

These evidences suggest that Pax3 and Pax7 may have both overlapping and distinct cell functions and are corroborated by comparative analysis of *Pax3* and *Pax7* mutant mice. During embryonic development, *Pax7* functions are partially compensated by *Pax3* as shown by the normal development of *Pax7* null mutant mice at birth (Kuang et al, 1996; Mansouri et al., 1996). However, abnormalities in neural crest derivates development have been reported in *Pax7* mutant mice (Mansouri et al., 1996). Double *Pax3/Pax7* mutant mice have more severe muscle defects than *Pax3* mutant mice (Franz et al., 1993; Relaix et al., 2004). Importantly, in post natal myogenesis, *Pax3* is unable to compensate for the loss of *Pax7* even in those muscles like the diaphragm where satellite cells co-express *Pax7* and *Pax3* (Seale et al., 2000; Kuang et al., 2006).

To date the only known Pax7 target gene is the myogenic regulatory factor *Myf5* (McKinnell et al., 2009; Soleimani et al., 2013). Proteomic studies have shown that Pax7 associates with a complex of proteins which includes chromatin modifiers such as the histone methyl transferases Ash2l, Wdr5 and Mll2 responsible for the opening of the chromatin at the *Myf5* locus (McKinnell et al., 2009).

Pax7 protein is regulated at multiple levels by post transcriptional modifications such as methylation (Kawabe et al., 2012), microRNAs (Chen et al., 2009 and 2010), caspase dependent degradation (Olguin, 2011) as well as by extrinsic signaling (Wen et al., 2012; Palacios et al., 2010).

The identification of Pax7 genetic requirements and their function will broaden our understanding of adult myogenesis and clearly constitutes a major research focus.

1.9. Regulation of satellite cells by the muscle stem cell niche

Satellite cells occupy a specific anatomical position along the muscle fiber which defines the muscle stem cell niche. The niche actively influences and it is influenced by its own stem cells during both tissue homeostasis and muscle regeneration (Gilbert et al., 2013; Bentzinger et al., 2013).

In physiological conditions, the satellite cells niche is defined mainly by the basal lamina on one side and the sarcolemma on the other. Interactions with extracellular matrix (ECM) components are mediated by multiple surface receptors including integrins and dystrophin-sarcoglycans proteins complex (Mauro et al. 1961; Yin H. et al, 2013; Cornelison et al., 2001; Mayer et al., 1997).

Substrate stiffness has been shown to maintain satellite cell self-renewal and enhance myoblasts fusion suggesting that satellite cells can “sense” the environment and have the ability to transduce mechanical cues (Gilbert et al., 2010; Serena et al., 2010). Importantly, the YAP/TAZ transcriptional complex has been shown to transduce mechanical cues from the cellular microenvironment into specific changes in cell shape to allow stem cells differentiation (Dupont et al., 2011).

Proximity to blood vessels (Christov et al., 2007) and innervations (Wu et al., 2012) has been shown to provide essential stimuli for the survival of satellite cells and to be integral components of the muscle stem cell niche.

External stimuli such as an injury or a stress to the muscle profoundly impact the architecture of the satellite cell niche and are accompanied by changes in ECM dynamics

(Bentzinger et al., 2013 and 2014) as well as release of cytokines and interleukins from immune cells or fibro adipogenic cells (Chazaud et al., 2003; Malerba et al., 2010; Joe et al., 2010). The release of systemic factors (Elabd et al., 2014; Conboy et al., 2005) and age dependent changes in signal transduction (Brack et al., 2008; Chakkalakal et al., 2012; Carlson et al., 2008) also modulate the niche environment.

1.10. Role of Notch signalling in adult myogenesis

One of the most important mechanisms of cell signaling is mediated by Notch. The *Notch* gene was identified almost 100 years ago while studying the mechanisms of Drosophila wing outgrowth (Morgan, 1917; Greenwold; 1998). Since then Notch has been found to be crucial for the development of all organisms from worms to humans (Kopan and Ilagan, 2009; Artavanis-Tsakonas et al., 1999; Bray et al., 2006; Poellinger and Lendhal 2008). The signaling relies on the interaction between two trans-membrane proteins, a Notch receptor and a Notch ligand (Figure 1.10). In mammalian cells there are 4 Notch receptors (Notch 1 to 4) and two families of Notch ligands (Jagged and Delta) (Bray et al., 2006; Kopan and Ilagan 2009). In the canonical signaling, upon receptor-ligand binding, the intracellular domain of the Notch receptor (NICD) is cleaved at two distinct sites and traslocates into the nucleus. NICD converts the transcription factor CSL-Rbp-j into an activator complex by dislocating co-repressors and recruiting co–activators proteins (Kopan et al. ,1996; Kao et al., 1998; Artavanis-Tsakonas,et al., 1999). Notch activated genes contain the CSL-Rbp-j sequence motif CGTGGGAA and the most well described Notch downstream targets are the *Hairy and Enhancer of Split related* bHLH repressors *Hes* and their homologous *Hey* genes (Figure 1.10) (Fortini et al., 1994; Bray et al., 2001).

Among all developmental pathways, the Notch signaling has been shown to play an essential role in the maintenance of satellite cells. Genetic inactivation of *Rbp-j* in Pax3+/Lbx1+ progenitors results in loss of satellite cells, smaller muscles and perinatal lethality (Vasutyna et al., 2007a). Residual satellite cells present at birth were MyoD+ and had already exit the cell cycle and were unable to contribute to post-natal muscle growth (Vasutyna et al., 2007b). Similarly transgenic mice bearing a hypomorphic *Delta 1* (*Dll1*) allele show reduced skeletal muscle mass due to the premature differentiation of progenitor cells (Schuster-Gossler et al., 2007). Transient exposure to *Dll1* signaling from migrating neural crests activate *Notch2* and up-regulate *Myf5* expression in dermomyotomal cells (Rios et al., 2011). While germline mutations of *Notch 1* and *Notch 2* results in disorganised somitogenesis and embryos die in utero by E9.0, *Notch 3* and *Notch 4* mutant mice develop normally suggesting a dominant role of *Notch 1* and *Notch 2* in embryonic development and possibly overlapping and redundant functions among the four receptors (Krebs et al., 2000; Hamada et al., 1999).

However, *Notch 3* mutant mice have higher number of satellite cells and show a hypertrophic phenotype upon repetitive injury (Kitamoto and Hanaoka, 2010). Genetic ablation of *Rbp-j* in adult satellite cells results in progressive decline of satellite cells number suggesting that Notch may be actively involved in the maintenance of satellite cells quiescence (Bjornson et al., 2012; Mourikis et al., 2012). Indeed, at least some downstream Notch target genes (*Hey1*, *Hey2*, *HeyL*) are highly expressed in quiescent cells and are down regulated upon activation(Bjorson et al.,2012; Fukada et al., 2007). In vitro studies of cell cycle kinetics showed that *Rbp-j* null satellite cells fail to enter the cycle and directly go through terminal differentiation bypassing the S-phase therefore

suggesting a potential regulation of cell cycle dependent genes by Notch (Bjornson et al., 2012). Interestingly ectopic activation of the Notch 1 intracellular domain (NICD1) can rescue satellite cells stalled in S-phase (Pisconti et al., 2010) and over expression of *Notch* 1 in primary myoblasts have been shown to promote cell cycle entry and proliferation (Conboy and Rando, 2002). Modulation of either extracellular matrix components such as collagen or cell adhesion molecules such as α7Integrin or Megf10 by Notch is required to anchor satellite cells to their niche and preserve their quiescent state (Brohl et al., 2010; Holterman et al., 2006).

NICD1 and Rbp-j have been shown to directly bind Pax7 and to promote satellite cell self-renewal (Wen et al., 2012) as well as inhibit terminal differentiation by preventing MyoD and MEF2C binding to the Myogenin promoter (Kuroda et al., 1999; Buas et al., 2009 and 2010) or by antagonizing pro differentiation signaling such as the p38/MAPK signalling (Jones et al., 2005; Kundoh et al., 2007). In agreement with these findings, inhibition of Notch results in precocious up-regulation of terminal myogenic differentiation genes (Conboy and Rando, 2002; Wen et al., 2012; Sun et al., 2007).

Figure 1.10

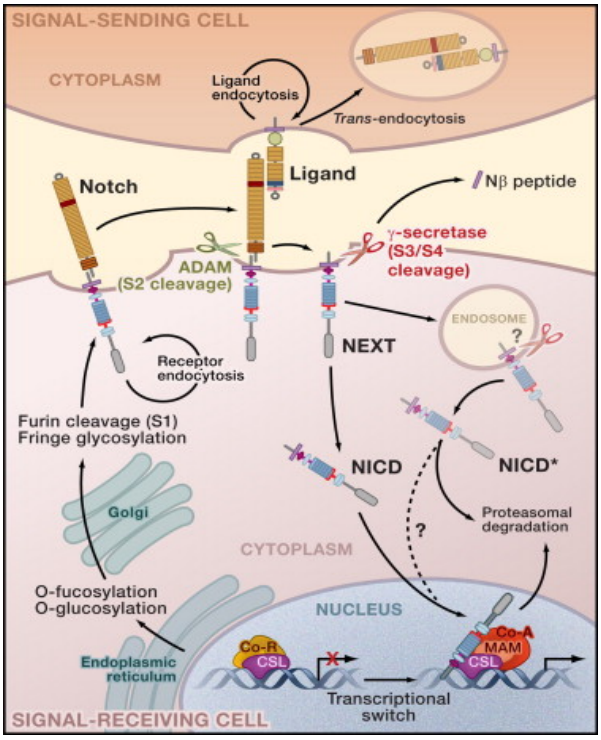

Figure 1.10. The Notch signaling pathway. Schematic of the transduction mechanism and regulation of the Notch pathway. The binding between a Notch receptor to a ligand results in the proteolytic cleavage and nuclear translocation of the Notch intracellular domain (NICD). Once in the nucleus, NICD then binds to the DNA-binding protein CSL (CBF1/RBPjκ/Su(H)/Lag-1). Allosteric changes determine the displacement of repressors and recruitment of the transcriptional coactivator Mastermind (MAM). NICD activity is regulated intracellularly by ubiquitin ligase dependent proteosomal degradation, glycosylation of the EGF-like repeats, or endocytosis [from Kopan and Ilagan, 2009].

1.11. Alternative sources of muscle regeneration

While not the focus of the current thesis, it is important to acknowledge the contribution of other stem cell types to muscle regeneration. Bone marrow stem cells (Ferrari et al., 1998) as well as side population (SP) stem cells (Gussoni et al., 1999) were among the first type of stem cells of non muscle origin to be shown to participate to muscle regeneration.

However, the most successful non muscle stem cells capable of regenerating and repair injured muscles are undoubtedly pericytes. Pericytes are blood vessel derived cells reminiscent of embryonal mesoangioblasts that can efficiently give rise to myogenic cells in vitro and are present in mouse, dogs as well as humans (Dellavalle et al., 2007; Tonlorenzi et al., 2007). When transplanted into mdx mice, a transgenic mouse line in which the lack of functional dystrophin protein results in continuous cycle of muscle regeneration-degeneration, pericytes can migrate into the host muscle from the vasculature bed and generate new muscle fibers as well as assume a satellite cell position (Sampaolesi et al., 2003 and 2006).

1.12. Relevance of studying muscle regeneration

With more than 600 different muscles accounting for approximately half of the total body mass, the skeletal muscle tissue is the second most abundant tissue, after the skin. While architecturally simple, the skeletal muscle tissue integrate and process multiple signals from transducing electrical stimuli from the nervous system, adapting to changes in the body metabolism, or sensing mechanical forces from the connective tissue and tendons.

1.13. Hypothesis and rationale

Pax7 is an essential regulator of post natal myogenesis. However the genetic requirements of *Pax7* in the regulation of satellite cells function remain elusive, partially due to technical difficulties isolating homogenous population of satellite cells from their tissue of origin.

The main objective of Chapter Two of the current thesis were to:

Identify the best strategy for the isolation of quiescent satellite cells from hindlimb muscles of adult mice. This was accomplished by testing different surface markers for the identification of satellite cells by Fluorescence Activated Cell Sorting (FACS);

The main objectives of Chapter Three of the current thesis were to:

Identify novel regulators of adult myogenesis. This was accomplished by performing RNA sequencing of FACS sorted *Pax7* null satellite cells as well as characterizing the behavior of *Pax7* null satellite cells in vitro.

Chapter Two – Isolation of Muscle Stem Cells by Fluorescence Activated Cell Sorting Cytometry

Summary

To investigate the role of Pax7 in adult satellite cells we made use of Fluorescence Activated Cell Sorting (FACS) coupled with gene expression analysis of *Pax7* null satellite cells. As many other stem cells, satellite cells are a heterogeneous population of cells. The identification of satellite cell specific transcripts depends on which surface markers are used to identify satellite cells, the time spent to isolate satellite cells, the degree of purity and integrity of the RNA as well as on the platform used to identify differentially expressed genes. Here we describe the optimization of a FACS protocol which allows the efficient isolation of a highly pure population of satellite cells from adult hindlimbs. The strategy described here provided also the foundation for gene expression studies carried out in Chapter 3.

Chapter 3

Isolation of Muscle Stem Cells by Fluorescence Activated Cell Sorting Cytometry

Alessandra Pasut, Paul Oleynik, and Michael A. Rudnicki

Abstract

Satellite cells are a heterogeneous population of muscle progenitors with stem cell properties responsible for the regeneration of adult skeletal muscle. Increasing interest in the therapeutic potential of satellite cells has challenged researchers with the need to purify a homogenous population of muscle progenitors. Here we provide a detailed protocol for the isolation of a pure population of satellite cells using fluorescence activated cell sorting. We give specific guidelines to ameliorate the reproducibility of the satellite cell isolation protocol with the goal to standardize procedures across labs. This protocol identifies satellite cells within adult skeletal muscle as an enriched population of Integrin $\alpha7^+$/$CD34^+$ double positive cells and CD45, CD31, CD11b, and Sca1 negative (Lin^-) cells (Integrin $\alpha7^+$/$CD34^+$/Lin^-). Functional assay shows that Integrin $\alpha7^+$/$CD34^+$/Lin^- satellite cells possess high myogenic potential and ability to regenerate muscle depleted satellite cells upon transplantation.

Key words: Satellite cells, Markers, FACS, Cytometry, Fluorochromes

1. Introduction

By providing a lifelong reservoir of muscle progenitors, satellite cells are the main contributors of muscle regeneration (1). Although accounting for only a small percentage of total myonuclei, satellite cells are able to repopulate damaged muscles by activating and differentiating into mature myofibers and at the same time self renew the original pool (2–5). Heterogeneity is a well-established and most likely unique feature of satellite cells (1, 4). Thus appropriate tools that guarantee the isolation of homogenous isolation of homogenous populations are central to the manipulation of satellite cells and to effectively establish the ability of different satellite cell subpopulations to regenerate injured muscles.

Joseph X. DiMario (ed.), *Myogenesis: Methods and Protocols*, Methods in Molecular Biology, vol. 798,
DOI 10.1007/978-1-61779-343-1_3,

Fluorescence activated cell sorting (FACS) is an assay in which single cell properties either physical or chemical are simultaneously analyzed in a fluid stream system and used to separate a heterogeneous sample into distinct groups of cells (6, 7). In a modern flow cytometer, a laser of a selected wavelength is directed toward a flowing stream of single cells and the properties of light scattering is used to infer parameters such as cell size, cell granularity, or DNA content (6, 7). The availability of fluorescently tagged antibodies that specifically recognize and bind to cell surface antigens is an efficient tool to further discriminate stem cells from more differentiated cells within adult tissues or to separate a subpopulation of stem cells within the same pool.

Satellite cell isolation by FACS is an incredibly resourceful but often challenging tool. When starting from a heterogeneous sample such as muscle tissue, several steps need to be performed to obtain a highly pure population of muscle progenitors. In this chapter we offer guidelines and suggestions to improve tissue digestion, single cell preparation, sample labeling, and sample sorting. Satellite cells do not express a unique stem cell marker; rather they can be distinguished from other muscle cells by using a combination of both negative and positive markers. The cell surface markers CXC motif receptor R-4 (CXCR4), the vascular cell adhesion molecule 1 (V-CAM-1), Integrins α7β1 or CD34 are used by different labs to identify satellite cells by FACS (2, 3, 5, 8–12). In the protocol herein described satellite cells are identified as an enriched population of Integrin α7/CD34 double positive cells and CD45, CD31, CD11b, and Sca1 negative (Lin^-) cells (Integrin $\alpha7^+/CD34^+/Lin^-$). More importantly, transplanted Integrin $\alpha7^+/CD34^+/Lin^-$ cells can efficiently regenerate muscles by both repairing and fusing with damaged fibers and contributing to a self-renewal pool (3, 5).

FACS coupled with high throughput gene expression studies allowed the elucidation of novel signaling pathways and molecules involved in satellite cell self-renewal and activation (5, 9). It is thus clear that the development of reproducible and standardized methods for the isolation of stem cells is of paramount importance especially in the context of translational research.

2. Materials

2.1. Reagents

1. Sterile surgical tools.
2. Netwell Mesh Filters, 74 μm (Costar).
3. CellTrics disposable filters, 50 μm (Partec).
4. Characterized Hyclone Fetal Bovine Serum (FBS; Thermo Scientific).

5. 2.5 U/mL Dispase II (Roche).
6. 2.5 U/mL Collagenase B (Roche).
7. Monoclonal antibody anti-mouse Integrin α7 clone 3C12 (MBL).
8. Alexa647 anti-mouse IgG1 (Molecular Probes, Invitrogen).
9. Phycoerythrin (PE) anti-mouse CD11b (eBioscience).
10. Phycoerythrin (PE) anti-mouse CD45 (eBioscience).
11. Phycoerythrin (PE) anti-mouse Ly-6A-E (Sca1; BD Bioscience).
12. Phycoerythrin (PE) anti-rat CD31 (BD Bioscience).
13. Biotin anti-mouse CD34 (eBioscience).
14. Streptavidin-APC-Cy7 (BD Bioscience).
15. Hoechst 33342 (Sigma).
16. Phosphate Buffer Saline (PBS).

2.2. Equipment

1. Cell sorter equipped with three lasers: 488 nm laser for the excitation of PE fluorochrome, 633 nm laser for the excitation of APC and APC-Cy7 fluorochrome, and UV for the excitation of Hoechst dye.

3. Methods

Mononuclear cells from a digested muscle preparation are processed using the Beckman-Coulter MoFlo cytometer (DakoCytomation) equipped with 488, 633 nm, and UV lasers. The Summit V4.3 software suite was used to analyze all results.

The protocol is divided into four sections: preparation of single cell suspension, cell staining, performing FACS, and downstream applications.

All procedures are to be performed at room temperature unless otherwise specified.

3.1. Single Cell Suspension

1. Dissect hind limb muscles from 6 to 8 week old mice for optimal satellite cell yield. Use a razor blade or other appropriate tools to first remove any hairs. Expose the muscle completely by cutting through the thick membrane surrounding the tissue. Dissect the muscles following their lengths and anatomy. Collect muscles in cold PBS until ready to proceed with all the samples.
2. If necessary, wash muscles in cold PBS a couple of times.
3. Using small scissors or other appropriate tools, carefully mince the muscles. If any bones are left, separate the bones from the muscles. Remove intramuscular fat pads (white and soft tissue).

4. Proceed with enzymatic digestion by adding 5 mL of collagenase-dispase solution (2.5 U/mL) per each muscle preparation (two hind limbs) and incubate for 10–12 min at 37°C.
5. Coat a plastic pipette with FBS to prevent cells from sticking to the pipette walls and resuspend minced muscles up and down a few times to help tissue digestion.
6. Repeat steps 4 and 5 until the tissue is almost entirely digested and appears as a homogenous solution with few or no tissue chunks. Depending on the enzyme activity, the incubation time can vary between 30 and 60 min.
7. Add 2 volumes of 10% FBS in PBS to inactivate enzyme activity and filter the solution through a 74 μm mesh filter. Centrifuge at 239 × *g* for 5 min. Keep the cell pellet and transfer the supernatant to a clean tube.
8. Centrifuge the supernatant one more time. Combine the two cell pellets in a new tube.

3.2. Cell Staining

1. Resuspend the cell pellet in 1 mL of 2% FBS in PBS. Take an aliquot (10 μL) and count the number of cells. It is recommended to dilute the aliquot at least 2 times to obtain an accurate measurement of total cell number. The staining protocol and corresponding volumes listed below are suitable for 10 million cells. *Optional*: if erythrocytes are presents in the cell pellet, before proceeding to count, add Red Blood Cell Lysis buffer (Sigma) as per manufacturer instruction and then proceed to count. Erythrocytes will anyway be excluded during the sorting strategy (see Subheading 3.3, step 2).
2. Prepare the following controls:
   (a) Set aside an aliquot of 50,000 cells to determine the threshold for cell autofluorescence (unstained control) (see Subheading 3.3, step 3).
   (b) Set aside three aliquots of 50,000 cells to be used as single color controls. In this specific case, the single color controls are Alexa647, APC-Cy7, and PE. The ratio of labeled antibody to cell number is the same used for the actual sample. The purpose of this control will be discussed in Subheading 3.3, steps 4 and 5.

       Dilute each control up to 500 μL in 2% FBS in PBS and filter the cell suspension using a 50 μm disposable filter to ensure a single cell suspension. Keep solutions on ice, protected from light until ready to process.
3. Adjust the final volume of the actual sample to 1 mL before proceeding further.
4. Add to the cell suspension 5 μL of monoclonal antibody anti-mouse Integrin α7 (1 mg/mL) and 10 μL of biotin anti-mouse

CD34 (0.5 mg/mL) per 10 million cells. Because different batches of antibodies might have slightly different concentrations, it is always recommended to titrate each new batch of antibody (see Note 1).

5. Incubate cells on ice for 15 min and gently shake cell suspension every 5 min to prevent cell clumps.
6. Add 9 mL of cold 2% FBS in PBS and centrifuge for 5 min at 239 × *g* to wash unbound primary antibody.
7. Resuspend the pellet in 1 mL of cold 2% FBS in PBS. Add 5 µL of Alexa647 anti-mouse IgG (2 mg/mL) and 2.5 µL of Streptavidin APC-Cy7 (0.2 mg/mL). Add 2.5 µL of PE anti-mouse CD45 (0.2 mg/mL), 2.5 µL of PE anti-mouse CD11b (0.2 mg/mL), 2.5 µL of PE anti-mouse Sca1 (0.2 mg/mL), and 2.5 µL of PE anti-rat CD31 (0.2 mg/mL), also referred to as Lin^-. If a UV laser is available, add 5 µL of Hoechst dye (1 mg/mL). Incubate cells on ice for 15 min protected from light. If a UV laser is not available, use another cell viability dye such as propidium iodide (PI) to discriminate dead-live cells (see Note 2).
8. Add 9 mL of cold 2% FBS in PBS and centrifuge for 5 min at 239 × *g* to wash unbound secondary antibody.
9. Resuspend cells in 500 µL of cold 2% FBS in PBS and filter cell suspension through a 50 µm disposable filter to ensure a single cell suspension. Keep cells on ice until ready to sort.

3.3. Performing FACS

These are general rules that should be followed when sorting satellite cells. Instrument calibration, cleaning procedure, or other routine operations are here omitted due to space limitations.

1. The following dot plots are used to create a satellite cell sorting profile on Summit or any equivalent flow cytometry/FACS software:
   (a) Side scatter (SSC) in logarithmic scale (log) vs. forward scatter (FSC) in linear scale (lin). SSC represents the light scattered and collected at a 90° angle. It is an indication of intrinsic cellular granularity. FSC represents the light scattered and collected at a 180° angle. It is an indication of cell size.
   (b) FSC linear vs. pulse width is also known as doublet discrimination. It distinguishes between singlets (single cells) and doublets (two cells joined together). This plot is needed to guarantee that a purified population of single cells is sorted.
   (c) SSC log vs. PE log distinguishes between Lin^- and Lin^+ cells.
   (d) Alexa647 log vs. APC-Cy7 log for compensation purposes.

(e) SSC log vs. Hoechst log distinguishes between dead (Hoechst$^-$) and live (Hoechst$^+$) cells.

(f) SSC log vs. Alexa647 log distinguishes between Integrin $\alpha7^-$ and Integrin $\alpha7^+$ cells.

(g) SSC log vs. APC-Cy7 log distinguishes between CD34$^-$ and CD34$^+$ cells.

2. Analyze the autofluorescence control by running the sample at a rate of roughly 1,000 events (cells)/s. Since these cells do not contain any label, they will appear as negative events. While analyzing the sample on cycle (noncumulatively), adjust the sensitivities of each detector until the events are displayed in the first decade of the *X*-axis in the corresponding fluorescence plots (PE, Alexa647, Alexa647-Cy7, and Hoechst). Collect and save the data for 50,000 events by switching to cumulatively data collection (turn cycle off). In the SSC-log vs. FSC lin plot (see Fig. 1a) draw a region (R1) being careful to exclude the line of events that have extremely low FSC and variable SSC. These events represent dead cells, debris, and erythrocytes. Satellite cells have low FSC and low-medium SSC.

3. In the FSC lin vs. pulse width plot (see Fig. 1b), draw a region (R2) that encompasses the majority of the events. These are the singlets. Doublets are characterized by large pulse width and should not be included in R2. Doublets account for a maximum of 10% of a properly prepared sample. Any result larger than this indicates the lack of a single cell suspension and the sample should be refiltered. Inclusion of doublets could also result in the collection of false positives.

4. Analyze the single color controls separately and save 50,000 events each. These cells will be viewed as negative events in the corresponding fluorescence plot. In the SSC log vs. PE log plot (see Fig. 1c) draw a region around the negative population. This region (R3) represents Lin$^-$ (PE$^-$) cells and accounts for 70% of total events.

5. Analyze the Alexa647 single color control. Compensate out any Alexa647 signal detected on the APC-Cy7 plot (see Note 3). Analyze the sample and save 50,000 events.

6. In the SSC log vs. Hoechst log plot (see Fig. 1d), draw a region (R4) around the Hoechst$^+$ cells. Hoechst$^+$ cells should account for 70–90% of total events.

7. In the SSC log vs. Alexa647 log plot (see Fig. 1e), construct and apply a gate (G1) that includes R1, R2, R3, and R4. Satellite cells should appear as a small, tight population of events with low-medium SSC and high Alexa647 signal. Draw a region (R5) around this population.

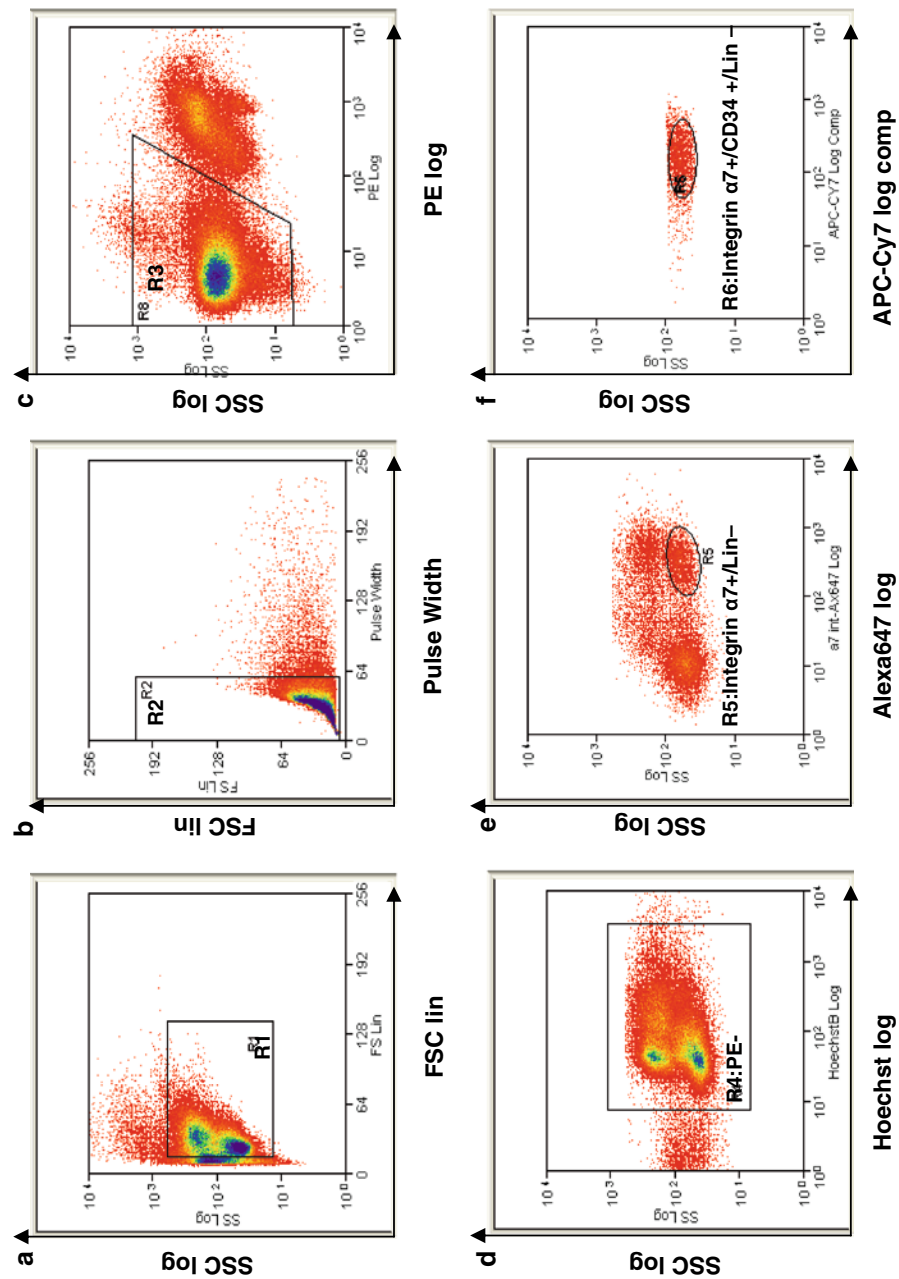

Fig. 1. Isolation of satellite cells from a heterogeneous muscle preparation by FACS. *Dot plots* representing the sequential gating strategy used to identify satellite cells from a heterogonous muscle sample. (**a**) Satellite cells appear as low FSC and low to medium SSC events. FSC is shown in linear scale while SSC is shown in logarithmic scale. (**b**) Doublets discrimination ensures that only a single cell suspension is analyzed and sorted. (**c**) Hoechst is used to discriminate between live (Hoechst$^+$) and dead (Hoechst$^-$) events. (**d**) CD45 and CD11b blood lineage cells, Sca1 mesenchymal progenitors, and CD31 endothelial cells are excluded by gating on PE-events. PE-events account for ~70% of the total events in a standard muscle preparation (**e**) The round gate represents a distinct population of Integrin $\alpha7$ and Lin$^-$ cells in the Alexa647 log vs. SC log plot. (**f**) The majority of satellite cells are double positive for the cell surface markers Integrin $\alpha7$ and CD34. Integrin $\alpha7^+$/CD34$^+$/Lin$^-$ satellite cells account for 1–4% of total events. The Summit softwareV4.3 is used to derive FACS analysis.

8. In the SSC log vs. APC-Cy7 log plot (see Fig. 1f), construct and apply a new gate (G2) that includes R1, R2, R3, R4, and R5. Satellite cells appear in a similar location as found in Fig. 1e. Draw a region (R6) around these cells.
9. The sort logic applied to collect satellite cells is R1 + R2 + R3 + R4 + R5 + R6. This sorting strategy identifies satellite cells as Integrin $\alpha7^+/CD34^+/Lin^-$ cells. Sort into collection tubes containing 2% FBS in PBS kept on ice. To facilitate and ameliorate cell recovery, the sort is performed under low pressure with a maximum flow rate of 3,000 events/s while using a 100 μm nozzle. Higher concentration serum or alternative media (i.e.: primary myoblasts medium) can be used to collect cells during the sort. After the first sort is complete, it is possible to run the sample another time for highest purity; however, the final yield of satellite cells might be heavily depleted because of either cell death or decreased fluorescence intensity of the antibodies resulting in higher rates of false negatives.

3.4. Downstream Applications

Each cell sorting must be followed by a careful characterization of the phenotype which should include immunostaining on freshly cytospunned cells and real time PCR (Q-PCR) for satellite cell specific markers to confirm the nature of the sorted population. This protocol allows for the isolation of an extremely pure population of satellite cells with the ability to both participate in new fiber formation as well as replenish satellite cell pools in impaired muscles (3, 5, 8).

If performing immunostaining on freshly sorted cells, resuspend cells in low volume (max 200 μL) and cytospin at 700 rpm (Cytospin 4, ThermoShendon) for 5 min using appropriate coated slides (Shandon Double Cytoslide coated). Increasing the speed might result in damaging cell integrity and poor quality staining. Care should also be taken during the immunostaining. Gentle washing is recommended to avoid losing cells. Integrin $\alpha7^+/CD34^+/Lin^-$ satellite cells contain more than 90% $Pax7^+$ satellite cells and express satellite cell specific markers by Q-PCR (5).

When sorting satellite cells for gene expression analysis (microarray), it is recommended to decontaminate the FACS sorter and minimize the presence of RNAse by using specific RNAse-free products and cleaning solutions. After the sorting, briefly centrifuge the cells to remove serum. Sorted cells do not pellet very easily, so extreme care should be taken to avoid disturbing the pellet. Resuspend the pellet in an appropriate volume of Trizol or other suitable RNA extraction buffer and immediately proceed with the isolation. Addition of Glycol Blue or other RNA carriers during the RNA isolation protocol might be useful to identify the pellet. When combining multiple sortings, it is best to isolate RNA after each sorting and then concentrate RNA at the desired volume using a speed-vacuum centrifuge system. Freezing-thawing Trizol-cell pellets decreases the final RNA yield.

3.5. Conclusion

Flow cytometry and FACS are undoubtedly valuable tools to obtain homogenous populations of stem cells. Continuous advances in technology made FACS suitable for different downstream applications such as gene expression studies, transplantation studies or single cell analysis. However, the increasing number of publications using FACS data requires unifying and standardizing the procedures to obtain and properly interpret FACS data. Here we summarize and emphasize the importance of the following information: (1) Machine settings: model of cytometer, number of lasers and sorting parameters (nozzle diameter and pressure); (2) Sample handling: if starting from heterogeneous sample, the type of tissue dissociation (sonication, homogenization, enzymatic, mechanical), antibodies list and dilutions, number of labeled cells, type of live-dead assay. (3) Flow analysis: software used to perform the sorting, sorting scheme, description of compensation, and type of controls used (i.e., fluorescence minus one (FMO) or single control). A detailed list of minimum accompanying information is also provided by Lee et al. (13). Flow data must always be accompanied by a complete functional assay. The use of standard procedures to isolate and identify satellite cells from muscle tissues and a careful description of the sorting strategy will allow interpreting and comparing flow data across labs and impact the reproducibility of FACS derived data.

4. Notes

1. *Antibody labeling optimization (Titration)*. Flow cytometry is informative under saturating labeling condition (5). The goal with an antibody titration is to optimize the ratio of labeled antibody to cell number. To perform an antibody titration, prepare aliquots containing the same number of cells. Save one aliquot as an unstained (autofluorescence) control. To the rest, add an increasing amount of the antibody of interest. Analyze each aliquot on a flow cytometer/FACS instrument from the lowest antibody concentration to the highest. The fluorescence intensity should increase in strength until it reaches a maximum above which the signal does not increase anymore. The corresponding antibody concentration is called saturating condition and represents the amount of labeled antibody that should be used. When titrating an antibody for the first time, it is also useful to determine whether the antibody of choice can nonspecifically bind to antigen or other receptors on target cells thus contributing to either increased cell autofluorescence or increased background signal. To do so, it is recommended to run isotype controls for each antibody used for FACS. Isotype controls must match the species, the isotype and the

fluorochrome of the antibody of interest and be used at the same saturating condition to obtain meaningful information. Isotype controls do not substitute for single color controls.

2. *Viability staining*. The goal of viability staining is to distinguish between live and dead cells in a FACS profile and to exclude dead cells from the sorted cells. We have employed Hoechst (where Hoechst$^+$ cells are live cells) because its fluorescence emission is significantly separated from the other fluorochromes here employed. Other viability stains include propidium iodide (PI) or costained with PI and Hoechst.
3. *Compensation*. Compensation is a procedure by which it is possible to remove artifacts (i.e., inclusion of false positives) when fluorochromes with spectral overlap (spillover) are used in the same sample (14). In the present sort, Alexa647 and the tandem dye APC-Cy7 are the two fluorochromes with spectral overlap. When performing FACS using multiple fluorochromes it is best to follow these simple rules: (1) Low abundant or weak antigens should be labeled with the brightest fluorochromes available. (2) If compensation due to spectral overlap needs to be performed, it is preferable to choose dyes with sufficiently distinct spectral overlap to clearly distinguish negative from positive cells and minimize the inclusion of contaminants. In this case, the two antigens used to identify satellite cells (Integrin α7 and CD34) are conjugated with APC and APC-Cy7, respectively, which do not show spectral overlap with PE thus decreasing the inclusion of contaminants in the final sort. Here compensation is applied only to remove any Alexa647 signal from the APC-Cy7 plot. To do this, load the autofluorescence control and draw quadrant regions on SSC log vs. APC-Cy7 log (see Fig. 2a). Then, load the Alexa647 single color control on the same plot (see Fig. 2b). As shown in Fig. 2b, Alexa647 spillover into the APC-Cy7 channel results in the appearance of APC-Cy7 positive cells. Apply compensation until no APC-Cy7 positive events are seen (see Fig. 2c). For accurate description of compensation using Summit Software refer to Summit Software training guide (15). Alongside single color controls, FMO controls should also be analyzed. To prepare FMO controls, label the sample with all the antibodies except for one (i.e., Alexa647-FMO: cells are stained with all antibodies except Alexa647).

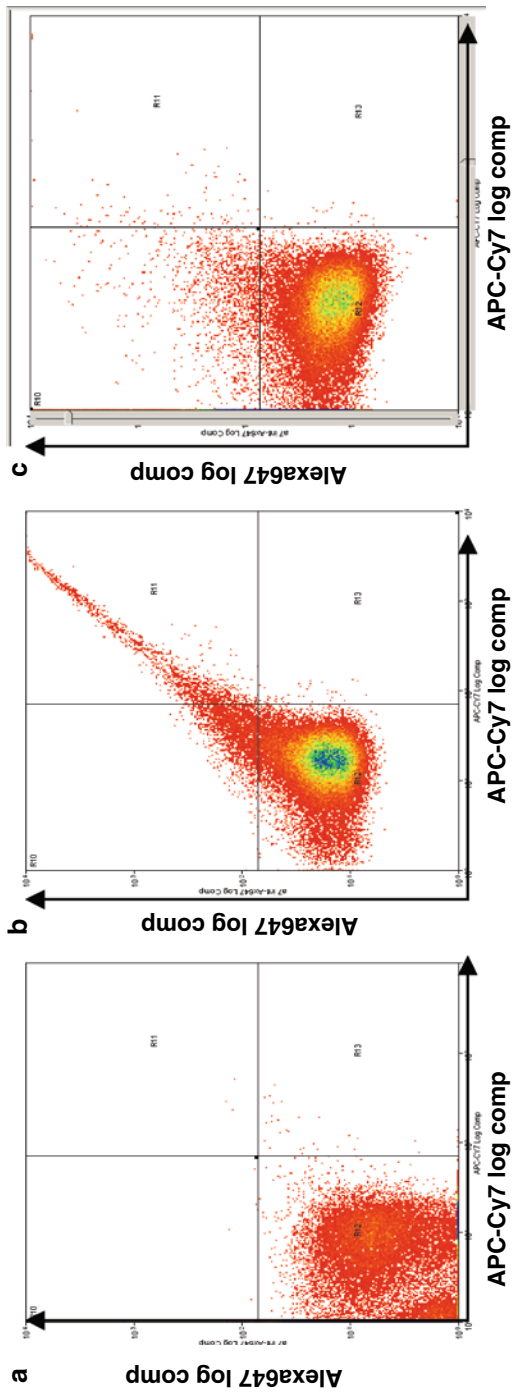

Fig. 2. Compensation strategy. Alexa647 and APC-Cy7 tandem dye have similar emission spectra. For this reason, any spillover of the Alexa647 in the APC-Cy7 channel must be corrected. (**a**) All events in the autofluorescence control sample should appear as double negative on the APC-Cy7 vs. Alexa647 plot. (**b**) Alexa647 spillover into the APC-Cy7 channel results in the appearance of false positive events. (**c**) After compensation is applied no Alexa647 cells are detected into the APC-Cy7 channel. The Summit softwareV4.3 is used to derive compensation analysis.

References

1. Rudnicki MA, Le Grand F, McKinnell I, Kuang S (2008) The molecular regulation of muscle stem cell function. Cold Spring Harb Symp Quant Biol. 73:323–31
2. Kuang S, Kuroda K, Le Grand F, Rudnicki MA (2007) Asymmetric self-renewal and commitment of satellite stem cells in muscle. Cell 129(5):999–1010
3. Sacco A, Doyonnas R, Kraft P, Vitorovic S, Blau HM (2008) Self-renewal and expansion of single transplanted muscle stem cells. Nature 456(7221):502–6
4. Collins CA, Olsen I, Zammit PS, Heslop L, Petrie A, Partridge TA, Morgan JE (2005) Stem cell function, self-renewal, and behavioral heterogeneity of cells from the adult muscle satellite cell niche. Cell 122(2):289–301
5. Le Grand F, Jones AE, Seale V, Scimè A, Rudnicki MA (2009) Wnt7a activates the planar cell polarity pathway to drive the symmetric expansion of satellite stem cells. Cell Stem Cells 5;4(6):535–47
6. HM Shapiro (2003) Practical Flow Cytometry. Fourth edition, Wiley-Liss Inc
7. Hoffman RA (2007) Current Protocols in Cytometry. Wiley Interscience
8. Blanco-Bose WE, Yao C-C, Kramer RH, Blau HM (2001) Purification of mouse primary myoblasts based on α7 Integrin expression. Exp Cell Res 265:212–220
9. Fukada S, Uezumi A, Ikemoto M, Masuda S, Segawa M, Tanimura N, Yamamoto H, Miyagoe-Suzuki Y, Takeda S (2007) Molecular signature of quiescent satellite cells in adult skeletal muscle. Stem Cells 25(10):2448–59
10. Cerletti M, Jurga S, Witczak CA, Hirshman MF, Shadrach JL, Goodyear LJ, Wagers AJ (2008) Highly efficient, functional engraftment of skeletal muscle stem cells in dystrophic muscles. Cell 134(1):37–47
11. Fukada S, Higuchi S, Segawa M, Koda K, Yamamoto Y, Tsujikawa K, Kohama Y, Uezumi A, Imamura M, Miyagoe-Suzuki Y, Takeda S, Yamamoto H (2004) Purification and cell-surface marker characterization of quiescent satellite cells from murine skeletal muscle by a novel monoclonal antibody. Exp Cell Res 296(2):245–55
12. Beauchamp JR, Heslop L, Yu DS, Tajbakhsh S, Kelly RG, Wernig A, Buckingham ME, Partridge TA, Zammit PS (2000) Expression of CD34 and Myf5 defines the majority of quiescent adult skeletal muscle satellite cells. J Cell Biol 151(6):1221–34
13. Lee JA, Spidlen J, Boyce K, Cai J, Crosbie N, Dalphin M, Furlong J, Gasparetto M, Goldberg M, Goralczyk EM, Hyun B, Jansen K, Kollmann T, Kong M, Leif R, McWeeney S, Moloshok TD, Moore W, Nolan G, Nolan J, Nikolich-Zugich J, Parrish D, Purcell B, Qian Y, Selvaraj B, Smith C, Tchuvatkina O, Wertheimer A, Wilkinson P, Wilson C, Wood J, Zigon R; Scheuermann RH, Brinkman RR (2008) MIFlowCyt: the minimum information about a flow cytometry experiment. Cytometry A 73(10):926–30
14. Roederer M (2001) Spectral Compensation for Flow Cytometry: Visualization Artifacts, Limitations, and Caveats. *Cytometry* 45:194–205
15. Prursley S (2007) Summit Software Training Guide, Beckman Coulter Inc

Chapter 3-Notch1 Rescues Pax7-deficient Satellite Cell Loss and Induces Brown Adipogenesis.

Notch 1 Rescues *Pax7*-deficient Satellite Cell Loss and Induces Brown Adipogenesis.

Alessandra Pasut [1,2] , Christopher Porter [2], Vahab Soleimani, Melanie Lacaria [1,2], Hong Ming [2],Robin Parks[1,2], Theodore Perkins [2], Michael A Rudnicki [1, 2,]

1. Cellular and Molecular Medicine Department
   Faculty of Medicine
   University of Ottawa, Ottawa
   ON, K1H8M5
   Canada

2. Sprott Center for Stem Cell Research
   Ottawa Hospital Research Institute
   Ottawa, ON, K1H8L6,
   Canada

Summary

Successful muscle growth and regeneration depend on a population of muscle stem cells known as satellite cells. Here we performed genome wide expression studies of quiescent satellite cells and show that *Pax7* is essential for satellite cell identity in postnatal skeletal muscles. We show that Notch signaling is impaired in *Pax7* null satellite cells and identify a novel and functional Pax7 binding site 28 kb upstream *Notch1* transcriptional start site. We demonstrate that over expression of Notch1 (NICD1) is sufficient to rescue loss of *Pax7*-deficient satellite cells due to precocious differentiation. Strikingly, *Pax7*$^{-/-}$ satellite cells expressing activated Notch1 are capable of proliferation but undergo highly-efficient default differentiation into brown adipocytes. Therefore, we conclude that *Notch 1* is a direct target gene of Pax7 in satellite cells, which functions to maintain satellite cell homeostasis and facilitate proliferation. In the absence of Pax7 and specification of myogenic identity, Notch1 functions as a novel regulator of brown adipogenesis.

Introduction

Satellite cells are widely acknowledged as the driving force of muscle regeneration in adult myogenesis (Chang et al., 2014). A steady number of satellite cells is required to ensure the maintenance of skeletal muscle turnover and guarantee its repair upon successive waves of injury. In homeostatic conditions, satellite cells are found in a state of reversible quiescence, which they can exit upon muscle injury (Yin et al., 2013; Chang et al., 2014). The exit from quiescence and entry in the cell cycle are followed by a phase of extensive proliferation whereby cycling satellite cells give rise to a transient population of cells called primary myoblasts. Primary myoblasts will then withdraw from the cell cycle and fuse to irreversibly differentiate into myotube which will either contribute to repair damaged fibers or make new ones. At the same time, asymmetric divisions of satellite stem cells is responsible for the maintenance of a self-renewing population of cells (Kuang et al., 2007).

All satellite cells express the paired box transcription factor *Pax7* (Seale et al., 2000). Genetic deletion of *Pax7* results in impaired post natal muscle growth and regeneration due to the progressive post natal decline in satellite cells (Seale et al., 2000; Kuang et al., 2007). Similarly, inactivation of *Pax7* in adult skeletal muscles via tamoxifen inducible Cre recombination of the *Pax7*locus results in loss of satellite cells, impaired muscle regeneration and massive fibrotic and fat infiltration (Lepper et al., 2009 and 2010; Gunther et al., 2013; vonMaltzhan et al., 2013). The current understanding is that in the absence of *Pax7* satellite cells are lost due to precocious differentiation

Together with intrinsic signalings, extrinsic signalings from the niche influence and modulate stem cell functions (Brack et al., 2008; Pisconti et al., 2010; Brohl et al., 2012;

reviewed in Bentzinger et al., 2014). The Notch pathway is an evolutionary conserved signaling triggered by the physical interaction between a Notch ligand expressed by one cell (sending cell) and a Notch receptor expressed by a neighbouring cell (receiving end) (Kopan and Ilagan, 2009). The binding of the Notch receptor to one of the ligands results in two sequential cleavages of the Notch intracellular domain (NICD), which translocates into the nucleus where it associates with the transcription factor Rbp-j. NICD binding to Rbp-j results in the recruitment of co-activators factors such as Malm and p300. Canonical Notch target genes include the family of basic helix loop helix (bHLH) transcription factors *Hes* and *Hey* (Bray et al., 2001).

Gene expression studies and immunofluorescence of adult skeletal muscles have shown that several components of the Notch signaling pathway are expressed in both quiescent and activated satellite cells but not in differentiating fibers (Conboy et al. 2002; Kuang et al., 2006; Fukada et al., 2007; Brohl et al., 2012; Bjorson et al., 2012; Mourikis et al., 2012). *Hey1*, a Notch downstream target gene, has been shown to inhibit terminal myogenic differentiation by antagonizing MyoD and MEF2 binding to *Myogenin* promoter (Kuroda et al., 1999; Buas et al., 2009 and 2010) and up-regulation of *Notch1* has been shown to promote satellite cell proliferation and self-renewal in a cell-dependent context (Conboy et al., 2002; Wen et al., 2012).

Interestingly, similarly to the Pax7 mutant phenotype, genetic inactivation of Notch in embryonic progenitors results in complete loss of satellite cells and impaired fetal myogenesis (Vasutyna et al., 2007). Tamoxifen induced deletion of *Rbp-j* in adult satellite cells, results in precocious exit from quiescence and impaired expansion due to precocious differentiation (Mourikis et al., 2012; Bjornson et al., 2012). These similarities may suggest the existence of a genetic interaction between Pax7 and Notch.

By performing genome wide studies here we show that Pax7 maintains satellite cell identity through the regulation of discrete class of genes, involved in cellular, developmental and metabolic functions. Here we report that Notch signaling is impaired in *Pax7* null satellite cells. We demonstrate that re-activation of the Notch pathway by over expression of the intracellular domain of *Notch1* (NICD1) is sufficient to rescue *Pax7* null satellite cell from precocious differentiation and to re-establish satellite cell homeostasis. NICD1 over expressing *Pax7* null satellite cells escape myogenic differentiation and instead differentiate into brown adipocytes and contribute to the formation of ectopic brown fat depots in vivo. We conclude that Notch 1 partially fulfills Pax7 functions in adult myogenesis and acts at different levels to control satellite cell homeostasis and lineage progression.

Results

Pax7 is required to maintain satellite cell identity and prevent differentiation

In the absence of *Pax7*, muscle regeneration is severely impaired (Seale et al., 2000). To identify biological functions associated with loss of *Pax7*, genome wide analysis of *Pax7* wild type and *Pax7* $^{LacZ/LacZ}$ (*Pax7* null) satellite cells was performed. In *Pax7*$^{LacZ/LacZ}$ mice (*Pax7*$^{-/-}$), the *Pax7* gene is replaced by *β- galactosidase*, such that no functional Pax7 protein is produced.

Satellite cells were isolated from 4 week old *Pax7* $^{lacZ/lacZ}$ or wild type mice by Fluorescence Activated Cell Sorting (FACS) using a well established protocol (Kuang et al., 2006; Sacco et al., 2008; Juan et al., 2011; Pasut et al., 2012) (Figure 1A-B and Figure S1). Genome wide RNA sequencing was performed using an Illumina platform. Equal number of reads and similar genome coverage were recovered from both samples (Figure S2). Gene expression was calculated as Fragments Per Kilobase of exon per Million fragments mapped

(FPKM) and significant genes were determined by using standard criteria (log 2 fold change >2 and p-value<0.05) (Figure S2).

A total of 722 genes were found significantly differentially expressed (DE) (Figure 1C). The functional annotation clustering tool provided by DAVID Bioinformatics resources (Huang et al., 2009) allowed identifying the most significantly enriched gene ontology (GO) functions in *Pax7* null satellite cells compared to wild type (Supplementary Tables 1-4). Significantly enriched GO terms included cell migration, cell adhesion, extra cellular matrix components, cytoskeleton proteins, calcium and ion channel trafficking, inflammation, lipid metabolism, fatty acid synthesis, RNA processing and regulation of transcription (Figure 1D-E; Supplementary Tables 1-4). Of interest, functions associated with positive regulation of growth, cell fate and skeletal muscle development were significantly under represented. Similarly, satellite cells and stem cell specific markers such as *Pax7*, *Myf5*, *c-Met*, *CD34*, *Calcr*, *V-Cam*, *Megf-10*, *Cxcr4*, *Sdc4*,were down-regulated (Supplementary Table 5) while genes usually expressed by terminally differentiated fibers such as myosins, sarcomeric proteins, neuromuscular junction proteins and proteins involved in muscle contraction were up-regulated (Supplementary Table 6).

In parallel, single fibers were isolated from *Pax7* null and wild type mice and cultured for 48 hours to allow satellite cell activation. We found that *Pax7* null EDL fibers have a significant decreased number of ki67 expressing (proliferating) satellite cells compared to wild type fibers (48.86+/- 4.45 vs 83.6 +/-12 %) (Figure 2A-B). Importantly the decrease in proliferation was not due to enhanced self-renewal as the number of satellite cells decreased over time in *Pax7* null compared to wild type mice (Figure S3).

To determine whether the decrease in proliferation was due to increase differentiation, we enumerated the number of satellite cells expressing MyoD and Myogenin cells at 48 hours in

culture. As shown in Figure 2C and D, most wild type satellite cells express MyoD but do not express Myogenin, suggesting that at this time, satellite cells are still proliferating and haven't yet committed to terminal differentiation. By contrast, the number of committed MyoD/Myogenin expressing satellite cells was 6 fold higher in *Pax7* null fiber cultures compared to wild type (18.99+/-5.7 vs 3.44+/-2.7, expressed in %) (Figure 2C-D). Additionally a minority (5.58+/- 1.5) of *Pax7*$^{-/-}$ satellite cells had already down regulated MyoD and up-regulated Myogenin (Figure 2C-D).

***Notch1* is a novel Pax7 target**

Genetic inactivation of *Rbp-j* has been shown to result in loss of satellite cells and precocious differentiation (Vasutyna et al., 2007; Bjorson et al, 2012; Mourikis et al., 2012). The similarity between the *Pax7* $^{-/-}$ satellite cell phenotype and the *Rbp-j* phenotype led us to test the hypothesis that Notch signaling was perturbed in *Pax7* null satellite cells. According to our RNA-seq data, some Notch genes such as *Notch2*, *Rbp-j*, *Notch3*, *Hey1*, *HeyL*, *Hes6* and *Dtx4* were down-regulated in *Pax7* null satellite cells (Supplementary Table 7).

We performed qRT-PCR on freshly sorted satellite cells to assess the level of expression of core components of the Notch pathway. As shown in Figure 3A, FACS sorted *Pax7* null satellite cells have significantly lower levels of *Notch1* and *Notch2* mRNAs compared to wild type cells. Similar results were obtained by performing transient RNA knock-down of *Pax7* in primary myoblasts and showed that *Notch 1* and *Notch 2* were the most highly significant down regulated genes (Figure 3B). Previous literature has shown that *Notch3* is highly retained by quiescent satellite cells (Kuang et al., 2006; Fukada et al., 2007). However our q-RT-PCR data show that *Notch3* expression was not significantly perturbed between *Pax7* null and *Pax7* wild

type satellite cells (Figure 3A). *Rbp-j* and *Hey1* expression were only slightly affected (Figure 3A).

Next, we interrogated our previously reported Pax7 Chromatin Immunoprecipitation (ChIP) sequencing data (Soleimani et al., 2012) and found putative Pax7 binding peaks upstream *Notch1* and *Notch2* transcriptional start sites (TSS). ChIP-qPCR was performed to validate Pax7 enrichment at those genomic loci (Figure 4A). As shown in Figure 4A, Pax7 enrichment at the -28kb site upstream of *Notch 1* was 5 fold higher relative to control, while the enrichment at the *Notch2* genomic site was not significant. Importantly both Pax7 homeobox and paired domain sequences were spanning the center of the *Notch1* peak (Figure 4B). Luciferase assay was performed to validate the ability of Pax7 to activate transcription from the *Notch1* site. The Pax7 trans-activator plasmid (Pax7 VP16) was co-trasfected into 293T cells in the presence or absence of the -28*Notch1* element. As shown in Figure 4C, Pax7 binding to the -28kb *Notch1* regulatory element was sufficient to increase *Luciferase* expression by 2.5 fold compared to control (VP16, empty vector). Co-transfection of 293 cells with a Pax7 mutated construct (Pax7 G/N) abolished the binding and didn't show any significant changes in Luciferase expression.

Similarly to loss of *Pax7*, inhibition of *Notch1* by siRNA in primary myoblasts decreased cell proliferation and enhanced myogenic differentiation as assessed by immunofluorescence for Myogenin and ki67 (Figure 4F). Inhibition of *Notch1* did not affect *Pax7* expression while *MyoD* and *Myf5* expression were up-regulated (Figure 4D-E; S4).

Altogether these results showed that the expression of several Notch genes is impaired in *Pax7* null satellite cells which precociously exit the cell cycle and differentiate. Additionally we identified *Notch1* as a novel Pax7 target gene.

***In vivo* activation of Notch signaling rescues *Pax7* null satellite cell number**

Our previous results showing that Notch and Pax7 genetically interact led us to speculate whether Notch gain of function could rescue *Pax7* null satellite cells. To address this question, we used a genetic approach. An advantage of this strategy is that it allows studying satellite cells in their physiological environment and with minimal external manipulation. Briefly, *Pax7* null mice were generated by crossing *Pax7* ^{CreER} (*Pax7* $^{CE/+}$) mice with *Pax7* $^{floxed/floxed}$ (*Pax7* $^{f/f}$) mice (Lepper et al., 2009 and 2010). In *Pax7* $^{f/CE}$ animals upon tamoxifen injection, Cre recombinase activity, driven from the *Pax7* promoter, results in the generation of a *Pax7* null allele from the *Pax7* floxed site (Lepper et al., 2009 and 2010) (Figure 5A). To constitutively activate Notch in adult satellite cells, 6 week old *Pax7* $^{f/CE}$ (*Pax7* null) or *Pax7* $^{f/+}$ (WT) mice were crossed with the *Rosa* ^{Notch} mouse strain (Murtaugh et al.,2003). In these latter mice, the active intracellular domain of *Notch 1* (NICD1) and the Green Fluorescent Protein GFP are expressed from the *Rosa* locus, upon Cre dependent recombination of the two *loxP* sites flanking the STOP sequence placed between NICD1 and the *ROSA26* promoter. GFP expression is localized to the nucleus such that all cells that have successfully over expressed NICD1 can be traced by nuclear GFP (Figure 5A). In *Pax7* $^{f/CE}$ *Rosa* ^{Notch} mice Cre recombinase from the *Pax7* locus results in the simultaneous inactivation of the *Pax7* gene and constitutive activation of NICD1. These mice are hereafter referred to as OE-NICD1 *Pax7* null. *Pax7* $^{f/+}$ *Rosa* ^{Notch} were used as controls. Tamoxifen was administered at 6 weeks of age and mice were sacrificed at 8 weeks for downstream analysis (Figure 5B).

Single fibers were isolated from EDL muscles as described in Pasut et al., 2013. As expected, *Pax7* $^{f/CE}$ (*Pax7* null*)* mice showed a significant reduction in the number of satellite cells (α7Integrin expressing cells) per fiber compared to control littermates (1.26 +/- 0.36 vs 5.98

+/- 0.72) (Figure 5C). Remarkably, the number of satellite cells was 3 fold increased in the presence of activated NICD1 (4.43 +/- 1.17 vs. 1.26+/- 0.36) and not significantly different from wild type (Figure 5C). GFP was expressed by OE-NICD1 *Pax7* null satellite cells only as confirmed by immunofluorescence staining of GFP on single EDL fibers (Figure 5D). However not all satellite cells were GFP positive potentially suggesting inefficient Cre recombination (Figure 5E-F). Importantly GFP and Pax7 expression were mutually exclusive (Figure S5B), clearly excluding the possibility that the rescuing effect is dependent on residual Pax7 expression. Additionally, staining on muscle sections showed that OE-NICD1 *Pax7* null satellite cells were found in a typical sublaminal position (Figure S5A).

Overall these data show that in vivo over expression of NICD1 is sufficient to rescue the loss of satellite cells observed in Pax7 mutant mice and therefore provide biological significance to the genetic interaction between Pax7 and Notch1.

Activated Notch rescues proliferation and prevents differentiation

To investigate the effect of Notch gain of function on activated satellite cells, single EDL fibers were cultured on horse serum coated dishes for 48 hours in high serum medium. Under these culture conditions, most wild type satellite cells exit quiescence and extensively proliferate as assessed by the nuclear expression of ki67, a marker of cell proliferation (Figure 6A-B).

However satellite cell activation is perturbed in *Pax7* null fibers, and consistent with previous findings the majority of *Pax7* null satellite cells were ki67 negative and only a minor fraction (23.9+/-2.4 %) was ki67 positive (Figure 6A-B). Remarkably, the number of ki67 expressing satellite cells was three times higher in the presence of NICD1 as quantified in Figure 6A. Of note, ki67 positive cells were also GFP positive, a clear indication that the proliferation was dependent on the activation of NICD1 (Figure 6B). However, it should be noted that a

minority of satellite cells over expressing NICD1were also ki67 negative (Figure 6B, white arrows). Occasionally GFP negative, ki67 positive satellite cells were also found. However, most GFP negative cells were ki67 negative. Our results imply that at least within a 48 hours time window NICD1 is permissive to both proliferation (Conboy et al., 2002) as well as self-renewal (Wen et al., 2012).

Activation of Notch has been shown to inhibit terminal differentiation (Kuroda et al., 1999; Conboy et al., 2005; Buas et al., 2009 and 2010; Bjorson et al., 2012; Mourikis et al., 2012). We next determined the number of MyoD expressing cells at 48 hours as MyoD expression marks satellite cells commitment toward the myogenic lineage. As expected, MyoD was up-regulated in most wild type and *Pax7* null satellite cells (Figure 7A). Remarkably, no MyoD expressing satellite cells were found on single EDL fibers isolated from OE-NICD1 *Pax7* null mice (Figure 7A). Importantly MyoD and GFP expression were mutually exclusive (Figure S6). In vitro activation of NICD1 in primary myoblasts isolated from $Pax7^{f/f}$ $Rosa^{Notch/+}$ mice infected with adenovirus expressing Cre recombinase (AdCre) showed significant down regulation of all three MRFs mRNAs (*MyoD, Myf5* and *Myog*enin) compared to control cultures (Figure 7B). Of note, when cultured in low serum conditions OE-NICD1 *Pax7* null primary myoblasts were unable to differentiate into myotubes and detached from the plate (data not shown). No discernible defects in cell differentiation were observed in control cultures of primary myoblasts infected with control adenovirus (AdRFP).

These findings clearly demonstrate that Notch is sufficient to inhibit the up-regulation of MRFs expression rather than inhibiting their DNA binding activity (Buas et al., 2010)

Notch signaling regulates satellite cell fate

We previously demonstrated that satellite cells have the ability to undergo both myogenic and adipogenic differentiation (Yin et al., 2013). However the mechanisms regulating satellite cell lineage fate are not well understood. The complete absence of MyoD positive cells in OE-NICD1 *Pax7* null fibers led us to address whether Notch regulates satellite cell lineage fate. Single EDL fibers were cultured on matrigel coated slides under adipogenic conditions. *Pax7* ^{CreER} *ROSA*^{YFP} mice, which allow lineage tracing of wild type satellite cells,were used as control. As expected, most wild type satellite cells give rise to multinucleated myotubes (Figure 7C). A small percentage of satellite cell derived progeny expressed both YFP and perilipin, a marker of mature adipocytes thus confirming that adult satellite cells do retain a bi-potential ability (Figure 7C, yellow arrows).

Remarkably all GFP positive cells from OE-NICD1 *Pax7* null fibers give rise to perilipin positive cells (Figure 7D) and no GFP expressing myotubes were found. Of note GFP expressing cells were also PRDM16 positive, a marker of brown fat adipocytes (Figure S7). Of interest we found that in vitro activation of NICD1 in primary myoblasts isolated from *Pax7*$^{f/f}$ *Rosa* $^{Notch/+}$ mice and infected with adenovirus expressing Cre recombinase (AdCre) results in the down-regulation of miR-133, which we previously showed to inhibit PRDM16 expression (Figure S7B) (Yin et al., 2013). Preliminary experiments in Pax7 wild type mice over expressing NICD1 also showed similar results and suggest that over expression of Notch induces satellite cells to differentiate into brown adipocytes, possibly by inhibiting both MyoD and miR-133 (Figure S8).

Activated Notch induces brown adipocytes during muscle regeneration in vivo

To address the effect of Notch over expression in vivo, muscles from wild type, *Pax7* null and OE-NICD1 *Pax7* null mice were injected with tamoxifen for 5 consecutive days and then injured

on the fifth day with cardiotoxin (Figure 8A). Mice were sacrificed 15 days later and immunohistological analysis was performed to assess the degree of muscle repair. As expected, wild type muscles successfully regenerated in response to cardiotoxin damage as evidenced by the homogenous appearance of centrally nucleated fibers and absence of fibrotic or fat infiltration (Figure 8B). On the other hand, *Pax7* null muscles showed extensive presence of mononuclear cells in the interstitial space, possibly indicating fibrosis (Figure 8B, black arrows) and local areas of fat infiltration as shown by haematoxylin and eosin staining (Figure 8B, yellow arrows). Remarkably, staining of muscle sections with Oil Red O which specifically labels lipid filled droplets, showed that OE-NICD1 *Pax7* null muscles had a significant higher amount of ectopic fat depots (Figure 8B and C). Centrally located fibers indicative of a certain degree of regenerative response were occasionally observed throughout the muscle, potentially due to inefficient or incomplete tamoxifen excision of the *Pax7* gene. No GFP positive fibers were observed in regenerating muscles from OE-NICD1 *Pax7* null mice (not shown) arguing against the contribution of activated NICD1 expressing cells to myogenic differentiation.

Increased fat infiltration was accompanied by a significant loss of muscle mass as shown in Figure 8D. Examination of un-injured controlateral muscles did not show any significant morphological differences across the three genotypes, arguing against the existence of pre-injured conditions that may have affected the outcome (Figure 8B, upper panel). Pax7 expression was also similar in OE-NICD1 and *Pax7* null satellite cells suggesting similar level of *Pax7* excision (data not shown). The number of satellite cells in injured wild type muscle was higher compared to non injured EDL, indicative of efficient satellite cells self-renewal upon injury (Figure 8E). Non- injured OE-NICD1 *Pax7* null EDL muscle had higher number of satellite cells (α7Integrin positive) per fiber compared to non injured *Pax7* null muscle (Figure 8E).

However, the number of satellite cells in injured muscles was similar between OE-NICD1 *Pax7* null and *Pax7* null EDLs (Figure 8E). While the experiments were limited to a small number of mice (n=3 for each genotype) and did not reach significance, we can speculate that increasing the number of animals would allow to better appreciate the effect of NICD1 on satellite cells in the context of injury.

Overall these results show that aside from its function in the maintenance of satellite cells, Notch 1 function as a novel regulator of brown adipogenesis.

Discussion

Satellite cells are the primary executioners of muscle regeneration and growth.

All satellite cells are unanimously identified by their expression of the paired box transcription factor *Pax7*, which extensive evidence has shown to be an essential requirement of postnatal myogenesis (Seale et al., 2000; Kuang et al., 2006; Lepper et al., 2009 and 2010; Gunther et al., 2013; von Maltzahn et al., 2013).

By performing genome wide analysis of *Pax7* null satellite cells we show that Pax7 maintains satellite cell identity through the regulation of multiple cell functions such as cell migration and adhesion (Cornelison et al., 2001; Alfaro et al., 2011), regulation of cell-extracellular matrix interactions (Pisconti et al., 2010), maintenance of quiescence (Fukada et al, 2007) and modulation of inflammation and chemotaxis (Chazaud et al., 2003). At the same time, bio-informatic analysis of RNA-seq data also highlights potential novel regulators of satellite cell function in postnatal myogenesis including genes involved in lipid metabolism (Yuzuf and Scadden, 2012), control of genome integrity (Cheung and Rando, 2014) or ion signaling (Sugimura et al., 2012).

Pax7 null satellite cells have impaired Notch signaling and we report the identification of a novel and functional Pax7 binding regulatory element located 28kb upstream of *Notch1*. Further, over expression of the constitutively active intracellular domain of *Notch 1* (NICD1) is sufficient to rescue the progressive loss of satellite cells in a tamoxifen inducible *Pax7* null mouse model. The mechanisms by which Notch maintains satellite cells homeostasis are not well understood. It has recently been shown that the binding satellite cells-ECM interactions are modulated by the binding between Syndecan 3 and Notch 1 at the cell membrane and that over expression of Notch 1 rescues Syndecan 3 null myoblasts impaired proliferation from differentiating (Pisconti et al., 2010). Additionally, modulation of ECM components expression by active Notch may contribute to maintain satellite cell quiescence by anchoring them to their niche (Brohl et al., 2012).

Inhibition of terminal differentiation by Notch over expression allows satellite cell expansion during the early phases of muscle regeneration (Conboy et al., 2002). Indeed, recent evidences showed that *Rbp-j* null satellite cells precociously differentiate (Bjorson et al., 2012 and Mourikis et al., 2012). In agreement with these results, we found that over expression of NICD1 rescues *Pax7* null impaired proliferation. Heterochronic parabiosis experiments have shown that the Notch ligand *Delta 1 (Dll1)* rescues the age-dependent decline in satellite cell number and their proliferation (Conboy et al., 2005) suggesting that transient exposure to Notch ligands may be a mechanism by which Notch activity is modulated during muscle regeneration.

Muscle regeneration ultimately relies on the commitment of satellite cells to the myogenic lineage. During embryonic development, muscle progenitors expressing *Pax3* and *Pax7* contribute to the formation of fetal muscles (Buckingham, 2001; Kassar-Duchossoy et al., 2005; Relaix et al., 2005). Importantly, lineage tracing experiments have shown that Pax7

expressing cells can be found in the dermis and in brown fat and that brown but not white adipocytes derive from a *Myf5* expressing embryonic progenitor (Lepper et al., 2009; Seale et al., 2008). Recent evidence has shown that adult satellite cells retain the ability to differentiate into both myogenic cells and brown adipocytes (Yin et al., 2013).

Here we show that Notch is an important player in the regulation of satellite cell lineage commitment as evidenced by the dramatic increase in brown adipogenesis observed in OE-NICD1 *Pax7* null satellite cells. Because these experiments were performed on a *Pax7* null background, we do not exclude the possibility that lack of *Pax7* may have also contributed to enhanced adipogenesis. Thus the most cautious explanation for our results is that Notch promotes satellite cell adipogenesis in the absence of a myogenic cue.

Previous studies using a similar genetic approach showed that over expression of Notch in wild type mice results in increase satellite cell self-renewal at the expense of muscle regeneration (Wen et al., 2012). These results were based on analysis of satellite cells from short term fiber culture (48 hours). Our preliminary experiments based on long term fiber culture analysis (2 weeks) show that over expression of Notch in wild type satellite cells also results in increased adipogenesis (Figure S8) and we are currently addressing the long term effect of Notch activation in wild type regenerating muscles. Based on our results, we can speculate that the long term effect of Notch on satellite cell lineage specification may override the transient effect that is may have on satellite cell self-renewal.

The up-regulation and maintenance of MyoD expression by muscle progenitors play a crucial role in the establishment of the myogenic identity (Rudnicki et al., 1993). Remarkably, MyoD and Myf5 have been shown to directly maintain *miR-133* expression during embyonic development (Sweetman et al., 2008). Of interest, the 3'UTR of *Rbp-j* contains a putative seed

sequence motif for *miR-133*, and it is thus tempting to speculate that *miR-133* expression reinforced by MyoD and Myf5 may restrict Notch activity by inhibiting *Rbp-j* expression (Figure 9).

Additionally, post translational modifications at the C-terminus Notch 1 PEST domain (Kopan and Ilagan, 2009), crosstalk with other signalings (Brack et al., 2008) or interactions with the atypical Delta like ligand homologue 1 (*Dlk1*) may also negatively regulate Notch1 expression (Bray et al., 2001). Of interest, the *Rosa* ^{Notch} mouse strain used here lack the PEST domain (Murtaugh et al., 2003).

In conclusion, we show that maintenance of satellite cell homeostasis relies on the genetic interaction between Pax7 and Notch1 and identify Notch1 as a novel regulator of brown adipogenesis (Figure 9). We propose that satellite cells are differentially responsive to Notch and that in homeostatic conditions the constitutive activation of the Notch pathway is responsible for the maintenance of the satellite cell pool (Bjorson et al., 2012; Mourikis et al., 2012). Instructive signals from the niche may positively reinforce this mechanism by engaging in circuitry of positive feedback (Brohl et al., 2012). Notch signaling is only transiently up-regulated in activated satellite cells to allow satellite cell expansion (Conboy et al., 2002) or self-renewal (Wen et al., 2012). Transient up-regulation of Notch ligands (Conboy et al., 2005) or Notch inhibitors may ultimately result in the specification of different genetic programs (Figure 9).

Material and Methods

Mice and animal procedures

Sv129 mice carrying the *Pax7*^{LacZ} allele which have the *β-galactosidase* gene knock into the *Pax7* locus (Mansouri et al., 1996) were maintained as heterozygous animals and interbred to generate *Pax7* $^{LacZ/LacZ}$ and *Pax7*$^{+/+}$ littermate control. Tamoxifen inducible *Pax7* null mice were

generated by crossing *Pax7*^{CE} mice (Jackson Laboratory), which express a Cre recombinase estrogen receptor fusion protein from the *Pax7* locus with *Pax7* $^{floxed/floxed}$ (*Pax7* $^{f/f}$) mice (Jackson laboratory) in which *Pax7* exon 2 is flanked by two flox sites and after Cre mediated recombination becomes a null *Pax7* allele (Lepper et al., 2009 and 2010). For study of Notch over expression, *Rosa* $^{Notch/Notch}$ mice (Murtaugh et al., 2003) were crossed with *Pax7*$^{CE/f}$ mice. *Pax7* $^{CreER/+}$ (Nishijo et al., 2009) were provided by Dr Charles Keller and cross with *Gt(Rosa)26*$^{Sortm9(CAG-YFP)}$ mice (Jackson laboratories) to generate *Pax7* $^{CreER/+}$ *Rosa*$^{YFP/YFP}$ mice in which Cre recombination driven from the *Pax7* locus results in the permanent expression of the fluorescent protein YFP. Cre expression was induced by injecting Tamoxifen (Sigma T5648) pre-dissolved in corn oil at a concentration of 20mg/ml intraperitoneally in 6 week old mice via 5 consecutive injections. For muscle regeneration studies, 50 µl of a cardiotoxin solution was administered intramuscularly to anesthetized animals. Cardiotoxin was prepared by dissolving Latoxan (Sigma) in physiological saline to a final concentration of 10 µM. Mice were sacrificed at either 8 or 12 week of age, as specified. All mice were maintained within the University of Ottawa animal facility and all experiments were performed according to the University of Ottawa regulation for animal care.

Fluorescence activated cell sorting (FACS) and cell culture

Satellite cells were isolated from hindlimb muscles as described in Pasut et al., 2011. Briefly, muscle dissection was followed by a 45 min digestion at 37ºC in collagenase B (Roche) and dispaseII (Roche) solution at a final concentration of 2.5U/ml. Mononuclear cell suspension was incubated in PBS supplemented with 2% horse serum at 4ºC with the following antibodies: APC-α7integrin (AbLab, 1:250), biotinCD34 (BD Bioscience, 1:100), PE-CD45 (BD Bioscience, 1:500), PE-Sca-1 (BD Bioscience, 1:500), PE-CD11b (BD Bioscience, 1:500) and PE-CD31 (

BD Bioscience, 1:500). Secondary APC-Cy7 streptavidin conjugated antibody (BD Bioscience, 1:500) was used to detect biotin labelled CD34. Hoechst 33342 (Sigma) was add at a final concentration of 1mg/ml. FACS was performed on a Moflo cytometer (Dako Cytomation) equipped with 3 lasers. The Summit v4.3 Suite was used for data acquisition and image processing.

For long term culture, satellite cells derived primary myoblasts were maintained on collagen coated plates in Ham's F10 (Wisent Inc) supplemented with penicillin and streptomycin (P/S, Wisent Inc), 20% Fetal Bovine Serum (FBS, Thermo Scientific) and 25ng/µl basic Fibroblast Growth Factor(bFGF Millipore).

siRNA transfection of primary myoblasts

Primary myoblasts were seeded into collagen coated 6-well plates at a density of 20*10^5 cells/ well. Cell transfection was performed using the RNAiMax Lipofectamine reagent (Invitrogen) according to manufacturer's instruction. *Pax7* on target plus siRNAs oligos were purchased from Dharmacon). *Notch 1* Silencer Select siRNAs (#70700 and #70699) and negative siRNA silencer select control oligos were purchased from Ambion. RNA was collected 48 hours from the trasfection. Quantitative PCR was performed using the Stratagene Mx3000P thermocycler. *Ppia* or *Gapdh* were used as reference genes, as specified. Fold expression was determined using the ΔΔCt formula. Statistical significance was performed on three independent replicates.

Single fiber isolation and culture

Single EDL fibers were isolated as described in Pasut et al., 2013. Briefly, single EDL muscles were dissected and digested at 37ºC in 2% collagenase (Sigma) till fibers were starting to dissociate. Isolation of single fibers was performed under a dissecting microscope in DMEM supplemented with Sodium Pyruvate (Invitrogen) and penicillin and streptomycin (P/S, Wisent

Inc). Single fibers were either fixed right after the isolation or cultured in DMEM supplemented with Sodium Pyruvate (Invitrogen), 20% Fetal Bovine Serum (FBS, Wisent Inc), 1% Chicken Embryo Extract (CEE, EnglandBio lab) and penicillin and streptomycin (P/S, Wisent Inc). For short term culture, fibers were cultured in suspension in horse serum coated dishes. For long term culture, fibers were maintained in suspension for 24 hours in horse serum coated dishes and then transferred into Matrigel™ (BD Matrigel) coated dishes and cultured for up to 2 weeks. Medium was changed every two days. Adipogenic differentiation was induced as described in Yin et al., 2013.

Immunostaining

Fiber and cells were fixed in 2% or 4% PFA (Sigma) respectively, followed by permeabilization in 0.5% Triton (Sigma) in PBS and overnight blocking in 10% horse serum in PBS. Primary antibodies were diluted in blocking buffer and used as follows: Pax7 (Developmental Study Hybridoma Bank, mouse monoclonal 1:2); β-gal (Developmental Study Hybridoma bank, mouse monoclonal, undiluted); MyoD (Santa Cruz, rabbit polyclonal 1:10); Myogenin (Developmental Study Hybridoma bank, mouse monoclonal, 1:2); ki67 (AbCam, rabbit monoclonal 1:500); Perilipin (Vala Science, mouse monoclonal1:1000); α7Integrin (Cedarlane, mouse monoclonal, 1:250); GFP (Abcam; chicken polyclonal, 1:1000).Respective secondary antibodies (Alexa, Invitrogen) were diluted in PBS and used at a 1:1000 dilution. DAPI (10mg/ml Sigma) was used to counter stain nuclei at a final dilution of 1:50.000. Images were acquired using a Zeiss Axio Observer microscope or Zeiss Axioplan 2 microscope equipped with an AxioCam HR.

Chromatin Immunoprecipitation and quantitative PCR

Stable over expressing Pax7-FLAG (OE-Pax7) or empty vector-FLAG primary myoblasts were cross linked in 1% formaldehyde (Sigma) in PBS for 10 min at room temperature (RT),

immediately followed by a 5 min incubation in quenching solution (0.125M Glycine in PBS). Cell lysates were collected in PBS and then cell pellet was resuspended in ChIP lysis Buffer (40mm Tris-HCl pH 8.0; 1% Triton; 4mM EDTA; 300mM NaCl) followed by sonication. FLAG immunoprecipitation (IP) was performed at 4ºC for 2 hours using a mouse monoclonal anti FLAG antibody conjugated to agarose beads (Sigma). Upon elution from the beads, DNA was reversed cross-linked overnight at 65ºC followed by proteinase K digestion at 37ºC for 1hour. Phenol chloroform extraction was then performed to isolate DNA. Enrichment of Pax7 on particular genomic loci was determined by q-PCR using the Stratagene Mx3000P thermocycler. Fold enrichment relative to empty vector was determined using the ΔΔCt formula. An unbound genomic region on chromosome 1 was used as reference. Statistical significance was performed on three independent IPs.

Luciferase reporter assay

293T cells were seeded into 48-well plates and transfection was performed at a cell density of 3*10^4 cells/ well. Cells were transfected using Lipofectamine2000 (Invitrogen) according to manufacture‘s intructions. Reporter vectors (Pax7WT-VP16, Pax7 GN-VP16, emptyVP16) were used at a final concentration of 250ng and were co-trasfected with a pRL-TK Renilla Luciferase vector at a ratio of 50:1 respectively. The Notch -28 kb element was cloned into the pgl4.23 vector (Promega) to generate the luciferase responsive Notch element and 250 ng of plasmid were used per each transfection reaction. Cells were lysed 48hours after transfection and Luciferase activity was measured using the Dual Luciferase System (Promega) with a Lumistar Optima fluorescence reader (BMG labtech).

Adenoviral infection

Adenoviruses containing either Cre (AdCre) or Red Fluorescent Protein (AdRFP) were provided by Dr Robin Parks. Primary myoblasts isolated from *Pax7* $^{f/f}$ *Rosa* $^{Notch/Notch}$ mice were seeded

into 6-well plate at a density of 20*10^5 cells per well. Virus infection was performed 24h after in HAM's F10 without antibiotics, supplemented with 10% fetal bovine serum (FBS, Wisent Inc). After 8h, media was replaced with regular primary myoblasts growth media. Cells were lysed in TRizol and gene expression was determined using the Stratagene Mx3000P thermocycler. Fold expression was determined using the ΔΔCt formula. Statistical analysis was performed on 3 independent replicates.

Sectioning and Immunofluorescence analysis

Tibialis anterior (TA) muscles were dissected, embedded into OCT-30% sucrose and directly frozen in liquid nitrogen. Histological and immunofluorescence staining were performed on 15µm and10 µm thick cryosections respectively. Briefly, sections were fixed in 4% PFA (Sigma) for 15 min followed by extensive PBS washes. Sections were incubated with MOM kit (for mouse monoclonal antibodies staining) or in blocking solution (10% horse serum, 0.5% Triton in PBS) overnight. Primary antibodies were diluted in blocking solution as follows: Pax7 (Developmental Study Hybridoma bank, mouse monoclonal, 1:2); Laminin (Sigma, rabbit polyconal 1:1000); GFP (Abcam; chicken polyclonal 1:1000). For GFP staining, muscles were prefixed in 4% PFA overnight and then washed in increasing solutions of sucrose followed by final embedding into OCT-30% sucrose.

RNA sequencing and bioinformatic analysis. RNA was isolated immediately after the sorting using the Arcturus Picopure Rna Isolation Kit (AB Applied Biosystems) according to manufacturer's instructions. RNA–Seq libraries were generated by using the Ovation® RNA-Seq system (Nugen) according to manufacturer's instructions. Sequencing was performed on Solexa GIIx station. mRNAs expression values were calculated using the TopHat/Cuff link software. The Ensembl Suite 6.7 release was used for gene annotations. Gene Ontology (GO) analysis was

performed using the DAVID functional annotation bioinformatics resources (http://david.abcc.ncifcrf.gov/).

Statistical analysis

All quantitative data are expressed as means +/- standard error of the mean (SEM), represented as error bars. Statistical analysis was performed on at least three replicates and significance was determined by Student t-test or by ANOVA. Individual p-values are indicated in each figure.

Acknowledgments

This work was supported by grants to MAR from the Canadian Institute of Health Research (CIHR), the National Institute of Health (NIH) and the Canada Research Chair Program. MAR holds a Canada Research Chair in Molecular genetics. AP is supported by a CIHR-Training Program in Regenerative Medicine (TPRM) fellowship and holds an Excellence Scholarship from the University of Ottawa.

Contributions of authors

AP conducted most experiments. VSD provided Pax7 over expressing cells used in Figure 4. RP provided adeno virus construct used in Figure 7 and S7. HM performed Luciferase and ChIP experiments shown in Figure 4. ML performed cardiotoxin injury and performed statistical analysis shown in Figure 8. CP and TP analyzed RNA-seq data and contributed to Figure1 and S2. AP and MAR analyze data and wrote the manuscript.

References

Alfaro, L.A., Dick, S.A., Siegel, A.L., Anonuevo, A.S., McNagny, K.M., Megeney, L.A., Cornelison, D.D., and Rossi, F.M. (2011). CD34 promotes satellite cell motility and entry into proliferation to facilitate efficient skeletal muscle regeneration.Stem Cells *29*, 2030–2041.

Bentzinger, C.F., Wang, Y,X., Dumont ,N.A., and Rudnicki, M.A.(2013). Cellular dynamics in the muscle satellite cell niche. EMBO Rep. 14, 1062-72.

Bjornson, C.R., Cheung, T.H., Liu, L., Tripathi, P.V., Steeper, K.M.,and Rando, T.A.(2012) Notch signaling is necessary to maintain quiescence in adult muscle stem cells. Stem Cells. *30,* 232-42.

Brack, A.S., Conboy, I.M., Conboy, M.J., Shen, J., and Rando, T.A. (2008). A temporal switch from Notch to Wnt signaling in muscle stem cells is necessary for normal adult myogenesis. Cell Stem Cell *2*, 50-9.

Bray, S. and Furriols, M. (2001). Notch pathway: making sense of suppressor of hairless. Curr. Biol. *11*, 217-221.

Bray, S.J., Takada, S., Harrison, E., Shen, S.C., and Ferguson-Smith, A.C.(2008). The atypical mammalian ligand Delta-like homologue 1 (Dlk1) can regulate Notch signalling in Drosophila. BMC Dev Biol. *8*, 8-11.

Bröhl, D., Vasyutina, E., Czajkowski, M.T., Griger, J., Rassek ,C., Rahn, H.P., Purfürst, B., Wende, H., and Birchmeier, C.(2012). Colonization of the satellite cell niche by skeletal muscle progenitor cells depends on Notch signals. Dev Cell. *23*, 469-81.

Buas,M.F., Kabak, S.,and Kadesch, T. (2010). The Notch effector Hey1 associates with myogenic target genes to repress myogenesis.J Biol Chem.*285*, 1249-58.

Buas,M.F., Kabak, S., and Kadesch, T.(2009). Inhibition of myogenesis by Notch: evidence for multiple pathways. J Cell Physiol. *218*, 84-93.

Buckingham, M. (2001). Skeletal muscle formation in vertebrates. Curr Opin Genet Dev *11*, 440-8

Chang, N.C., and Rudnicki, M.A. (2014). Satellite cells: the architects of skeletal muscle. Curr Top Dev Biol. *107*, 161-81. Nature.*490*, 355-60.
Chazaud, B., Sonnet, C., Lafuste, P., Bassez, G., Rimaniol, A.C., Poron, F., Authier, F.J., Dreyfus, P.A., and Gherardi, R.K. (2003). Satellite cells attract monocytes and use macrophages as a support to escape apoptosis and enhance muscle growth.J Cell Biol. *163*, 1133-43.

Cheung, T.H and Rando, T.A. (2013). Molecular regulation of stem cell quiescence. Nat Rev Mol Cell Biol. *14*, 329-40.

Conboy, I.M., and Rando, T.A. (2002). The regulation of Notch signaling controls satellite cell activation and cell fate determination in postnatal myogenesis. Dev. Cell *3*, 397-409

Conboy, I.M., Conboy, M.J., Wagers, A.J., Girma, E.R., Weissman, I.L., and Rando, T.A.(2005). Rejuvenation of aged progenitor cells by exposure to a young systemic environment. Nature. *433*, 760-4.

Cornelison, D.D., Filla, M.S., Stanley, H.M., Rapraeger, A.C., and Olwin, B.B. (2001) Syndecan-3 and syndecan-4 specifically mark skeletal muscle satellite cells and are implicated in satellite cell maintenance and muscle regeneration. Dev. Biol. *239*, 79–94.

Fukada, S., Uezumi, A., Ikemoto, M., Masuda, S., Segawa, M., Tanimura, N., Yamamoto, H., Miyagoe-Suzuki, Y., and Takeda, S. (2007). Molecular signature of quiescent satellite cells in adult skeletal muscle. Stem Cells *25*, 2448-2459

Günther, S., Kim, J., Kostin, S., Lepper, C., Fan, C.M.,and Braun, T. (2013). Myf5-positive satellite cells contribute to Pax7-dependent long-term maintenance of adult muscle stem cells. Cell Stem Cell. *13*, 590-601.

Kassar-Duchossoy, L., Giacone, E., Gayraud-Morel, B., Jory, A., Gomes, D., and Tajbakhsh, S. (2005). Pax3/Pax7 mark a novel population of primitive myogenic cells during development. Genes Dev 19, 1426-1431.

Kopan, R., and Ilagan, M.X.(2009). The canonical Notch signaling pathway: unfolding the activation mechanism. Cell. *137*, 216-33.

Kuang, S., Kuroda, K., Le Grand, F., and Rudnicki, M.A. (2007). Asymmetric self-renewal and commitment of satellite stem cells in muscle. Cell 129, 999-1010.

Kuroda, K., Tani, S., Tamura, K., Minoguchi, S., Kurooka, H., and Honjo, T.(1999). Delta-induced Notch signaling mediated by RBP-J inhibits MyoD expression and myogenesis.J Biol Chem. *274*, 7238-44.

Lepper, C., Conway, S.J., and Fan, C.M. (2009). Adult satellite cells and embryonic muscle progenitors have distinct genetic requirements. Nature 460, 627-631.

Lepper, C., Fan, C.M. (2010). Inducible lineage tracing of Pax7-descendant cells reveals embryonic origin of adult satellite cells. Genesis. *7*, 424-36.

Mourikis, P., Gopalakrishnan, S., Sambasivan, R., and Tajbakhsh, S.(2012). Cell-autonomous Notch activity maintains the temporal specification potential of skeletal muscle stem cells. Development. *139*, 4536-48.

Murtaugh, L.C., Stanger, B.Z., Kwan, K.M., and Melton, D.A. (2003). Notch signaling controls multiple steps of pancreatic differentiation. Proc Natl Acad Sci *100,* 14920-5.

Pasut, A., Oleynik, P., and Rudnicki, M.A.(2012). Isolation of muscle stem cells by fluorescence activated cell sorting cytometry. Methods Mol Biol. *798*, 53-64.

Pasut, A., Jones, A.E., and Rudnicki, M.A.(2013). Isolation and culture of individual myofibers and their satellite cells from adult skeletal muscle. J Vis Exp. *73*, e50074.

Pisconti, A., Cornelison, D.D., Olguín, H.C., Antwine, T.L., and Olwin B.B.(2010). Syndecan-3 and Notch cooperate in regulating adult myogenesis. J Cell Biol. *190*, 427-41.

Relaix, F., Rocancourt, D., Mansouri, A., and Buckingham, M. (2005). A Pax3/Pax7-dependent population of skeletal muscle progenitor cells. Nature *435*, 948-953.

Seale, P., Sabourin, L.A., Girgis-Gabardo, A., Mansouri, A., Gruss, P., and Rudnicki, M.A.(2000). Pax7 is required for the specification of myogenic satellite cells. Cell *102*,
777-786.

Seale, P., Bjork, B., Yang, W., Kajimura, S., Chin, S., Kuang, S., Scimè, A., Devarakonda, S., Conroe, H.M., Erdjument-Bromage, H., Tempst, P., Rudnicki, M.A., Beier, D.R.,and Spiegelman, B.M. (2008). PRDM16 controls a brown fat/skeletal muscle switch. Nature. *454*, 7961-7.

Sugimura, R., He, X.C., Venkatraman, A., Arai, F., Box, A., Semerad, C., Haug, J.S., Peng, L., Zhong, X.B., Suda, T, and Li, L.(2012). Noncanonical Wnt signaling maintains hematopoietic stem cells in the niche. Cell. 2012 Jul 20;150(2):351-65. doi: 10.1016/j.cell.2012.05.041.

Sweetman, D., Goljanek, K., Rathjen, T., Oustanina, S., Braun, T., Dalmay, T., and Münsterberg, A. (2008). Specific requirements of MRFs for the expression of muscle specific microRNAs, miR-1, miR-206 and miR-133. Dev Biol. *321*, 491-9.

Vasyutina, E., Lenhard, D.C., Wende, H., Erdmann, B., Epstein, J.A., and Birchmeier C.(2007). RBP-J (Rbpsuh) is essential to maintain muscle progenitor cells and to generate satellite cells. Proc Natl Acad Sci *104*, 4443-8.

von Maltzahn, J., Jones, A.E., Parks, R.J., and Rudnicki, M.A.(2013). Pax7 is critical for the normal function of satellite cells in adult skeletal muscle. Proc Natl Acad Sci. *110*, 16474-9.

Wen, Y., Bi, P., Liu, W., Asakura, A., Keller, C., and Kuang, S. (2012). Constitutive Notch activation upregulates Pax7 and promotes the self-renewal of skeletal muscle satellite cells. Mol Cell Biol. *32*, 2300-11.

Yin, H., Price, F., and Rudnicki, M.A. (2013). Satellite Cells and the Muscle Stem Cell Niche. Physiol Rev *93*, 23-67.

Yin, H., Pasut, A., Soleimani, V.D., Bentzinger, C.F., Antoun, G., Thorn, S., Seale, P., Fernando, P, van Ijcken, W., Grosveld, F., Dekemp, R.A., Boushel, R., Harper, M.E., and Rudnicki, M.A.(2013). MicroRNA-133 controls brown adipose determination in skeletal muscle satellite cells by targeting Prdm16. Cell Metab. *17*, 210-24.

Yusuf, R.Z., and Scadden, D.T.(2012). Fate through fat: lipid metabolism determines stem cell division outcome. Cell Metab. 16, 411-3.

Figures

Figure 1

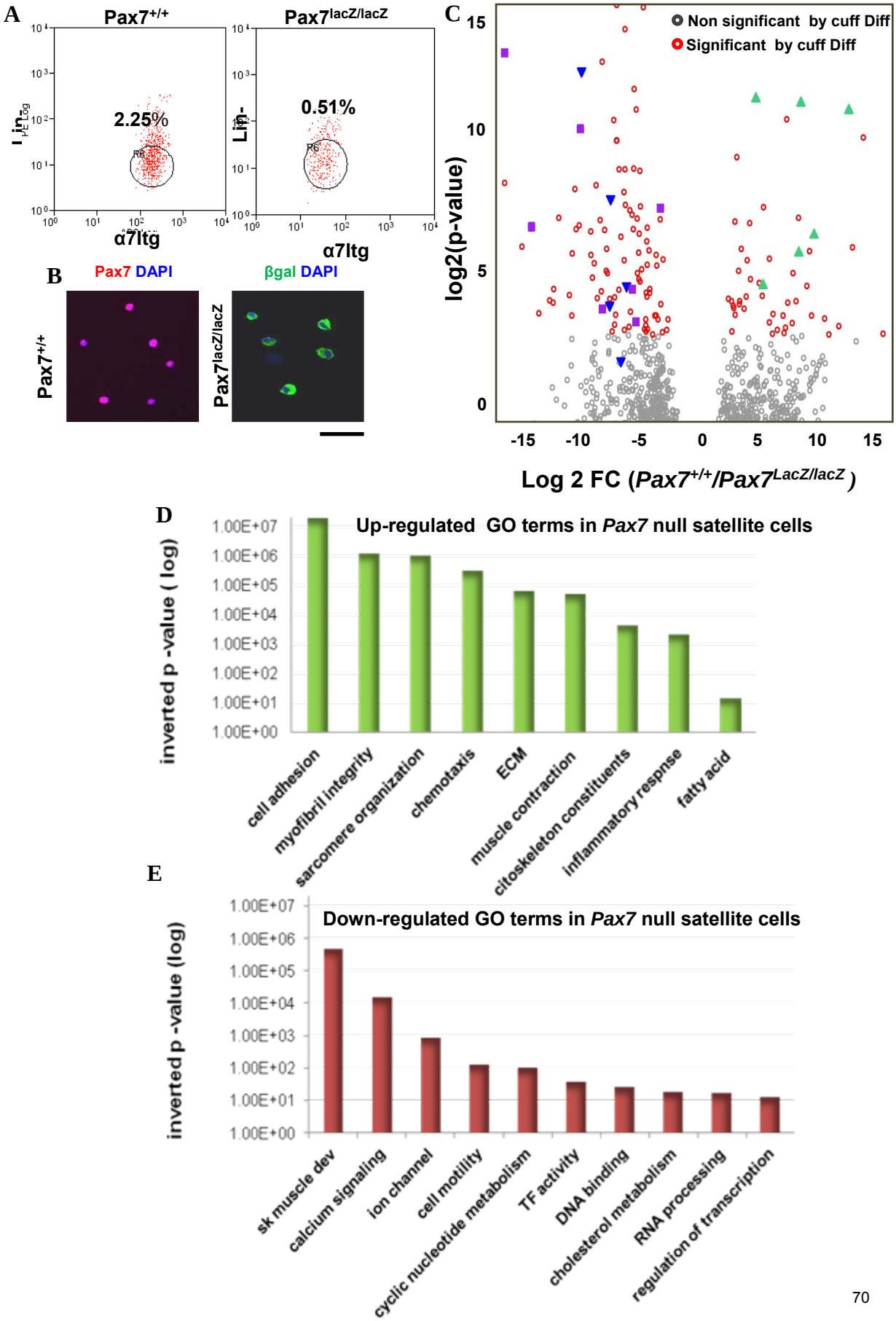
A
Pax7+/+
Pax7lacZ/lacZ
2.25%
0.51%
Lin-
α7Itg
B
Pax7 DAPI
βgal DAPI
Pax7+/+
Pax7lacZ/lacZ
C
Non significant by cuff Diff
Significant by cuff Diff
log2(p-value)
Log 2 FC (Pax7+/+/Pax7LacZ/lacZ)
D
Up-regulated GO terms in Pax7 null satellite cells
inverted p -value (log)
cell adhesion
myofibril integrity
sarcomere organization
chemotaxis
ECM
muscle contraction
citoskeleton constituents
inflammatory respnse
fatty acid
E
Down-regulated GO terms in Pax7 null satellite cells
inverted p -value (log)
sk muscle dev
calcium signaling
ion channel
cell motility
cyclic nucleotide metabolism
TF activity
DNA binding
cholesterol metabolism
RNA processing
regulation of transcription

Figure 1. RNA-sequencing analysis of *Pax7 LacZ/LacZ* satellite cells. A. FACS plots of *Pax7* +/+ and *Pax7 LacZ/LacZ* (*Pax7* null) satellite cells isolated from whole hind limb muscles of 4 week old mice. Gates and percentage of cells within each gate are shown. Satellite cells were identified as Lineage (Lin-) negative and α7Integrin (α7Itg) positive cells. Lineage markers include: CD45, CD11b, Sca-1, and CD31. Hoechst was used to identify live cells. **B.** Immunofluorescence staining of freshly sorted satellite cells citospunned after the sort and stained with Pax7 (red) or βeta-galactosidase (β-gal) (Green). Nuclei were counterstained with DAPI. Bar=50μm**.C**. The volcano plot shows gene expression values calculated as log2 fold change (FC) in the x-axis and correspondent p-value in y-axis in logarithmic scale. Negative FC values identify down- regulated genes in *Pax7* null satellite cells. Conversely positive FC values identify up-regulated genes in *Pax7* null satellite cells. Red dots represent top 2% significant genes (total of 722 genes) as estimated by CuffDiff. Blue triangles identify satellite and stem cell specific markers. Green squares represents fiber specific and muscle differentiation genes. **D-E**. Bar graphs show enriched Gene Ontology (GO) functions over-represented (D) and under-represented (E) in *Pax7* null satellite cells according to DAVID analysis.

Figure 2

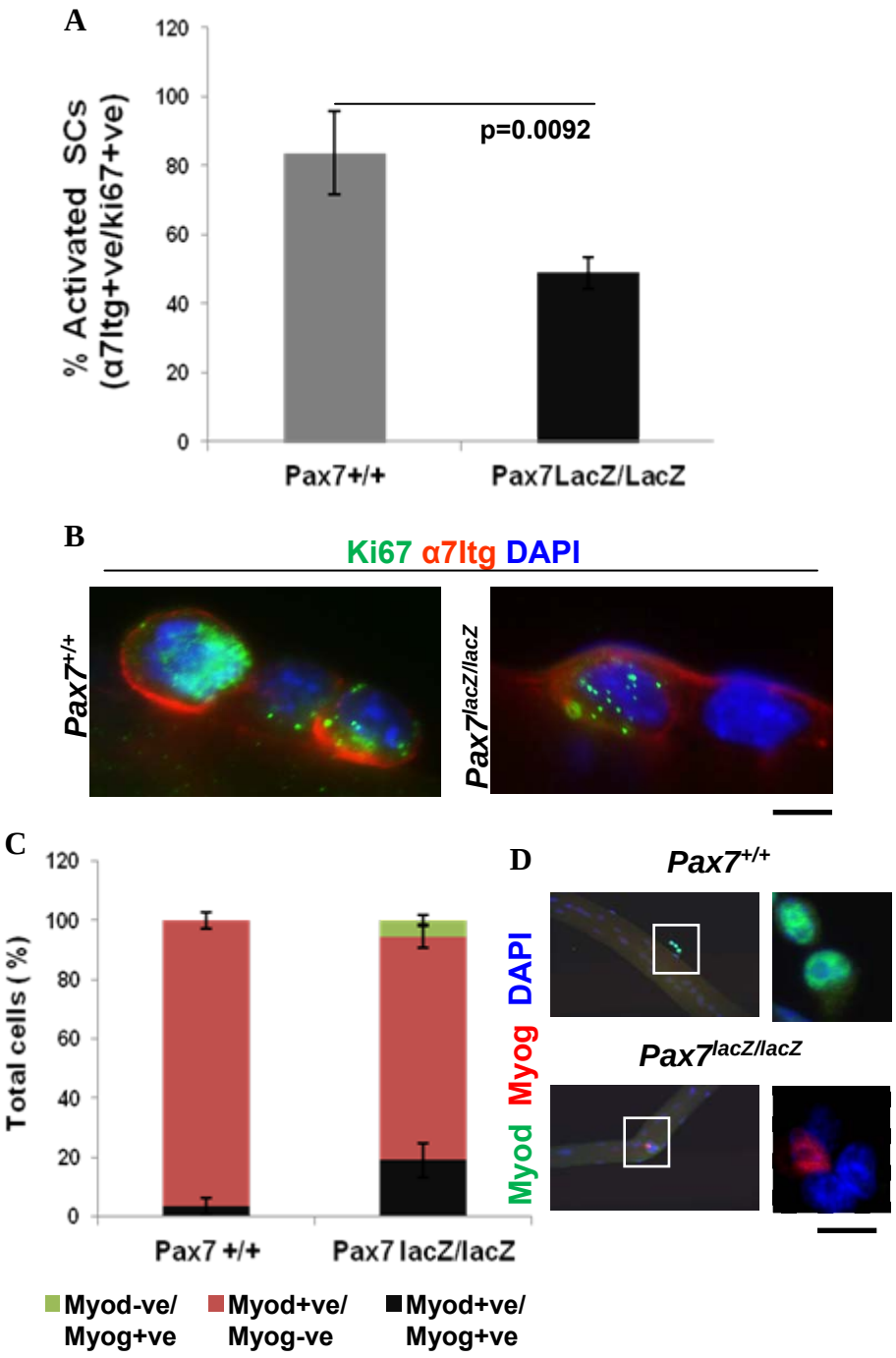
A
% Activated SCs (α7Itg+ve/ki67+ve)
120
100
80
60
40
20
0
p=0.0092
Pax7+/+
Pax7LacZ/LacZ
B
Ki67 α7Itg DAPI
Pax7+/+
Pax7lacZ/lacZ
C
Total cells (%)
120
100
80
60
40
20
0
Pax7 +/+
Pax7 lacZ/lacZ
Myod-ve/ Myog+ve
Myod+ve/ Myog-ve
Myod+ve/ Myog+ve
D
Pax7+/+
Pax7lacZ/lacZ
Myod Myog DAPI

Figure 2. Loss of *Pax7* results in impaired proliferation due to precocious differentiation. A. Single EDL fibers were isolated from 4 week old *Pax7* wild type (*Pax7 +/+)* and *Pax7* null (*Pax7 LacZ/LacZ*) mice and cultured for 48 hours in high serum medium. Satellite cells on fibers were stained for α7Integrin (α7Itg) and ki67. Graph shows the percentage (%) of activated satellite cells expressed as α7Itg;ki67 double positive cells. Error bars represent SEM. t-test was performed on 3 independent experiments. p-values are shown. **B**. Immunofluorescence staining of satellite cells on single fibers fixed after 48 hours in culture. α7Integrin is shown in red, ki67 is shown in green. Nuclei were counterstained with DAPI (blue). Bar= 50µm. **C**. Graph shows the percentage (%) of MyoD positive, Myogenin (Myog) positive and MyoD/Myog double positive cells over total number of satellite cells. Error bars represent SEM. **D**. Immunofluorescence staining of MyoD and Myogenin positive cells on fibers. MyoD is shown in green, Myogenin is shown in red. Nuclei were counterstained with DAPI (blue). Bar= 100µm.

Figure 3

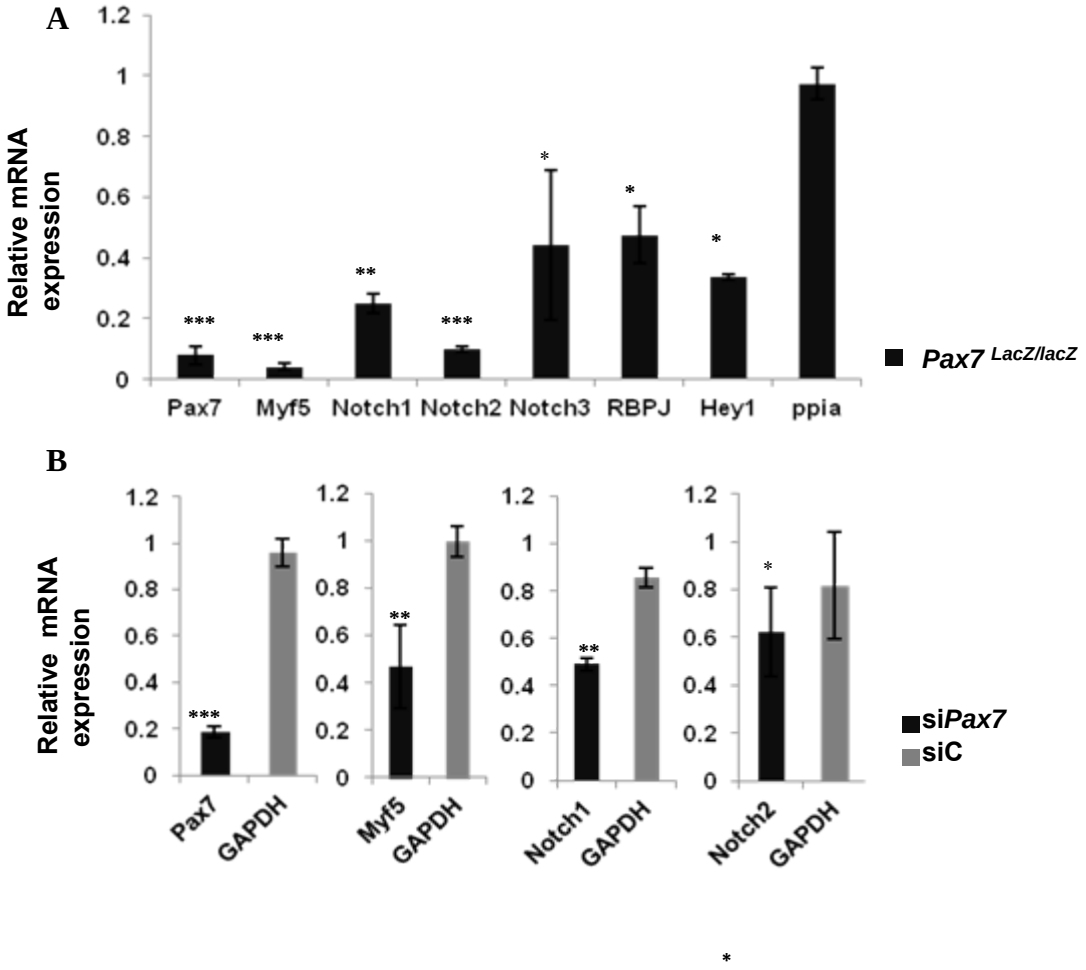

Figure 3. Notch signaling is impaired in *Pax7* null satellite cells. A. qRT-PCR analysis of Notch genes in *Pax7* LacZ/lacZ relative to *Pax7* +/+ freshly sorted satellite cells. *Ppia* was used as control for gene normalization. N= 3 independent sorts. Error bars represent SEM. t-test was used for significance. *p<0.5; **p<0.05;***p<0.005. **C**. Cultured primary myoblasts were transfected with a cocktail of siRNAs against *Pax7* (si*Pax7*).Cells transfected with a negative siRNA construct were used as control (siC). RNA was extracted 48 hours after. Graph shows qRT-PCR of *Pax7*, *Myf5*, *Notch1* and *Notch2* relative to *Gapdh*. N=3 independent replicates. Error bars represent SEM. t-test was used for significance. *p<0.5; **p<0.05;***p<0.001.

Figure 4

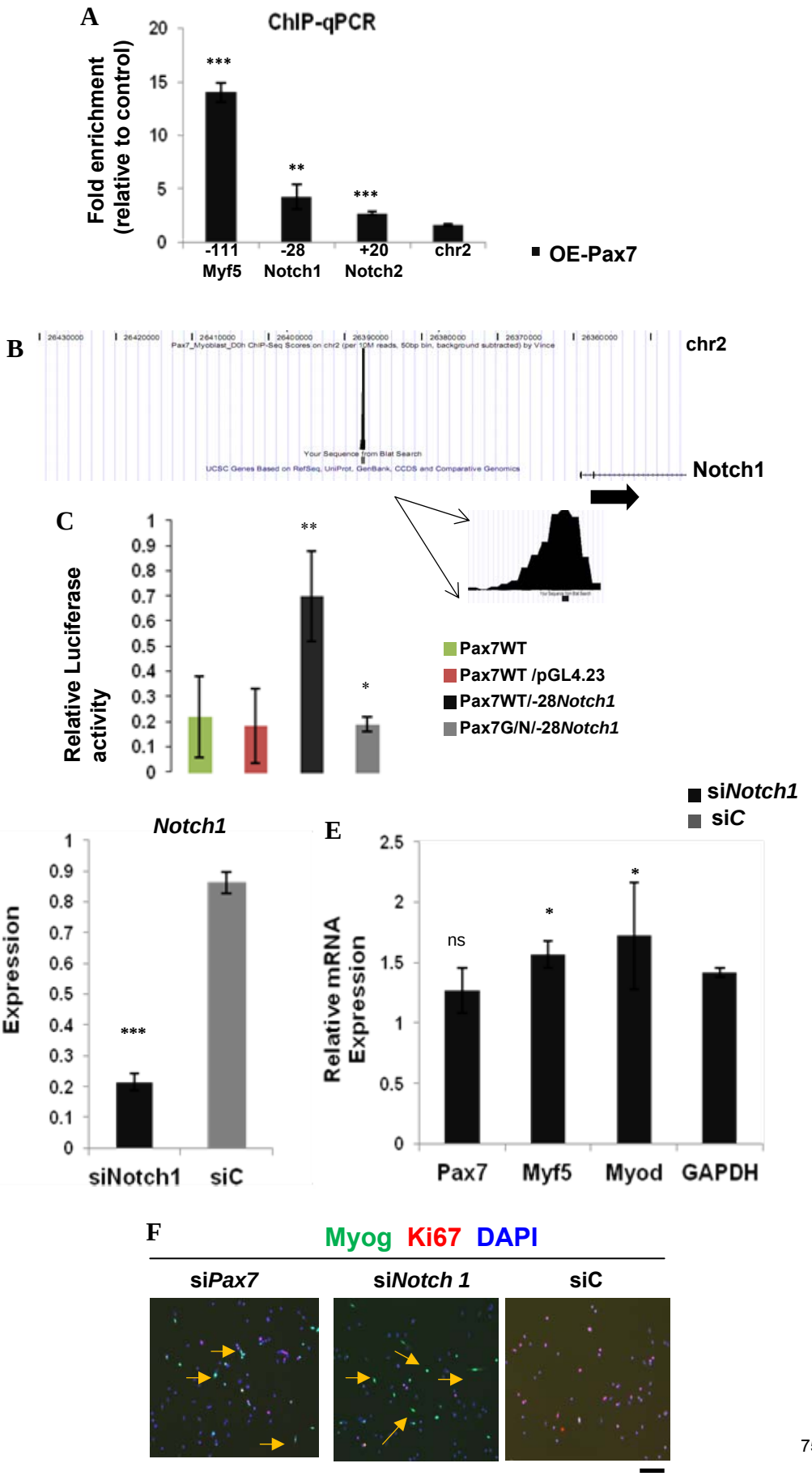
A
ChIP-qPCR
Fold enrichment (relative to control)
20
15
10
5
0
***
**
***
-111 Myf5
-28 Notch1
+20 Notch2
chr2
OE-Pax7
B
chr2
Notch1
C
Relative Luciferase activity
1
0.9
0.8
0.7
0.6
0.5
0.4
0.3
0.2
0.1
0
**
*
Pax7WT
Pax7WT /pGL4.23
Pax7WT/-28Notch1
Pax7G/N/-28Notch1
siNotch1
siC
D
Notch1
Relaive mRNA Expression
***
siNotch1
siC
E
Relative mRNA Expression
2.5
2
1.5
1
0.5
0
ns
*
*
Pax7
Myf5
Myod
GAPDH
F
Myog Ki67 DAPI
siPax7
siNotch 1
siC

Figure 4. *Notch 1* is a Pax7 target gene. A. Primary myoblasts stably over expressing Pax7-FLAG construct (OE-Pax7) and empty vector-FLAG primary myoblasts (EV) were used to perform Pax7 Chromatin Immunprecipitation (ChIP) followed by q-RT-PCR. Graph shows Pax7 enrichment for the following sites: -111kb *Myf*5, -28kb *Notch1* and +20kb*Notch 2* respectively. Fold change was normalized to a genomic region on chromosome 2 with no Pax7 binding. The *Myf*5-111kb element was used as positive control. N=3. Error bars represent SEM. t-test was used for significance. *p<0.5; **p<0.05; ***p<0.005. **B**. Track shows the location of the -28kb *Notch1* element on chromosome 2 and relative distance from *Notch1* transcriptional start site. Black arrow indicates direction of transcription. Enlargement shows the position of the Pax7 paired (GTCACGGT) and homeobox (TAATTGATTA) domains relative to the center of the peak. **C**. Luciferase assay was performed on 293T cells transfected with the -28kb*Notch1* cloned into the pGL4.23 luciferase vector. The Pax7 wild type minimal transactivator domain (Pax7WT) and the Pax7 mutant DNA binding domain (Pax7G/N) constructs were cloned within the pCDNA3 vector and co-transfected with the -28kb*Notch1* reporter vector or pGL4.23 alone. Luciferase activity was normalized to Renilla activity. N=3 replicates. **D-E**. qRT-PCR of cultured primary myoblasts transfected with a cocktail of siRNAs against *Notch1* (si*Notch1*) or negative control (siC). Gene expression was normalized to GAPDH. N=3 independent replicates. Error bars represent SEM. The Student t-test was used for significance. *p<0.5; **p<0.05; ***p<0.005. **F**. Primary myoblasts transfected with si*Notch1*, si*Pax7* or negative control (siC), were fixed after 48 hours and stained for Myogenin (green) and ki67 (red). Nuclei were counterstained with DAPI (blue).Bar=100µm.

Figure 5

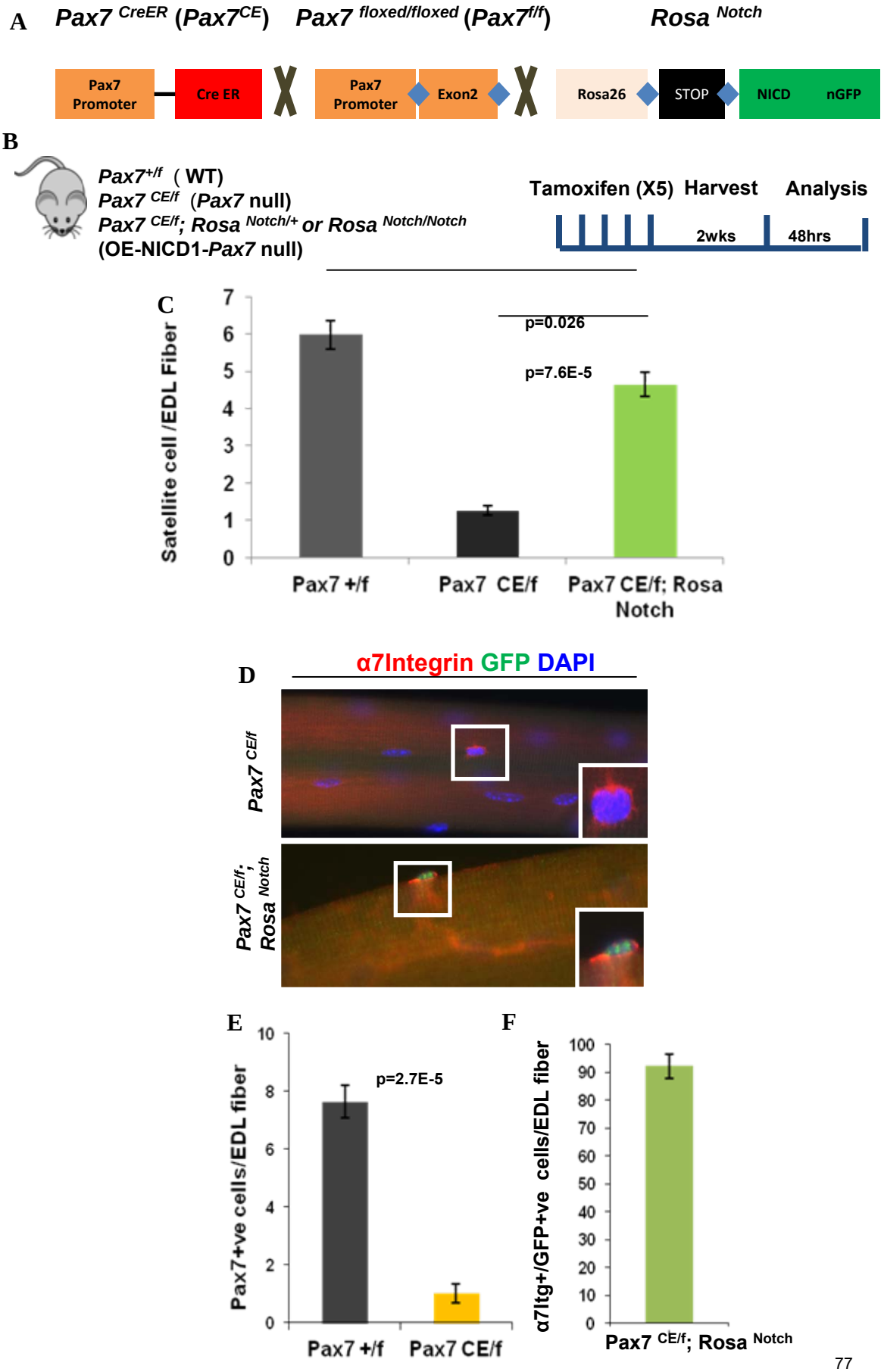
A
Pax7 CreER (Pax7CE)
Pax7 floxed/floxed (Pax7f/f)
Rosa Notch
Pax7 Promoter
Cre ER
Pax7 Promoter
Exon2
Rosa26
STOP
NICD
nGFP
B
Pax7+/f (WT)
Pax7 CE/f (Pax7 null)
Pax7 CE/f; Rosa Notch/+ or Rosa Notch/Notch
(OE-NICD1-Pax7 null)
Tamoxifen (X5)
Harvest
Analysis
2wks
48hrs
C
Satellite cell /EDL Fiber
p=0.026
p=7.6E-5
Pax7 +/f
Pax7 CE/f
Pax7 CE/f; Rosa Notch
D
α7Integrin GFP DAPI
Pax7 CE/f
Pax7 CE/f; Rosa Notch
E
Pax7+ve cells/EDL fiber
p=2.7E-5
Pax7 +/f
Pax7 CE/f
F
α7Itg+/GFP+ve cells/EDL fiber
Pax7 CE/f; Rosa Notch

Figure 5. Notch gain of function rescues *Pax7* null satellite cells. A. Schematic overview of the mouse strains used in this study**.** In the *Pax7 CreER* (*Pax7CE*) mouse strain Cre recombinase is driven from the *Pax7* locus. In the *Pax7 floxed/floxed* (*Pax7f/f*) mouse strain exon 2 of *Pax7* is flanked by two *loxP* sites which upon Cre recombination give rise to a non functional *Pax7* allele. In the *Rosa Notch* mouse strain the expression of the intracellular domain of *Notch1* (NICD1) from the constitutively active *Rosa* locus is blocked by a STOP codon flanked by two *loxP* sites. Cre recombinase activity drives NICD1 constitutive expression. **B**. Schematic of the genotypes used in this study. *Pax7 +/f* (WT), *Pax7 CE/f* (Pax7 null) and *Pax7 CE/f*; *Rosa Notch* (OE-NICD1 *Pax7* null) mice were given 5 consecutive injections of tamoxifen 24 hours apart. Mice were sacrificed 2 weeks after the first injection for subsequent analysis. **C**. Number of satellite cells (α7Integrin positive cells) per EDL fiber at time 0 from 8 week old mice. Error bars represent SEM. N=4. The student t-test was used to determined significance. Individual p-values are shown. **D**. Immunofluorescence staining of satellite cells stained for α7Integrin (red) and GFP (green). Nuclei were counterstained with DAPI (blue) Bar=100µm.**E**. Number of Pax7 positive cells at time 0 per EDL fibers from 8 week old mice. Bars represent SEM. N=4. Student t-test was used to determine significance. p-values are shown**. F**. Number of GFP and α7Integrin double positive satellite cells at time 0. Bar represent SEM.N=4.

Figure 6

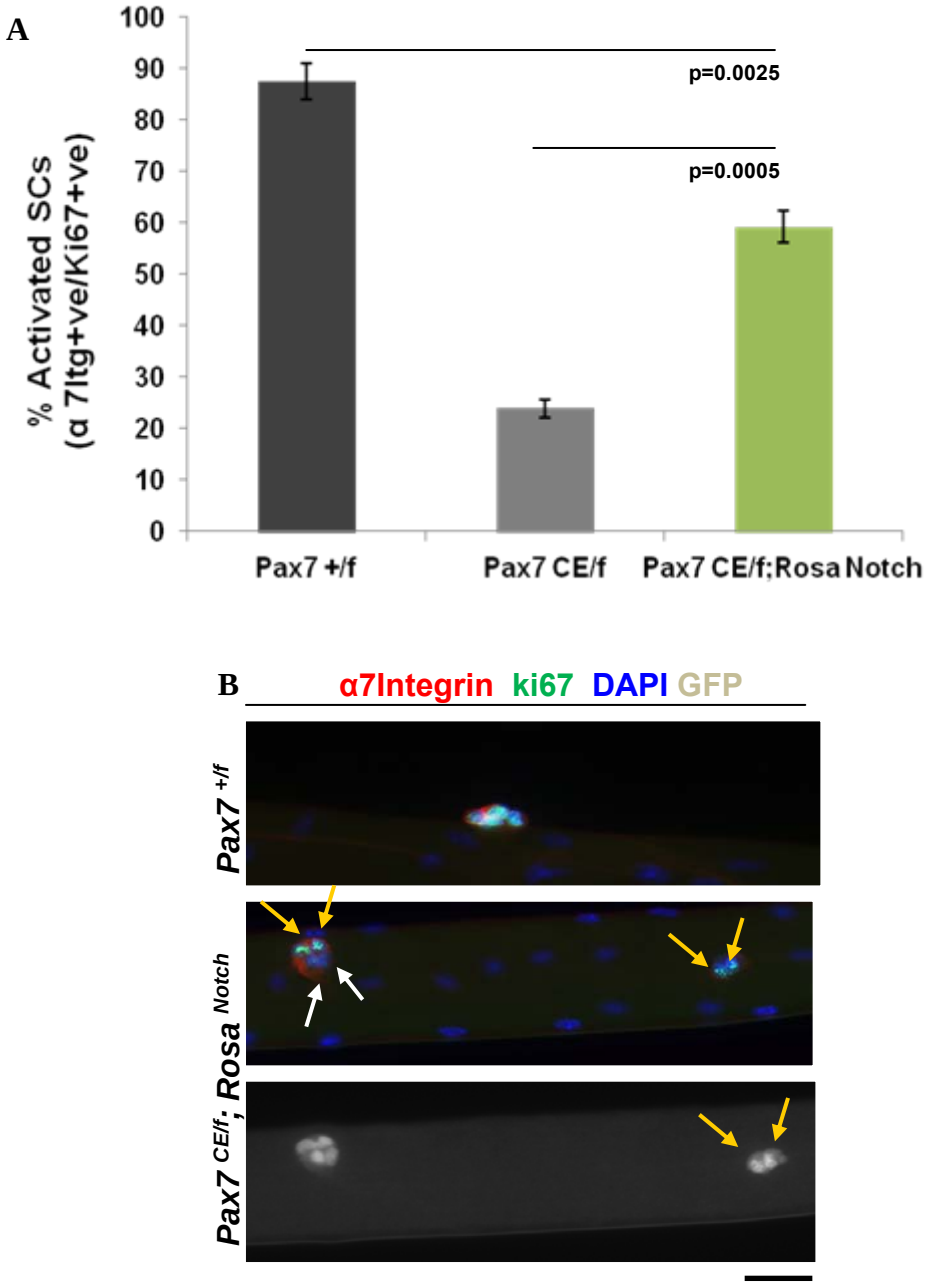

Figure 6. Notch gain of function rescues *Pax7* null satellite cells proliferation. A. EDL fibers were cultured on horse serum coated dishes for 48 hours to allow satellite cell activation. The number of activated satellite cells (α7Integrin/ki67 double positive cells) was scored after 48 hours in culture. Error bars represent SEM. N=4. Student t-test was used to determine significance. P-values are shown. **B**. EDL fibers were fixed in PFA and stained for α7Integrin (red), ki67 (green) and GFP (grey). Nuclei were counterstained with DAPI (blue). Yellow arrows point to GFP positive, ki67 positive cells. White arrows point to GFP positive, ki67 negative cells. Bar=100µm.

Figure 7

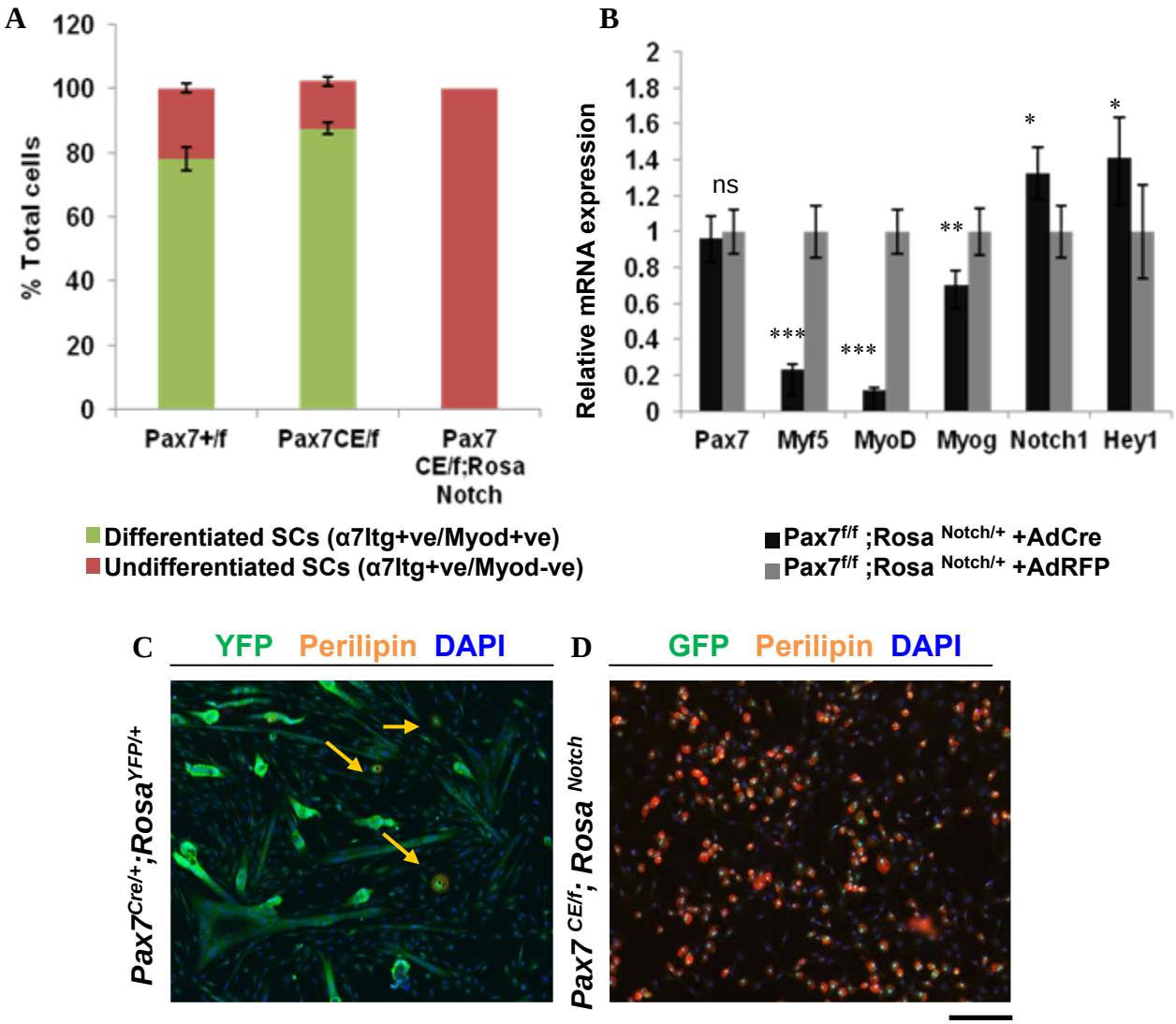

Figure 7. Notch gain of function inhibits *Pax7* null differentiation. A. Graph shows the number (%) of α7Integrin positive, MyoD positive (differentiated) and α7Integrin positive, Myod negative (undifferentiated) satellite cells at 48 hrs in culture. Error bars represent SEM. N=4. **B**. qRT-PCR of *Pax7*, *Myf5*, *MyoD*, *Myogenin* (*Myog*), *Notch1* and *Hey1* from *Pax7* f/f; *Rosa Notch/+*primary myoblasts infected with an adenovirus expressing Cre recombinase (AdCre) or a control virus expressing the Red Fluorescent Protein RFP (AdRFP). Cell lysates were collected after 48 hours. Gene expression was normalized to GAPDH.N=3 replicates. Error bars represent SEM. Student t-test was used to determine significance. *p<0.5; **p<0.05; ***p<0.001.**C-D**. Immunofluorescence staining of satellite cells derived adipocytes isolated from 8 week old *Pax7 CreER; Rosa YFP/YFP* or *Pax7 f/CE Rosa Notch/Notch* mice and cultured on matrigel coated slides under adipogenic condition. GFP is shown in green. Perilipin is shown in red. Nuclei were counterstained with DAPI (blue).Bar=200µm.

Figure 8

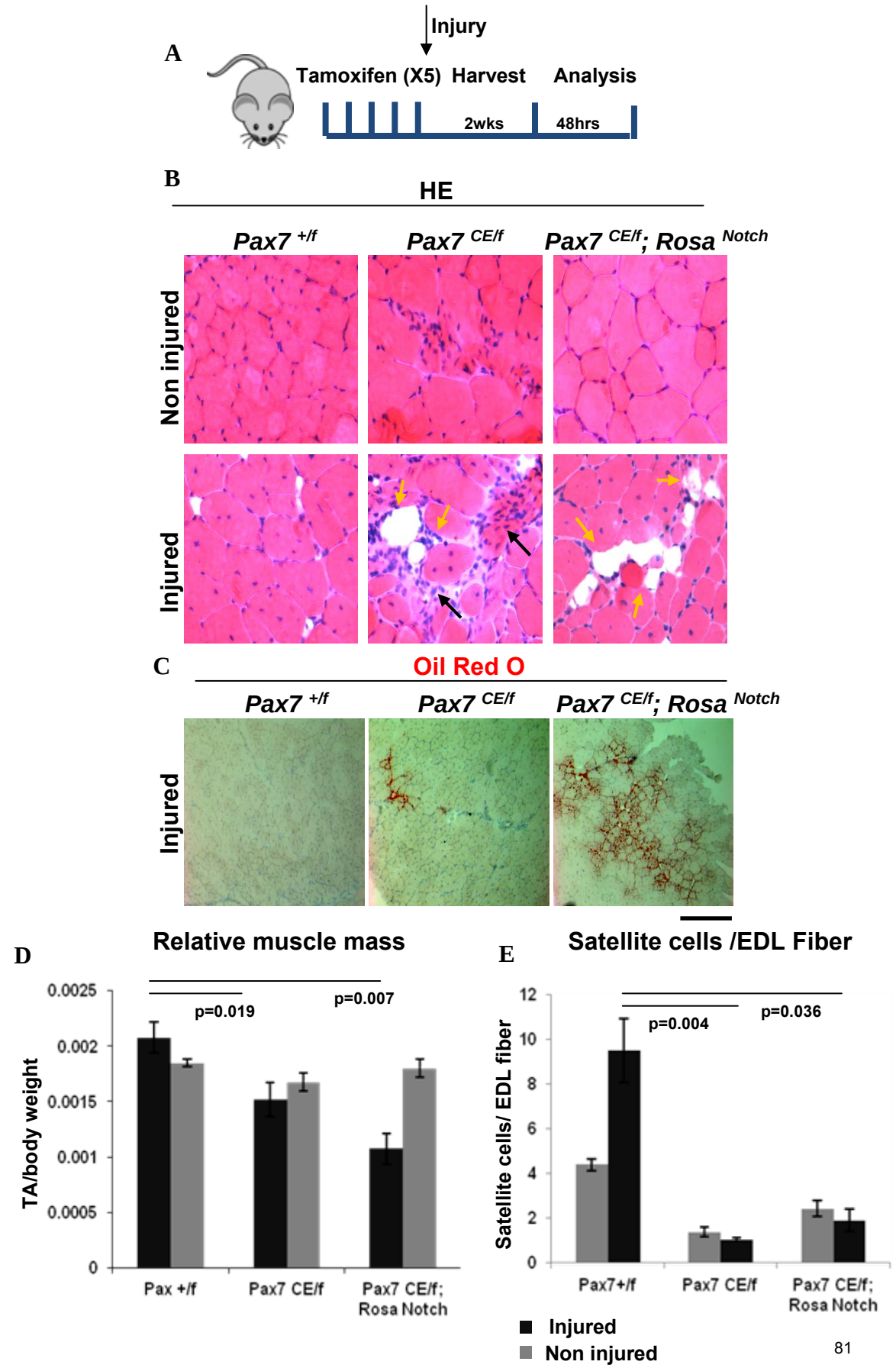
A
Injury
Tamoxifen (X5)
Harvest
Analysis
2wks
48hrs
B
HE
Pax7 +/f
Pax7 CE/f
Pax7 CE/f; Rosa Notch
Non injured
Injured
C
Oil Red O
Pax7 +/f
Pax7 CE/f
Pax7 CE/f; Rosa Notch
Injured
D
Relative muscle mass
TA/body weight
0.0025
0.002
0.0015
0.001
0.0005
0
p=0.019
p=0.007
Pax +/f
Pax7 CE/f
Pax7 CE/f; Rosa Notch
E
Satellite cells /EDL Fiber
Satellite cells/ EDL fiber
12
10
8
6
4
2
0
p=0.004
p=0.036
Pax7+/f
Pax7 CE/f
Pax7 CE/f; Rosa Notch
Injured
Non injured

Figure 8. Over expression of Notch signaling induces satellite cells adipogenesis in vivo. A. Schematic overview of the regeneration experiment**.** Mice were injected with tamoxifen for 5 consecutive days and cardiotoxin was administered intramuscularly on the fifth day. Muscles were harvested 2 weeks later for analysis. **B.** Representative Hematoxilin and Eosin (HE) staining of non- injured (upper panel) and injured (lower panel) Tibialis Anterior (TA) muscles. Yellow arrows point to fat depots. Black arrows point to fibrotic tissue **C**. Histological images of TA sections stained with Oil Red O solution. Lipid droplets are stained in red, nuclei in dark blue, cytoplasm stained white to pale yellow. Bar=100μm **D.** Graph shows TA muscle mass normalized by total body weight of injured (black bars) and non injured (grey bars) muscles respectively. N=3 each genotype**.** Errors bars represent SEM. ANOVA was used to calculate significance. p-values are shown. **E**. Number of satellite cells (α7 Integrin positive cells) per EDL fiber from wild type, *Pax7* null and OE-NICD1 *Pax7* null injured (black bars) and non-injured (grey bars) EDL. Error bars represent SEM. N=3. The student t-test was used to calculate significance. p-values are shown.

Figure 9

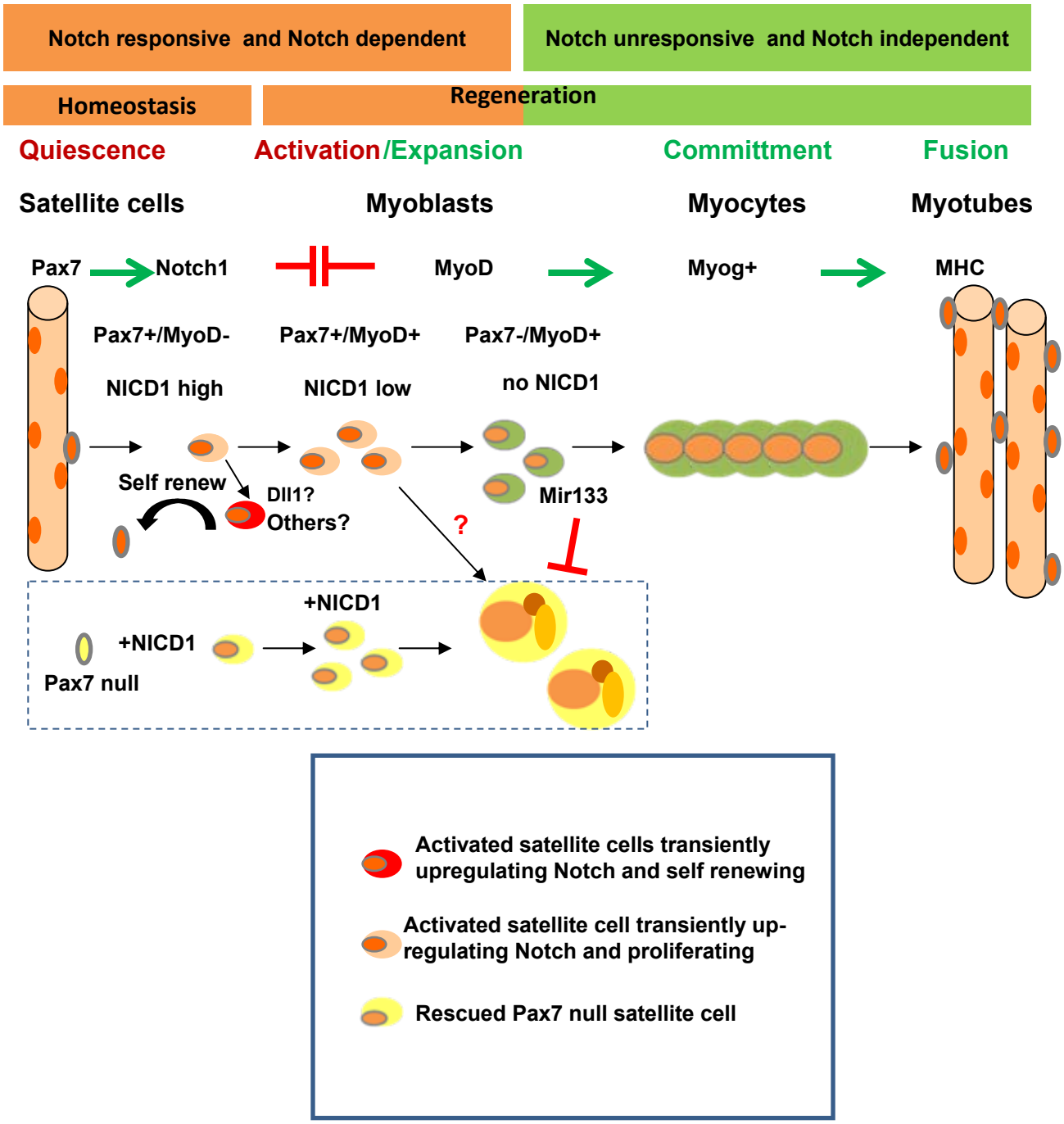

Figure 9. Requirement of Notch signalling in adult myogenesis. Schematic model of the Notch requirement in adult myogenesis. In quiescent satellite cells Pax7 maintais Notch expression which is required to prevent loss of satellite cells. During the early phase of muscle regeneration, NICD1 promotes satellite cell expansion and self-renewal where it inhibits MyoD up-regulation. In a Pax7 null background constitutive over expression of Notch results in enhanced brown adipogenesis.

Supplementary Figures

S1

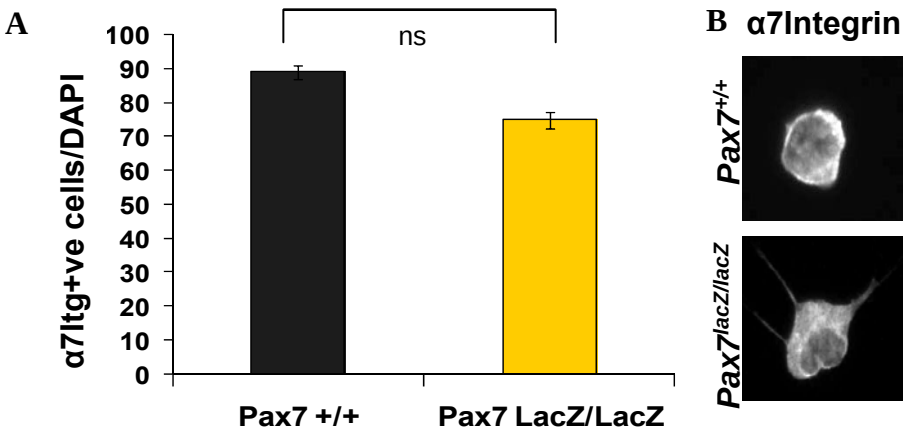

Figure S1. FACS quality control. A. Quantification of the number of α7 Integrin (α7Itg) positive cells from freshly sorted *Pax7 +/+* and *Pax7 LacZ/LacZ* samples. DAPI was used to identify nuclei. N=3 independent sort. Errors bars represent SEM. Student t-test was used to calculate significance. p-value>0.5.**B**. Immunofluorescence staining of citospunned α7 Integrin positive satellite cells isolated by FACS from *Pax7 +/+* and *Pax7 LacZ/LacZ* mice .

S2

A

Sample	Total Reads	Mapped reads	%Unique reads
Pax7 $^{+/+}$	30,035,687	28, 065, 118	70.53
Pax7 $^{-/-}$	35, 303, 208	32, 476, 561	57.57

B

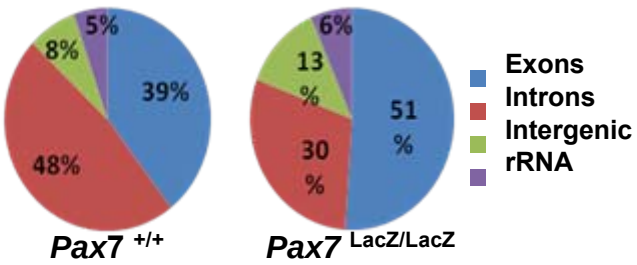

C

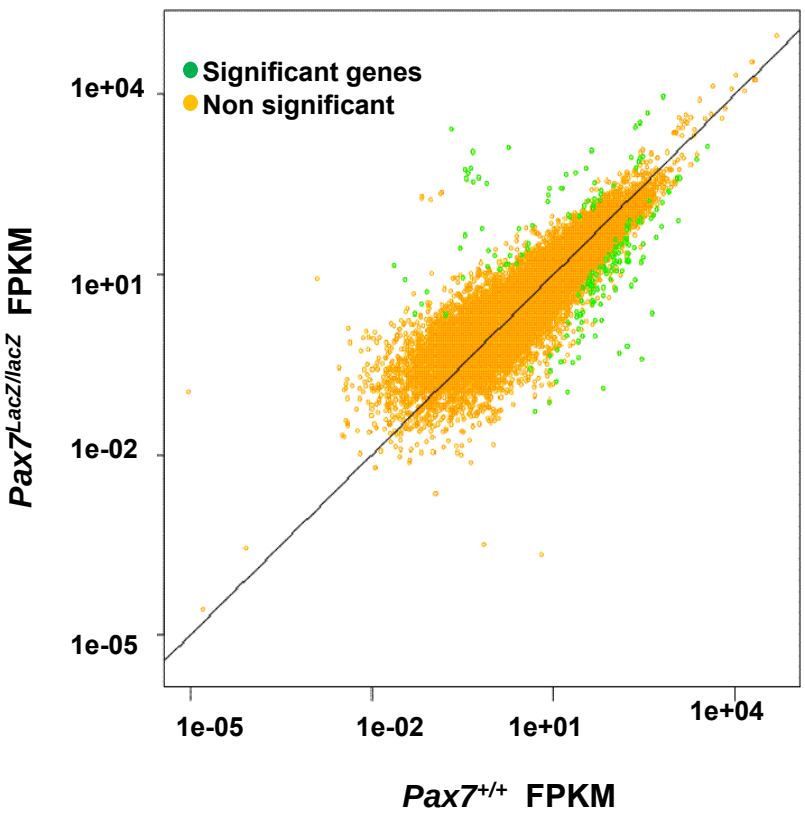

Figure S2. RNA-seq quality control. A. Table shows the number of total, unque and mapped reads for *Pax7* +/+ and *Pax7* LacZ/LacZ samples. **B**. Distribution of reads across the genome.**C**. Graph shows gene expression calculated as FPKM (**F**ragments **P**er **K**ilobase of exon per **M**illion fragments mapped). x-axis identifies *Pax7* +/+ gene values, y-axis identifies *Pax7* LacZ/LacZ gene values. Yellows dots represent non significant genes. Green dots represent differentially expressed genes as estimated by the CuffDiff.

S3

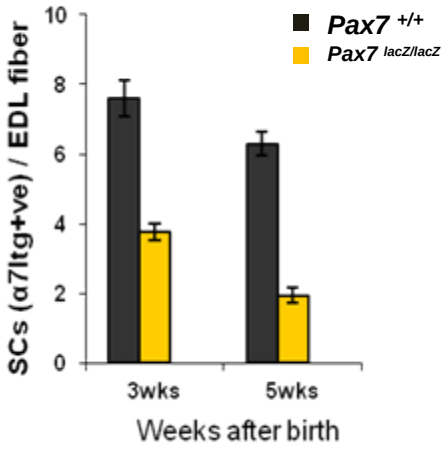

Figure S3. Post natal decrease in satellite cells number in *Pax7* null mice. Graph shows the number of satellite cells (SCs) as α7 Integrin (α7Itg) cells per EDL fiber in 3 and 5 week old wild type (*Pax7* +/+) and *Pax7* null (*Pax7* LacZ/LacZ) mice. N=4. Error bars represent SEM. Student t-test was performed to determine significance. P<0.0001.

S4

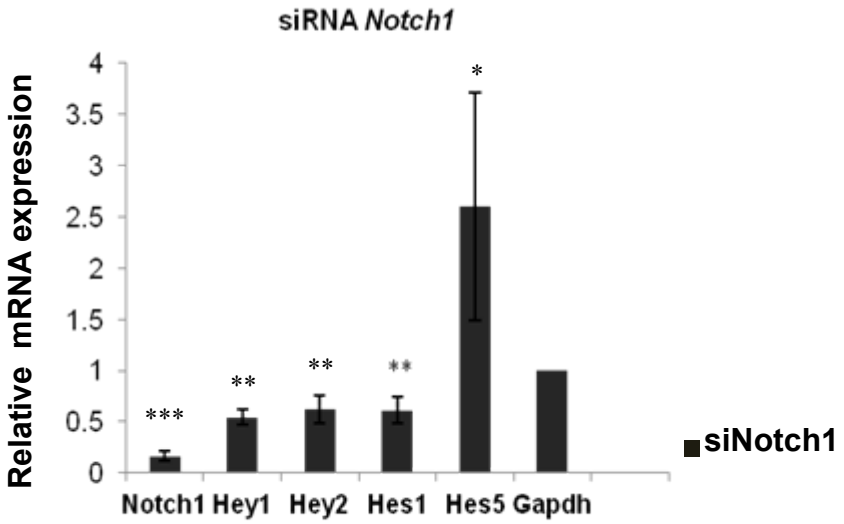

Figure S4. Transient knock down of *Notch*1 in primary myoblasts. Cultured primary myoblasts were transfected with two siRNAs oligonucleotides against *Notch 1* (si*Notch1*) or with a negative control siRNA (siC). Cell lysates were collected after 48 hours from the transfection. qRT-PCR of *Notch1* and downstream target genes *Hey1*, *Hey2*, *Hes1* and *Hes5* is shown. N=3. Error bars represent SEM. Student t-test was performed to determine significance. ***p<0.0001; **p<0.05.*p<0.5.

S5

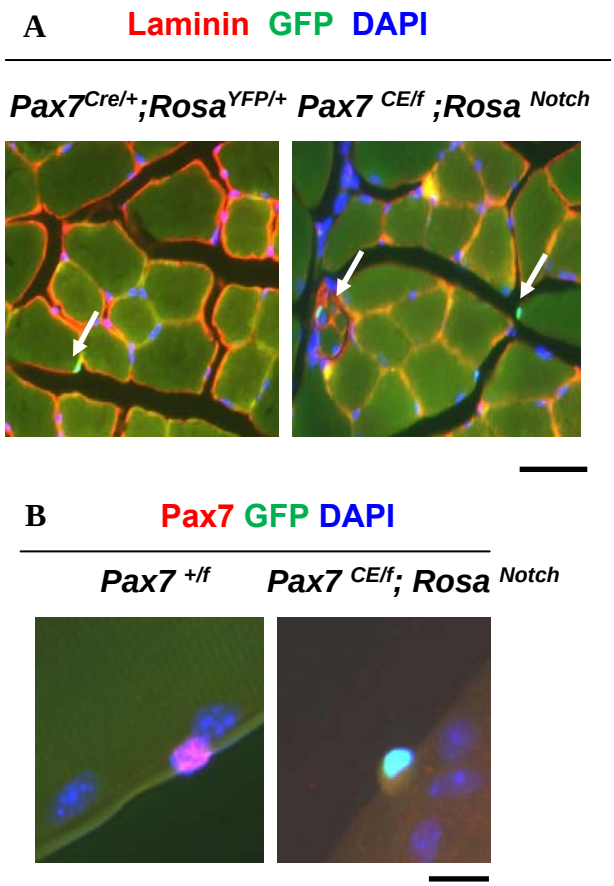

Figure S5. Sublaminal satellite cells on Tibialis Anterior muscle sections. **A.** Immunofluorescence staining of GFP positive satellite cells from wild type muscle (*Pax7 Cre/+; Rosa YFP/+*) and OE-NICD1 *Pax7* null (*Pax7 CE/f; Rosa Notch/+*). Laminin is shown in red, GFP in green, nuclei were counterstained with DAPI (blue). Bar= 50µm. **B**. Immunofluorescence of satellite cells stained for Pax7 (red) and GFP (green). Nuclei were counterstained with DAPI (blue). Bar=100µm.

S6

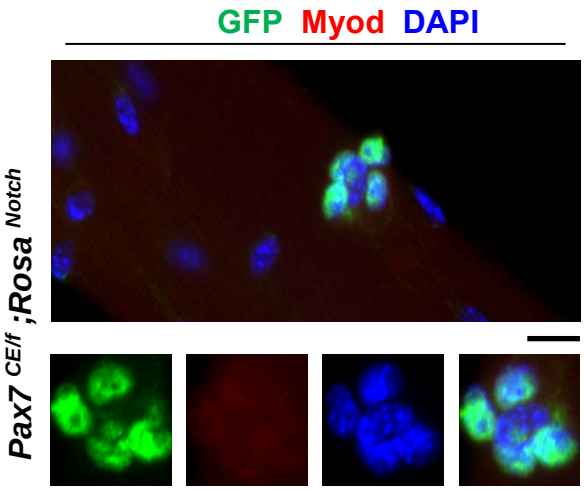

Figure S6. Activated NICD1 *Pax7* null satellite cells do not express MyoD.
Immnofluorescence staining of activated NICD1 *Pax7* null satellite cells at 48 hours in culture. Over expressing *Notch 1* satellite cells were stained with GFP (green) and MyoD (red). Nuclei were counterstained with DAPI (blue). Bar=100µm.

S7

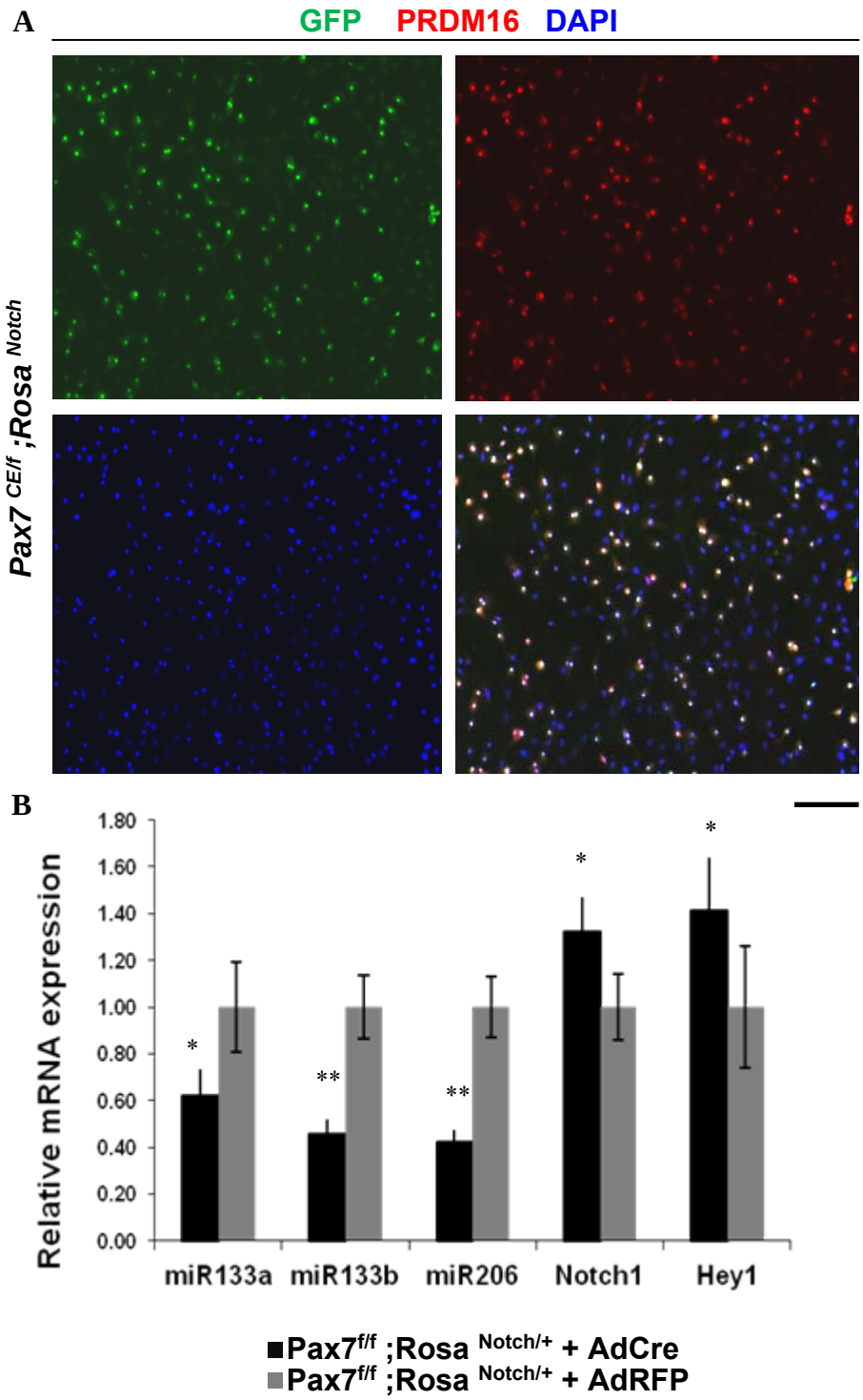
A
GFP
PRDM16
DAPI
Pax7 CE/f ;Rosa Notch
B
Relative mRNA expression
1.80
1.60
1.40
1.20
1.00
0.80
0.60
0.40
0.20
0.00
*
**
**
*
*
miR133a
miR133b
miR206
Notch1
Hey1
Pax7f/f ;Rosa Notch/+ + AdCre
Pax7f/f ;Rosa Notch/+ + AdRFP

Figure S7. NICD1 *Pax7* null derived satellite cells differentiate into brown adipocytes. **A**. Immunofluorescence staining of activated NICD1 *Pax7* null satellite cells cultured in adipogenic conditions for 10 days and stained with GFP (green) and PRDM16 (red). Nuclei were counterstained with DAPI (blue). Bar=200μm. **B**. qRT-PCR of *miR-133*, *miR-206*, *Notch1* and *Hey1* from *Pax7* f/+; *Rosa Notch/+*primary myoblasts infected with an adenovirus encoding for Cre recombinase (AdCre) or a control vector encoding for the Red Fluorescent Protein RFP (AdRFP). Cell lysates were collected after 48 hours. Gene expression was normalized to GAPDH.N=3 replicates. Error bars represent SEM. Student t-test was used to determine significance. *p<0.5; **p<0.05; ***p<0.001.

S8

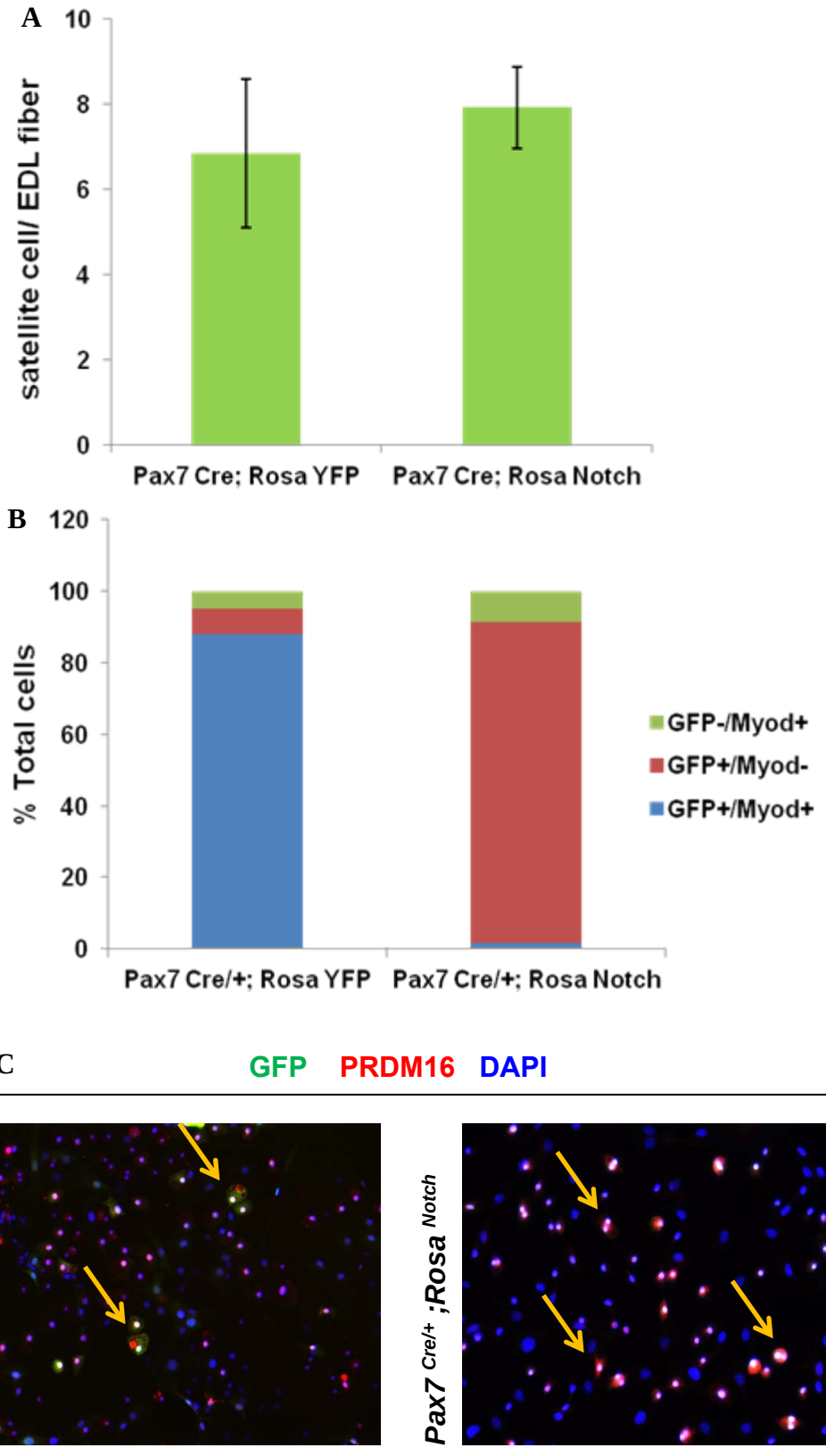
A
satellite cell/ EDL fiber
0
2
4
6
8
10
Pax7 Cre; Rosa YFP
Pax7 Cre; Rosa Notch
B
% Total cells
0
20
40
60
80
100
120
Pax7 Cre/+; Rosa YFP
Pax7 Cre/+; Rosa Notch
GFP-/Myod+
GFP+/Myod-
GFP+/Myod+
C
GFP
PRDM16
DAPI
Pax7 Cre/+;Rosa YFP
Pax7 Cre/+ ;Rosa Notch

Figure S8. Pax7 wild type OE-NICD1 satellite cells differentiate into brown adipocytes. **A.** EDL fibers were isolated from *Pax7Cre/+; Rosa YFP* and *Pax7 Cre/+; Rosa Notch* mice. In *Pax7Cre/+; Rosa YFP* mice Cre recombinase from the *Pax7* locus drives the constitutive expression of YFP. YFP is cytoplasmic. In *Pax7 Cre/+; Rosa Notch* mice Cre recombinase from the *Pax7* locus drives the constitutive over expression of NICD1 and GFP. GFP is nuclear. GFP is localized to the nucleus. Graph shows the number of satellite cells (Pax7+GFP+ expressing cells) at time 0. N=3. **B.** Graph shows the number of GFP+/MyoD+; GFP+/MyoD- and GFP-/MyoD+ cells at 48 hours in culture. N=1 **C.** Immunofluorescence staining of satellite cells derived adipocytes from *Pax7Cre/+; Rosa YFP* and *Pax7 Cre/+; Rosa Notch* mice. GFP is shown in green, PRDM16 is shown in red, nuclei were counterstained with DAPI. Yellow arrows point to YFP/GFP+ PRDM16+ cells.

Supplementary Tables

Table S1. List of pathways down-regulated in *Pax7* $^{-/-}$ satellite cells

KEGG ID	Count	%	p-value	Benjamini	Fold enrich
Calcium signaling	11	4.3	8.1E-5	7.0E-3	4.7
Purine metabolism	7	2.7	1.1E-2	3.8E-1	3.7
MAP kinase signaling	9	3.5	1.4E-2	3.2E1	2.8
Regulation of cytoskeleton	7	2.7	4.5E-2	6.3E-1	2.6

Table S2. List of enriched GO terms down-regulated in *Pax7* $^{-/-}$ satellite cells

GO ID	Count	%	p-value	Benjamini	Fold enrich
Ion channel activity	14	5.4	6.0E-4	8.9E-2	3.1
Cell morphogenesis	13	5.1	4.6E-4	1.5E-1	3.4
ECM	13	5.1	4.1E-4	2.4E-2	3.4
Cell projections	19	7.4	3.7E-4	3.4E-2	2.6
Neuronal projections	12	4.7	2.9E-4	5.4E-2	3.8
Cell motion	15	5.8	1.9E-4	1.2E-1	3.3
Cell fate commitment	7	2.7	9.9E-3	4.0E-1	3.8
Skeletal Muscle Development	10	3.9	9.0E-3	3.9E-1	4.4
Cell motility	10	3.9	8.8E-3	3.9E-1	2.8
Muscle dev	7	2.7	6.9E-3	3.3E-1	4.1
Positive regulation of catalytic activity	10	3.9	5.2E-3	2.7E-1	3.1
Cell adhesion	16	6.2	4.1E-3	2.9E-1	2.7
Positive regulators of multicellular processes	8	3.1	4.1E-3	2.8E-1	3.9
Regulation of system process	9	3.5	3.5E-3	2.9E-1	3.9
Metal ion transporter	11	4.3	3.2E-3	1.8E-1	3.1
Intracellular signaling	23	8.9	2.0E-3	2.2E-1	2.0
Plasma membrane	55	4.4	1.3E-3	4.8E-1	1.5
Regulation of metabolic processes	27	10.5	4.4E-2	7.2E-1	1.5
Regulation of growth	8	3.1	4.2E-2	7.0E-1	2.5
Ion transport	17	6.6	1.5E-2	5.0E-1	1.9
TF activity	18	7	1.5E-2	5.0E-1	1.9
Leukocyte activation	8	31	1.9E-2	5.4E-1	2.9
Regulation of transcription	24	9.3	2.4E-2	6.0E-1	1.6
DNA binding	32	12.5	2.9E-2	6.4E-1	1.4
Homeostatic processes	14	5.4	2.9E-2	6.5E-1	1.9

Table S3. List of pathways (KEGG) up-regulated in *Pax7* $^{-/-}$ satellite cells

KEDD ID	Count	%	p-value	Benjamini	Fold enrich
ECM-receptor interaction	11	2.8	1.4E-5	1.5E-3	5.8
Focal adhesion	14	3.6	4.6E-4	2.4E-2	3.1
Cell adhesion	10	2.6	7.5E-3	2.3E-1	2.9
Cytokine-Receptor interaction	12	3.1	2.1E-2	4.2E-1	2.2

Table S4. List of enriched GO terms up-regulated in *Pax7* $^{-/-}$ satellite cells

GO ID	Count	%	p-value	Benjamini	Fold enrich
Cell adhesion	33	8.5	4.1E-8	6.8E-5	3
Myofibril	14	3.6	6.2E-8	1.7E-5	7.2
Sarcomere	12	3.1	9.7E-7	8.9E-5	7
Chemotaxis	13	3.3	1.3E-6	7.0E-4	6.1
Contractile fibers	12	3.1	2.0E-6	1.0E-4	6.5
Plasma membrane	95	24.4	5.3E-6	2.4E-4	1.5
Extracellular region	59	15.1	1.2E-4	4.5E-3	1.6
Regulation of protein kinase	13	33	2.7E-4	8.6E-2	3.6
ECM	18	4.6	3.5E-4	1.1E-2	2.7
Response to wounding	17	4.4	1.2E-3	1.4E-1	2.5
Actin-Cytosleleton	13	3.3	1.5E-3	3.7E-2	3.0
Citoskeleton organization	16	4.1	1.7E-3	1.7E-1	2.5
Citokine activity	11	2.8	3.0E-3	3.8E-1	3.1
Heart development	12	3.1	4.2E-3	3.2E-1	2.8
Ion channel	10	2.6	6.8E-3	1.2E-1	3
Regulation of metabolic processes	14	3.6	5.9E-3	3.7E-1	2.4
Cell-cell adhesion	12	3.1	6.3E-3	3.8E-1	2.6
Neuron projections	10	2.6	7.3E-3	2.9	4.1E-1
Calcium ion binding	28	7.2	7.9E-3	3.8E-1	1.7
hemopoeisis	12	3.1	9.8E-3	4.7E-1	2.5
Immune response	18	4.6	1.0E-2	4.6E-1	2
Lymphocyte activation	10	2.6	1.2E-2	4.0E-1	2.7

Table S5. RNA-seq values for satellite cells markers

gene	log2(FC)	p-value	q-value
Fgfr1	-2.23574	1.85E-11	3.85E-08
Pax7	-4.758	2.98E-09	2.23E-06
Fgfr4	-3.29699	7.00E-08	3.37E-05

Met	-3.54006	9.64E-07	0.000368
Calcr	-9.03758	3.44E-06	0.000991
Bmp6	-2.87366	4.97E-05	0.008767
Vcam1	-3.58053	0.000119	0.017157
Ncam1	-2.07068	0.000302	0.036888
Cd34	-2.22693	0.000685	0.067497
Myf5	-3.11103	0.001479	0.119266
Cxcr4	-2.16758	0.010321	0.414466
Notch2	-2.05186	0.025004	0.637897
Megf10	-2.51371	0.003212	0.205863
Pax3	-0.07805	0.074684	0.940467
Sdc4	-1.57791	0.094373	0.967613
Sdc3	0.88838	0.348318	0.999281

Table S6. RNA-seq values of fiber specific genes

gene	log2 (FC)	p-value	q-value
Tnnt3	4.41181	2.22E-16	1.39E-12
Myl1	4.83622	3.24E-11	6.06E-08
Trdn	9.2989	1.54E-09	1.25E-06
Ttn	2.53828	1.04E-08	6.49E-06
Myh4	4.42115	1.27E-08	7.66E-06
Myoz2	6.42798	1.77E-08	1.00E-05
Tpm2	2.27577	2.94E-06	0.000886
Ckm	4.97337	4.97E-06	0.001293
Tnnc2	4.33559	1.11E-05	0.002541
Tnc	3.10494	1.46E-05	0.003182
Myh2	2.52873	0.000794	0.076138
Myoz1	3.43985	0.012851	0.466912
Myt1	3.84357	0.014152	1
Myom2	2.34965	0.032731	0.723607

Table S7. RNA-seq values for components of the Notch signaling pathways

gene	log2(FC)	p-value	q-value
Notch2	-2.05186	0.025004	0.637897
Rbpj	-0.84611	0.253199	0.999281
Notch3	-0.16324	0.86484	0.999281
Notch4	2.07645	0.0061	0.301963
Dll3	0.891919	0.518035	0.999281
Dll4	1.50267	0.178476	0.993581
Jag1	0.163689	0.801484	0.999281
Jag2	0.900814	0.500257	0.999281
Hes1	0.755793	0.408267	0.999281
Hes5	1.70E+00	0.12842	1
Hes6	-1.49942	0.208478	0.999281
Hey1	-0.98472	0.276791	0.999281
Hey2	0.307057	0.803619	0.999281

Lfng	1.87032	0.184968	0.997945
Numb	-0.67022	0.170715	0.98295
Numbl	0.186248	0.776173	0.999281
Dtx4	-3.37407	0.000293	0.036025
Heyl	-1.07023	0.103916	0.967613
Dll1	-1.10032	0.208405	0.999281
Notch1	fail	fail	fail
Gxylt2	-5.14	1.15E-05	0.002602
Adam12	2.32701	0.011274	0.435874
Cir1	-0.53287	0.549698	0.999281
Mfng	-0.45896	0.664147	0.999281
Rfng	-0.47062	0.694404	0.999281
Dvl1	-0.64549	0.355041	0.999281
Dvl2	-0.5911	0.431723	0.999281
Dvl3	-0.0828	0.887241	0.999281
Dtx1	-0.00121	0.99938	1
Dtx2	0.176159	0.815661	0.999281
Dtx3	0.657138	0.220629	0.999281
Crebbp	-0.05713	0.950472	0.999281
Ep300	-0.00521	0.995211	0.999871
Kat2a	-0.93744	0.08185	0.967613
Kat2b	-0.53126	0.407638	0.999281
Snw1	-0.4177	0.662915	0.999281
Ctbp1	-0.43358	0.657836	0.999281
Ctbp2	-0.13539	0.831491	0.999281
Hdac1	-0.21055	0.73171	0.999281
Hdac11	-2.70855	0.009824	0.402265
Hdac2	-0.87309	0.064781	0.922515
Ptcra	0	1	1
Ncstn	-0.51279	0.324514	0.999281
Aph1c	-0.21684	0.872133	0.999281
Aph1a	0.251634	0.806481	0.999281
Aph1b	-0.14237	0.888562	0.999281

Table S8. List of primers sequences used for qRT-PCR

Gene	Forward	Reverse	Yse
Pax7	GACGACGAGGAAGGAGACAA	ACATCTGAGCCCTCATCCAG	qRT-PCR
Myf5	ACAGCAGCTTTGACAGCATC	AAGCAATCCAAGCTGGACAC	
MyoD	GGCTACGACACCGCCTACTA	GTGGAGATGCGCTCCACTAT	
Myogenin	CAGTGAATGCAACTCCCACAG	ATGGACGTAAGGGAGTGCAGA	
Rbp-j	CCTTCGGTCCCAGACAGTTA	ATACAGGGTCGTCTGCATCC	
Hes1	CCAAGCTAGAGAAGGCAGACA	TGATCTGGGTCATGGAGTTG	
Hes5	GCAGCATAGAGCAGCTGAAG	TAGTCCTGGTGCAGGCTCTT	
Hes6	CGGATCAACGAGAGTCTTCAG	TCAGCTGAGACAGTGGCATC	
Hey1	CTGTGTTCCATGTCCCCAAC	GTGTGCAGCATTTTCAGGTG	
Hey2	TGAAGATGCTCCAGGCTACA	GCACAGGTGCTGAGATGAGA	

Notch3	GTCCAGACTGGGGCTTACTG	GGCCCTTGTCTATGCACTTT	
Notch2	CCGCCGAGACTCTAGCAAT	TGTCCCAGAACCAATCAGGT	
Notch1	CCGTTACATGCAGCAGTTTC	AGCCAGGATCAGTGGAGTTG	
mir133	TTTGGTCCCCTTCAACCAGCTG	GCATACGAGCTCTTCCGATCT	
mir206	TGGAATGTAAGGAAGTGTGTGG	GCATACGAGCTCTTCCGATCT	
mir1	TGGAATGTAAAGAAGTATGTAT	GCATACGAGCTCTTCCGATCT	
Ppia	CACTGCCAAGACTGAATG	GTCGGAAATGGTGATCTTC	
Gapdh	TGTCCGTCGTGGATCTGAC	GGTCCTCAGTGTAGCCCAAG	
Myf5-111	CATCCCACATAATCCAATCAC	ACACAGATGGATGGGAAAGA	ChIP
Notch1-28	GACCACATAGGGCAAAGAGG	AGGCACCTGCTTGTCTCATT	
Notch2 +20	CCTGGGGAGAAGAATGAGAA	CACTGAGGAAAGGGTCCATC	
Chr 2 -200	CTCAGAAATCCGGCTGACTC	CAGGGTTCAGAGCTTTCACA	

Chapter 4- General Discussion

Discussion

4.1. General overview

This project aimed to characterize the genetic requirements of *Pax7* and their functional relevance in adult myogenesis, as it was previously shown that *Pax7* is critically required for the maintenance of satellite cells and muscle regeneration (Seale et al., 2000; Kuang et al., 2006; Lepper et al., 2009 and 2010; Gunther et al., 2013; vonMaltzhan et al., 2013). To achieve this goal, we used *Pax7* null mutant mice as a model system in combination with gene expression studies and cellular techniques.

4.2 FACS based approach for gene expression studies of stem cells

The isolation of stem cells from their tissue of origin is a critical aspect of gene expression studies. While being fairly low abundant, recent estimates of the total number of satellite cells in adult muscles showed that the satellite cell population size may outnumber that of other stem cells such as hematopoietic stem cells (Bentzinger et al., 2012). However, compared to hematopoietic stem cells, which are fairly accessible, satellite cells are embedded within adult muscle fibers. Their isolation requires both enzymatic and mechanical dissociations which results in loss of stem cell quiescence and satellite cell activation.

Traditionally Fluorescence Activated Cell Sorting (FACS) based approaches have been used to study stem cells at the genetic level (Fukada et al., 2007; Sacco et al., 2008). Our efforts were therefore initially focused on optimizing a FACS protocol for the isolation of satellite cells from wild type as well as *Pax7* null mutant mice. For this purpose we screened several markers previously identified using Representational Difference Analysis (RDA) approach of satellite stem cells and satellite committed cells. Immunohistochemistry and qPCR analysis identified *β1Integrin* (Kuang et al., 2006), *Notch3* (Fukada et al., 2007) and *Frizzled7* (Le Grand et al.,

2009) as markers of quiescent satellite cells. However, currently available antibodies did not prove to be suitable to identify satellite cells by FACS. The use of α7Integrin (Blanco-Bose et al., 2001) and CD34 (Alfaro et al., 2011) surface markers in conjunction with lineage negative markers including CD45 (red blood lineage), Sca-1 (hematopoietic lineage), CD11b (immune cell lineage) and CD31 (endothelial lineage) represent a successful strategy to unambiguously identify satellite cells in vivo (Kuang et al., 2006; Sacco et al., 2008; Juan et al., 201; Pasut et al., 2012). Together with pilot experiments aimed to identify the optimal saturating conditions for antibody labeling, the optimization of the protocol also involved titration measurement of the speed and pressure of the sorting to achieve optimal cell recovery in the least amount of time while preserving cell viability and RNA integrity. With this regard we found that 2 hour long sorting at a medium pressure (maximum number of total cells ~20 millions) guarantees an abort rate lower than 0.6% and allows the recovery of good quality RNA.

4.3 Gene expression studies of *Pax7* null satellite cells

Gene expression studies require usually between 1-2 µg of total RNA. We estimated that the average amount of RNA collected from two wild type mice in a 2 hour sort is 100-150ng. Conversely, the average amount of RNA collected from three *Pax7* null mice in 2 hours of sorting is <50 pg. The significant difference in RNA amount partially reflects the decrease number of satellite cells in *Pax7* null mice, as shown in Figure 1 and S3 of Chapter 3. This required collecting RNA from multiple sorts. An additional challenge was represented by the low survival of *Pax7* null mice most of which (>50%) die perinatally within the first two-three weeks of age (Kuang et al., 2006). Even in the most ideal conditions, the amount of recovered RNA is in the order of ng. Microarray platform such as the Affymetrix Mouse Exon 1.0 ST array requires a minimum of 500 ng of total RNA for each replicate and a total of three replicates for

statistical analysis. Pre-amplification of RNA has been shown to introduce bias in gene expression changes compared to non amplified RNA especially for low abundant transcripts when methods based on hybridized probes-template detection systems are used (Canales et al., 2006; Vermeulen et al., 2009).

For these reasons, the best option in our case was the use of genome wide sequencing platforms (Zhao et al., 2014). The digital nature of RNA sequencing (RNA-Seq) provides an unbiased coverage of the whole transcriptome at a higher resolution than other available platforms for gene expression studies (Zhao et al., 2014). Indeed, while microarrays cover at best around 20% of the length of a gene, the digital nature of RNA sequencing allows entire coverage of a gene transcript (Illumina genome analyzer *IIx*, user guide).

RNA-Seq is also more sensitive and accurate at discriminating subtle fold changes. This is due to the fact that RNA reads counts can be approximated to a Poisson distribution when at least 50 million of reads are collected (Illumina genome analyzer *IIx*, user guide). Statistically this implies that RNA-seq can accurately detect difference in fold change as low as 1.25. Even when as low as 10 million reads are collected, RNA-seq is 5 times more sensitive than microarray and allows identifying up to 44% more differentially expressed genes. Microarray sensitivity has been estimated to be comparable to RNA-seq of approximately 2 million reads (Illumina genome analyzer *IIx*, user guide).

By combining FACS and Illumina high throughput genome wide sequencing, we successfully identify a total of 722 differentially expressed genes (Figure 1). Bioinformatic analysis of our data showed that lack of *Pax7* results in the loss of satellite cell identity and acquisition of a more differentiated phenotype as suggested by the down-regulation of satellite cell specific markers (Table S5, Chapter 3) and up-regulation of genes such as myosins and

sarcomeric protein (Table S6, Chapter 3). Regulation of cell migration and cell adhesion, cell-cell and cell-ECM interactions, control of chemotaxis and positive regulation of growth and homeostasis as well as regulation of skeletal muscle development, were among the most highly enriched GO terms associated with Pax7. These findings are in agreement with previous gene expression studies (Fukada et al., 2007) but also highlight novel class of genes, including regulators of calcium homeostasis, metabolic functions, DNA or RNA processes, which may be implicated in the maintenance of quiescence (Tables S1-4, Chapter 3).

4.4 Regulation of Notch signaling by Pax7

In parallel with gene expression studies, we performed in vitro fiber culture studies of *Pax7* null satellite cells and observed that *Pax7* null satellite cells precociously differentiate. These findings led us to focus on genes involved in the inhibition of myogenic differentiation as potential targets of Pax7. Interestingly, *Rbp-j* null mice have a strikingly similar phenotype to *Pax7* null mice and *Rbp-j* null satellite cells are lost due to precocious differentiation (Vasutyna et al., 2007 and 2010). These similarities led us to test whether Notch genes were perturbed in *Pax7* null satellite cells. While pathway analysis performed using DAVID did not show a perturbation in the Notch pathway (Supplementary table S1 and S3), we found that several Notch genes including core components of the Notch pathway such as *Notch2* (log2 FC -2.05), *Rbp-j* (log 2FC -0.8), *Hes6* (log 2FC -1.4), *Hey 1*(log 2FC -0.9), *Numb* (log2 FC-0.6), *Hey1* (log2 FC-1.0) and *Dll1* (log2FC-1.0)were down-regulated in *Pax7* null satellite cells (Table S7, Chapter 3) (FC=fold change). Ancillary components of the Notch pathway which were also found down-regulated included the histone deacetyalse *HDAC11* (log2 FC-2.7), the ubiquitin ligase *Dtx4* (log2 FC-3.3) and the xylosil transferase *Gxlty2* (log2 FC-5.4).

qRT-PCR on freshly sorted satellite cells showed that *Notch 1* and *Notch 2* were significantly down-regulated compared to other tested genes. Additionally ChIP-Seq data identified a putative Pax7 binding peak upstream of *Notch 1* transcriptional start site (TSS) which we further validated by performing ChIP-qPCR and luciferase. The results gathered form qRT-PCR, ChIP-qPCR, Luciferase and single knock down led us to conclude that *Notch 1* was a novel Pax7 target gene. Pathway analysis, performed by DAVID on our RNA-seq data, did not show a global perturbation in the Notch pathway. We could speculate that in this case, gene set enrichment analysis (GSEA) or other integrative tools such as Cytoscape may be better suited to identify differential expressed signalling and networks of interactions among a given set of enriched genes (Mootha et al., 2003; Tian et al., 2005).

4.5 Notch signaling partially fulfills Pax7 requirements in adult myogenesis

The combination of gene expression and in vitro experiments led us to identify a genetic interaction between Pax7 and Notch1. Next we sought to address the extent to which Notch1 participates in the regulation of satellite cell function by performing a series of "rescue" experiments. To do this, we over expressed the constitutively active intracellular domain of *Notch1* (NICD1) in *Pax7* null mice (Figure 5A and B). The comparison between *Pax7* null and *Pax7* null over expressing NICD1 (OE-NICD1) satellite cells would ultimately allowed us to pinpoint the exact requirements of *Notch1* in adult myogenesis.

In resting conditions muscle is a low turnover tissue and satellite cells are normally found in a sub-laminal position along each muscle fibers in a quiescent state (Charge and Rudnicki, 2004; Yin et al., 2013). Our experiments show that the constitutively active intracellular domain of *Notch1* (NICD1) is sufficient to restore satellite cell number in *Pax7* null mice and therefore led us to conclude that *Notch1* is required to maintain satellite cell quiescence. As *Rbp-j* null

satellite cells precociously exit quiescence (Bjorson et al., 2012; Mourikis et al., 2012), we can speculate that this function is mediated by the canonical Notch signalling pathway (Kopan and Ilagan, 2009), possibly through the modulation of cell-niche interactions (Pisconti et al., 2010; Brohl et al., 2012)

In order to efficiently repair muscles, quiescent satellite cells must enter the cell cycle and undergo a phase of extensive proliferation before committing to differentiate. NICD1 over expression was sufficient to restore satellite cell proliferation in *Pax7* null mice. These findings are in agreement with previous evidences showing that Notch is required to sustain proliferation (Conboy and Rando, 2002; Sun et al.,2007) and supported by the fact that transient knock down of *Notch1* in primary myoblasts or inactivation of *Rbp-j* in satellite cells leads to growth arrest and terminal differentiation (Vasutyna et al., 2007; Bjornson et al., 2012). However, Wen et al., showed that NICD1 over expression in vivo promotes satellite cells self-renewal (Wen et al., 2012). The dual role of Notch signaling is well documented in the hematopoietic system where *Notch1* has been shown to act as both an oncogene by promoting cell growth and proliferation and a tumor suppressor by suppressing hematopoietic stem cell expansion (Kannan et al., 2011; Yatim et al., 2012; Pajcini et al., 2011).

While the dynamic of receptor–ligand engagement are generally poorly defined, transient up-regulation of Notch by its ligand *Delta1* (*Dll1*) has been shown to mediate the establishment of muscle progenitors in the embryo (Rios et al., 2005) and to rescue the age dependent decline in satellite cell number (Conboy et al., 2005). Therefore, we propose a model in which it is not the level of expression of Notch 1 specifically but the transient exposure to different Notch ligands that instruct or prime satellite cells to engage in different programs (Figure 9, Chapter 3). Additionally, Notch1 has also been shown to act independently from Rbp-j and activate gene

transcription in a non-canonical fashion (Ross and Kadesch, 2001; Brack et al., 2008; Perumalsamy et al., 2009). Given this evidence we could also speculate that context dependent crosstalk with other signalling may modulate alternative cell fate choices.

4.6 Role of Pax7 and Notch in lineage progression

While primarily involved in muscle regeneration, lineage tracing experiments have shown that adult satellite cells, similarly to their embryonic progenitors, also contribute to the formation of ectopic brown adipose tissue (Seale et al., 2008; Lepper et al., 2009; Yin et al., 2013). Both skeletal muscle and brown fat have the ability to dissipate energy in the form of heat either through exercise or exposure to cold temperature, respectively (Tseng et al., 2003). Adaptive thermogenesis is controlled at the level of mitochondria.Specifically, the mithochondrial uncoupling proteins UCP 1-5 function to uncouple oxidative phosphorylation and use hydrogen protons (H+) to produce heat instead of ATP (Nederggard et al., 2005). The mechanisms that regulate the switch between muscle and brown fat are not well understood.

Unexpectedly we found that Notch signalling promotes brown adipogenesis of *Pax7* null satellite cells. The first conclusion from these findings is that while the quiescent state and early phases of muscle regeneration depends on Notch signaling, *Notch1* is completely dispensable for myogenic differentiation (Figure 9, Chapter 3). Because our experiments were performed on a *Pax7* null background, we conclude that Notch promotes brown adipogenesis in the absence of a myogenic cue. Indeed, RNA-seq data shows that genes related with cell fate determination are enriched in *Pax7* null satellite cells (Table S2) and we do not exclude that in *Pax7* null mice satellite cells may be lost partially due to the acquisition of alternative cell fates.

To address this issue, we over-expressed NICD1 in Pax7 wild type satellite cells in vivo (Figure S8). Remarkably, Pax7 wild-type over expressing NICD1 satellite cells fail to up-

regulate *MyoD* and instead differentiate into brown adipocytes (Figure S8 B and C). While additional in vivo analysis needs to be performed, these results suggest that Notch signaling promotes brown adipogenesis even in the presence of Pax7.

One obvious explanation is the inhibition of MyoD by Notch (Kuroda et al., 1999; Buas et al., 2009 and 2010). Given the complete absence of MyoD+ satellite cells in over-expressing NICD1 mice, we conclude that rather than inhibiting MyoD activity, Notch1 most likely inhibits the up-regulation of MyoD expression. During embryonic development, MyoD and Myf5 drive the expression of *miR-133* which is required by embryonic and adult muscle cells to reinforce their myogenic identity (Chen et al., 2009 and 2010; Sweetman et al., 2008; Yin et al., 2013). Interestingly ChIP-Seq data identified conserved MyoD and Pax7 binding sites on *miR-133* upstream regulatory regions (Soleimani et al., 2012) and thus it is tempting to speculate that MyoD and Pax7 synergistically act to up-regulate *miR-133* and thus allow myogenic commitment of satellite cells. As we previously showed that miR-133 inhibits brown adipogenesis by targeting the brown lineage determinator *PRDM16*, it is possible that Notch may enhance brown fat differentiation of satellite cells by reducing *miR-133* level of expression (Figure S7).

4.7 Future directions

Based on our findings, we conclude that satellite cells engagement in muscle regeneration depends on the establishment of different thresholds of Notch activity (Figure 9 Chapter 3). While in quiescent satellite cells Pax7 maintains *Notch 1* expression which is required to ensure satellite cell homeostasis, during muscle regeneration a threshold of Notch signaling may be required to promote self renewal, proliferation or differentiation of satellite cells.

Recent evidences have shown that the regulation of gene expression by transcription factors is affected by the transient establishment of intra and inter chromosomal interactions which bring long distance enhancer elements in close proximity to the transcription apparatus (Phillips-Cremins et al., 2013; Fraser and Bickmore, 2007). ChIP-seq data show that Pax7 binding sites are predominantly located away from the transcriptional start site (TSS) (Soleimani et al., 2012). The use of high-throughput technology coupled with chromosome conformation capture techniques (Hi-C) may provide additional insights on how Pax7 regulates gene transcription and be useful to address the functional requirements of nuclear architecture in the transition of satellite cells from quiescence to activation to differentiation.

It is clear that the maintenance of stem cell quiescence involves the regulation of cell intrinsic and cell extrinsic pathways among which Notch signalling stands up as a major player. The mammalian genome encodes four Notch receptor of which 3 (*Notch1, 2, 3*) are highly expressed by satellite cells. The issue of receptor redundancy is a major hurdle in the field of Notch signalling transduction. In which processes (ie: satellite cell heterogeneity or stem cell division) do Notch homologues have redundant or opposite functions? And what are the molecular mechanisms that regulate such differences? (Kopan et al., 1996; Conboy et al., 2002; Kuang et al., 2006; Kitamoto et al., 2010). The development of imaging tools to follow Notch activity in vivo may provide additional insights and help solving some of these issues (Souilhol et al., 2006; Villas Boas et al., 2011; Ilagan et al., 2011; Nowotzkin et al., 2013).

A more comprehensive analysis of the effect of Notch signaling in stem cell regulation may come from researching how Rbp-j and NICD1 interacts at the genomic level. Recent chromatin immunoprecipation studies coupled with high throughput sequencing of Rbp-j alone and NICD-Rbp-j complex in C2C12 muscle cells showed that Rbp-j is dynamically recruited to

the DNA by NICD and that most Rbp-j regulatory elements are also co-occupied by NICD (Castel et al., 20103). However, a minor fraction of DNA sites is statically bound by Rbp-j alone independently from NICD. This may suggest the existence of both NICD-Rbp-j dependent and NICD independent but Rbp-j dependent genomic regulatory elements. Whether these elements are functionally distinct is not clear (Barolo et al., 2002; Kreyci and Bray 2007). Additional studies of the Notch interactome may be useful to understand whether NICD heterotypic interactions occur at specific genes promoters and whether they have a biological significance (Yatim et al., 2012).

4.8. Relevance

Pax7 has been shown to have oncogenic properties in 22% of patients affected by rhabdomyosarcoma (RMS), a rare form of skeletal muscle soft tissue sarcoma which primarily affects children and young adolescents caused by the translocation of chromosome 13 into either chromosomes 1 (60% cases) or 2 (22% cases) resulting in the generation of a Pax3 or Pax7 fusion oncogenic proteins (Barr et al., 2001).

A hallmark of cancer is the acquisition of a growth advantage by the tumor initiating cells which are incapable of differentiating. Recent studies have shown that satellite cells are the cell of origin of rhabdomyosarcoma (Keller et al., 2004; Rubin et al., 2011). Therefore, understanding the mechanisms by which satellite cells maintain quiescence or regulate their activation may result in the identification of potential tumor suppressor genes (Tremblay et al., 2014).

4.9. Conclusive remarks

Our studies as well as others have shown that muscle regeneration is the result of the synergistic interactions between intrisinc and extrinsic signaling that fuel each other through mechanisms of feed forward loops or antagonize each other by engaging in negative feedback circuits. The knowledge gained over more than 50 years of research in the muscle stem cells field has greatly contributed to our understanding of tissue regeneration and homeostasis.

Collaborative research efforts to navigate the complex network of interactions that regulate gene expression at the genomic or metagenomic levels, coupled with the use of mouse genetic and the development of imaging tools that allow to follow the fate of single molecule in vivo will undoubtly foster the development and design of new tools for the manipulation of satellite cells and their use in regenerative medicine.

References

Abou-Khalil,R., and Brack ,A.S.(2010). Muscle stem cells and reversible quiescence: the role of sprouty. Cell Cycle. *9*, 2575-80.

Aguiari, P., Leo, S., Zavan, B., Vindigni, V,, Rimessi, A., Bianchi, K., Franzin, C., Cortivo, R., Rossato, M., Vettor, R., Abatangelo, G., Pozzan, T., Pinton, P., and Rizzuto, R.(2008). High glucose induces adipogenic differentiation of muscle-derived stem cells. Proc Natl Acad Sci U S A. *105*, 1226-31.

Albini, S., Coutinho, P., Malecova,B., Giordani, L., Savchenko, A., Forcales, S.V.,and Puri, P.L.(2013). Epigenetic reprogramming of human embryonic stem cells into skeletal muscle cells and generation of contractile myospheres. Cell Rep.*3*, 661-70.

Alfaro, L.A., Dick, S.A., Siegel, A.L., Anonuevo, A.S., McNagny, K.M., Megeney, L.A., Cornelison, D.D., and Rossi, F.M. (2011). CD34 promotes satellite cell motility and entry into proliferation to facilitate efficient skeletal muscle regeneration.Stem Cells *29*, 2030–2041.

Aragona, M., Panciera, T., Manfrin, A., Giulitti, S., Michielin, F., Elvassore, N., Dupont, S.,and Piccolo, S.(2013). A mechanical checkpoint controls multicellular growth through YAP/TAZ regulation by actin-processing factors.Cell *154*, 1047-59.

Artavanis-Tsakonas, S., Rand, M. D. and Lake, R. J. (1999). Notch signaling: Cell fate control and signal integration in development. Science *284*,770 -776.

Asakura, A., Komaki, M., and Rudnicki, M. (2001). Muscle satellite cells are multipotential stem cells that exhibit myogenic, osteogenic, and adipogenic differentiation. Differentiation *68*, 245–253.

Bajard, L., Relaix, F., Lagha, M., Rocancourt, D., Daubas, P., and Buckingham, M.E.(2006). A novel genetic hierarchy functions during hypaxial myogenesis: Pax3directly activates Myf5 in muscle progenitor cells in the limb. Genes Dev *20*, 2450-2464.

Barolo, S., Stone, T., Bang, A.G., and Posakony, J.W.(2002). Default repression and Notch signaling: Hairless acts as an adaptor to recruit the corepressors Groucho and dCtBP to Suppressor of Hairless. Genes Dev. *16*, 1964-76.

Barr, F.G. (2001). Gene fusions involving PAX and FOX family members in alveolar rhabdomyosarcoma. Oncogene *20*, 5736-5746.

Bartel, D.P. (2004). MicroRNAs: Genomics, biogenesis, mechanism, and function. Cell *116*, 281–297.

Beauchamp, J.R., Heslop, L., Yu, D.S., Tajbakhsh, S., Kelly, R.G., Wernig, A., Buckingham, M.E,Partridge, T.A., and Zammit, P.S.(2000). Expression of CD34 and Myf5 defines the majority ofquiescent adult skeletal muscle satellite cells. J Cell Biol *151*, 1221–1234.

Bentzinger, C.F., Wang, Y,X., Dumont ,N.A., and Rudnicki, M.A.(2013). Cellular dynamics in the muscle satellite cell niche. EMBO Rep. 14, 1062-72.

Bentzinger, C.F., Wang, Y.X., von Maltzahn, J., Soleimani, V.D., Yin, H., Rudnicki, M.A.(2013). Fibronectin regulates Wnt7a signaling and satellite cell expansion. Cell Stem Cell. *12*, 75-87.

Bentzinger, C.F., Wang, Y.X., and Rudnicki, M.A.(2012). Building muscle: molecular regulation of myogenesis. Cold Spring Harb Perspect Biol. *4*, 1-18.

Berkes, C.A., and Tapscott, S.J. (2005). MyoD and the transcriptional control of myogenesis. Semin Cell Dev Biol. *16*, 585-95.

Bischoff, R. (1994). The satellite cell and muscle regneration. In Myology, A.G. Engel, and C. Franzini-Armstrong, eds. (New York, McGraw-Hill), pp. 97-118.

Bjornson, C.R., Cheung, T.H., Liu, L., Tripathi, P.V., Steeper, K.M.,and Rando, T.A.(2012) Notch signaling is necessary to maintain quiescence in adult muscle stem cells. Stem Cells. *30*, 232-42.

Blanco-Bose, W.E., Yao, C.C, Kramer, R.H, and Blau, H.M. (2001). Purification of mouse primary myoblasts based on alpha 7 integrin expression. Exp Cell Res. *265*, 212-20.

Borello, U., Berarducci, B., Murphy, P., Bajard, L., Buffa, V., Piccolo, S., Buckingham, M, and Cossu, G. (2006). The Wnt/β-catenin pathway regulates Gli-mediated Myf5 expression during somitogenesis. Development *133*, 3723–3732.

Bosnakovski, D., Xu, Z., Li, W., Thet, S., Cleaver, O., Perlingeiro, R.C., and Kyba, M.(2008). Prospective isolation of skeletal muscle stem cells with a Pax7 reporter. Stem Cells. *26*, 3194-204.

Boutet, S.C., Cheung, T.H., Quach, N.L., Liu, L., Prescott, S.L., Edalati, A., Iori, K.,and Rando, T.A.(2012). Alternative polyadenylation mediates microRNA regulation of muscle stem cell function. Cell Stem Cell. *10*, 327-36.

Brack, A.S., Conboy, I.M., Conboy, M.J., Shen, J., and Rando, T.A. (2008). A temporal switch from Notch to Wnt signaling in muscle stem cells is necessary for normal adult myogenesis. Cell Stem Cell, *2*, 50-9.

Brack, A.S., Conboy, M.J., Roy, S., Lee, M., Kuo, C.J., Keller, C., and Rando, T.A. (2007).
Increased Wnt signaling during aging alters muscle stem cell fate and increases fibrosis. Science *317*, 807-810.

Braun, T., Bober, E., Rudnicki, M.A., Jaenisch, R., and Arnold, H.H. (1994). MyoD expression marks the onset of skeletal myogenesis in Myf-5 mutant mice. Development *120*, 3083-3092.

Braun, T., Rudnicki, M.A., Arnold, H.H., and Jaenisch, R. (1992). Targeted inactivation of the muscle regulatory gene Myf-5 results in abnormal rib development and perinatal death. Cell *71*, 369-382.

Braun, T., Winter, B., Bober, E., and Arnold, H.H. (1990). Transcriptional activation domain of the muscle-specific gene-regulatory protein myf5. Nature *346*, 663-665.

Bray, S.J. (2006). Notch signalling: a simple pathway becomes complex. Nat. Rev. Mol. Cell Biol. *7*, 678–689.

Bray, S. and Furriols, M. (2001). Notch pathway: making sense of suppressor of hairless. Curr. Biol. *11*, 217-221.

Bröhl, D., Vasyutina, E., Czajkowski, M.T., Griger, J., Rassek ,C., Rahn, H.P., Purfürst, B., Wende, H., and Birchmeier, C.(2012). Colonization of the satellite cell niche by skeletal muscle progenitor cells depends on Notch signals. Dev Cell. *23*, 469-81.

Brunelli, S., Relaix, F., Baesso, S., Buckingham, M., and Cossu, G. (2007). β-Catenin-independent activation of MyoD in presomitic mesoderm requires PKC and depends on Pax3 transcriptional activity. Dev Biol *304*, 604–614.

Buas,M.F., Kabak, S., and Kadesch, T. (2010). The Notch effector Hey1 associates with myogenic target genes to repress myogenesis.J Biol Chem.*285*, 1249-58.

Buas,M.F., Kabak, S., and Kadesch, T.(2009). Inhibition of myogenesis by Notch: evidence for multiple pathways. J Cell Physiol. *218*, 84-93.

Buckingham, M. (2001). Skeletal muscle formation in vertebrates. Curr Opin Genet Dev *11*, 440-8

Buckingham, M., Bajard, L., Chang, T., Daubas, P., Hadchouel, J., Meilhac, S., Montarras, D., Rocancourt, D., and Relaix, F. (2003). The formation of skeletal muscle: from somite to limb. J Anat *202*, 59-68.

Buckingham, M., and Relaix, F. (2007). The role of Pax genes in the development of tissues and organs: Pax3 and Pax7 regulate muscle progenitor cell functions. Annu Rev Cell Dev Biol *23*, 645-673.

Buckingham, M., and Rigby, P.W.(2014). Gene regulatory networks and transcriptional mechanisms that control myogenesis. Dev Cell.*28*, 225-38.

Buckingham M. (2009).Muscle stem cell behavior is modified by microRNA-27 regulation of Pax3 expression.Proc Natl Acad Sci.*106*, 13383–13387.

Canales, R.D., Luo, Y., Willey, J.C., Austermiller, B., Barbacioru, C.C., Boysen, C., Hunkapiller, K., Jensen, R.V, Knight, C.R., Lee, K.Y., Ma, Y., Maqsodi, B., Papallo, A., Peters, E.H., Poulter, K., Ruppel, P.L., Samaha, R.R., Shi, L., Yang, W., Zhang, L., and Goodsaid, F.M.(2006). Evaluation of DNA microarray results with quantitative gene expression platforms. Nat Biotechnol. *9*,1115-22.

Caretti, G., Schiltz, R.L., Dilworth, F.J., Di Padova, M., Zhao, P., Ogryzko, V., Fuller-Pace, F.V., Hoffman, E.P., Tapscott, S.J., and Sartorelli, V.(2006). The RNA helicases p68/p72 and the noncoding RNA SRA are coregulators of MyoD and skeletal muscle differentiation. Dev Cell. *11*, 547-60.

Carlson, M.E., Hsu, M, and Conboy, I.M. (2008). Imbalance between pSmad3 and Notch induces CDK inhibitors in old muscle stem cells. Nature. *454*, 528-32.

Castel, D., Mourikis, P., Bartels, S.J., Brinkman, A.B., Tajbakhsh, S., and Stunnenberg, H.G.(2013). Dynamic binding of RBPJ is determined by Notch signaling status. Genes Dev. *27*, 1059-71.

Chakkalakal, J.V., Christensen, J., Xiang, W., Tierney, M.T., Boscolo, F.S, Sacco, A., and Brack, A.S. (2014). Early forming label-retaining muscle stem cells require p27kip1 for maintenance of the primitive state. Development. *141*, 1649-59.

Chakkalakal, J.V., Jones, K.M., Basson, M.A., and Brack, A,S. (2012). The aged niche disrupts muscle stem cell quiescence.

Chang, N.C., and Rudnicki, M.A. (2014). Satellite cells: the architects of skeletal muscle. Curr Top Dev Biol. *107*, 161-81. Nature.*490*, 355-60.

Charge, S.B., and Rudnicki, M.A. (2004). Cellular and molecular regulation of muscle regeneration. Physiol Rev *84*, 209-238.

Chazaud, B., Sonnet, C., Lafuste, P., Bassez, G., Rimaniol, A.C., Poron, F., Authier, F.J., Dreyfus, P.A., and Gherardi, R.K.(2003). Satellite cells attract monocytes and use macrophages as a support to escape apoptosis and enhance muscle growth.J Cell Biol. *163*, 1133-43.

Chen, J.F., Mandel, E.M., Thomson, J.M., Wu, Q., Callis, T.E., Hammond, S.M., Conlon,F.L., and Wang, D.Z. (2006). The role of microRNA-1 and microRNA-133 in skeletal muscle proliferation and differentiation. Nat Genet *38*, 228-233.

Chen, J.F., Tao, Y., Li, J., Deng, Z., Yan, Z., Xiao, X., and Wang, D.Z. (2010). microRNA-1 and microRNA-206 regulate skeletal muscle satellite cell proliferation and differentiation by repressing Pax7. J Cell Biol *190*, 867-879.

Cheung, T.H and Rando, T.A. (2013). Molecular regulation of stem cell quiescence. Nat Rev Mol Cell Biol. *14*, 329-40.

Cheung, T.H., Quach, N.L., Charville, G.W, Liu, L., Park ,L., Edalati, A., Yoo, B., Hoang, P., and Rando, T.A.(2012). Maintenance of muscle stem-cell quiescence by microRNA-489. Nature. *482*, 524-8.

Choi, J., Costa, M.L., Mermelstein, C.S., Chagas, C., Holtzer, S., and Holtzer, H. (1990).MyoD converts primary dermal fibroblasts, chondroblasts, smooth muscle, andretinal pigmented epithelial cells into striated mononucleated myoblasts and multinucleated myotubes. Proc Natl Acad Sci *87*, 7988-7992.

Christov, C., Chrétien, F., Abou-Khalil, R., Bassez, G., Vallet, G., Authier, F.J., Bassaglia, Y., Shinin, V., Tajbakhsh, S., Chazaud, B., and Gherardi RK.(2007). Muscle satellite cells and endothelial cells: close neighbors and privileged partners. Mol Biol Cell. *18*, 1397-409.

Collins, C.A., Olsen, I., Zammit, P.S., Heslop, L., Petrie, A., Partridge, T.A., and Morgan, J.E. (2005). Stem cell function, self-renewal, and behavioral heterogeneity of cells from the adult muscle satellite cell niche. Cell. 122, 289-301.

Collins, C.A., Gnocchi, V.F., White, R.B., Boldrin, L., Perez-Ruiz, A., Relaix, F., Morgan,J.E., and Zammit, P.S. (2009). Integrated functions of Pax3 and Pax7 in the regulation of proliferation, cell size and myogenic differentiation. PloS one 4, e4475.

Conboy, I.M., and Rando, T.A. (2002). The regulation of Notch signaling controls satellite cell activation and cell fate determination in postnatal myogenesis. Dev Cell *3*, 397-409.

Conboy, I.M., Conboy, M.J., Wagers, A.J., Girma, E.R., Weissman, I.L., and Rando, T.A.(2005). Rejuvenation of aged progenitor cells by exposure to a young systemic environment. Nature. *433*, 760-4.

Cornelison, D.D., Filla, M.S., Stanley, H.M., Rapraeger, A.C., and Olwin, B.B. (2001) Syndecan-3 and syndecan-4 specifically mark skeletal muscle satellite cells and are implicated in satellite cell maintenance and muscle regeneration. Dev Biol *239*, 79–94.

Cornelison, D.D., and Wold, B.J. (1997). Single-cell analysis of regulatory gene expression in quiescent and activated mouse skeletal muscle satellite cells. Dev Biol. *191*, 270-83.

Crist,C.G., and Buckingham, M.(2009a). microRNAs gain magnitude in muscle.Cell Cycle. 8, 3627-8.

Crist,C.G., Montarras, D., Pallafacchina, G., Rocancourt, D., Cumano, A., Conway, S.J.,and Buckingham M.(2009b). Muscle stem cell behavior is modified by microRNA-27 regulation of Pax3 expression. Proc Natl Acad Sci. *106*, 13383-7.

Crist, C.G., Montarras, D., and Buckingham, M. (2012). Muscle satellite cells are primed for myogenesis but maintain quiescence with sequestration of Myf5 mRNA targeted by microRNA-31 in mRNP granules.Cell Stem Cell. *11*,118-26.

Daston, G., Lamar, E., Olivier, M., and Goulding, M. (1996). Pax-3 is necessary for migration but not differentiation of limb muscle precursors in the mouse.Development *122*, 1017-1027.

Davis, R.L., Weintraub, H., and Lassar, A.B. (1987). Expression of a single transfectedcDNA converts fibroblasts to myoblasts. Cell *51*, 987-1000.

Dellavalle, A., Sampaolesi, M., Tonlorenzi, R., Tagliafico, E., Sacchetti, B., Perani, L., Innocenzi, A., Galvez, B.G., Messina, G., Morosetti, R., Li, S., Belicchi, M., Peretti, G., Chamberlain, J.S., Wright, W.E., Torrente, Y., Ferrari, S., Bianco, P., and Cossu ,G.(2007) Pericytes of human skeletal muscle are myogenic precursors distinct from satellite cells.Nat Cell Biol. *9*, 255-67.

Dilworth, F.J., and Blais, A.(2011). Epigenetic regulation of satellite cell activation during muscle regeneration. Stem Cell Res Ther. *19*, 18-47.

Di Padova, M., Caretti, G., Zhao, P., Hoffman, E.P.,and Sartorelli, V.(2007). MyoD acetylation influences temporal patterns of skeletal muscle gene expression. J Biol Chem. *282*, 37650-9.

Dupont, S., Morsut, L., Aragona, M., Enzo, E., Giulitti, S., Cordenonsi, M., Zanconato, F., Le Digabel, J., Forcato, M., Bicciato, S., Elvassore.N., and Piccolo, S. (2011). Role of YAP/TAZ in mechanotransduction. Nature *474*, 179-183.

Elabd, C., Cousin, W., Upadhyayula, P., Chen, R.Y., Chooljian, M.S., Li, J., Kung, S., Jiang, K.P., and Conboy I.M. (2014). Oxytocin is an age-specific circulating hormone that is necessary for muscle maintenance and regeneration. Nat Commun. *5*, 4082.

Epstein, J.A., Shapiro, D.N., Cheng, J., Lam, P.Y., and Maas, R.L. (1996). Pax3 modulates expression of the c-Met receptor during limb muscle development. Proc Natl AcadSci *93*, 4213-4218.

Faralli, H., and Dilworth, F.G. (2012). Turning on Myogenin in Muscle: A Paradigm for Understanding Mechanisms of Tissue-Specific Gene Expression. Comp Funct Genomics *2012*, 1-10.

Ferrari, G., Cussela-De Angelis, G., Coletta, M., Paolucci, E., Stornaiuolo, A., Cossu, G., and Mavilio, F. (1998). Muscle regeneration by bone marrow-derived myogenic progenitors. Science *279*, 1528-1530.

Forsberg, E.C., Passegué ,E., Prohaska, S.S., Wagers ,A.J., Koeva, M., Stuart, J.M., Weissman, I.L.(2010). Molecular signatures of quiescent, mobilized and leukemia-initiating hematopoietic stem cells. PLoS One.*5*:e87875.

Fortini, M. E. and Artavanis-Tsakonas, S. (1994). The Suppressor of Hairless protein participates in Notch receptor signaling. Cell *79*,273 -282.

Franz, T., Kothary, R., Surani, M.A., Halata, Z., and Grim, M. (1993). The Splotch mutation interferes with muscle development in the limbs. Anat Embryol (Berl) *187*, 153-160.

Fraser,P., and Bickmore, W. (2007). Nuclear organization of the genome and the potential for gene regulation. Nature *447*, 413–417. Fukada, S., Uezumi, A., Ikemoto, M., Masuda, S., Segawa, M., Tanimura, N., Yamamoto, H., Miyagoe-Suzuki, Y., and Takeda, S. (2007). Molecular signature of quiescent satellite cells in adult skeletal muscle. Stem Cells *25*, 2448-2459

Fulco, M., Schiltz, R.L., Iezzi, S., King, M.T., Zhao, P., Kashiwaya, Y., Hoffman, E., Veech, R.L., and Sartorelli V.(2003). Sir2 regulates skeletal muscle differentiation as a potential sensor of the redox state. Mol Cell. *12*, 51-62.

Fulco, M., Cen, Y., Zhao, P., Hoffman, E.P., McBurney, M.W., Sauve, A.A., and Sartorelli, V.(2008). Glucose restriction inhibits skeletal myoblast differentiation by activating SIRT1 through AMPK-mediated regulation of Nampt. Dev Cell. *14*, 661-73.

Gibb,S., Maroto, M., and Dale,J.K.(2010). The segmentation clock mechanism moves up a notch. Trends in Cell Biology *20*, 593-600.

Gilbert, P.M., and Blau, H.M. (2011). Engineering a stem cell house into a home. Stem Cell Res Ther. 2011 *2*, 3-9.

Gilbert, P.M., Havenstrite, K.L., Magnusson, K.E., Sacco, A., Leonardi, N.A., Kraft, P., Nguyen, N.K., Thrun, S., Lutolf, M.P., and Blau, H.M.(2010). Substrate elasticity regulates skeletal muscle stem cell self-renewal in culture. Science. *329*,1078-81.

Gillespie, M.A., Le Grand, F., Scimè, A., Kuang, S., von Maltzahn, J., Seale, V., Cuenda, A., Ranish, J.A., and Rudnicki M.A. (2009). J Cell Biol. *187*, 991-1005.

Gnocchi,V.F., White, R.B., Ono, Y., Ellis, J.A., Zammit, P.S.(2009). Further characterisation of the molecular signature of quiescent and activated mouse muscle satellite cells. PLoS One. *4*:e5205.

Goldman, YE. (1987). Kinetics of the actomyosin ATPase in muscle fibers. Ann. Rev. of Physiol.49, 637-654.

Goulding, M., Lumsden, A., and Paquette, A.J. (1994). Regulation of Pax-3 expression in the dermomyotome and its role in muscle development. Development 120, 957-971.

Gray H.(1918-1961).Anatomy of the human body, Chapter IV, 20thed. Philadelphia:lea and Febger, 1918; New York: Bartleby.com, 2000.

Greenwald, I. (1998). LIN-12/Notch signaling: lessons from worms and flies. Genes Dev. *12*, 1751 -1762.

Grifone, R., Demignon, J., Giordani, J., Niro, C., Souil, E., Bertin, F., Laclef, C., Xu, P.X., and Maire ,P. (2007). Eya1 and Eya2 proteins are required for hypaxial somitic myogenesis in the mouse embryo. Dev Biol *302*, 602–616.

Gros, J., Manceau, M., Thome, V.,*and* Marcelle, C. (2005). A common somitic origin for embryonic muscle progenitors and satellite cells. Nature *435*, 954–958.

Günther, S., Kim, J., Kostin, S., Lepper, C., Fan, C.M.,and Braun, T. (2013). Myf5-positive satellite cells contribute to Pax7-dependent long-term maintenance of adult muscle stem cells. Cell Stem Cell. *13*, 590-601.

Gussoni, E., Soneoka, Y., Strickland, C.D., Buzney, E.A., Khan, M.K., Flint, A.F., Kunkel, L.M., and Mulligan, R.C. (1999). Dystrophin expression in the mdx mouse restored by stem cell transplantation. Nature *401*, 390-394.

Hamada, Y., Kadokawa, M., Okabe, M., Ikawa, J.R., Coleman, Y.,and Tsujimoto Y.(1999).Mutation in ankyrin repeats of the mouse Notch2 gene induces early embryonic lethality. Development *126* , 3415–3424.

Hasty, P., Bradley, A., Morris, J.H., Edmondson, D.G., Venuti, J.M., Olson, E.N., and Klein,W.H. (1993). Muscle deficiency and neonatal death in mice with a targeted mutation in the myogenin gene. Nature *364*, 501-506.

Hirsinger, E., Duprez, D., Jouve, C., Malapert, P., Cooke, J., and Pourquie, O. (1997).Noggin acts downstream of Wnt and Sonic Hedgehog to antagonize BMP4 in avian somite patterning. Development *124*, 4605-4614.

Hofmann, M., Schuster-Gossler, K., Watabe-Rudolph, M., Aulehla, A., Herrmann, B.G., and Gossler, A. (2004). WNT signaling, in synergy with T/TBX6, controls Notch signaling by regulating Dll1 expression in the presomitic mesoderm of mouse embryos. Genes Dev *18*, 2712–2717.

Holterman, C.E., Le Grand, F., Kuang, S., Seale, P., and Rudnicki, M.A. (2007). Megf10 regulates the progression of the satellite cell myogenic program. J Cell Biol *179*, 911-922.

Hopkins, PM. (2006). Muscle Physiology. Contin Educ Anaesth Crit Care Pain *6*, 1-6.Horst, D., Ustanina, S., Sergi, C., Mikuz, G., Juergens, H., Braun, T., and Vorobyov, E.(2006). Comparative expression analysis of Pax3 and Pax7 during mouse myogenesis. The International journal of developmental biology *50*, 47-54.

Huang, D.W., Sherman, B.T, and Lempicki, R.A. (2009).Systematic and integrative analysis of large gene lists using DAVID Bioinformatics Resources. Nature Protoc. *4*, 44-57.

Illumina genome analyzer *IIx*, user guide SCS v2.10 (2012). pagg 91-103 and 107-131.

Ishibashi,J., Perry, R.L., Asakura, A and Rudnicki, MA.(2005) MyoD induces myogenic differentiation through cooperation of its NH2- and COOH-terminal regions. J Cell Biol. *17*, 471-82.

Jiang, W., Xiaojuan, S., Min, Z., Chongtao. Z., Bin, C., Yongqing, X.,Jun, O., Hua, L., and Xiaozhong, Q., (2012). Correlation between innervation of skeletal muscles and myoblast stem ells. Int. J. Morphol.*30*, 1532-1537.

Joe, A.W., Yi, L., Natarajan, A., Le Grand, F., So, L., Wang, J., Rudnicki, M.A., and Rossi, F.M.(2010). Muscle injury activates resident fibro/adipogenic progenitors that facilitate myogenesis. Nat Cell Biol. *12*, 153-63.

Jones, N.C., Tyner, K.J., Nibarger, L., Stanley, H.M., Cornelison, D.D., Fedorov, Y.V., and Olwin, B.B.(2005). The p38alpha/beta MAPK functions as a molecular switch to activate the quiescent satellite cell. J Cell Biol. *169*, 105-16.

Juan, A.H., Derfoul, A., Feng, X, Ryall, J.G, Dell'Orso, S., Pasut, A., Zare, H., Simone, J.M., Rudnicki, M.A, and Sartorelli V.(2011). Polycomb EZH2 controls self-renewal and safeguards the transcriptional identity of skeletal muscle stem cells. Genes Dev. *25*, 789-94.

Kablar, B., Krastel, K., Ying, C., Tapscott, S.J., Goldhamer, D.J., and Rudnicki, M.A. (1999). Myogenic determination occurs independently in somites and limb buds. Dev Biol *206*, 219-231.

Kamminga, L.M., Bystrykh, L.V., de Boer, A., Houwer, S., Douma, J., Weersing, E., Dontje, B., de Haan, G.(2006). The Polycomb group gene Ezh2 prevents hematopoietic stem cell exhaustion. Blood. *107*, 2170-9.

Kannan, S., Fang, W., Song, G., Mullighan, C.G., Hammitt, R., McMurray, J., and Zweidler-McKay, P.A.(2011). Notch/HES1-mediated PARP1 activation: a cell type-specific mechanism for tumor suppression. Blood. 117, 891-900.

Kao, H. Y., Ordentlich, P., Koyano-Nakagawa, N., Tang, Z., Downes, M., Kintner, C. R., Evans, R. M. and Kadesch, T. (1998). A histone deacetylase corepressor complex regulates the Notch signal transduction pathway. Genes Dev. *12*, 2269 -2277.

Kassar-Duchossoy, L., Giacone, E., Gayraud-Morel, B., Jory, A., Gomes, D., and Tajbakhsh, S. (2005). Pax3/Pax7 mark a novel population of primitive myogenic cells during development. Genes Dev 19, 1426-1431.

Katz, B.(1961). The terminations of the afferent nerve fibre in the muscle spindle of the frog. Philos Trans Royal Soc Lond [Biol]. *243*, 221–24.

Kawabe, Y., Wang, Y.X., McKinnell, I.W., Bedford, M.T., and Rudnicki MA.(2012). Carm1 regulates Pax7 transcriptional activity through MLL1/2 recruitment during asymmetric satellite stem cell divisions. Cell Stem Cell. *11*, 333-45.

Keller, C., Hansen, M.S., Coffin, C.M., and Capecchi, M.R. (2004). Pax3:Fkhr interferes with embryonic Pax3 and Pax7 function: implications for alveolar rhabdomyosarcoma cell of origin. Genes Dev *18*, 2608-2613.

Kitamoto ,T., and Hanaoka, K.(2010). Notch3 null mutation in mice causes muscle hyperplasia by repetitive muscle regeneration. Stem Cells. *12*, 2205-16.

Kopan, R., Schroeter, E.H., Weintraub, H., and Nye, J.S. (1996). Signal transduction by activated mNotch: Importance of proteolytic processing and its regulation by the extracellular domain. Proc. Natl. Acad. Sci. *93*, 1683–1688.

Kopan, R., and Ilagan, M.X.(2009). The canonical Notch signaling pathway: unfolding the activation mechanism. Cell. *137*, 216-33.

Krebs, L.T., Xue, Y., Norton, C.R., Shutter, J.R., Maguire, M., Sundberg, J.P., Gallahan, D., Closson, V., Kitajewski, J., Callahan, R., Smith, G.H., Stark, K.L., and Gridley, T.(2000). Notch signaling is essential for vascular morphogenesis in mice. Genes Dev. *14*, 1343-52.

Krejcí, A., and Bray, S.(2007). Notch activation stimulates transient and selective binding of Su(H)/CSL to target enhancers.Genes Dev. *11*, 1322-7.

Kuang, S., Charge, S.B., Seale, P., Huh, M., and Rudnicki, M.A. (2006). Distinct roles for Pax7 and Pax3 in adult regenerative myogenesis. J Cell Biol 172, 103-113.

Kuang, S., Kuroda, K., Le Grand, F., and Rudnicki, M.A. (2007). Asymmetric self-renewal and commitment of satellite stem cells in muscle. Cell 129, 999-1010.

Kondoh, K., Sunadome, K., and Nishida, E.(2007). Notch signaling suppresses p38 MAPK activity via induction of MKP-1 in myogenesis. J Biol Chem. *282*, 3058-65.

Kuroda, K., Tani, S., Tamura, K., Minoguchi, S., Kurooka, H., and Honjo, T.(1999). Delta-induced Notch signaling mediated by RBP-J inhibits MyoD expression and myogenesis.J Biol Chem. *274*, 7238-44.

Lagha, M., Kormish, J.D., Rocancourt, D., Manceau, M., Epstein, J.A., Zaret, K.S., Relaix,F., and Buckingham, M.E. (2008). Pax3 regulation of FGF signaling affects the progression of embryonic progenitor cells into the myogenic program. Genes Dev*22*, 1828-1837.

Le Grand, F., Jones, A.E., Seale, V., Scime, A., and Rudnicki, M.A. (2009). Wnt7a activates the planar cell polarity pathway to drive the symmetric expansion of satellite stem cells. Cell Stem Cell *4*, 535-547.

Lepper, C., Conway, S.J., and Fan, C.M. (2009). Adult satellite cells and embryonic muscle progenitors have distinct genetic requirements. Nature 460, 627-631.

Lepper, C., Fan, C.M. (2010). Inducible lineage tracing of Pax7-descendant cells reveals embryonic origin of adult satellite cells. Genesis. *7*, 424-36.

Ling, B.M., Bharathy, N., Chung, T.K., Kok, W.K., Li, S., Tan, Y.H., Rao, V.K., Gopinadhan, S., Sartorelli, V., Walsh, M.J., and Taneja, R.(2012). Lysine methyltransferase G9a methylates the transcription factor MyoD and regulates skeletal muscle differentiation. Proc Natl Acad Sci *109*, 841-6.

Malerba, A., Pasut, A., Frigo, M., De Coppi, P., Baroni, M.D., and Vitiello, L.(2010). Macrophage-secreted factors enhance the in vitro expansion of DMD muscle precursor cells while preserving their myogenic potential. Neurol Res. *32*, 55-62.

Mansouri, A., Stoykova, A., Torres, M., and Gruss, P. (1996). Dysgenesis of cephalic neural crest derivatives in Pax7-/- mutant mice. Development 122, 831-838.

Mansouri, A., Stoykova,A. and Gruss,P. (1994). Pax genes in development. Journal of Cell Science, *18*, 35-42

Maroto, M., Reshef, R., Munsterberg, A.E., Koester, S., Goulding, M., and Lassar, A.B. (1997). Ectopic Pax-3 activates MyoD and Myf-5 expression in embryonic mesoderm and neural tissue. Cell *89*, 139-148.

Mauro, A. (1961). Satellite cell of skeletal muscle fibers. J Biophys Biochem Cytol. *9*,493–495

Mayer, U., Saher, G., Fässler, R., Bornemann, A., Echtermeyer, F., von der Mark, H., Miosge, N., Pöschl, E., and von der Mark, K.(1997). Absence of integrin alpha 7 causes a novel form of muscular dystrophy. Nature Genetics. *17*, 318-23.

McKinnell, I.W., Ishibashi, J., Le Grand, F., Punch, V.G., Addicks, G.C., Greenblatt, J.F.,Dilworth, F.J., and Rudnicki, M.A. (2008). Pax7 activates myogenic genes by recruitment of a histone methyltransferase complex. Nature cell biology *10*, 77-84.

Megeney, L.A., and Rudnicki, M.A. (1995). Determination versus differentiation and the MyoD family of transcription factors. Biochem Cell Biol *73*, 723-732.

Miner, J., Miller, J.,and Wold, B.J. (1992). Skeletal muscle phenotypes initiated by ectopic MyoD in transgenic mouse heart. Development *114*, 853-860.

Molkentin, J.D., and Olson, E.N. (1996). Combinatorial control of muscle development by basic helix-loop-helix and MADS-box transcription factors. Proc Natl Acad Sci *93*, 9366-9373.

Montarras, D., Morgan, J., Collins, C., Relaix, F., Zaffran, S., Cumano, A., Partridge, T., and Buckingham ,M.(2005). Direct isolation of satellite cells for skeletal muscle regeneration. Science. *309*, 2064-7.

Mootha, V.K., Lindgren, C.M., Eriksson, K.F., Subramanian, A., Sihag, S., Lehar, J., Puigserver, P., Carlsson, E., Ridderstråle, M., Laurila, E., Houstis, N., Daly, M.J., Patterson, N., Mesirov, J.P., Golub, T.R., Tamayo, P., Spiegelman, B., Lander, E.S., Hirschhorn, J.N., Altshuler, D.,and Groop, L.C.(2003). PGC-1alpha-responsive genes involved in oxidative phosphorylation are coordinately downregulated in human diabetes. Nat Genet. *34*, 267-73.

Morgan, T.H. (1917). The theory of the gene. Am. Nat. *51*,513-544.

Moss, F.P., and Leblond, C, P.(1970). Nature of dividing nuclei in skeletal muscle of growing rats.J Cell Biol *44*, 459–462.

Mourikis, P., Gopalakrishnan, S., Sambasivan, R., and Tajbakhsh, S.(2012). Cell-autonomous Notch activity maintains the temporal specification potential of skeletal muscle stem cells.Development. *139*, 4536-48.

Munsterberg, A.E., Kitajewski, J., Bumcrot, D.A., McMahon, A.P., and Lassar, A.B. (1995). Combinatorial signaling by Sonic hedgehog and Wnt family members induces myogenic bHLH gene expression in the somite. Genes Dev *9*, 2911-2922.

Nabeshima, Y., Hanaoka, K., Hayasaka, M., Esumi, E., Li, S., Nonaka, I., and Nabeshima, Y. (1993). Myogenin gene disruption results in perinatal lethality because of severe muscle defect. Nature *364*, 532-535.

Nedergaard, J., Ricquier, D., and Kozak, L.P.(2005). Uncoupling proteins: current status and therapeutic prospects. EMBO Rep.*6*, 917-21.

Nishijo, K., Hosoyama, T., Bjornson, C.R., Schaffer,B.S., Prajapati, S.I., Bahadur, A.N., Hansen, M.S., Blandford, M.C., McCleish, A.T., Rubin, B.P., Epstein, J.A., Rando, T.A., Capecchi, M.R, and Keller C.(2009). Biomarker system for studying muscle, stem cells, and cancer in vivo. FASEB J. *23*, 2681-90.

Olguín, H.C. (2011). Regulation of Pax7 protein levels by caspase-3 and proteasome activity in differentiating myoblasts. Biol Res. *44*, 323-7.

Olguin, H.C., and Olwin, B.B. (2004). Pax-7 up-regulation inhibits myogenesis and cell cycle progression in satellite cells: a potential mechanism for self-renewal. Dev
Biol *275*, 375-388.

Ott, M.O., Bober, E., Lyons, G., Arnold, H., and Buckingham, M. (1991). Early expression of the myogenic regulatory gene, myf-5, in precursor cells of skeletal muscle in the mouse embryo. Development *111*, 1097-1107.

Palacios, D., Mozzetta C., Consalvi, S., Caretti, G., Saccone, V., Proserpio, V., Marquez, V.E., Valente, S., Mai, A., Forcales, S.V., Sartorelli, V., and Puri, P.L. (2010). TNF/p38α/polycomb signaling to Pax7 locus in satellite cells links inflammation to the epigenetic control of muscle regeneration. Cell Stem Cell. *7*, 455-69.

Pallafacchina, G., Francois, S., Regnault, B., Czarny, B., Dive, V., Cumano, A., Montarras, D., and Buckingham M. (2010). An adult tissue-specific stem cell in its niche: a gene profiling analysis of in vivo quiescent and activated muscle satellite cells. Stem Cell Res *4*, 77–91.

Pajcini, K.V., Speck, N.A., and Pear, W.S.(2011). Notch signaling in mammalian hematopoietic stem cells. Leukemia. *10*, 1525-32.

Pardo, P.S., and Boriek, A.M. (2011). The physiological roles of Sirt1 in skeletal muscle. Aging (Albany NY) *4*, 430-7.

Pasut, A., Oleynik, P., and Rudnicki, M.A.(2012). Isolation of muscle stem cells by fluorescence activated cell sorting cytometry. Methods Mol Biol. *798*, 53-64.

Pasut, A., Jones, A.E., and Rudnicki, M.A.(2013). Isolation and culture of individual myofibers and their satellite cells from adult skeletal muscle. J Vis Exp. *73*, e50074.

Perumalsamy, L.R., Nagala, M., Banerjee, P. and Sarin, A.(2009). A hierarchical cascade activated by non-canonical Notch signaling and the mTOR-Rictor complex regulates neglect-induced death in mammalian cells. Cell Death Differ. 16, 879-89.

Phillips-Cremins, J.E., Sauria, M.E., Sanyal, A., Gerasimova, T.I., Lajoie, B.R., Bell, J.S., Ong, C.T., Hookway, T.A., Guo, C., Sun, Y., Bland,M.J., Wagstaff, W., Dalton, S., McDevitt, T.C., Sen, R., Dekker, J., Taylor, J., and Corces, V.G.(2013). Architectural protein subclasses shape 3D organization of genomes during lineage commitment. Cell. *153*, 1281-95.

Pisconti, A., Cornelison, D.D., Olguín, H.C., Antwine, T.L., and Olwin B.B. (2010). Syndecan-3 and Notch cooperate in regulating adult myogenesis. J Cell Biol. *190*, 427-41.

Poellinger, L., and Lendahl, U. (2008). Modulating Notch signaling by pathway-intrinsic and pathway-extrinsic mechanisms. Curr. Opin. Genet. Dev. *18*, 449–454.

Pourquie,O., Fan,CM., Coltey,M., Hirsinger,E., Watanabe,Y., Bre,C., Francis-West,P., Brickell,P., Tessier-Lavigne,P., and Le Douarin, M.N.(1996(Lateral and Axial Signals Involved in Avian Somite Patterning: A Role for BMP4. Cell *84*, 461–471.

Punch, V.G., Jones, A.E., and Rudnicki, M.A. (2009). Transcriptional networks that regulate muscle stem cell function. Wiley Interdisciplinary Reviews: Systems Biology and Medicine *1*, 128-140.

Puri, L. and Sartorelli, V. (2000). Regulation of muscle regulatory factors by DNA-binding, interacting proteins, and post-transcriptional modifications. J Cell Physiol *185*, 155-173.

Rawls, A., Valdez, M.R., Zhang, W., Richardson, J., Klein, W.H., and Olson, E.N. (1998). Overlapping functions of the myogenic bHLH genes MRF4 and MyoD revealed in double mutant mice. Development *125*, 2349-2358.

Relaix, F., Rocancourt, D., Mansouri, A., and Buckingham, M. (2004). Divergent functions of murine Pax3 and Pax7 in limb muscle development. Genes Dev *18*, 1088-1105.

Relaix, F., Rocancourt, D., Mansouri, A., and Buckingham, M. (2005). A Pax3/Pax7-dependent population of skeletal muscle progenitor cells. Nature *435*, 948-953.

Reshef, R., Maroto, M., and Lassar, A.B. (1998). Regulation of dorsal somitic cell fates: BMPs and Noggin control the timing and pattern of myogenic regulator expression.Genes Dev *12*, 290-303.

Rhodes, S.J., and Konieczny, S.F. (1989). Identification of MRF4: a new member of the muscle regulatory factor gene family. Genes Dev 3, 2050-2061.

Ridgeway, A.G., Petropoulos, H., Wilton, S., and Skerjanc, I.S. (2000). Wnt signaling regulates the function of MyoD and myogenin. J Biol Chem *275*, 32398-32405.

Ridgeway, A.G., and Skerjanc, I.S. (2001). Pax3 is essential for skeletal myogenesis and the expression of Six1 and Eya2. J Biol Chem *276*, 19033-19039.

Rios, A.C., Serralbo, O., Salgado, D., Marcelle, C.(2011). Neural crest regulates myogenesis through the transient activation of NOTCH. Nature *473*, 532-5.

Rodgers, J.T., King, K.Y., Brett, J.O., Cromie, M.J., Charville, G.W., Maguire, K.K., Brunson, C., Mastey, N., Liu, L., Tsai, C.R., Goodell, M.A., and Rando, T.A.(2014). mTORC1 controls the adaptive transition of quiescent stem cells from G0 to G(Alert). Nature. *510*, 393-6.

Ross, D.A, and Kadesch, T.(2001). The notch intracellular domain can function as a coactivator for LEF-1.Mol Cell Biol. *22*, 7537-44.

Rossi, C.A., Pozzobon, M., Ditadi, A., Archacka, K., Gastaldello, A., Sanna, M., Franzin, C., Malerba, A., Milan, G., Cananzi, M., Schiaffino, S., Campanella, M., Vettor, R., and De Coppi P.(2010). Clonal characterization of rat muscle satellite cells: proliferation, metabolism and differentiation define an intrinsic heterogeneity. PLoS One. *5*:e8523.

Rubin, B.P., Nishijo, K., Chen, H.I., Yi, X., Schuetze, D.P., Pal, R., Prajapati, S.I., Abraham, J., Arenkiel, B.R., Chen, Q.R., Davis, S., McCleish, A.T., Capecchi, M.R., Michalek, J.E., Zarzabal, L.A., Khan, J., Yu, Z., Parham, D.M., Barr, F.G., Meltzer, P.S., Chen ,Y., and Keller C.(2011). Evidence for an unanticipated relationship between undifferentiated pleomorphic sarcoma and embryonal rhabdomyosarcoma. Cancer Cell. 19, 177-91.

Rudnicki, M.A., Braun, T., Hinuma, S., and Jaenisch, R. (1992). Inactivation of MyoD in mice leads to up-regulation of the myogenic HLH gene Myf-5 and results in apparently normal muscle development. Cell *71*, 383-390.

Rudnicki, M.A., and Jaenisch, R. (1995). The MyoD family of transcription factors and skeletal myogenesis. Bioessays *17*, 203-209.

Rudnicki, M.A., Schnegelsberg, P.N., Stead, R.H., Braun, T., Arnold, H.H., and Jaenisch, R.(1993). MyoD or Myf-5 is required for the formation of skeletal muscle. Cell *75*,1351-1359.

Rudnicki, M.A., Le Grand, F., McKinnell, I., and Kuang, S.(2008). The molecular regulation of muscle stem cell function. Cold Spring Harb Symp Quant Biol *7*, 323–331.

Sabourin, L.A., Girgis-Gabardo, A., Seale, P., Asakura, A., and Rudnicki MA.(1999) Reduced differentiation potential of primary MyoD-/- myogenic cells derived from adult skeletal muscle.J Cell Biol., *144*, 631-43.

Sacco, A., Doyonnas, R., Kraft, P., Vitorovic, S., and Blau, H.M.(2008). Self-renewal and expansion of single transplanted muscle stem cells. Nature. *456*, 502-6.

Sambasivan, R., Yao, R., Kissenpfennig, A., Van Wittenberghe, L., Paldi, A., Gayraud-Morel, B., Guenou, H., Malissen, B., Tajbakhsh, S., and Galy, A. (2011). Pax7-expressing satellite cells are indispensable for adult skeletal muscle regeneration. Development. *138*, 3647-56.

Sampaolesi, M., Blot, S., D'Antona, G., Granger, N., Tonlorenzi, R., Innocenzi, A., Mognol, P., Thibaud, J.L., Galvez, B.G., Barthélémy, I., Perani, L., Mantero ,S., Guttinger, M., Pansarasa, O., Rinaldi, C., Cusella, De Angelis, M.G., Torrente, Y., Bordignon, C., Bottinelli, R.,and Cossu, G.(2006). Mesoangioblast stem cells ameliorate muscle function in dystrophic dogs.Nature *444*, 574-9.

Sandmann, T., Jensen, L.J., Jakobsen, J.S., Karzynski, M.M., Eichenlaub, M.P., Bork, P., and Furlong, E.E. (2006). A temporal map of transcription factor activity mef2 directly regulates target genes at all stages of muscle development. Dev Cell *10*, 797-807.

Sassoon, D., Lyons, G., Wright, W.E., Lin, V., Lassar, A., Weintraub, H., and Buckingham,M. (1989). Expression of two myogenic regulatory factors myogenin and MyoD1 during mouse embryogenesis. Nature *341*, 303-307.

Schafer, K., and Braun, T. (1999). Early specification of limb muscle precursor cells by the homeobox gene Lbx1h. Nat Genet *23*, 213-216.

Schienda, J., Engleka, K.A., Jun, S., Hansen, M.S., Epstein, J.A., Tabin, C.J., Kunkel, L.M.,and Kardon, G. (2006). Somitic origin of limb muscle satellite and side population
cells. Proc Natl Acad Sci U S A *103*, 945-950.

Schultz, E., Gibson, M.C., and Champion, T. (1978). Satellite cells are mitotically quiescent in mature mouse muscle: an EM and radioautographic study. J Exp Zool *206*, 451–456.

Seale, P., Sabourin, L.A., Girgis-Gabardo, A., Mansouri, A., Gruss, P., and Rudnicki, M.A.(2000). Pax7 is required for the specification of myogenic satellite cells. Cell *102*,
777-786.

Seale, P., Bjork, B., Yang, W., Kajimura, S., Chin, S., Kuang, S., Scimè, A., Devarakonda, S., Conroe, H.M., Erdjument-Bromage, H., Tempst, P., Rudnicki, M.A., Beier, D.R.,and Spiegelman, B.M. (2008). PRDM16 controls a brown fat/skeletal muscle switch. Nature. *454*, 7961-7.

Sebastian,S., Faralli,H., Yao,Z., Rakopoulos,P., Palii,C., Cao,Y., Singh,K., Liu, Q.C., Chu, A.,Aziz,A., Brand, M., Tapscott, S.J., and Dilworth, F.J., (2013).Tissue-specific splicing of a ubiquitously expressed transcription factor is essential for muscle differentiation. Genes Dev. *27*, 1247-59.

Serena, E., Zatti, S., Reghelin, E., Pasut, A., Cimetta, E.,and Elvassore, N.(2010). Soft substrates drive optimal differentiation of human healthy and dystrophic myotubes. Integr Biol (Camb). *4*,193-201.
Shea, K.L., Xiang, W., LaPorta, V.S., Licht, J.D., Keller, C., Basson, M.A., and Brack ,A,S.(2010). Sprouty1 regulates reversible quiescence of a self-renewing adult muscle stem cell pool during regeneration. Cell Stem Cell. *6*, 117-29.

Schuster-Gossler, K., Cordes, R., and Gossler, A.(2007). Premature myogenic differentiation and depletion of progenitor cells cause severe muscle hypotrophy in Delta1 mutants.(2007). Proc Natl Acad Sci *104*; 537-42.

Soleimani, V.D., Yin, H., Jahani-Asl, A., Ming, H., Kockx ,C.E., van Ijcken, W.F., Grosveld, F., and Rudnicki, M.A. (2012). Snail regulates MyoD binding-site occupancy to direct enhancer switching and differentiation-specific transcription in myogenesis. Mol Cell. *47*, 457-68.

Soleimani, V.D., Punch, V.G., Kawabe, Y., Jones, A.E., Palidwor, G.A., Porter, C.J., Cross, J.W., Carvajal, J.J., Kockx, C.E., van IJcken, W.F., Perkins, T.J., Rigby, P.W., Grosveld, F., and Rudnicki, M.A.(2012). Transcriptional dominance of Pax7 in adult myogenesis is due to high-affinity recognition of homeodomain motifs. Dev Cell. *22*, 1208-20.

Sun, H., Li, L., Vercherat, C., Gulbagci, N.T., Acharjee, S., Li, J., Chung, T.K., Thin, T.H., and Taneja, R.(2007). Stra13 regulates satellite cell activation by antagonizing Notch signaling. J Cell Biol. 177, 647-57.

Sweetman, D., Goljanek, K., Rathjen, T., Oustanina, S., Braun, T., Dalmay, T., and Münsterberg, A. (2008). Specific requirements of MRFs for the expression of muscle specific microRNAs, miR-1, miR-206 and miR-133. Dev Biol. *321*, 491-9.

Tajbakhsh, S., Rocancourt, D., Cossu, G., and Buckingham, M. (1997). Redefining the genetic hierarchies controlling skeletal myogenesis: Pax- 3 and Myf-5 act upstream
of MyoD. Cell *89*, 127-138.

Tajbakhsh, S. (2009). Skeletal muscle stem cells in developmental versus regenerative myogenesis. J Intern Med *266*, 372–389.

Thayer, M.J., Tapscott, S.J., Davis, R.L., Wright, W.E., Lassar, A.B., and Weintraub, H.(1989). Positive autoregulation of the myogenic determination gene MyoD1. Cell
58, 241-248.

Tian, L., Greenberg, S.A., Kong, S.W., Altschuler, J., Kohane, I.S., and Park, P.J.(2005). Discovering statistically significant pathways in expression profiling studies. Proc Natl Acad Sci *102*, 13544-9.

Tonlorenzi, R., Dellavalle, A., Schnapp, E., Cossu, G., Sampaolesi, M.(2007). Isolation and characterization of mesoangioblasts from mouse, dog, and human tissues. Curr Protoc Stem Cell Biol. Chapter 2, Unit 2B.1.

Tremblay, A.M., Missiaglia, E., Galli, G.G., Hettmer, S., Urcia, R., Carrara, M., Judson, R.N., Thway, K., Nadal, G., Selfe, J.L., Murray, G., Calogero, R.A., De Bari, C., Zammit, P.S., Delorenzi, M., Wagers, A.J., Shipley, J., Wackerhage, H., and Camargo, F.D.(2014). The Hippo Transducer YAP1 Transforms Activated Satellite Cells and Is a Potent Effector of Embryonal Rhabdomyosarcoma Formation.Cancer Cell. *26*, 273-87.

Tremblay, P., Dietrich, S., Mericskay, M., Schubert, F.R., Li, Z., and Paulin, D. (1998). A crucial role for *Pax3* in the development of the hypaxial musculature and the long-range migration of muscle precursors. Dev Biol *203*, 49–61.

Tseng, Y.H., Cypess, A.M., and Kahn, C.R.(2010). Cellular bioenergetics as a target for obesity therapy. Nat Rev Drug Discov. *9*, 465-82.

Vasyutina, E., Lenhard, D.C., Wende, H., Erdmann, B., Epstein, J.A., and Birchmeier C.(2007). RBP-J (Rbpsuh) is essential to maintain muscle progenitor cells and to generate satellite cells. Proc Natl Acad Sci *104*, 4443-8.

Vasyutina, E., Lenhard, D.C., and Birchmeier, C.(2007). Notch function in myogenesis.Cell Cycle. 6, 1451-4.

Vermeulen, .J, Derveaux, S., Lefever, S., De Smet, E., De Preter, K., Yigit, N., De Paepe, A., Pattyn, F., Speleman, F., and Vandesompele, J. (2009). RNA pre-amplification enables large-scale RT-qPCR gene-expression studies on limiting sample amounts. BMC Res Notes. *2*, 235-256.

von Maltzahn, J., Jones, A.E., Parks, R.J., and Rudnicki, M.A.(2013). Pax7 is critical for the normal function of satellite cells in adult skeletal muscle. Proc Natl Acad Sci. *110*, 16474-9.

Weintraub, H., Dwarki, V.J., Verma, I., Davis, R., Hollenberg, S., Snider, L., Lassar, A., and Tapscott, S.J. (1991). Muscle-specific transcriptional activation by MyoD. Genes Dev *5*, 1377-1386.

Wen, Y., Bi, P., Liu, W., Asakura, A., Keller, C., and Kuang, S. (2012). Constitutive Notch activation upregulates Pax7 and promotes the self-renewal of skeletal muscle satellite cells. Mol Cell Biol. *32*, 2300-11.

White, R.B., and Ziman, M.R. (2008). Genome-wide discovery of Pax7 target genes during development. Physiol Genomics *33*, 41-49.

Wright, W.E., Sassoon, D.A., and Lin, V.K. (1989). Myogenin, a factor regulating myogenesis, has a domain homologous to MyoD. Cell *56*, 607-617.

Yatim, A., Benne, C., Sobhian, B., Laurent-Chabalier, S., Deas, O., Judde, J.G., Lelievre, J.D., Levy, Y., and Benkirane, M.(2012). NOTCH1 nuclear interactome reveals key regulators of its transcriptional activity and oncogenic function. Mol Cell. *48*, 445-58.

Yennek, S., Burute, M., Théry, M., and Tajbakhsh, S. (2014). Cell adhesion geometry regulates non-random DNA segregation and asymmetric cell fates in mouse skeletal muscle stem cells. Cell Rep. *7*, 961-70.

Yin, H., Price, F., and Rudnicki, M.A. (2013). Satellite Cells and the Muscle Stem Cell Niche. Physiol Rev *93*, 23-67.

Yin, H., Pasut, A., Soleimani, V.D., Bentzinger, C.F., Antoun, G., Thorn, S., Seale, P., Fernando, P, van Ijcken, W., Grosveld, F., Dekemp, R.A., Boushel, R., Harper, M.E., and Rudnicki, M.A.(2013). MicroRNA-133 controls brown adipose determination in skeletal muscle satellite cells by targeting Prdm16. Cell Metab. *17*, 210-24.

Zammit, P.S., Relaix, F., Nagata, Y., Ruiz, A.P., Collins, C.A., Partridge, T.A., andBeauchamp, J.R. (2006). Pax7 and myogenic progression in skeletal muscle satellite cells. J Cell Sci *119*, 1824-1832.

Zammit, P.S., Golding, J.P., Nagata, Y., Hudon, V., Partridge, T.A., and Beauchamp, J.R. (2004). Muscle satellite cells adopt divergent fates: a mechanism for self-renewal? J Cell Biol *166*, 347-357.
Zhang, X.M., Ramalho-Santos, M., and McMahon, A.P. (2001). Smoothened mutants reveal redundant roles for Shh and Ihh signaling including regulation of L/R asymmetry by the mouse node. Cell *105*, 781–792.

Zhang, W., Behringer, R.R., and Olson, E.N. (1995). Inactivation of the myogenic bHLH gene MRF4 results in up-regulation of myogenin and rib anomalies. Genes Dev *9*, 1388-1399.

Zhao P., and Hoffman, P.E. (2004). Embryonic myogenesis pathways in muscle regeneration. Dev Dyn *229*, 380-392.

Zhao,S., Fung-Leung, W.P., Bittner, A., Ngo, K.,and Liu, X.(2014). Comparison of RNA-Seq and microarray in transcriptome profiling of activated T cells. PLoS One. *9*, e78644

Appendix A

Video Article

Isolation and Culture of Individual Myofibers and their Satellite Cells from Adult Skeletal Muscle

Alessandra Pasut[1,2], Andrew E. Jones[1,2], Michael A. Rudnicki[1,2]

[1]Sprott Center for Stem Cell Research, Ottawa Hospital Research Institute

[2]Department of Cellular and Molecular Medicine, University of Ottawa

URL: http://www.jove.com/video/50074
DOI: doi:10.3791/50074

Keywords: Stem Cell Biology, Issue 73, Cellular Biology, Molecular Biology, Medicine, Biomedical Engineering, Bioengineering, Physiology, Anatomy, Tissue Engineering, Stem Cells, Myoblasts, Skeletal, Satellite Cells, Skeletal Muscle, Muscular Dystrophy, Duchenne, Tissue Culture Techniques, Muscle regeneration, Pax7, isolation and culture of isolated myofibers, muscles, myofiber, immunostaining, cell culture, hindlimb, mouse, animal model

Date Published: 3/22/2013

Citation: Pasut, A., Jones, A.E., Rudnicki, M.A. Isolation and Culture of Individual Myofibers and their Satellite Cells from Adult Skeletal Muscle. *J. Vis. Exp.* (73), e50074, doi:10.3791/50074 (2013).

Abstract

Muscle regeneration in the adult is performed by resident stem cells called satellite cells. Satellite cells are defined by their position between the basal lamina and the sarcolemma of each myofiber. Current knowledge of their behavior heavily relies on the use of the single myofiber isolation protocol. In 1985, Bischoff described a protocol to isolate single live fibers from the Flexor Digitorum Brevis (FDB) of adult rats with the goal to create an *in vitro* system in which the physical association between the myofiber and its stem cells is preserved [1]. In 1995, Rosenblattmodified the Bischoff protocol such that myofibers are singly picked and handled separately after collagenase digestion instead of being isolated by gravity sedimentation [2, 3]. The Rosenblatt or Bischoff protocol has since been adapted to different muscles, age or conditions [3-6]. The single myofiber isolation technique is an indispensable tool due its unique advantages. First, in the single myofiber protocol, satellite cells are maintained beneath the basal lamina. This is a unique feature of the protocol as other techniques such as Fluorescence Activated Cell Sorting require chemical and mechanical tissue dissociation [7]. Although the myofiber culture system cannot substitute for *in vivo* studies, it does offer an excellent platform to address relevant biological properties of muscle stem cells. Single myofibers can be cultured in standard plating conditions or in floating conditions. Satellite cells on floating myofibers are subjected to virtually no other influence than the myofiber environment. Substrate stiffness and coating have been shown to influence satellite cells' ability to regenerate muscles [8, 9] so being able to control each of these factors independently allows discrimination between niche-dependent and -independent responses. Different concentrations of serum have also been shown to have an effect on the transition from quiescence to activation. To preserve the quiescence state of its associated satellite cells, fibers should be kept in low serum medium [1-3]. This is particularly useful when studying genes involved in the quiescence state. In serum rich medium, satellite cells quickly activate, proliferate, migrate and differentiate, thus mimicking the *in vivo* regenerative process [1-3]. The system can be used to perform a variety of assays such as the testing of chemical inhibitors; ectopic expression of genes by virus delivery; oligonucleotide based gene knock-down or live imaging. This video article describes the protocol currently used in our laboratory to isolate single myofibers from the Extensor Digitorum Longus (EDL) muscle of adult mice (6-8 weeks old).

Video Link

The video component of this article can be found at http://www.jove.com/video/50074/

Protocol

All experiments were handled according to the University of Ottawa regulations for animal care and handling.

See **Table 1** for an overview of the protocol.

1. Before Starting the Isolation

1. Prepare the following solutions:

   0.2% Collagenase type I in DMEM (Dulbecco's modified Eagle's medium; high glucose, L-glutamine with 110 mg/ml sodium pyruvate). For two EDL muscles prepare 2 ml of 0.2% Collagenease in DMEM. Filter the solution through 0.22 µm filter. 10 min before the isolation, prewarm at 37 °C in a water bath. Additional aliquots of undiluted collagenase can be frozen at -20 °C for later use.

   Note: use DMEM with sodium pyruvate throughout all of the procedure. Fibers do not survive in sodium pyruvate-free medium.

- Washing media (use to perform all the washes). Supplement DMEM with 1% Penicillin/Streptomycin. Filter through 0.22 µm filter before use.
- Myofiber culture media. Supplement DMEM with 20% FBS, 1% Chicken Embryo extract and 1% Penicillin/Streptomycin. Filter through 0.22 µm filter before use.
- Matrigel coated dishes. To culture fibers for long period of time, we recommend using Matrigel as coating substrate. To prepare Matrigel coated dishes, thaw an aliquot of Matrigel at 4 °C overnight. The day after, dilute Matrigel 1:10 in DMEM. Keep Matrigel at 4 °C at all times and avoid abrupt temperature changes as this will create microscopic crystals within the Matrigel solution resulting in uneven coating. Place dishes to be coated on ice. Coat dishes with just enough volume to cover the surface. Let it sit for 1 min. Completely remove the leftover Matrigel. Let dishes dry at 37 °C for at least 3 hr prior to use or overnight.

Note: aliquots of diluted Matrigel can be re-used multiple times for coating purpose if stored at 4 °C.

2. Lastly, be sure to clean the microscope station and dissecting tools with 70% ethanol.
3. For two EDL isolations (one mouse) prepare five plastic Petri dishes (60*15mm) as follows:
   - Four dishes for the isolation (1 for muscle dissociation, 3 for serial washes). All dishes must be coated with horse serum (HS) to prevent myofibers from attaching to plastic. To coat, pipette 3 ml of horse serum into each dish, swirl to allow even coating, remove the horse serum and let the dish dry for at least 30 min. Add 4 ml of DMEM to each dish. Keep dishes at 37 °C in a 5% CO_2 incubator prior to use.

Note: Horse serum can be re-used multiple times, if kept sterile. Alternatively, a solution of 10% HS in DMEM can be used to coat dishes. Use HS coated dishes throughout the whole protocol and when culturing myofibers on floating conditions.

- One dish will be used to culture myofibers after the isolation. Alternative dish sizes or formats can be used for the final culture of myofibers depending on downstream applications. However, we do not suggest dish sizes larger than 60*15mm. Myofibers can be kept in suspension for no longer than 96 hr before hyper contraction occurs. For longer culture times, we recommend using Matrigel coated dishes or plates.

4. For one fiber isolation (2 EDL), prepare two sterile Pasteur pipettes: one large bore pipette for muscle handling and one small bore pipette for myofiber manipulation. Use a diamond pen to cut each glass pipette to the desired length and heat polish to smooth pipette's edges. By using the flame, curve the tip of the small bore pipette. This will help handling single fibers. Flame to sterilize. Coat each pipette with HS before use.

2. Muscle Dissection and Digestion

1. For the purpose of these experiments, 8 week old SV129, *Pax7 CreER^{Cklr};Rosa26TdTomato* (*Pax7Cre-TdTomato*) and *Myf5-Cre;Rosa26YFP* were used.
2. Spray hind limbs with 70% ethanol. Pin the animal (face up) to a support board to have a better grasp of the hind limb during the procedure.
3. With the help of scissors, cut through the entire length of the limb and expose the underlying muscle. Remove the skin as well as any hair or fur (**Figure 1A**).
4. With a fine scissor, cut through the thin fascia without damaging the underlying muscles. Visually localize the EDL. The EDL is found in the anterior compartment of the hind limb just underneath the Tibialis Anterior (TA) muscle.
5. With the help of two forceps, expose the distal tendons.
6. Cut the distal tendons (of both the TA and EDL) with sharp Cohann-Vannas spring scissors.
7. With the help of forceps hold both TA and EDL muscles by their tendons and delicately pull the muscles up towards the proximal end. At this point you should be able to clearly see the EDL muscle just underneath the TA muscle. Now, separate the EDL from the TA muscle by pulling the two tendons in opposite directions (**Figure 1B**). Avoid stretching the EDL muscle while performing this operation as this will damage the myofibers.
8. Expose the EDL tendon. To better visualize the proximal tendon it may help at this point to remove the TA muscle. It may also help to cut off some the connective tissue around the knee (**Figure 1C**).
9. Cut the proximal tendon and gently remove the EDL (**Figure 1D**).
10. By holding the muscle through its tendons, transfer it to 2 ml of previously prepared collagenase solution. Incubate at 37 °C in a water bath.

Note: for successful fiber isolation, it is important to isolate the EDL from tendon to tendon so that the myofiber integrity is maintained. Steps 2.3 to 2.9 can be performed under a dissecting microscope. Alternatively, the use of a magnifying glass may also help to have a better view of the muscles.

11. Repeat steps 2.3 to 2.9 to isolate the second EDL. Transfer the second EDL in the same tube. To avoid uneven digestion, isolation of the second EDL should be completed no more than 5 min after the first.

Note 1: incubation time may need to be adjusted depending on collagenase activity. Longer or shorter incubation might be required depending on the size, age and/or muscle condition (*e.g.* fibrotic muscles need longer digestion time).

Note 2: If examining satellite cells behavior under quiescence conditions, agitation during muscle digestion time may activate satellite cells [10].

12. During the digestion time, regularly check the muscle to avoid over-digestion. Stop the digestion when muscles start to loosen up and myofibers are visible. To stop digestion, carefully transfer both muscles to a prewarmed Petri dish with 4 ml of DMEM (dissociation dish). Use the large bore size pipette to perform this operation.

Note: avoid muscle overdigestion as this inevitably results in the isolation of hyper contracted myofibers.

3. Single Myofiber Dissociation and Culture

1. To release myofibers, use the large bore glass pipette to flush the muscle with warm medium until fibers naturally start being released. Do not triturate the muscle as this will inevitably result in damaging fibers. Perform this and the following steps under a dissecting microscope.
2. Continue releasing myofibers until the desired number is reached. If the dish is required at room temperature for more than 10 min allow a 5 min (minimum) incubation at 37 °C, 5% CO_2 to re-equilibrate the medium.

   Note: if medium reaches temperatures below physiological (37 °C) for an extended time myofibers will die.
3. Using the small size bore pipette, transfer live single myofibers to a new prewarmed dish (first of three consecutive washes). Handle each myofiber individually instead of transferring bulk of myofibers all at once. If necessary, incubate at 37 °C, 5% CO_2 for 10-15 min to re-equilibrate the medium.
4. Repeat step 3.3 for 2 more times or until all dead myofibers and debris are removed. We recommend at least three consecutive washes for proper clean-up.

   Note: dead myofibers will appear as short and hyper contracted under the microscope light.
5. Incubate single myofibers at 37 °C, 5% CO_2 in the last wash dish (DMEM only) for at least one hr prior to switching to culture medium. This allows myofibers to adjust to the *in vitro* conditions in the absence of serum. We found that immediate culture of myofibers in serum rich medium increases fiber shrinking.
6. After one hr, transfer myofibers to a new prewarmed dish or to the appropriate culture format depending on the downstream application. Culture fibers in high serum medium to allow satellite cell activation. Alternatively, different concentrations of serum or chicken embryo extract can also be used. Change medium every other day.

4. Downstream Applications

1. *Immunostaining*. Live myofibers can be fixed and stained at any time point during the isolation. Immunofluorescence can be performed on both floating and substrate-attached myofibers. If staining floating myofibers, use a small bore glass pipette to transfer myofibers from one solution to another. Alternatively, it is possible to keep myofibers in the same well throughout all the procedure and add/remove solutions using a glass pipette. Avoid standard aspiration as this will result in the removal of the myofibers as well. Briefly, completely remove culture medium; fix myofibers in prewarmed 4% paraformaldehyde (PFA) for 5 min. Extensively wash in PBS several times. Incubate myofibers in 1% glycine in PBS or other standard quenching solutions to minimize PFA background staining. If necessary, permeabilize myofibers with 0.1% Triton X-100 in PBS for 10 min followed by a 5 min wash in PBS. Incubate fibers in blocking solution (10% horse serum, 0.1% Triton X-100, 1% NaN) for 1 hr at room temperature or preferably overnight at 4 °C. Alternative blocking solutions may be used, depending on the antibody of interest. Wash once in PBS for 5 min. Incubate with the appropriate primary antibody diluted in blocking solution for 1 hr at room temperature or overnight at 4 °C. Wash fibers 3 times at 5 min per wash in PBS to remove any unbound antibody. Incubate with the appropriate secondary antibody for 45 min to 1 hr at room temperature. Wash 3 times at 5 min per wash in PBS. Counterstain nuclei with 1 mg/ml DAPI. If staining floating fibers, transfer each fiber to a glass slide suitable for microscopy. Remove any excess of PBS or medium. Apply mounting medium and then add coverslip. Proceed to visualize myofibers under a fluorescence microscope. See **Figure 4** for representative immunofluorescence on EDL myofibers. Alternative staining procedures using stronger fixatives are described in Verma, M. *et al.* [11] and Wosniak, A.C. *et al.* [12].
2. *Oligonucleotide or plasmid transient transfection*. Live myofibers can be transfected with plasmid or siRNA for specific gene/s of interest. When using siRNA, double transfection is recommended for efficient gene knockdown. We suggest performing the first transfection after 8 hr from the isolation. Six hr after the transfection, replace with fresh medium. For siRNA transfection, we suggest starting by using a final concentration of 50 nM. Gene expression knockdown can be analyzed by RNA extraction or preferably by immunostaining.
3. *Viral infection*. Infection of live myofibers is possible although the incidence of cell death is higher than with oligo transfection and the efficiency of infection may be variable depending on muscle conditions and age. For instance, intact adult muscle myofibers are particularly non responsive to viral infection due to the presence of the basal lamina which has been shown to provide a protective barrier against host infection [13, 14]. Lentiviral vectors are preferred over retroviral vectors because they can infect quiescent (non mitotic) cells. For viral infection, it is advisable to culture fibers on a Matrigel coated dish or plate and let myofibers adjust to media conditions for the first 24 hr.
4. *Live Imaging*. Live imaging of myofibers is particularly time consuming and necessitates a microscope equipped with a 37 °C, 5% CO_2 chamber. It is useful when assessing the behavior of single satellite cells. Work done using this technique has been instrumental for the discovery of satellite cell heterogeneity and to study their behavior on fibers (15 and 16).

Representative Results

Here we described the isolation of single myofibers from the EDL muscle of adult mice. Successful myofibers yield depend on several factors, such as collagenase activity or muscle conditions or age. Most importantly, the isolation of the muscle from tendon to tendon results in long, intact myofibers from EDL muscle. **Figure 1** shows a step by step graphical representation of the "tendon to tendon" isolation. Once the muscle is fully digested, myofibers are released by applying gentle pressure to the muscle. **Figure 2A** shows a representative picture of a myofiber isolation experiment after the first wash. At this point the culture contains a mixture of bundles of single myofibers which appear as long and shining tubular structures, hyper contracted myofibers which are dark and short and debris from the digestion process. By the end of at least three consecutive washes, only single live myofibers should remain in the dish for culture or downstream analysis (**Figure 2B**). **Figure 2C** shows a long, live fiber as compared to a hyper contracted fiber (C'). At the time of the isolation, satellite cells appear as tiny protuberances on the myofiber surface (**Figure 3A**). If maintained in serum rich medium, satellite cells activate, proliferate, migrate and eventually fuse into myotubes (B). After 15 days in culture, all myotubes express the Myf5 reporter YFP (C) suggesting that muscle regeneration in the adult is performed by cells that at some point during their development had expressed the myogenic determinant factor Myf5. All satellite cells express the paired box transcription factor Pax7 [17]. The reporter mouse line *Pax7Cre-TdTomato* can be used to trace satellite cells via the expression of the TdTomato

fluorescent signal (**Figures 3D** and **E**). **Figure 4** shows a representative immunofluorescence of double Pax7+/Myod satellite cells. Classically double Pax7+/Myod+ satellite cells are considered proliferative committed muscle progenitors which will either complete the differentiation program by down regulating Pax7 while maintaining Myod expression or return to quiescence by down regulating Myod and maintaining Pax7 expression [18]

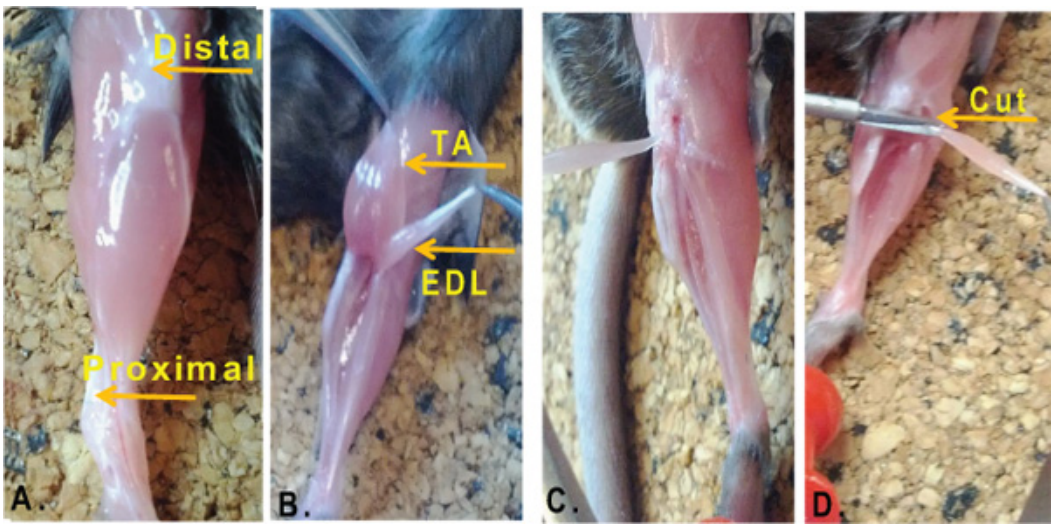

Figure 1. EDL muscle isolation from mouse hindlimb. A . Hindlimb of an 8 week old adult mouse. Arrows indicates the distal (knee) tendon and the proximal (foot) tendon. **B**. Anatomical position of the Tibialis Anterior (TA) muscle and the Extensor Digitorum Longus (EDL) muscle. **C**. By holding the EDL through the proximal tendon, the muscle is pulled toward the knee to expose the distal tendon. **D**. The distal tendon is cut and the EDL is released.

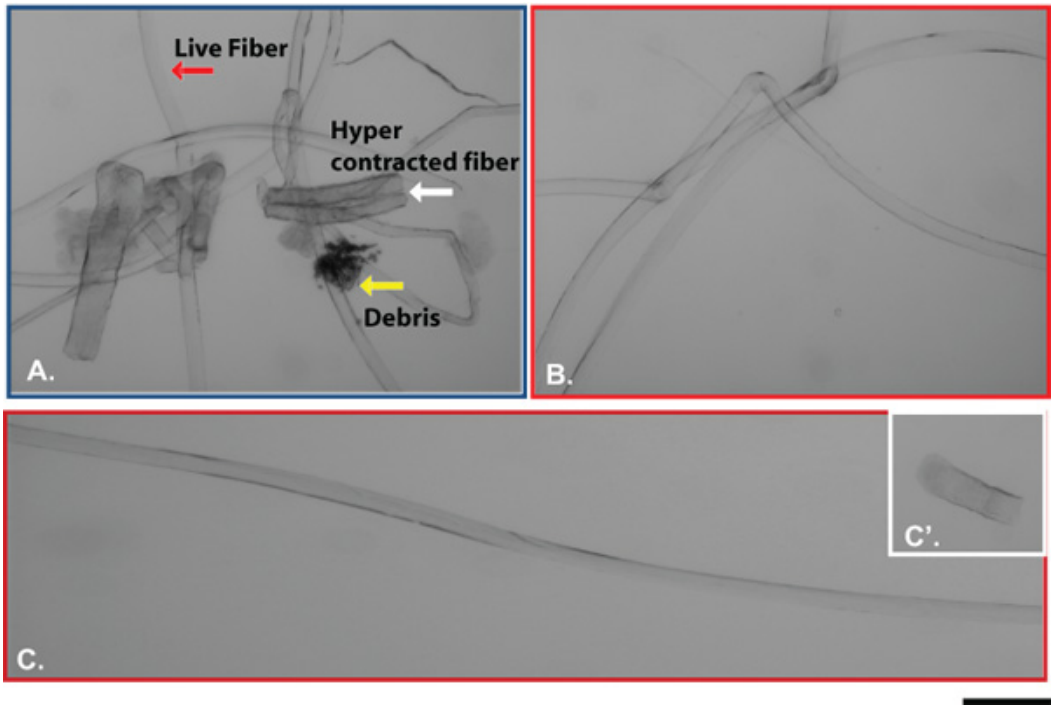

Figure 2. Representative results of a single myofiber isolation experiment. A . Bright field picture of a myofiber isolation experiment at the first wash step. Red arrow indicates live myofibers, white arrow indicates hyper contracted myofibers and yellow arrow indicates cells, myofiber or ECM debris. **B**. After consecutive washes in DMEM, only live myofibers remain. **C** and **C'**. Image represents a long intact live myofiber (**C**) and a short hyper contracted myofiber (**C'**). Bar 10 µm. Pictures were taken with a Zeiss Axio Observer Z1 microscope equipped with AxioCam HR.

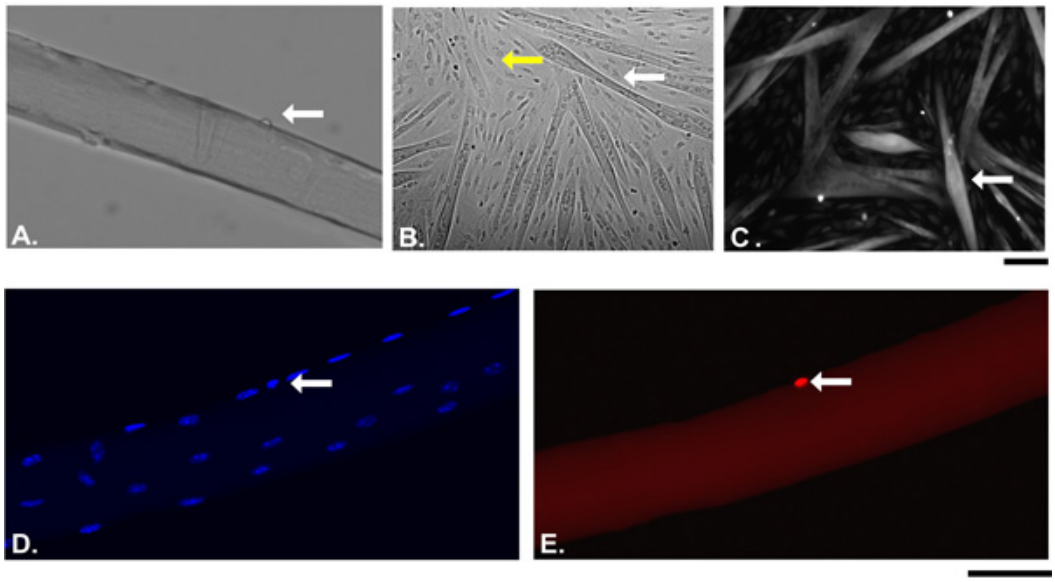

Figure 3. Representative results of a single myofiber culture experiment. A . Bright field picture of a single, live myofiber with its associated satellite cell (arrow) right after the isolation (Time 0). **B**. Single myofibers were plated on Matrigel and cultured in serum rich medium for 15 days. White arrow indicates differentiated myotubes as compared to single cells (yellow arrow) **C**. Single myofibers from a *Myf5Cre;RosaYFP* mouse were cultured as in **B**. Arrow indicates Myf5 derived myotubes. **D** and **E**. Single myofibers from *Pax7Cre;TdTomato* were isolated and fixed right after. Arrows indicate Pax7 positive quiescent satellite cell (**E**, red). Nuclei were counterstained with DAPI (**D**). Bar: 50 µm. Pictures were taken with a Zeiss Axio Observer Z1 microscope equipped with AxioCam HR.

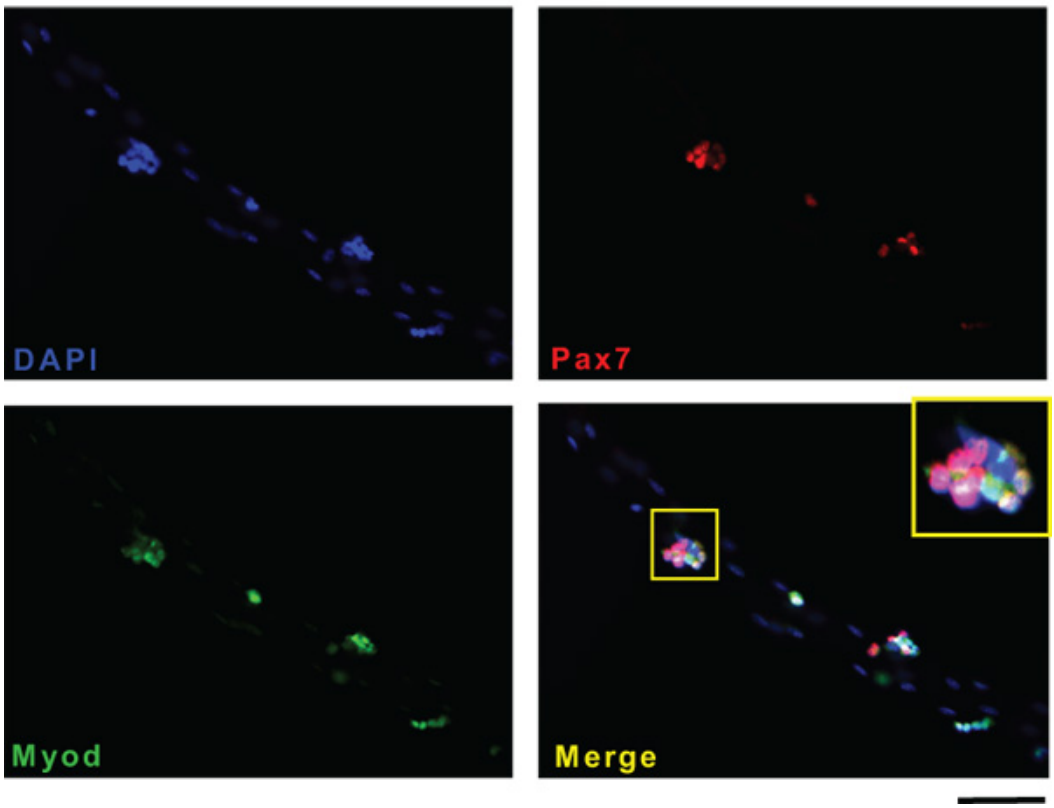

Figure 4. Example of immunofluorescence staining of satellite cells on myofibers. Single myofibers were isolated and cultured for 72 hr in floating conditions. Satellite cells on myofibers were stained for the satellite cell specific marker Pax7 (**B**, red) and the myogenic regulatory factor Myod (**C**, green). Nuclei were counterstained with DAPI (**A**). Bars: 50 µm. Pictures were taken with a Zeiss Axio Observer Z1 microscope equipped with AxioCam HR.

Muscle Dissection (5 min each muscle)	• Tendon to tendon isolation • Sharp tools • Minimal muscle damage
Muscle Digestion (30-45 min)	• Temperature sensitive • Avoid overdigestion
Fiber isolation	• Avoid over manipulation of fibers • Eliminate debris with several washes
Fiber Culture (Up to 3-4 weeks)	• Format: any • Coating: horse serum, Matrigel • Medium: basal or high serum

Table 1. Overview of the myofiber isolation protocol. The myofiber isolation protocol consists of 4 major steps. For each step, the approximate time and major critical points are discussed. For detailed discussion of each step, refer to the protocol text.

Discussion

The isolation and culture of single myofibers from intact muscles provides an excellent *in vitro* model to study the process of muscle regeneration. A unique feature of this system is the preservation of satellite cells in their physiological environment beneath the basal lamina. Most importantly, the technique can be used to investigate muscle stem cell behavior in both quiescence and activated states. Over the past 20 years, the myofiber culture system has provided meaningful insights into the biology of the satellite cell population with respect to both intrinsic and extrinsic determinants. By culturing individual myofibers, satellite cell heterogeneity with respect to myofiber, muscle type or regenerative potential has been addressed [15]. Elaborate studies using live imaging of single cultured fibers allowed for the gaining information on satellite cell migration pattern [16]. The acquisition of quantitative data is also possible. Although time consuming, it provides significant information on the distribution and occurrence of specific events (stem cells asymmetric division, proliferation and differentiation ratio, etc.). Together with previously described applications, protein or RNA extraction from single fibers is also possible, although isolation of pure population of satellite cells by FACS or other means may provide a better platform to investigate protein or gene expression changes at a molecular level. In our experience, the most critical step for successful fiber isolation is the "tendon to tendon" isolation (steps 2.5 to 2.9 in the protocol text). This guarantees that after muscle digestion, fibers are released from the EDL with minimal or no damage thus increasing their performance in the following steps.

Disclosures

No competing interests.

Acknowledgements

We would like to thank Sarah Dick for providing critical reading and comments. M.A.R. holds the Canada Research Chair in Molecular Genetics and is an International Research Scholar of the Howard Hughes Medical Institute. This work was supported by grants to MAR from the National Institutes of Health, the Howard Hughes Medical Institute, the Canadian Institutes of Health Research, the Muscular Dystrophy Association and the Canada Research Chair Program.

References

1. Bischoff, R. Proliferation of muscle satellite cells on intact myofibers in culture. *Dev. Biol.* **115** (1), 129-139 (1986).
2. Rosenblatt, J.D., Lunt, A.I., Parry, D.J., & Partridge, T.A. Culturing satellite cells from living single muscle fiber explants. *In Vitro Cell Dev. Biol. Anim.* **31** (10), 773-9 (1995).
3. Anderson, J.E., Wozniak, A.C., & Misunoya W. Single muscle fiber isolation and culture for cellular molecular, pharmacological, and evolutionary studies. *Methods Mol. Biol.* **798**, 85-102, Humana Press, New York, NY, 10013, USA, (2012).
4. Shefer, G. & Yablonka-Reuveni, Z. Isolation and culture of skeletal muscle myofibers as a means to analyze satellite cells. *Methods Mol. Biol.* **290**, 281-304, Human Press Inc, Totowa, NJ, (2005).
5. White, R.B., Biérinx, A.S., Gnocchi,V.F., & Zammit, P.S. Dynamics of muscle fibre growth during postnatal mouse development. *BMC Developmental Biology.* **10** (21), 1-11 (2010).
6. Siegel, A.L., Kuhlmann, P.K., & Cornelison, D.D. Muscle satellite cell proliferation and association: new insights from myofiber time-lapse imaging. *Skeletal Muscle.* **2** (1), 1-7 (2011).
7. Pasut, A., Oleynik, P., & Rudnicki, M.A. Isolation of muscle stem cells by fluorescence activated cell sorting cytometry. *Methods Mol. Biol.* **798**, 53-64, Humana Press, New York, NY, 10013, USA, (2012).
8. Engler, A.D., Griffin, M.A., Sen, S., Bonnemann, C.G., Sweeney, H.L., & Discher, D.E. Myotubes differentiate optimally on substrates with tissue-like stiffness: pathological implications for soft or stiff microenvironments. *J. Cell. Biol.* **166** (4), 877-87 (2004).
9. Boonen, K.J. & Post, M.J. The muscle stem cell niche: regulation of satellite cells during regeneration. *Tissue Eng. Part B Rev.* **14** (4), 419-31 (2008).
10. Wozniak, A.C. & Anderson, J.E. Single-fiber isolation and maintenance of satellite cell quiescence. *Biochem. Cell Biol.* **83** (5), 674-6 (2005).

11. Verma, M. & Asukura, A. Efficient Single Muscle Fiber Isolation from Alcohol-Fixed Adult Muscle following β-Galactosidase Staining for Satellite Cell Detection. *J. Histochem. Cytochem.* **59** (1), 60-7 (2001).
12. Wosniak, A.C., Pilipowics, O., *et al.* C-Met expression and mechanical activation of satellite cells on cultured muscle fibers. *J. Histochem. Cytochem.* **51** (11), 1437-45 (2003).
13. Huard, J., Feero, W.G., Watkin, S.C., Hoffman, E.P., Rosenblatt, J.D., & Glorioso, J.C. The basal lamina is a physical barrier to herpes simplex virus-mediated gene delivery to mature muscle fibers. *J. Virol.* **70** (11), 8117-23 (1996).
14. Feero, W.G., Rosenblatt, J.D., *et al.* Viral gene delivery to skeletal muscle: insights on maturation-dependent loss of fiber infectivity for adenovirus and herpes simplex type 1 viral vectors. *Hum. Gene Ther.* **8** (4), 371-80 (1997).
15. Kuang, S., Kuroda, K., Le grand, F., & Rudnicki, M.A. Asymmetric self-renewal and commitment of satellite stem cells in muscle. *Cell.* **129** (5), 999-1010 (2007).
16. Siegel, A.L, Atchison, K., Fisher, K.E., Davis, G.E., & Cornelison, DD. 3D timelapse analysis of muscle satellite cell motility. *Stem Cells.* **27** (10), 2527-38 (2009).
17. Seale, P., Sabourin, L.A., Girgis-Gabardo, A., Mansouri, A., Gruss, P., & Rudnicki, M.A. Pax7 is required for the specification of myogenic satellite cells. *Cell.* **102** (6), 777-86 (2000).
18. Zammit, P., Golding, J.P., Nagata, Y., Hudon, V., Partridge, T.A., & Beauchamp J.R. Muscle satellite cells adopt divergent fates: a mechanism for self-renewal? *J. Cell Biol.* **166** (3), 347-57 (2004).

Appendix B

Cell Metabolism
Article

MicroRNA-133 Controls Brown Adipose Determination in Skeletal Muscle Satellite Cells by Targeting Prdm16

Hang Yin,[1] Alessandra Pasut,[1] Vahab D. Soleimani,[1] C. Florian Bentzinger,[1] Ghadi Antoun,[2] Stephanie Thorn,[3] Patrick Seale,[4] Pasan Fernando,[3,5] Wilfred van IJcken,[6] Frank Grosveld,[6] Robert A. Dekemp,[3] Robert Boushel,[7] Mary-Ellen Harper,[2] and Michael A. Rudnicki[1,*]

[1]Regenerative Medicine Program, Ottawa Hospital Research Institute, Ottawa, ON K1H 8L6, Canada
[2]Department of Biochemistry, Microbiology, and Immunology, Faculty of Medicine, University of Ottawa, Ottawa, ON K1H 8M5, Canada
[3]University of Ottawa Heart Institute, Ottawa, ON K1Y 4W7, Canada
[4]Institute for Diabetes, Obesity, and Metabolism, University of Pennsylvania School of Medicine, Philadelphia, PA 19104, USA
[5]Nordion, Ottawa, ON K2K 1X8, Canada
[6]Department of Cell Biology and Genetics, Erasmus MC, Dr. Molewaterplein 50, 3015 GE Rotterdam, The Netherlands
[7]Department of Biomedical Sciences, University of Copenhagen, Department of Anaesthesia, Bispebjerg Hospital, 2400 Copenhagen NV, Denmark
*[redacted]

http://dx.doi.org/10.1016/j.cmet.2013.01.004

SUMMARY

Brown adipose tissue (BAT) is an energy-dispensing thermogenic tissue that plays an important role in balancing energy metabolism. Lineage-tracing experiments indicate that brown adipocytes are derived from myogenic progenitors during embryonic development. However, adult skeletal muscle stem cells (satellite cells) have long been considered uniformly determined toward the myogenic lineage. Here, we report that adult satellite cells give rise to brown adipocytes and that microRNA-133 regulates the choice between myogenic and brown adipose determination by targeting the 3′UTR of *Prdm16*. Antagonism of microRNA-133 during muscle regeneration increases uncoupled respiration, glucose uptake, and thermogenesis in local treated muscle and augments whole-body energy expenditure, improves glucose tolerance, and impedes the development of diet-induced obesity. Finally, we demonstrate that miR-133 levels are downregulated in mice exposed to cold, resulting in de novo generation of satellite cell-derived brown adipocytes. Therefore, microRNA-133 represents an important therapeutic target for the treatment of obesity.

INTRODUCTION

Obesity is associated with increased risks of type 2 diabetes, cardiovascular diseases, and cancer and thus poses a demanding challenge for global health care. Although diet and exercise are well-known defenses against obesity, the exacerbating epidemic of obesity has raised a major interest to develop alternative therapeutic strategies. Two distinct types of adipose tissues exist—white and brown. When dietary energy exceeds total body energy needs, the energy is stored mainly as triglycerides in white adipocytes. By contrast, brown adipocytes are specialized to dissipate energy in the form of body heat (thermogenesis) and are characterized by expression of uncoupling protein Ucp1 in their abundant mitochondria (Frontini and Cinti, 2010).

Active brown adipose tissue (BAT) can provide a natural defense against obesity. However, BAT is relatively scarce in adult humans, and its prevalence was not unequivocally recognized until recently (Cypess et al., 2009; Nedergaard et al., 2007; Ouellet et al., 2012; Saito et al., 2009; van Marken Lichtenbelt et al., 2009; Virtanen et al., 2009; Zingaretti et al., 2009). Intriguingly, the level of BAT activity in adult humans is negatively correlated to body mass index (Cypess et al., 2009; Nedergaard et al., 2010; Pfannenberg et al., 2010; van Marken Lichtenbelt et al., 2009). Experimental induction of BAT function in animal models is associated with a lean and healthy phenotype (Ghorbani and Himms-Hagen, 1997; Kopecky et al., 1995). As such, expanding and activating BAT thermogenesis opens a new avenue toward preventing/treating obesity and obesity-related metabolic disorders (Cypess and Kahn, 2010).

Lineage-tracing experiments have indicated that BAT is derived during embryogenesis from Pax7/Myf5-expressing skeletal muscle precursors located within dermomyotome (Atit et al., 2006; Lepper and Fan, 2010; Seale et al., 2008). Importantly, Prdm16, a zinc-finger transcription factor, has been demonstrated to be necessary and sufficient to establish the identity of the BAT lineage (Seale et al., 2007, 2008). In vitro, loss of function of Prdm16 promotes the myogenic differentiation of committed preadipocytes isolated from BAT, whereas Prdm16 gain of function leads to brown adipogenesis of the C2C12 myoblast cell line and myoblasts isolated from newborn mice (Seale et al., 2008). Similarly, Prdm16 is also both necessary and sufficient for the emergence of beige adipocytes in subcutaneous WAT (browning), which is linked with improved metabolic phenotypes (Seale et al., 2011).

Prdm16 determines BAT identity by activating the complete complement of brown fat genes while also repressing

WAT-specific (Kajimura et al., 2008) and muscle-specific programs (Seale et al., 2008). Notably, ablation of Prdm16 in BAT abolishes the expression of brown adipocyte-specific thermogenic genes (e.g., *Ucp1*), yet spares the terminal adipogenic differentiation and the expression of adipogenic markers that are common to both white and brown adipocytes (Seale et al., 2008). As such, Prdm16 represents a "master regulator" of brown adipogenesis particularly critical for brown adipose lineage determination.

The potent fate-switching function of Prdm16 in vitro implies that its expression be tightly regulated in myogenic cells in vivo. Satellite cells are adult skeletal muscle stem cells, which reside closely juxtaposed with contractile myofibers beneath the basal lamina (Chargé and Rudnicki, 2004). Satellite cells are quiescent in vivo under physiological conditions, whereas they can be activated in response to resistance training or muscle injury. When activated, satellite cells migrate from the myofibers and proliferate as committed myogenic precursors (myoblasts), which in turn undergo terminal myogenic differentiation (myogenesis) and fuse into multinucleated muscle cells (myotubes) (Chargé and Rudnicki, 2004). Notably, satellite cells are believed to be uniformly committed to the myogenic lineage, and it has been reported that they do not differentiate into adipocytes in vitro (Joe et al., 2010). This is consistent with the observation that Prdm16 is not detectable in satellite cells nor their daughter myogenic precursor cells (Seale et al., 2011).

Here we show that satellite cells are multipotent and can give rise to both myogenic and brown adipogenic lineages. The brown adipose determination of satellite cells is controlled by a myogenic microRNA, miR-133 that directly targets the 3′UTR of the *Prdm16* mRNA to repress Prdm16 expression. Inhibition of microRNA-133 during muscle regeneration elicits brown adipogenic commitment of satellite cells in vivo and induces their differentiation into interstitial brown adipocytes. Cold exposure results in downregulation of miR-133 and de novo generation of satellite cell-derived brown adipocytes. Taken together, our data reveal a central function of miR-133 in controlling Prdm16-dependent lineage determination of satellite cells and suggest a promising strategy for inducing active BAT in vivo from skeletal muscle stem cells.

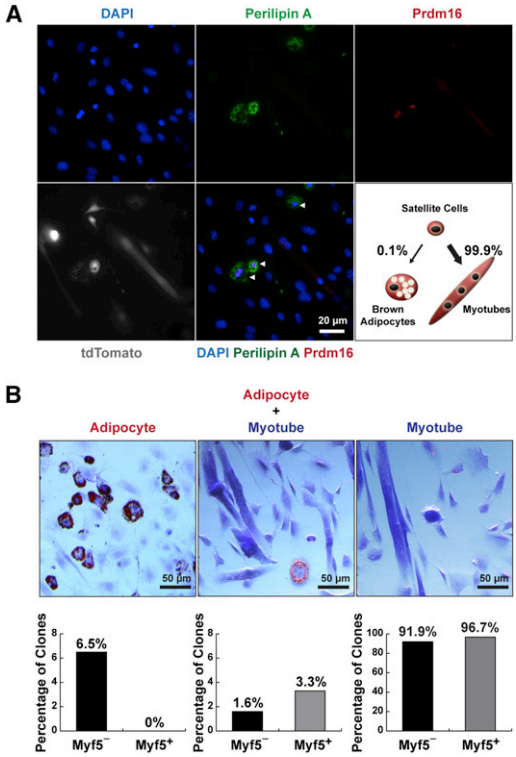

Figure 1. Satellite Cells Differentiate into Brown Adipocytes

(A) Satellite cells differentiated into brown adipocytes (arrowheads) in myofiber cultures under proadipogenic conditions. Myofibers (n > 600) with resident satellite cells were isolated from *Pax7-CreER/R26R-tdTomato* EDL muscles and cultured for 12 days in proadipogenic medium. Lineage-marked satellite cell-derived brown adipocytes expressed tdTomato and Prdm16, Perilipin A. (B) Clonal analysis of FACS-isolated single satellite stem cells and satellite myogenic progenitors (n > 2,000 for each cell type) indicates some satellite cells are bipotential. Approximately 1.6% of satellite stem cells and 3.3% satellite myogenic progenitors gave rise to mixed muscle and adipocyte-containing colonies. In addition, 6.5% of satellite stem cells clones but none of satellite myogenic progenitors gave rise to colonies uniformly composed of adipocytes. Shown are representative images of three types of clones derived from clonal satellite cell cultures stained with ORO, and the corresponding percentages from satellite stem cells ($Myf5^{-}$) and satellite myogenic progenitors ($Myf5^{+}$) clones.

See also Figure S1.

RESULTS

Single Satellite Cells Are Multipotent and Differentiate into Brown Adipocytes

In adult muscle, satellite cells are characterized by their specific expression of Pax7 in both quiescent and activated states (Seale et al., 2000). To investigate the capability of satellite cells in adult skeletal muscle to undergo brown adipogenic differentiation, we utilized a Cre/LoxP-based system for satellite cell lineage tracing (Nishijo et al., 2009). *Pax7-CreER;R26R-tdTomato* mice were injected with tamoxifin for 5 consecutive days at 6 weeks of age to induce permanent tdTomato expression in satellite cells and their descendants (see Figure S1A online).

From the extensor digitorum longus (EDL) muscles of these mice, we isolated single myofibers (n > 600), carrying labeled satellite cells embedded within their native niche, and cultured them under established proadipogenic conditions (Seale et al., 2008). We observed adipocytes at a low frequency, characterized by the presence of oil droplets and expression of cytoplasmic Perilipin A (a marker for differentiated adipocytes), mixed together with elongated multinucleated myotubes (Figure 1A). Importantly, these adipocytes were brown adipocytes, as evidenced by their nuclear expression of Prdm16 (Figure 1A). As expected, all multinucleated myotubes were labeled with tdTomato, indicating their satellite cell origin. Notably, $Prdm16^{pos}$ brown adipocytes were similarly labeled with tdTomato, indicating that they derived from Pax7-expressing satellite cells (Figure 1A). Overall, satellite-cell-derived brown adipocytes (SC_BA) accounted for 0.1% of tdTomato-labeled cells in these cultures. By contrast, brown adipogenic differentiation of satellite cells was not observed under promyogenic culture conditions (Kuang et al., 2007) (Figure S1B).

Satellite cells represent a heterogeneous population containing stem cells and committed cells (Wang and Rudnicki, 2012).

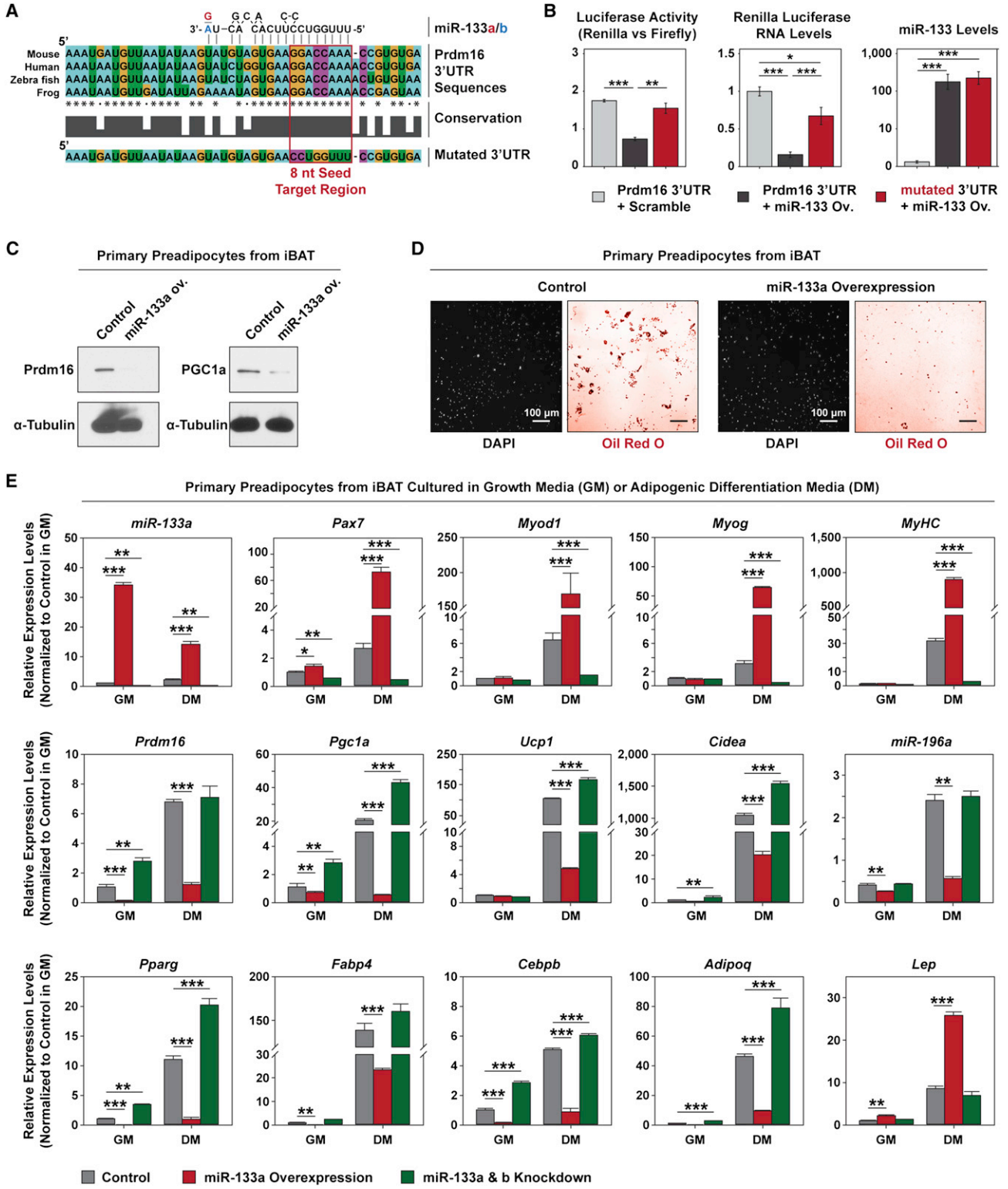

Figure 2. Prdm16 Is Targeted by miR-133

(A) *Prdm16* 3′UTR contains a conserved target site for both miR-133a and miR-133b. The absolutely conserved 8 nt seed sequences in multiple genomes and a mutated seed sequence used in this study (Prdm16_mutUTR) were enclosed in a red frame.

(B) Luciferase assays and RT-qPCR indicate miR-133 targets *Prdm16* 3′UTR and this repression depends on the predicted 8 nt seed sequence. Ectopic miR-133 was overexpressed in HEK293T cells together with *Renilla* luciferase reporter constructs containing either intact or mutated *Prdm16* 3′UTR. The repression of luciferase activity and expression by miR-133 was abolished by mutating the predicted 8 nt seed sequence.

(legend continued on next page)

By lineage tracing, we have previously identified a satellite stem cell population (Pax7^{pos}, Myf5-Cre-YFP^{neg}) that can undergo asymmetric cell divisions to generate committed satellite myogenic progenitors (Pax7^{pos}, Myf5-Cre-YFP^{pos}) (Kuang et al., 2007). To measure the potential of these two satellite cell subpopulations to undergo brown adipogenesis, we employed fluorescence-activated cell sorting (FACS) to isolate total satellite cells from *Pax7-ZsGreen;Myf5-Cre;R26R-tdTomato* mice on the basis of their ZsGreen fluorescence (Bosnakovski et al., 2008), and further separate into satellite stem cell (ZsGreen^{pos}, Myf5-Cre-tdTomato^{neg}) and satellite myogenic progenitor (ZsGreen^{pos}, Myf5-Cre-tdTomato^{pos}) subpopulations by tdTomato fluorescence (Figures S1C and S1D).

To address whether these two subpopulations of satellite cells are multipotent (myogenic and adipogenic) at the clonal level, we sorted single satellite stem cells or satellite myogenic progenitors into individual wells (n > 2,000 for each cell type). The reliability of sorting single satellite cells into individual wells was confirmed by visual inspection of all wells (Figure S1E). We found that 6.5% of single satellite stem cell-derived clones contained exclusively oil red O (ORO)-positive adipocytes, whereas this kind of clone was not observed from satellite myogenic progenitor clones (Figure 1B, left). Notably, 1.6% of satellite stem cell clones and 3.3% of satellite progenitor clones contained mixed adipocytes and myotubes, supporting the notion that satellite cells are multipotent (Figure 1B, middle). The majority of satellite cell clones exclusively formed muscle-containing colonies (Figure 1B, right). These data demonstrate that satellite cells are multipotent and can clonally give rise to both myogenic and brown adipogenic cells.

Prdm16 Is Targeted by miR-133

We hypothesized that brown adipose determination of satellite cells is controlled by microRNAs, which regulate the expression of Prdm16 or other brown adipose determinants. Therefore, we performed whole-transcriptome RNA sequencing (RNA-Seq) for satellite cells and brown preadipocytes isolated from adult hindlimb muscles and interscapular BAT (iBAT), respectively, by established FACS schemes (Scimè et al., 2005) (Figure S2A). We identified 580 mRNAs and 88 microRNAs, which are differentially expressed between two cell lineages (Figures S2B and S2C, Table S1, and Table S2).

Satellite cell-enriched microRNAs and their predicted transcription factor targets enriched in brown preadipocytes were plotted to identify negative regulatory networks (Figure S2D). Analysis of the network suggested that Prdm16 is repressed by the satellite cell-enriched miR-133a and miR-133b. We identified a highly conserved target site for miR-133a and miR-133b with an absolutely conserved 8 nt seed sequence in the 3′UTR of *Prdm16* mRNA (Figure 2A). The conservation of the seed sequence suggests biological relevance of these microRNAs in regulating Prdm16 expression in humans.

We performed luciferase assays and RT-qPCR to investigate the direct targeting of *Prdm16* 3′UTR by miR-133. HEK293T cells transfected with reporter plasmids containing the *Prdm16* 3′UTRs showed markedly decreased luciferase activity and luciferase mRNA level in the presence of ectopic miR-133 (Figure 2B). Mutation of the conserved 8 nt seed sequence abrogated the miR-133-induced repression of the *Prdm16* 3′UTR. Similar results were also observed in C2C12 myoblasts (Figure S2E).

miR-133 belongs to a group of myomiRs, which are enriched in muscle tissue and myogenic cells (Chen et al., 2006; Williams et al., 2009). We confirmed the inverse expression patterns of Prdm16 and miR-133 in FACS-sorted BAT progenitors, satellite cell populations, and cultured primary myoblasts (Figure S2F). Thus, we hypothesized that direct targeting of Prdm16 by miR-133 represents a potential regulatory mechanism in brown adipose determination.

Overexpression of miR-133 Impairs Lineage Commitment of Brown Preadipocytes

Primary brown preadipocytes express low but evident levels of miR-133 (Walden et al., 2009). Therefore, we tested the effects of miR-133 overexpression on the brown adipose lineage fate of primary brown preadipocytes. To avoid "off-target" and "overloading" side effects, we utilized a lentivirus-based microRNA expression system to elevate the endogenous levels of miR-133 in primary brown preadipocytes within a physiological range.

Lentiviral overexpression of miR-133 resulted in markedly reduced protein levels of Prdm16 and Pgc1-α, which is a Prdm16 target and critical for BAT-specific thermogenic gene expression (Seale et al., 2007) (Figure 2C). Moreover, overexpression of miR-133 strongly impaired adipogenic differentiation of brown preadipocytes at confluent density, as evidenced by reduced number of ORO^{pos} adipocytes in the differentiation cultures (Figure 2D).

We further performed RT-qPCR to investigate gene expression signatures associated with lineage commitment of brown preadipocytes in response to miR-133 overexpression or repression (Figure 2E). Overexpression of miR-133 decreased the expression of brown adipogenic markers (*Prdm16*, *Pgc1a*, *Ucp1*, *Cidea*, and *miR-196a*) as well as genes associated with general adipogenesis (*Pparg*, *Fabp4*, *Cebpb*, and *Adipoq*). Notably, overexpression of miR-133 led to markedly increased expression levels of myogenic transcription factors, *Pax7*, *MyoD*, and *Myogenin* as well as a myogenic differentiation

(C) Immunoblots reveals that lentiviral miR-133 overexpression (ov.) in primary brown preadipocytes repressed Prdm16 and Pgc1-α protein levels.

(D) Representative images depict that adipogenic differentiation from primary brown preadipocytes was severely impaired by miR-133 overexpression. ORO staining revealed drastically reduced number of differentiated adipocytes with oil droplets in the miR-133 ov. culture, while DAPI staining of the same fields indicated that same near-confluent density of cells were present for both cultures.

(E) RT-qPCR shows lentiviral overexpression of miR-133 or inhibition of miR-133 by antisense oligos impaired or enhanced brown adipogenic commitment in primary brown preadipocytes, respectively. Notably, impaired brown adipogenic commitment in the miR-133 ov. culture was companied with the emergence of myogenic differentiation, as evidenced by increased expression of myogenic markers (*Pax7*, *MyoD*, *Myog*, *MyHC*), and white adipogenic differentiation, as evidenced by increased expression of *Leptin*.

Error bars, SEM. See also Figure S2.

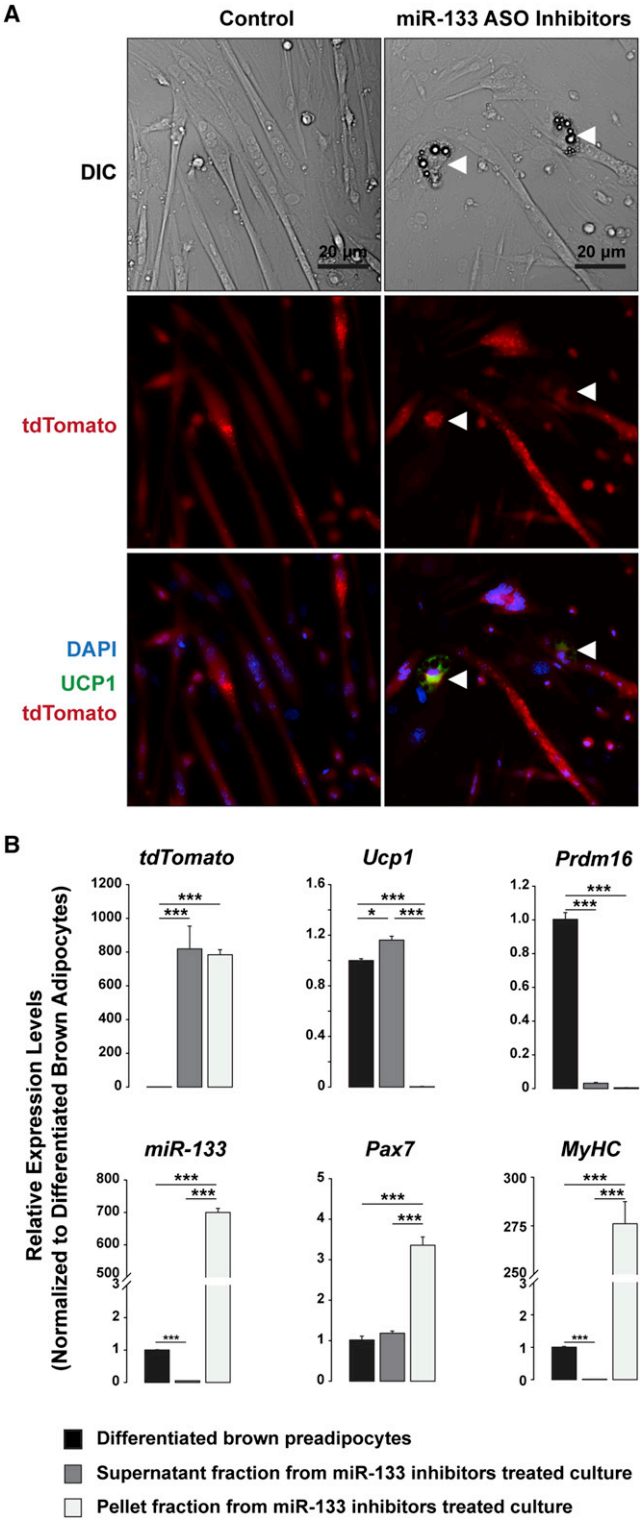

Figure 3. miR-133 Prevents Brown Adipose Determination in Satellite Cells

(A) Inhibition of miR-133 induced satellite cells to differentiate into brown adipocytes (arrowheads) in myofiber cultures under proadipogenic conditions. Myofibers (n > 300) with resident satellite cells were isolated from *Pax7-CreER/R26R-tdTomato* EDL muscles and transfected with mixed inhibitors for miR-133a and miR-133b or a control scramble inhibitor. Lineage-marked satellite cell-derived brown adipocytes (SC_BA) expressed tdTomato and Ucp1.

(B) RT-qPCR reveals gene expression signatures of SC_BAs as compared to those of myotubes and differentiated primary brown adipocytes. miR-133 inhibitor-treated myofiber cultures were centrifuged to separate the supernatant faction enriched for SC_BAs and the pellet fraction which contains mostly myotubes.

Error bars, SEM. See also Figure S3.

marker, *myosin heavy chain 2* (*MyHC*). A white adipocyte-specific marker, *Leptin*, was also increased in miR-133 overexpression culture. By contrast, inhibition of miR-133 enhanced brown adipogenic commitment and differentiation, as evidenced by increased expression of *Prdm16*, *Pgc1a*, *Ucp1*, *Cidea*, *Pparg*, *Cebpb*, and *Adipoq*, as well as decreased expression of *Pax7*, *MyoD*, *Myogenin*, and *MyHC* (Figure 2E). These data indicate that miR-133 regulates brown adipose determination in primary brown preadipocytes by targeting Prdm16.

miR-133 Prevents Brown Adipose Determination in Satellite Cells

To investigate whether knockdown of miR-133 promotes brown adipose determination, we transfected satellite cells embedded within individual myofibers with mixtures of either antisense oligonucleotide (ASO) inhibitors or mimetics for miR-133a and miR-133b (>300 myofibers per treatment group) (Figure S3A). Remarkably, inhibition of miR-133 resulted in a pronounced increase of brown adipocytes in the culture, characterized by their nuclear Prdm16 staining and presence of oil droplets (Figure S3B, right). Conversely, no brown adipocytes were observed in myofiber cultures transfected with miR-133 mimetics (Figure S3B, middle).

To confirm that these brown adipocytes were derived from satellite cells, tdTomato-labeled satellite cells on myofibers isolated from *Pax7-CreER;R26R-tdTomato* mice (>300 myofibers per treatment group) were transfected with miR-133 ASO inhibitors (Figure 3A). Notably, we observed a dramatic 16-fold increase in the number of satellite cell-derived brown adipocytes (SC_BA), as evidenced by their Ucp1 and tdTomato double staining in response to miR-133 inhibition (Figure 3A). Thus, we conclude that miR-133 inhibition in satellite cells is sufficient to induce brown adipose determination.

The molecular nature of SC_BA was characterized following their enrichment by centrifugation based on their low density. After centrifugation, the supernatant fraction was enriched for SC_BA, whereas the pellet fraction was enriched for myotubes. The gene expression profiles of these SC_BA and myotube fractions were then compared with those of cultured differentiated brown preadipocytes originally also isolated from *Pax7-CreER;R26R-tdTomato* mice (Figure 3B). RT-qPCR revealed that the SC_BA-enriched supernatant fraction contained comparable levels of *tdTomato* mRNA relative to the myotube-enriched pellet fraction, consistent with the common satellite cell origin of these two types of cells. By contrast, the preadipocyte-derived brown adipocytes did not express *tdTomato*, confirming that Pax7 was not expressed in iBAT during tamoxifen induction. Intriguingly, SC_BA expressed a high level of *Ucp1* but less *Prdm16* relative to brown adipocytes, suggesting that a low level of Prdm16 is sufficient to support brown adipocyte determination

in vitro. Consistent with miR-133 inhibitor treatment, SC_BA contained lower *miR-133* levels relative to brown adipocytes. As expected, the myotube fraction was enriched for *miR-133*, *Pax7*, and *MyHC* yet devoid of *Ucp1* mRNA. Taken together, these data support the hypothesis that miR-133 expression enforces myogenic commitment of satellite cells by targeting Prdm16 expression and repressing brown adipogenic determination.

We next investigated whether miR-133 represses brown adipose determination by targeting genes in addition to Prdm16. To address this question, we transiently expressed ectopic miR-133 in C3H10T1/2 mesenchymal progenitors in the absence or presence of ectopic Prdm16 lacking its 3′UTR (Prdm16_CDS) during the adipogenic determination stage (before adipogenic induction). In this manner, we could assess whether miR-133 targets any other brown adipogenic determinants during adipogenic determination, whose repression cannot be rescued by Prdm16 ectopic expression (Figure S3C).

In the absence of Prdm16, ectopic expression of miR-133 moderately compromised the white adipose determination and differentiation of C3H10T1/2 progenitors, as evidenced by reduced Perilipin A expression combined with lack of Prdm16 or Ucp1 expression (Figures S3D and S3E). On the other hand, ectopic expression of Prdm16 markedly promoted brown adipose determination and differentiation, as evidenced by increased Perilipin A expression combined with strong induction of Ucp1 and Pgc1α. Critically, ectopic expression of miR-133 together with Prdm16 led to a comparable, if not improved, brown adipocyte phenotype as compared to Prdm16 overexpression alone. In addition, overexpression of miR-133 alone in C3H10T1/2 progenitors appeared not to induce myogenic determination as observed from brown preadipocyte cultures (Figure S3E, MyHC panel). These findings are consistent with the absence of miR-133 seed sequence in the 3′UTRs of *Pparg*, *Pgc1a/b*, *Cebpa/b/d*, and *Ucp1*. Therefore, we conclude that miR-133 prevents brown adipose determination by primarily targeting Prdm16.

Antagonism of miR-133 Induces Brown Adipose Determination of Satellite Cells during Muscle Regeneration

To investigate miR-133 function in brown adipose determination of satellite cells in vivo, we synthesized miR-133 antagomiR (miR-133 ASO) with an antisense sequence to both miR-133a and miR-133b, as well as a control "antagomiR" (control ASO) with the same chemical modifications and not antisense to any mouse gene or EST sequence (see the Experimental Procedures). We performed lineage tracing to distinguish effects of miR-133 ASO on satellite cells versus other cell types. Six-week-old *Pax7-CreER;R26R-tdTomato* mice were treated with tamoxifin as before (five consecutive daily injections), then aged to 10 weeks of age prior to initiating the experiment. Control ASO versus miR-133 ASO were injected into tibialis anterior (TA) muscles 3 days following saline injection (quiescent state) or cardiotoxin injection (to induce satellite cell activation) (Figure S4A). After 1 month, RT-qPCR was performed using RNA isolated from several tissues to evaluate the efficacy and scope of miR-133 ASO administration.

We detected striking reduction of both miR-133a and miR-133b expression within the TA muscles administrated with miR-133 ASO, with more prominent effects observed in resting muscles injected with miR-133 ASO (Figure 4A). In fact, miR-133 ASO injected into resting muscles also repressed miR-133a/b expression in the contralateral TA muscles, suggesting diffusion of this antagomiR under this condition. Such a "leaking" effect was not present when miR-133 ASO was injected into regenerating muscles. Notably, miR-133 expression in the myocardium was unaffected by the intramuscular administration of miR-133 ASO. In addition, miR-133 ASO had no effect on *let-7a* microRNA expression, confirming its specificity. Accordingly, we detected increased *Ucp1* mRNA within miR-133 ASO-injected regenerating muscle, yet not within other tissues or miR-133 ASO-injected resting muscle (Figure 4A). Similar repression of *miR-133a/b* and induction of *Ucp1* mRNA were detected after 3 months of a single miR-133 ASO injection in regenerating muscle, indicating long-lasting effects of this ASO in muscle (Figure S4B). Corroborating the RT-qPCR results, Ucp1 protein was specifically detected by immunoblotting of extracts from regenerated TA muscles that had received miR-133 ASO, but not in contralateral muscles or under other conditions (Figure 4B and Figure S4C). By comparison, Ucp3, a muscle abundant uncoupling protein, was largely unaffected by miR-133 ASO administration (Figure 4B). miR-133 ASO treatment following frozen injury-induced muscle regeneration similarly induced *Ucp1* mRNA level in treated TA muscle (Figure S4D).

To investigate whether miR-133 ASO was inducing satellite cells to undergo brown adipose determination in vivo, we performed immunofluorescence microscopy on cross-sections prepared from regenerating TA muscles treated with control- or miR-133 ASO (Figures 4C and 4D). Staining for Ucp1 and basal lamina-located Laminin confirmed Ucp1 staining only within miR-133 ASO-treated regenerating muscles. Moreover, we found that Ucp1^{pos} cells were located within muscle interstitium, distinct from surrounding myofibers ensheathed within the basal lamina (Figure 4C). In addition, we observed that these interstitial cells were immunoreactive to Perilipin A and nuclear Prdm16 (Figure 4D). Most importantly, the majority of these induced brown adipocytes were also labeled with tdTomato, indicating that they were derived from Pax7-expressing satellite cells (Figures 4C and 4D).

We observed markedly increased numbers of interstitial cells (Figure S4E) and ORO-stained cells (Figure S4F) located between regenerating myofibers in response to miR-133 ASO treatment. ASO-treated muscles contained on average 15.6 Ucp1^{pos} brown adipocytes per section, of which 83.3% were derived from satellite cells (Figure S4G). Also, each cross-section of miR-133 ASO-treated muscle contained on average 31.6 Prdm16^{pos} cells, of which 76.8% were derived from satellite cells (Figure S4H). Presumably, this difference reflects the expression of Prdm16 in lineage-committed yet undifferentiated brown preadipocytes. The remaining ~20% tdTomato^{neg} brown adipocytes may originate from unlabeled satellite cells or from other cell sources (data not shown).

Small amounts of BAT have previously been reported to exist in hindlimb muscles of obesity-resistant *129S6/SvEvTac* mice, but not in obesity-prone *C57BL/6* mice (Almind et al., 2007). By immunoblotting, we detected ectopically induced Ucp1 protein expression in miR-133 ASO-treated muscles (2 months after treatment) of *C57BL/6* mice fed with either a regular diet

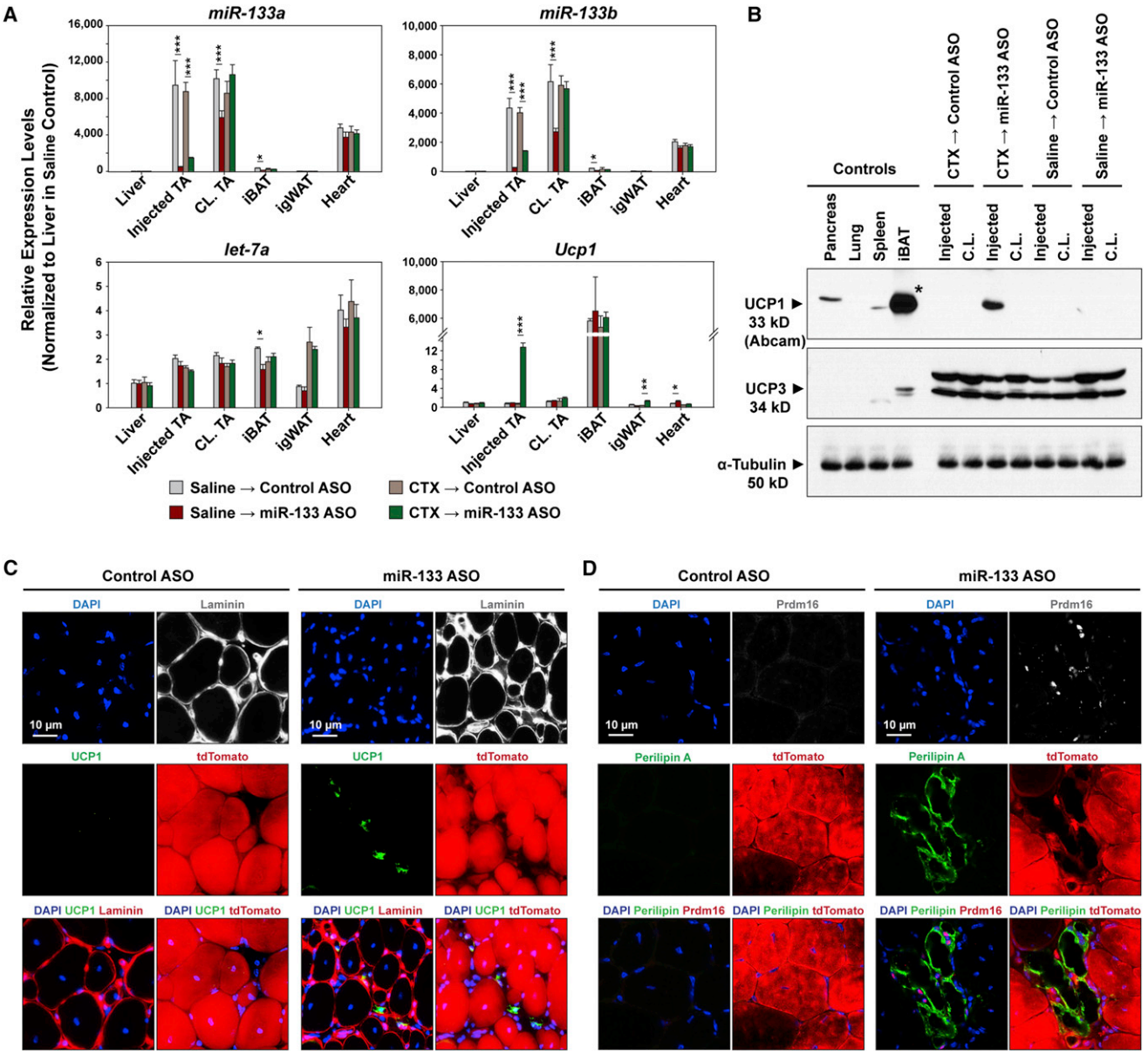

Figure 4. Antagonism of miR-133 Induces Brown Adipose Determination of Satellite Cells during Muscle Regeneration

(A) High efficacy and specificity of miR-133 antagomiR (ASO) in vivo. RT-qPCR indicates reduced expression of both *miR-133a* and *miR-133b*, but not *let-7a* in response to intramuscular miR-133 ASO administration. *Ucp1* mRNA was drastically induced in regenerating TA muscles by miR-133 ASO.

(B) Immunoblots reveal the evident induction of Ucp1, but not Ucp3, in regenerating TA muscles in response to miR-133 ASO treatment. Asterisk denotes that the loading of the iBAT lane on the Ucp1 immunoblot was 1/100 of other lanes to avoid overloading.

(C and D) miR-133 antagonism during muscle regeneration induced satellite cells to differentiate into brown adipocytes located within the muscle interstitium. Representative images of TA muscle cross-sections stained with Ucp1 and Laminin (C) or Prdm16 and Perilipin A (D) together with tdTomato native fluorescence revealed SC_BAs within the muscle interstitium.

Error bars, SEM. See also Figure S4.

(RD) or a high-fat diet (HFD) (Figure 5A). Consistently, we did not observe Ucp1 expression in either control ASO-treated muscles or contralateral resting muscles under either diet condition. H/E staining and Ucp1 immunohistochemistry further confirmed the efficacy of miR-133 ASO in inducing ectopic Ucp1^{pos} brown adipocytes within muscle interstitium of *C57BL/6* mice under both diet conditions (2 months after treatment) (Figure 5B).

miR-133 Antagonism Induces Metabolically Active Brown Adipocytes in Muscle

We next investigated whether miR-133 ASO-induced BAT in muscle is metabolic active and can function as authentic BAT. To quantify bioenergetic effects of miR-133 ASO-induced BAT in muscle, we performed high-resolution respirometry on TA muscles after 2 months of either control or miR-133 ASO

treatment (*C57BL/6* males fed on RD, n = 6 in each treatment group). We applied a two-step protocol that was specifically designed to reveal the metabolic functions of relatively rare BAT embedded within skeletal muscle (see the Supplemental Experimental Procedures). Compared to skeletal muscle, brown adipocytes have conspicuously higher uncoupled respiration rates particularly in response to fatty acids (FAs), which is due to their characteristic expression of mitochondrial Ucp1 (Cannon and Nedergaard, 2004). Thus, we first followed a well-established protocol to measure FA-induced uncoupled respiration in intact (nonpermeabilized) muscle preparations (Figure 5C) (Chance and Williams, 1955). We found that titration of octanoyl carnitine (a medium-chain FA covalently linked to carnitine, which can enter freely into intact cells and also into mitochrondrion via acylcarnitine translocase [Houten and Wanders, 2010]) increased mitochondrial respiration rate to 13.5 ± 1 $pmol \cdot s^{-1} \cdot mg^{-1}$ in miR-133 ASO-treated TA muscle compared to 7.7 ± 1 $pmol \cdot s^{-1} \cdot mg^{-1}$ in control (Figure 5D, uncoupled/intact cells). This marked difference in the response to FAs is highly consistent with reported acute activation of mitochondrial respiration rates in brown adipocytes exposed to FAs (Matthias et al., 2000).

We next sought to test whether this 1.75-fold increase in the respiration rate was due to potential changes in muscle cells. If these changes indeed occurred, we expected to detect similar increased lipid oxidative phosphorylation capacity in permeabilized muscle preparations (permeabilization allows various substrates to pass through the cell membrane; see the Supplemental Experimental Procedures). We measured maximal electron flow through electron-transferring flavoprotein (ETF) in a separate portion of TA muscles in the presence of ADP. In response to ADP, the lipid oxidative phosphorylation capacity was 13.0 ± 1 $pmol \cdot s^{-1} \cdot mg^{-1}$ in the control muscle as compared to 13.8 ± 3 $pmol \cdot s^{-1} \cdot mg^{-1}$ in the miR-133 ASO-treated muscles (Figure 5D, ETF/permeabilized cells). This observation strongly supports the notion that the higher respiration rate in intact miR-133 ASO-treated muscle is due to FA-induced uncoupling in brown adipocytes, not in muscle cells. Therefore, we estimate that the induction of uncoupling respiration by miR-133 ASO leads to an additional 0.3 $cal \cdot hr^{-1} \cdot mg^{-1}$ of energy expenditure in the treated TA muscle.

To further investigate possible bioenergetic effects of miR-133 ASO on muscle cells, we compared coupled state 3 respiration rates in treated and control permeabilized muscle tissues under full electron supply through complexes I and II (Figure 5D, permeabilized cells). No difference in electron transport through complex I (NADH dehydrogenase) between control and treated muscles was observed after electron transport through ETF was inhibited by the titration of glutamate (treated = 33 ± 3 $pmol \cdot s^{-1} \cdot mg^{-1}$, control = 28 ± 2 $pmol \cdot s^{-1} \cdot mg^{-1}$, p = 0.2). Maximal cellular state 3 respiration or oxidative phosphorylation capacity (P_{I+II}) was induced with the addition of succinate to provide additional electron flow through complex II (succinate dehydrogenase). This capacity reflects the maximal mitochondrial capacity to catalyze Redox reactions that are primarily coupled to the production of ATP via ATP synthase. Again, no difference in maximal coupled respiration between control and miR-133 ASO-treated muscles was observed (Figure 5D, P_{I+II}/permeabilized cells). Similar results were derived from contralateral soleus muscles of control or miR-133 ASO-treated mice (Figure S5A). As both glutamate and succinate are poor substrates for BAT mitochondria (Cannon and Nedergaard, 2001), these results rule out any significant bioenergetic effect of miR-133 ASO on skeletal muscle cells.

Altogether, these data support the assertion that miR-133 ASO treatment in regenerating muscle results in unaltered coupled respiration in treated muscle cells but elicits drastic increases in uncoupled respiration, presumably owing to ectopically induced brown adipocytes within the muscle interstitium.

Metabolically active BAT has been identified in adult human by [^{18}F]-fluorodeoxyglucose positron emission tomography ([^{18}F]-FDG PET), due to dramatic glucose uptake by this tissue after sympathetic activation (Nedergaard et al., 2007). To visualize active BAT within muscle, we performed [^{18}F]-FDG PET imaging on control or miR-133 ASO-treated mice (n = 5 for 133 ASO-treated mice, n = 4 for control-treated muscle; 2 months after treatment) after acute sympathetic activation by selective β3-adrenergic receptor agonist, CL316,243. We observed a dramatic increase of FDG uptake in miR-133 ASO-treated TA muscles compared to contralateral TA muscles or TA muscles within control ASO-treated mice (Figure 5E and Figure S5B). To rule out possible direct and indirect effects of CL316,243 on glucose/FDG uptake by skeletal muscle cells, we normalized FDG activities derived from regions of interest (ROIs) of treated TA muscles to those of contralateral TA muscles (Figure 5F). On average, miR-133 ASO-treated TA muscles after CL316,243-stimulated sympathetic activation exhibited a 1.3-fold increase of glucose/FDG uptake compared to control, strongly arguing that the ectopic-induced brown adipocytes in miR-133 ASO-treated TA muscles are metabolically active upon activation. Such a drastic increase was not observed without the sympathetic activation preceding anesthesia (baseline). As a reference, glucose/FDG uptake by iBAT expectedly increased 2.3- to 2.5-fold after CL316,243-stimulated sympathetic activation in both control and miR-133 ASO-treated mice (Figure 5F).

A hallmark of active brown adipocytes is their unique thermogenic capability via extensive uncoupled respiration in abundant mitochondria (Cannon and Nedergaard, 2004). Therefore, we directly assessed the thermogenic capability of muscle-embedded brown adipocytes by thermographic imaging of control- or miR-133 ASO-treated mice fed with either RD or HFD (n = 5 per treatment group per diet group; Figure 5G). We observed increased surface temperatures on miR-133 ASO-treated hindlimbs compared to contralateral hindlimbs or hindlimbs of control ASO-treated mice (Figure 5G). On average, the surface temperatures on miR-133 ASO-treated hindlimbs were 0.7°C or 0.9°C higher than control hindlimbs for mice fed with RD or HFD, respectively (Figure 5H). We observed no difference in expression of *IL-1β* and *TNF-α* between control and treated muscles, supporting the assertion that the temperature increase is not due to inflammation (Figure S5C).

Taken together, our data provide compelling evidence that the induced intramuscular BAT induced by miR-133 ASO treatment is metabolically active.

Antagonism of miR-133 during Muscle Regeneration Reduced Adiposity, Augmented Energy Expenditure, and Improved Glucose Tolerance

Intramuscular brown adipocytes have been described in *129S6/SvEvTac* mice and in *Lxr*$^{-/-}$ mice (deficient for Liver X receptors),

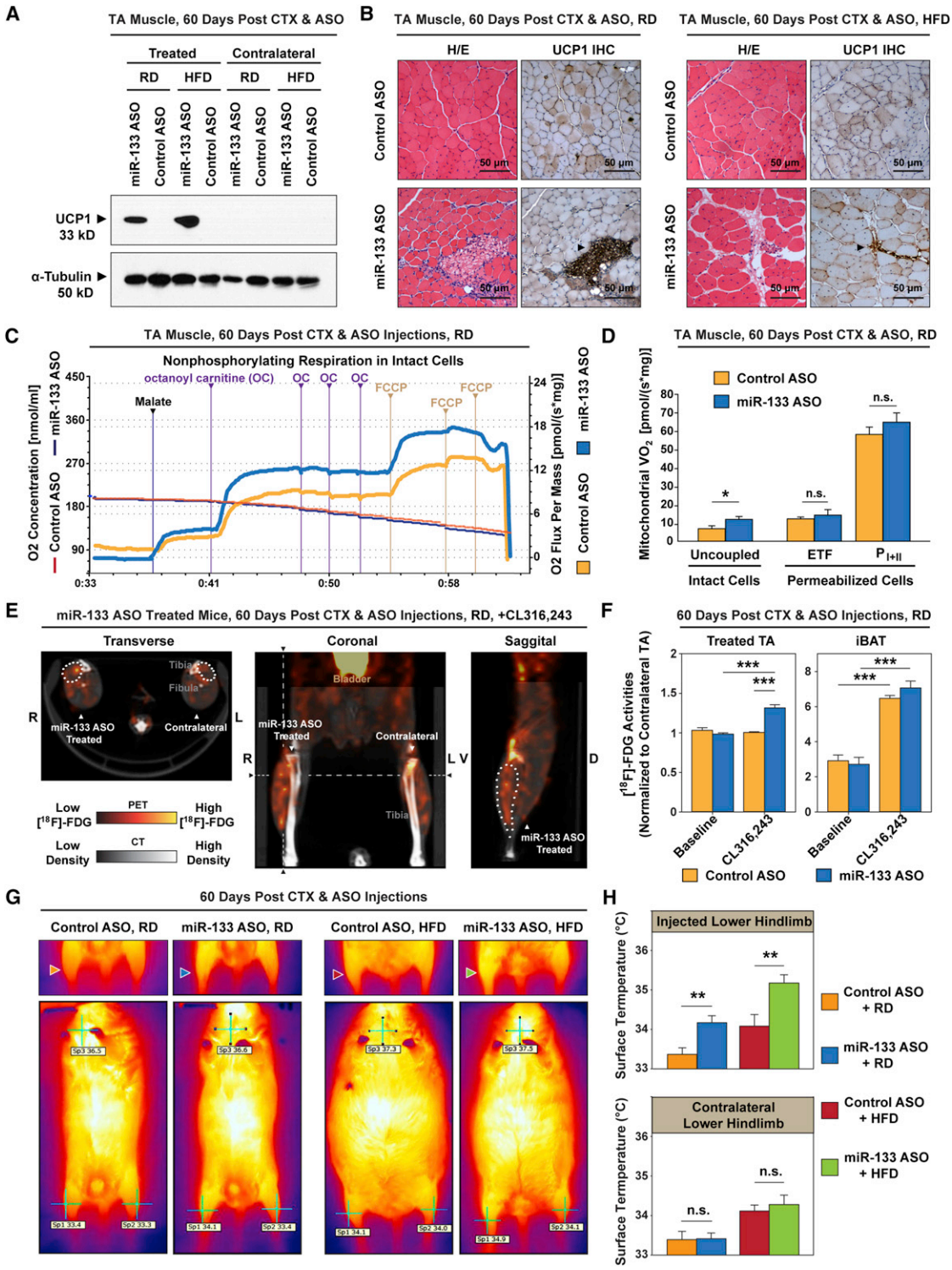

Figure 5. miR-133 Antagonism Induces Metabolically Active Brown Adipocytes in Muscle

(A) Immunoblots reveal the induction of Ucp1 in regenerating TA muscles by miR-133 antagonism in *C57BL/6* mice fed with either a regular diet (RD) or a high-fat diet (HFD). The contralateral TA muscles were included as control.

(B) Hematoxylin and eosin (H/E) staining and immunohistochemistry (IHC) of Ucp1 protein reveal that miR-133 antagonism-induced brown adipocytes located within the muscle interstitium (arrowheads) under both diet conditions.

(C) Representative oxygraph tracings from high-resolution respirometry depict markedly increased uncoupled (nonphosphorylating) respiration in intact (non-permeabilized) miR-133 ASO-treated TA muscles compared to control. Notably, octanoyl carnitine (OC) markedly increased the O_2 consumption in miR-133 ASO-treated TA muscles compared to control. Responses before reoxygenation (which showed no O_2 diffusion limitation) and titration of antimycin A are shown.

(legend continued on next page)

both of which display increased energy expenditure and resistance to obesity (Almind et al., 2007; Kalaany et al., 2005). We therefore assessed systematic metabolic consequences of miR-133 ASO treatment in regenerating TA muscle.

Treated and control *C57BL/6* male mice were raised on either RD or HFD in individual cages at 22°C (n = 5 per treatment per diet group). In both diet groups, miR-133 ASO-treated mice were obviously leaner than the control mice at 4 months after treatment (Figure 6A). Quantitatively, miR-133 ASO-treated mice displayed reduced gain in body weight over the 4 month period after ASO administration (Figure 6B). Close examination revealed significant reduction of weights in inguinal white fat depots (igWAT) and epididymal white fat depots (epiWAT), yet the mass of iBAT depots and treated TA muscles was unaffected (Figure S6A).

To assess whether miR-133 ASO treatment leads to increased whole-body energy expenditure, we carried out indirect calorimetry studies at 2–3 months after ASO treatment on control and miR-133 ASO-treated mice (*C57BL/6*, male, individually caged, n = 5 per treatment group per diet group; Figure 6C and Figure S6B). We detected a significant increase of total energy expenditure in miR-133 ASO-treated mice during light cycle (Figure 6C, left) without change in physical activities (Figure 6D, left). Intriguingly, this amount of energy expenditure is coincident with the increase of mitochondrial respirometry-measured energy expenditure in miR-133 ASO-treated TA muscles after adjustment with TA muscle mass (Figure S6A; 0.3 $cal \cdot hr^{-1} \cdot mg^{-1} \times 75\ mg = 0.0225\ kcal \cdot hr^{-1}$). Thus, we reasoned that increased uncoupled respiration due to ectopically induced intramuscular BAT likely contributes significantly to the total energy expenditure increase in light cycle. In dark cycle (when mice are active and feeding), the energy expenditure is conspicuously high in miR-133 ASO-treated mice (Figure 6C, right), which is associated with increased physical activities for the mice during the dark cycle (Figure 6D, right).

Similarly, we detected significantly increased total energy expenditure in miR-133 ASO-treated mice fed the HFD during light cycle (Figure S6B, left), without a difference in physical activities (Figure S6C, left). No significant increase in energy expenditure or physical activity was recorded in these mice over the dark cycle when compared to control mice (Figures S6B and S6C, right panels). This discrepancy may be related to the abnormally low respiratory exchange ratio (~0.76) in the control mice fed with HFD (Figure S6D), which indicates an increased proportion of lipid oxidation in the control mice. The 24 hr food intake in miR-133 ASO-treated mice was comparable to that of control mice for both diet groups (Figure S6E), suggesting the reduction of body weight is likely due to the enhanced thermogenesis, and hence lower food efficiency, in the mice. Intriguingly, miR-133 ASO treatment also led to much improved glucose tolerance in both diet groups (Figure 6E and Figure S6F). In addition, H/E staining and microscopy of tissue sections from fat depots and liver revealed that miR-133 ASO-treated mice exhibited reduced numbers of infiltrating inflammatory cells in epiWAT and reduced liver steatosis when fed the HFD (Figure S6G). Notably, the body weight and glucose tolerance status of our control mice resemble those of *C57BL/6* mice (in the same age) reported in numerous studies, which argues that the beneficial effects of miR-133 ASO treatment was not due to any cryptic effect of our control antagomiR.

Therefore, we conclude that miR-133 antagonism by ASO injection during muscle regeneration elicits profound changes in energy metabolism at the whole-body level, consistent with a leaner and healthier phenotype.

The Expression of miR-133 Is Downregulated In Skeletal Muscles after Cold Exposure, which Is Coincident with Emergence of Satellite Cell-Derived Brown Adipocytes

We next investigated whether the brown adipose determination of satellite cells occurs under physiological conditions that downregulate miR-133 expression. It has been reported that chronic cold exposure induces Ucp-1^{pos} adipocytes ("brite" or "beige" adipocytes), which morphologically resemble brown adipocytes yet arise from a non-Myf5 cell lineage, in subcutaneous WAT (Frontini and Cinti, 2010; Seale et al., 2011). We performed RT-qPCR using RNA isolated from multiple adipose and muscle tissues to evaluate the expression of miR-133 and BAT markers (Prdm16 and Ucp1) in response to cold exposure (1 week at 4°C; Figure 7A). We found cold exposure represses the expression of miR-133 in all investigated skeletal muscle

(D) High-resolution respirometry reveals a marked increase of uncoupled respiration in miR-133 ASO-treated TA muscles (intact cells) as well as comparable levels of fatty acid β-oxidation-mediated electron transport through electron-transferring flavoprotein (ETF) and maximal oxidative phosphorylation capacity (P_{I+II}) in control and miR-133 ASO-treated, permeabilized TA muscles (n = 6 per group). Notably, the respiration rate in miR-133 ASO-treated permabilized muscle was comparable to that of control muscle after titration of ADP (ETF).

(E) Representative ^{18}F-FDG microPET/CT images of miR-133 ASO-treated mice depict increased FDG uptake in the ASO-treated TA muscle compared to the contralateral nontreated TA muscle in response to acute CL316,243 treatment. Notably, hot spots with extremely high ^{18}F-FDG activities, presumably representing clusters of active brown adipocytes, were only present within miR-133 ASO-treated TA muscles. Dashed lines denote the levels for transverse and sagittal cross-sections. The position of miR-133 ASO-treated TA muscle was demarcated by dots on these cross-sections.

(F) Quantitative ^{18}F-FDG activities within regions of interest (ROIs) reveal marked increases of FDG uptake in miR-133 ASO-treated TA muscles after acute CL316,243 treatment (n = 5 for miR-133 ASO-treated group, n = 4 for control ASO-treated group). We normalized the ^{18}F-FDG activities within ROIs of treated TA muscles to those of contralateral TA muscles in order to cancel out potential effect of CL316,243 or physical activity on FDG uptake in differentiated muscle cells. ^{18}F-FDG uptake by interscapular BAT (iBAT) was also dramatically induced by CL316,243.

(G) Representative thermographic images depict evident increase of surface temperatures in the miR-133 ASO-treated hindlimbs of mice fed with either a regular diet (RD, blue arrowhead) or a high-fat diet (HFD, green arrowhead) compared to the contralateral hindlimbs or both hindlimbs in control ASO-treated mice. Arrowheads denote ASO treated right hindlimbs. Whole-body thermographic images (lower panels) are shown to denote the representative temperatures at both hindlimbs and neck areas.

(H) Quantitative temperature measurement by thermographic imaging reveals the marked increase of surface temperatures in hindlimbs that received miR-133 ASO treatment (n = 5 per treatment group per diet group).

Error bars, SEM. See also Figure S5.

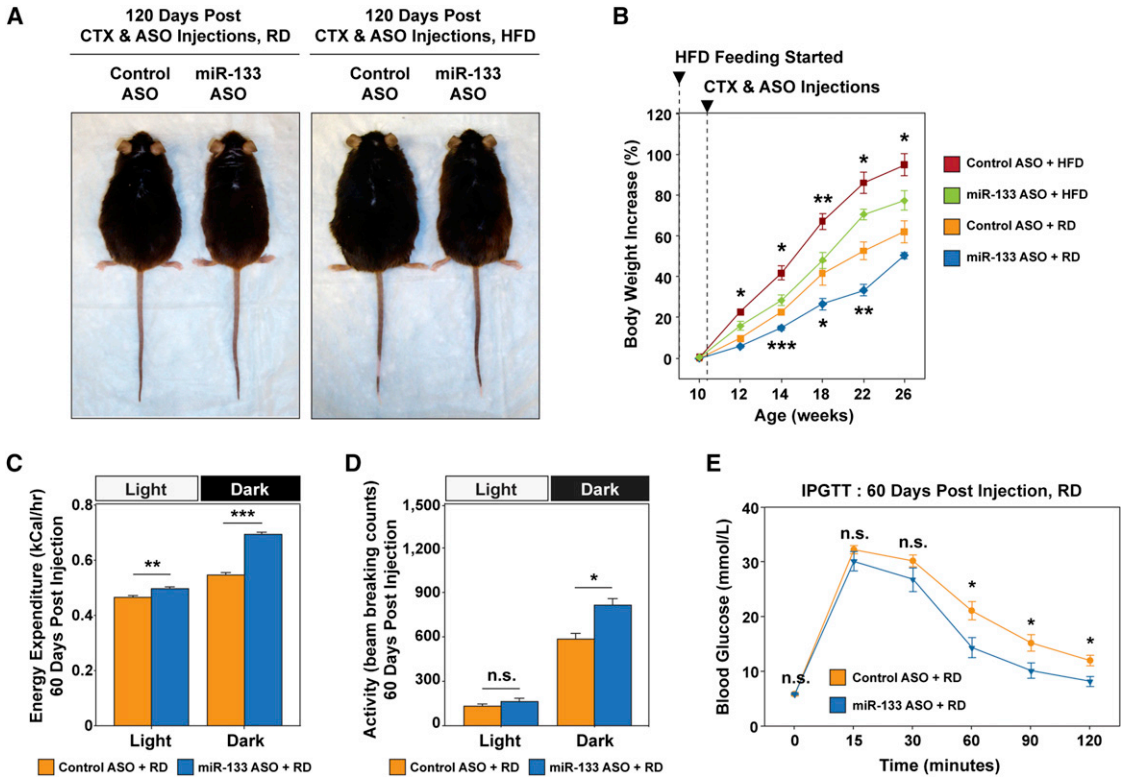

Figure 6. Antagonism of miR-133 during Muscle Regeneration Reduced Adiposity, Increased Total Energy Expenditure, and Improved Glucose Tolerance

(A) Representative images of direct comparisons of *C57BL/6* mice fed the RD or HFD and received control or miR-133 ASO treatment during TA muscle regeneration depict that the miR-133 ASO-treated mice displayed leaner phenotype.

(B) Retarded body weight increase over a 16 week body weight monitoring time course in mice that received miR-133 ASO treatment during TA muscle regeneration (n = 6 per treatment group per diet group).

(C) miR-133 ASO treatment increased total energy expenditure. Indirect calorimetry reveals that mice receiving miR-133 ASO treatment during TA muscle regeneration had a recorded higher energy expenditure than the control mice (n = 5 per group), measured at 22°C during light and dark cycles (fed the RD). Values of total energy expenditure were plotted without normalization to lean body mass.

(D) Physical activities measured within light and dark cycles during indirect calorimetry (C) reveal increased physical activities within the dark cycle for miR-133 ASO-treated mice (fed the RD). Physical activities are presented as arithmetic means of beam-breaking events at X, Y, and Z dimensions.

(E) IPGTT tests for *C57BL/6* mice received either control or miR-133 ASO treatment (fed the RD; n = 6 per group).

Error bars, SEM. See also Figure S6.

tissues and brown/white adipose tissues. Coincidently, induced brown adipose determination/differentiation (as evidenced by increased *Prdm16* and *Ucp1* mRNA levels) was also observed in subcutaneous WAT depots and chunk muscles (e.g., intercostal muscles, back muscles, and paraspinal muscles), but not limb muscles (e.g., tibialis anterior).

To confirm satellite cell-derived brown adipocytes were induced by cold exposure, we performed immunofluorescence microscopy on cross-sections prepared from paraspinal muscles of cold-exposed *Pax7-CreER;R26R-tdTomato* mice. Strikingly, we observed emerging tdTomato^{pos}, Ucp1^{pos} adipocytes located within the interstitium of paraspinal muscles after cold exposure (Figure 7B). Such adipocytes were not detected in paraspinal muscles of the control *Pax7-CreER;R26R-td Tomato* mice raised under room temperature (23°C). Therefore, our observations implicate miR-133 in the physiological regulation of brown adipose determination of satellite cells in response to cold exposure.

DISCUSSION

Using lineage tracing and clonal analysis, we found that satellite cells in adult muscle are bona fide bipotential stem cells that can give rise to brown adipogenic as well as myogenic progenitors. We also identified a microRNA expressed in satellite cells and upregulated as the myogenic program progresses—miR-133—that directly represses the expression of Prdm16 to enforce myogenic commitment in satellite cells. Thus miR-133 functions as a switch to regulate the lineage choice between brown adipogenic versus myogenic determination.

We demonstrated that antagonizing miR-133 function by antisense oligos (antagomiR) in activated satellite cells in response to muscle injury resulted in the efficient induction of brown adipocytes within the muscle interstitium. We estimate that each treated TA muscle would contain tens of thousands of brown adipocytes based on enumeration of these cells as well as Ucp1 protein levels (Figure 4). Notably, the stimulatory effect

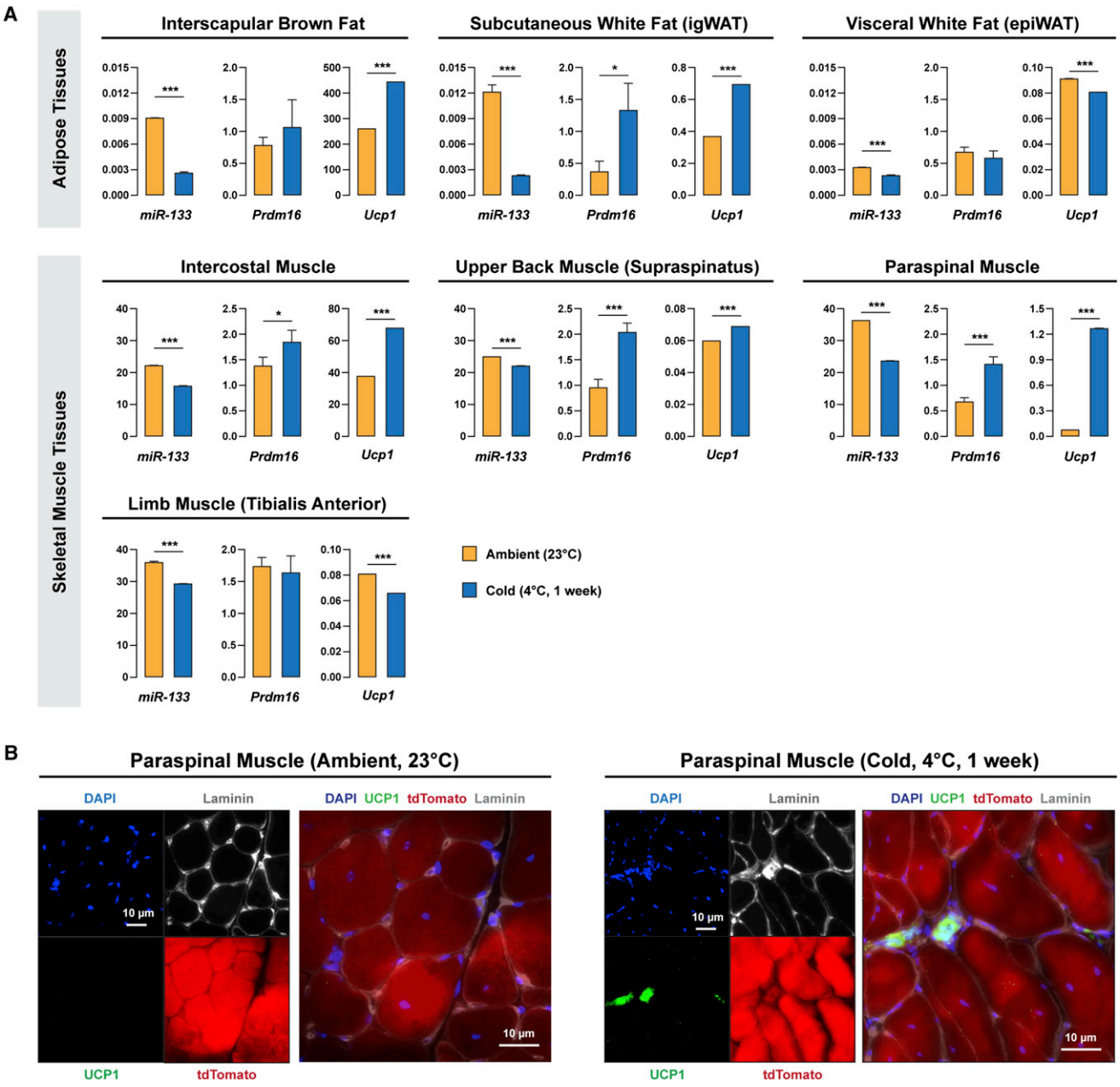

Figure 7. Cold Exposure Downregulates miR-133 Expression in Skeletal Muscles

(A) Cold exposure induced downregulation of *miR-133* (*miR-133a* and *miR-133b*) in multiple adipose and muscle tissues and increased expression of brown adipocyte markers, *Prdm16* and *Ucp1*, in subcutaneous WAT and trunk muscles. *C57BL/6* mice were raised under ambient temperature (23°C) or exposed to cold (4°C) for 1 week. Multiple tissues were dissected and investigated by RT-qPCR for the expressions of *miR-133*, *Prdm16*, and *Ucp1*.

(B) Cold exposure induced satellite cells to differentiate into brown adipocytes located within the muscle interstitium in paraspinal muscles. *Pax7-CreER;R26R-tdTomato* mice were raised under ambient temperature (23°C) or exposed to cold (4°C) for 1 week. Representative images of paraspinal muscle cross-sections stained with DAPI, Ucp1, and Laminin together with tdTomato native fluorescence revealed SC_BAs within the muscle interstitium.

Error bars, SEM.

of miR-133 ASO on brown adipose determination likely occurs in the early stage of muscle regeneration (within 2 weeks after muscle injury). Thus, satellite cell-derived brown adipocytes, once formed, do not require constant exposure to miR-133 ASO to maintain their function. The targeting specificity of miR-133 ASO argues for a pivotal role of miR-133 in BAT determination in muscle. However, it should also be noted that miR-133 may also target other biological processes in addition to de novo BAT formation in vivo. Future studies will reveal whether brown adipose determination of satellite cells occurs within muscles of miR-133 compound mutant mice (*miR-133a-1*$^{-/-}$; *miR-133a-2*$^{-/-}$; *miR-133b*$^{-/-}$).

We found that cold exposure represses the expression of miR-133 in multiple skeletal muscle tissues along with brown and white adipose tissues. Correspondingly, cold exposure also induced brown adipose determination/differentiation (as indicated by increased *Prdm16* and *Ucp1* mRNA levels) in subcutaneous WAT depots and trunk muscles. To explore whether the increased *Prdm16*/*Ucp1* expression in trunk muscles was due to induced satellite cell-derived brown adipocytes, we further exposed *Pax7-CreER;R26R-tdTomato* mice to cold and performed immunostaining (Figure S7B) on paraspinal muscle cross-sections. Strikingly, we observed satellite cell-derived brown adipocytes (tdTomato^{pos}, Ucp1^{pos}) located within paraspinal muscle interstitium. Recently, it was reported that miR-133 regulates Prdm16 in committed brown adipogenic cells, and cold treatment of cultured cells resulted in down-regulation of miR-133 and upregulation of Prdm16 and Ucp1 (Trajkovski et al., 2012). Taken together, these observations implicate regulation of miR-133 expression as a key thermoregulatory mechanism in the whole-animal response to acute and chronic cold.

Our investigation of the metabolic phenotypes associated with miR-133 ASO-treated TA muscles/hindlimbs indicated that the induced brown adipocytes in the muscle interstitium are metabolically active (Figure 5). This notion is supported by bioenergetics results of miR-133 ASO-treated TA muscles in vitro, which showed markedly increased uncoupled respiration in nonpermeabilized miR-133 ASO-treated muscle in response to Ucp1 activation by FAs. This increased uncoupled respiration rate has potentially important implications for energy expenditure and weight control in vivo. The difference in uncoupled respiration between control and miR-133 ASO treatment TA muscles is equivalent to ~0.023 kcal·hr^{-1}, which would fully account for the measured difference of total energy expenditure between control and miR-133 ASO-treated mice in the light cycle and ~15% of the difference found in the dark cycle (when more energy is used to support coupled, ATP synthase-dependent respiration during physical activity).

Our experiments also demonstrate that miR-133 ASO induced brown adipocytes in muscle function in the same manner as authentic BAT, in terms of their energy uptake ([^{18}F]-FDG/glucose uptake; Figures 5E and 5F) and energy expenditure (thermogenesis; Figures 5G and 5H). It is noteworthy that the markedly increased glucose/FDG uptake in miR-133 ASO-treated muscles was only revealed after selective β3-adrenergic receptor activation (CL316,243). Importantly, β3-adrenergic receptors express abundantly on brown adipocytes but little on muscle cells (Krief et al., 1993).

Skeletal muscle is a compatible tissue for adaptive thermogenesis of resident brown adipocytes. It has been well established that skeletal muscle cells are indirectly controlled by the sympathetic nervous system via diffusible adrenergic transmitters released from abundant vascular sympathetic innervations (Bowman and Nott, 1969). Thus, it is reasonable to speculate that interstitial satellite cell-derived brown adipocytes would be readily accessed by catecholamines from the vasculature relative to myofibers surrounded by basal lamina. The elevated glucose/FDG uptake in response to CL316,243 strongly implicates the presence of β3-adrenergic receptors on satellite cell-derived brown adipocytes.

Skeletal muscle has a very high metabolic capacity. Therefore, it is intriguing to hypothesize that the activation of muscle-embedded BAT may parallel sympathetic activation and dynamic regulation of oxygen/energy source supply via vasodilatation in response to need for muscle motor output. Indeed, the obesity resistance trait of *129S6/SvEvTac* mice has been attributed to ectopic intramuscular BAT, which appeared to be more sensitive to adrenergic agonists in Ucp1 induction as compared to iBAT (Almind et al., 2007). Similar to *129S6/SvEvTac* mice, obesity-prone *C57BL/6* mice showed reduced adiposity, augmented energy expenditure, and improved whole-body insulin sensitivity in response to miR-133 ASO treatment and BAT induction in muscle (Figure 6). These systemic effects of miR-133 ASO may associate with direct effects of ectopically induced satellite cell-derived brown adipocytes in muscle, or alternatively ensue from indirect effects from reduced body weight and adiposity (e.g., increased muscle insulin sensitivity may result from reduced adiposity or increased physical activity).

The data from mitochondrial respirometry clearly indicate that neither miR-133 ASO-treated TA muscles nor the contralateral soleus muscles have significantly increased oxidative phosphorylation capacity compared to the control muscles (Figure 5D and Figure S5A). The isolated activities of cytochrome oxidase in the contralateral soleus muscles, a marker for mitochondrial content (Larsen et al., 2012), were also comparable between treatment groups (miR-133 ASO treated, 130 ± 13 pmol·s^{-1}·mg^{-1}; control ASO treated, 113 ± 24 pmol·s^{-1}·mg^{-1}, $p = 0.5$). These results indicate that the miR-133 ASO treatment regime does not mimic a "training" effect in skeletal muscle cells. Further investigation may shed light on the cause(s) of increased physical activity levels in miR-133 ASO-treated mice. Nevertheless, the phenotypes linked with miR-133 ASO treatment evidently argue for positive influences of miR-133 ASO on metabolism.

Here, we demonstrate that satellite cells can differentiate into either myocytes or brown adipocytes. The lineage switch between myogenic and brown adipogenic commitment is controlled by myomiR miR-133, which is highly expressed in satellite cells. Functional brown adipocytes can be induced from satellite cells by inhibiting miR-133 function during muscle regeneration or by cold exposure accompanied with downregulation of miR-133 expression. Therefore, targeting miR-133 activity in adult muscle stem cells represents an attractive strategy to stimulate a physiological effective increase in the numbers of active brown adipocytes in vivo.

EXPERIMENTAL PROCEDURES

Induced Brown Adipocytes In Vivo by miR-133 AntagomiR

To induce brown adipocytes in vivo, 10 mg/mL cardiotoxin solution (50 μl) was intramuscularly injected into TA muscles of 10-week-old *Pax7-CreER/R26R-tdTomato* mice (Figure 4) or *C57BL/6* mice (Figure 5 and Figure 6). Alternatively, frozen injury was performed by applying liquid nitrogen-cooled tweezers tips directly onto the anterior sides of TA muscles (Figure S4H). After 3 days, 20 μg of miR-133 antagomiR or control antagomiR in saline (50 μl) was intramuscularly injected into the same injured TA muscles (on right hindlimbs). To test efficacy of miR-133 ASO in intact muscles, saline, instead of cardiotoxin, was injected to TA muscles before miR-133 ASO administration (Figures 4A and 4B). miR-133 antagomiR and scramble antagomiR were designed as previously described (Krützfeldt et al., 2005).

miR-133 antagomiR sequence and modifications were as follows: 5′-*mA*mUmAmGmCmUmGmGmUmUmGmAmAmGmGmGmGmAmC*mC*mA*mA*mAChl-3′; scramble antagomiR sequence and modifications, 5′-*mA*mAmGmAmAmUmGmAmCmGmAmUmCmGmGmUmAmGmG*mG*mC*mA*mCChl-3′. "m" represents a 2′-O-methyl-modified nucleotide. Asterisk indicates a phosphorothioate linkage. "Chl" denotes a 3′ cholesterol moiety.

Indirect Calorimetry

Whole-body O_2 consumption and CO_2 production were measured using an open-circuit four-chamber indirect calorimetry system with automatic temperature and light controls (Columbus Instruments). Physical activities during indirect calorimetry were measured using infrared laser beam sets. Mice had access ad libitum to food and water in respiration chambers. Data were recorded for a 24 hr period with light between 06:00 and 18:00.

[^{18}F]-FDG PET Imaging and X-ray Computed Tomography

All animal procedures comply with the Canadian Council on Animal Care's Guide to the Care and Use of Experimental Animals, the Animals for Research Act, and were approved by the Animal Care Committee at University of Ottawa. Mouse PET imaging was performed with an Inveon PET scanner (Siemens Preclinical Solutions, Knoxville, TN, USA). Control or miR-133 ASO-treated *C57BL/6* male mice fed with regular diet were anesthetized under 2% isoflurane. Mice were administrated with ~1 mCi [^{18}F] fluoro-2-deoxyglucose ([^{18}F] FDG) via tail vein injection and subjected to an 80 min dynamic scan. Data analysis was performed using the Inveon Research Workplace software to determine the standardized uptake values (SUVs) (activity concentration/injected dose × body weight) based on drawn ROIs at the end of the 80 min scanning period. Computed tomography (CT) with hindlimbs centered in the field of view was performed before the microPET imaging. Reconstructed CT images were registered with microPET images to precisely identify TA muscles on hindlimbs. To activate brown adipocytes, a β3-adrenergic selective agonist, CL-316,243, was administrated (1 mg/kg body weight; i.p. injection) 20 min before the anesthesia.

Thermographic Imaging

Mouse thermographic imaging was performed with a FLIR T640 infrared camera with highest sensitivity set to ~35°C. Control or miR-133 ASO-treated *C57BL/6* male mice fed with either a regular diet or a HFD were shaved at both of the hindlimbs 1 day before the imaging. Subject mice were quickly anesthetized under ~1% isoflurane, and thermographic images were taken immediately after the mice were anesthetized (within 2 min). Data analysis was performed using FLIR QuickReport software with measuring crosses set on the TA muscle areas on lower hindlimbs and the neck areas.

Statistical Analysis

Error bars are SEM. Asterisk indicates significant pairwise comparison by t test, *$p \leq 0.05$, **$p \leq 0.01$, ***$p \leq 0.001$.

SUPPLEMENTAL INFORMATION

Supplemental Information includes six figures, three tables, Supplemental Experiemental Procedures, and Supplemental References and can be found with this article at http://dx.doi.org/10.1016/j.cmet.2013.01.004.

ACKNOWLEDGMENTS

We thank Brianne Thrush for help on high-resolution respirometry, Christine Archer for help on microPET/CT imaging, Céline Aguer and Jian Xuan for help on indirect calorimetry, Paul Oleynick for fluorescent-activated cell sorting, and Jennifer Ritchie for animal husbandry. H.Y. was supported by fellowships from Canadian Institutes of Health Research (CIHR), CIHR Training Program in Regenerative Medicine, and the Ontario Research Fund. M.A.R. holds the Canada Research Chair in Molecular Genetics. This work was funded by the Canadian Institutes of Health Research grant MOP81288, NIH/NIAMS grant R01AR044031, and Ontario Research Fund grants (to M.A.R.), and by EuTRACC, a European Commission 6th Framework grant (to F.G.). H.Y., R.B., M-E.H., and M.A.R. conceived of and designed experiments, and prepared the manuscript. H.Y. executed most of the experiments and performed bioinformatic analyses. A.P. executed experiments in Figure 1 and Figure S3B. V.D.S. prepared retroviruses. C.F.B. executed experiments in Figures S4F and S4G. G.A. helped on experiments in Figures 5C and 5D and Figure S5A. P.S. provided anti-Prdm16 antibody. S.T., P.F., and R.A.D. designed experiments and analyzed data in Figures 5E and 5F and Figure S5B. W.v.I. and F.G. provided support to high-throughput sequencing of satellite cell transcriptome. R.B. designed and performed experiments and analyzed data in Figures 5C and 5D and Figure S5A.

Received: February 27, 2012
Revised: August 18, 2012
Accepted: January 11, 2013
Published: February 5, 2013

REFERENCES

Almind, K., Manieri, M., Sivitz, W.I., Cinti, S., and Kahn, C.R. (2007). Ectopic brown adipose tissue in muscle provides a mechanism for differences in risk of metabolic syndrome in mice. Proc. Natl. Acad. Sci. USA *104*, 2366–2371.

Atit, R., Sgaier, S.K., Mohamed, O.A., Taketo, M.M., Dufort, D., Joyner, A.L., Niswander, L., and Conlon, R.A. (2006). Beta-catenin activation is necessary and sufficient to specify the dorsal dermal fate in the mouse. Dev. Biol. *296*, 164–176.

Bosnakovski, D., Xu, Z., Li, W., Thet, S., Cleaver, O., Perlingeiro, R.C., and Kyba, M. (2008). Prospective isolation of skeletal muscle stem cells with a Pax7 reporter. Stem Cells *26*, 3194–3204.

Bowman, W.C., and Nott, M.W. (1969). Actions of sympathomimetic amines and their antagonists on skeletal muscle. Pharmacol. Rev. *21*, 27–72.

Cannon, B., and Nedergaard, J. (2001). Respiratory and thermogenic capacities of cells and mitochondria from brown and white adipose tissue. Methods Mol. Biol. *155*, 295–303.

Cannon, B., and Nedergaard, J. (2004). Brown adipose tissue: function and physiological significance. Physiol. Rev. *84*, 277–359.

Chance, B., and Williams, G.R. (1955). A simple and rapid assay of oxidative phosphorylation. Nature *175*, 1120–1121.

Chargé, S.B., and Rudnicki, M.A. (2004). Cellular and molecular regulation of muscle regeneration. Physiol. Rev. *84*, 209–238.

Chen, J.F., Mandel, E.M., Thomson, J.M., Wu, Q., Callis, T.E., Hammond, S.M., Conlon, F.L., and Wang, D.Z. (2006). The role of microRNA-1 and microRNA-133 in skeletal muscle proliferation and differentiation. Nat. Genet. *38*, 228–233.

Cypess, A.M., and Kahn, C.R. (2010). Brown fat as a therapy for obesity and diabetes. Curr. Opin. Endocrinol. Diabetes Obes. *17*, 143–149.

Cypess, A.M., Lehman, S., Williams, G., Tal, I., Rodman, D., Goldfine, A.B., Kuo, F.C., Palmer, E.L., Tseng, Y.H., Doria, A., et al. (2009). Identification and importance of brown adipose tissue in adult humans. N. Engl. J. Med. *360*, 1509–1517.

Frontini, A., and Cinti, S. (2010). Distribution and development of brown adipocytes in the murine and human adipose organ. Cell Metab. *11*, 253–256.

Ghorbani, M., and Himms-Hagen, J. (1997). Appearance of brown adipocytes in white adipose tissue during CL 316,243-induced reversal of obesity and diabetes in Zucker fa/fa rats. Int. J. Obes. Relat. Metab. Disord. *21*, 465–475.

Houten, S.M., and Wanders, R.J. (2010). A general introduction to the biochemistry of mitochondrial fatty acid β-oxidation. J. Inherit. Metab. Dis. *33*, 469–477.

Joe, A.W., Yi, L., Natarajan, A., Le Grand, F., So, L., Wang, J., Rudnicki, M.A., and Rossi, F.M. (2010). Muscle injury activates resident fibro/adipogenic progenitors that facilitate myogenesis. Nat. Cell Biol. *12*, 153–163.

Kajimura, S., Seale, P., Tomaru, T., Erdjument-Bromage, H., Cooper, M.P., Ruas, J.L., Chin, S., Tempst, P., Lazar, M.A., and Spiegelman, B.M. (2008). Regulation of the brown and white fat gene programs through a PRDM16/CtBP transcriptional complex. Genes Dev. *22*, 1397–1409.

Kalaany, N.Y., Gauthier, K.C., Zavacki, A.M., Mammen, P.P., Kitazume, T., Peterson, J.A., Horton, J.D., Garry, D.J., Bianco, A.C., and Mangelsdorf,

D.J. (2005). LXRs regulate the balance between fat storage and oxidation. Cell Metab. *1*, 231–244.

Kopecky, J., Clarke, G., Enerbäck, S., Spiegelman, B., and Kozak, L.P. (1995). Expression of the mitochondrial uncoupling protein gene from the aP2 gene promoter prevents genetic obesity. J. Clin. Invest. *96*, 2914–2923.

Krief, S., Lönnqvist, F., Raimbault, S., Baude, B., Van Spronsen, A., Arner, P., Strosberg, A.D., Ricquier, D., and Emorine, L.J. (1993). Tissue distribution of beta 3-adrenergic receptor mRNA in man. J. Clin. Invest. *91*, 344–349.

Krützfeldt, J., Rajewsky, N., Braich, R., Rajeev, K.G., Tuschl, T., Manoharan, M., and Stoffel, M. (2005). Silencing of microRNAs in vivo with 'antagomirs'. Nature *438*, 685–689.

Kuang, S., Kuroda, K., Le Grand, F., and Rudnicki, M.A. (2007). Asymmetric self-renewal and commitment of satellite stem cells in muscle. Cell *129*, 999–1010.

Larsen, S., Nielsen, J., Hansen, C.N., Nielsen, L.B., Wibrand, F., Stride, N., Schroder, H.D., Boushel, R., Helge, J.W., Dela, F., and Hey-Mogensen, M. (2012). Biomarkers of mitochondrial content in skeletal muscle of healthy young human subjects. J. Physiol. *590*, 3349–3360.

Lepper, C., and Fan, C.M. (2010). Inducible lineage tracing of Pax7-descendant cells reveals embryonic origin of adult satellite cells. Genesis *48*, 424–436.

Matthias, A., Ohlson, K.B., Fredriksson, J.M., Jacobsson, A., Nedergaard, J., and Cannon, B. (2000). Thermogenic responses in brown fat cells are fully UCP1-dependent. UCP2 or UCP3 do not substitute for UCP1 in adrenergically or fatty scid-induced thermogenesis. J. Biol. Chem. *275*, 25073–25081.

Nedergaard, J., Bengtsson, T., and Cannon, B. (2007). Unexpected evidence for active brown adipose tissue in adult humans. Am. J. Physiol. Endocrinol. Metab. *293*, E444–E452.

Nedergaard, J., Bengtsson, T., and Cannon, B. (2010). Three years with adult human brown adipose tissue. Ann. N Y Acad. Sci. *1212*, E20–E36.

Nishijo, K., Hosoyama, T., Bjornson, C.R., Schaffer, B.S., Prajapati, S.I., Bahadur, A.N., Hansen, M.S., Blandford, M.C., McCleish, A.T., Rubin, B.P., et al. (2009). Biomarker system for studying muscle, stem cells, and cancer in vivo. FASEB J. *23*, 2681–2690.

Ouellet, V., Labbé, S.M., Blondin, D.P., Phoenix, S., Guérin, B., Haman, F., Turcotte, E.E., Richard, D., and Carpentier, A.C. (2012). Brown adipose tissue oxidative metabolism contributes to energy expenditure during acute cold exposure in humans. J. Clin. Invest. *122*, 545–552.

Pfannenberg, C., Werner, M.K., Ripkens, S., Stef, I., Deckert, A., Schmadl, M., Reimold, M., Häring, H.U., Claussen, C.D., and Stefan, N. (2010). Impact of age on the relationships of brown adipose tissue with sex and adiposity in humans. Diabetes *59*, 1789–1793.

Saito, M., Okamatsu-Ogura, Y., Matsushita, M., Watanabe, K., Yoneshiro, T., Nio-Kobayashi, J., Iwanaga, T., Miyagawa, M., Kameya, T., Nakada, K., et al. (2009). High incidence of metabolically active brown adipose tissue in healthy adult humans: effects of cold exposure and adiposity. Diabetes *58*, 1526–1531.

Scimè, A., Grenier, G., Huh, M.S., Gillespie, M.A., Bevilacqua, L., Harper, M.E., and Rudnicki, M.A. (2005). Rb and p107 regulate preadipocyte differentiation into white versus brown fat through repression of PGC-1alpha. Cell Metab. *2*, 283–295.

Seale, P., Sabourin, L.A., Girgis-Gabardo, A., Mansouri, A., Gruss, P., and Rudnicki, M.A. (2000). Pax7 is required for the specification of myogenic satellite cells. Cell *102*, 777–786.

Seale, P., Kajimura, S., Yang, W., Chin, S., Rohas, L.M., Uldry, M., Tavernier, G., Langin, D., and Spiegelman, B.M. (2007). Transcriptional control of brown fat determination by PRDM16. Cell Metab. *6*, 38–54.

Seale, P., Bjork, B., Yang, W., Kajimura, S., Chin, S., Kuang, S., Scimè, A., Devarakonda, S., Conroe, H.M., Erdjument-Bromage, H., et al. (2008). PRDM16 controls a brown fat/skeletal muscle switch. Nature *454*, 961–967.

Seale, P., Conroe, H.M., Estall, J., Kajimura, S., Frontini, A., Ishibashi, J., Cohen, P., Cinti, S., and Spiegelman, B.M. (2011). Prdm16 determines the thermogenic program of subcutaneous white adipose tissue in mice. J. Clin. Invest. *121*, 96–105.

Trajkovski, M., Ahmed, K., Esau, C.C., and Stoffel, M. (2012). MyomiR-133 regulates brown fat differentiation through Prdm16. Nat. Cell Biol. *14*, 1330–1335.

van Marken Lichtenbelt, W.D., Vanhommerig, J.W., Smulders, N.M., Drossaerts, J.M., Kemerink, G.J., Bouvy, N.D., Schrauwen, P., and Teule, G.J. (2009). Cold-activated brown adipose tissue in healthy men. N. Engl. J. Med. *360*, 1500–1508.

Virtanen, K.A., Lidell, M.E., Orava, J., Heglind, M., Westergren, R., Niemi, T., Taittonen, M., Laine, J., Savisto, N.J., Enerbäck, S., and Nuutila, P. (2009). Functional brown adipose tissue in healthy adults. N. Engl. J. Med. *360*, 1518–1525.

Walden, T.B., Timmons, J.A., Keller, P., Nedergaard, J., and Cannon, B. (2009). Distinct expression of muscle-specific microRNAs (myomirs) in brown adipocytes. J. Cell. Physiol. *218*, 444–449.

Wang, Y.X., and Rudnicki, M.A. (2012). Satellite cells, the engines of muscle repair. Nat. Rev. Mol. Cell Biol. *13*, 127–133.

Williams, A.H., Liu, N., van Rooij, E., and Olson, E.N. (2009). MicroRNA control of muscle development and disease. Curr. Opin. Cell Biol. *21*, 461–469.

Zingaretti, M.C., Crosta, F., Vitali, A., Guerrieri, M., Frontini, A., Cannon, B., Nedergaard, J., and Cinti, S. (2009). The presence of UCP1 demonstrates that metabolically active adipose tissue in the neck of adult humans truly represents brown adipose tissue. FASEB J. *23*, 3113–3120.

Polycomb EZH2 controls self-renewal and safeguards the transcriptional identity of skeletal muscle stem cells

Aster H. Juan, Assia Derfoul, Xuesong Feng, et al.

Genes Dev. 2011 25: 789-794
Access the most recent version at doi:10.1101/gad.2027911

RESEARCH COMMUNICATION

Polycomb EZH2 controls self-renewal and safeguards the transcriptional identity of skeletal muscle stem cells

Aster H. Juan,[1] Assia Derfoul,[1,4] Xuesong Feng,[1,4] James G. Ryall,[1,4] Stefania Dell'Orso,[1,4] Alessandra Pasut,[2,4] Hossein Zare,[1] James M. Simone[3] Michael A. Rudnicki,[2] and Vittorio Sartorelli[1,5]

[1]Laboratory of Muscle Stem Cells and Gene Regulation, National Institute of Arthritis, Musculoskeletal, and Skin Diseases (NIAMS), National Institutes of Health, Bethesda, Maryland 20892, USA; [2]The Sprott Centre for Stem Cell Research, Regenerative Medicine Program, Ottawa Hospital Research Institute, Ottawa, Ontario K1H8L6, Canada; [3]Flow Cytometry Section, NIAMS, National Institutes of Health, Bethesda, Maryland 20892, USA

Satellite cells (SCs) sustain muscle growth and empower adult skeletal muscle with vigorous regenerative abilities. Here, we report that EZH2, the enzymatic subunit of the Polycomb-repressive complex 2 (PRC2), is expressed in both Pax7$^+$/Myf5$^-$ stem cells and Pax7$^+$/Myf5$^+$ committed myogenic precursors and is required for homeostasis of the adult SC pool. Mice with conditional ablation of *Ezh2* in SCs have fewer muscle postnatal Pax7$^+$ cells and reduced muscle mass and fail to appropriately regenerate. These defects are associated with impaired SC proliferation and derepression of genes expressed in nonmuscle cell lineages. Thus, EZH2 controls self-renewal and proliferation, and maintains an appropriate transcriptional program in SCs.

Supplemental material is available for this article.

Received January 1, 2011; revised version accepted March 3, 2011.

Adult skeletal muscle regenerates in response to traumatic injuries or degenerative conditions. This property is afforded mainly by satellite cells (SCs), a heterogeneous population of resident committed myogenic progenitors and noncommitted stem cells (Sherwood et al. 2004; Collins et al. 2005; Montarras et al. 2005; Kuang et al. 2007). In the mouse, postnatal SCs are mitotically active for the initial 2 wk after birth. After this period, they enter quiescence and their number declines. However, following muscle injury or degeneration, adult SCs undergo intense proliferation and efficiently differentiate. To replenish the reservoir, a subset of dividing SCs returns to the niche following a process of asymmetric and symmetric cell division (Shinin et al. 2006; Conboy et al. 2007; Kuang et al. 2007; Shea et al. 2010). Approximately 10% of noncommitted Pax7$^+$/Myf5$^-$ SCs can asymmetrically generate a self-renewing, noncommitted Pax7$^+$/Myf5$^-$ cell and a committed Pax7$^+$/Myf5$^+$ daughter cell in vivo. The noncommitted Pax7$^+$/Myf5$^-$ cell returns to the niche to maintain the SC reservoir, while the committed Pax7$^+$/Myf5$^+$ SC undergoes several rounds of cell division and the ensuing cells eventually differentiate into pre-existing or newly formed myofibers (Kuang et al. 2008).

Polycomb group (PcG) proteins regulate differentiation of totipotent embryonic stem (ES) cells and maintenance of multipotent and progenitor stem cell populations (Sauvageau and Sauvageau 2010). The Polycomb-repressive complex 2 (PRC2) subunit EZH2 methylates histone H3 Lys 27 (H3K27me3), establishing an epigenetic mark that identifies repressed chromatin regions. Ablation of PRC2 members in ES cells impairs their differentiation (Pasini et al. 2007; Chamberlain et al. 2008; Shen et al. 2008) and results in unscheduled expression of mixed cell lineage genes (Boyer et al. 2006; Lee et al. 2006). While PcG establishes and maintains positional patterning of the body axis through regulation of Hox genes in both *Drosophila* and mammals, its role in conferring cell identity by repressing inappropriate cell lineage-specific transcription in animal development has not been demonstrated. Indeed, derepression of mixed cell lineage genes does not occur in epidermal, neuronal, or pancreatic cells of *Ezh2* conditional null mice (Chen et al. 2009; Ezhkova et al. 2009; Hirabayashi et al. 2009).

We generated mice in which *Ezh2* was conditionally ablated in SCs (*Ezh2* muscle knockout, *Ezh2*^{mKO}). While EZH2 was dispensable for fetal muscle development, it was required for postnatal muscle growth and adult muscle regeneration, ensuring appropriate homeostasis of the SC pool. Unlike other progenitor cells, reduced H3K27me3 in *Ezh2*^{mKO} SCs was accompanied by RNA polymerase II (PolII) recruitment and transcriptional activation of genes normally repressed in SCs and expressed in other cell lineages, including cardiac progenitors, retinal cones, neurons, and chondrocytes. Thus, our findings indicate that EZH2, which regulates proliferation and maintains transcriptional identity of adult muscle stem cells, is an important molecular component of adult skeletal myogenesis.

Results and Discussion

Pax7 and Ezh2 are coexpressed in postnatal SCs

Pax7 is essential for SC specification and survival (Buckingham and Relaix 2007). While Pax7$^+$ cells were present at embryonic day 15.5 (E15.5) and E17.5, EZH2 could not be detected in skeletal muscle but was expressed in the epidermis (Supplemental Fig. S1A; Ezhkova et al. 2009). At postnatal day 1 (P1), EZH2 was expressed in limb muscles, where it remained detectable, along with Pax7, for ~14 d (P14) (Fig. 1A). Indeed, the vast majority of Pax7$^+$ cells coexpressed EZH2 in muscle cross-sections of P8 animals (Fig. 1B). Both EZH2 and Pax7 decreased and became undetectable by immunoblot after P21 (Fig. 1A), consistent with cessation of myonuclei accretion.

[*Keywords*: Polycomb; Ezh2; satellite cells; muscle growth; muscle regeneration]

[4]**These authors contributed equally to this work.**

[5]**Corresponding author.**

Article is online at http://www.genesdev.org/cgi/doi/10.1101/gad.2027911.

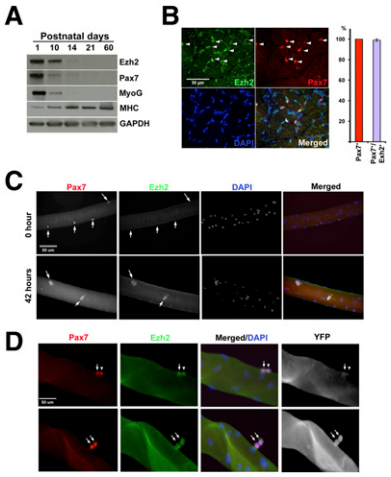

Figure 1. Ezh2 expression in limb muscles and SCs. (*A*) Limb muscle extracts from mice at P1–P60 probed with the indicated antibodies. (*B*) In P8 hindlimb muscles, EZH2 is expressed in Pax7$^+$ cells. Arrowheads indicate cells positive for Pax7 and EZH2. Quantification of Pax7$^+$/EZH2$^+$ cells in P8 EDL muscles. (*C*, *top* panel) Myofiber-associated quiescent (0 h) Pax7$^+$ SCs do not express a detectable level of EZH2. (*Bottom* panel) After 42 h, EZH2 is expressed in couplets of dividing Pax7$^+$ SCs. (*D*) In single myofibers of *Myf5-Cre/ROSA-YFP* mice cultured for 42 h, EZH2 is expressed in both Pax7$^+$/YFP$^-$ (*top* panel) and Pax7$^+$/YFP$^+$ (*bottom* panel) cells. Arrows indicate YFP$^+$ cells, and arrowheads indicate YFP$^-$ cells. Bars, 50 μm.

Ezh2 is expressed in both noncommitted and myogenically committed proliferating SCs

To evaluate EZH2 expression in quiescent and activated (i.e., cells that have entered the cell cycle) SCs, individual myofibers and their associated SCs were isolated from the extensor digitorus longus (EDL) muscle of 2-mo-old mice (P60) and either fixed immediately or cultured for 42 h to stimulate SC proliferation. While Pax7 was expressed in both conditions, EZH2 was detected only in Pax7$^+$ dividing SCs at 42 h (Fig. 1C). Neither Pax7 nor EZH2 was detected in myofiber nuclei (Fig. 1C). The low abundance of SCs at P21 prevented Pax7 detection (Fig. 1A).

The SC pool is composed of at least two hierarchical subpopulations (Kuang et al. 2007). Pax7$^+$/Myf5$^-$ cells are noncommitted self-renewing stem cells maintaining the SC compartment and giving rise to Pax7$^+$/Myf5$^+$ myogenic committed precursors fated to differentiate into myofibers. To investigate EZH2 expression in these two subpopulations, we used a lineage-tracing approach based on the *Myf5-Cre/ROSA-YFP* mouse, where cells that express or have ever expressed Myf5-Cre are YFP$^+$, while cells that have never expressed Myf5-Cre are YFP$^-$ (Kuang et al. 2007). Immunostaining with Pax7 and EZH2 antibodies of *Myf5-Cre/ROSA-YFP* myofibers cultured for 42 h in growth medium revealed that Pax7 and EZH2 were coexpressed in both YFP$^-$ (Fig. 1D, top panel) and YFP$^+$ (Fig. 1D, bottom panel) cells (Fig. 1D). Thus, EZH2 is expressed in both dividing Pax7$^+$/Myf5$^-$ noncommitted stem cells and Pax7$^+$/Myf5$^+$ muscle progenitors.

Mice with conditional ablation of Ezh2 in Pax7-derived muscle precursor cells have reduced muscle mass with smaller myofibers

Ezh2 was selectively ablated in Pax7-derived cells by crossing knock-in mice expressing Cre recombinase from the Pax7 locus (*Pax7*-Cre) (Keller et al. 2004) with mice bearing floxed *Ezh2* alleles (Su et al. 2003). In *Pax7*-Cre$^{+/-}$; Ezh2$^{fl/fl}$ mice (*Ezh2*^{mKO}), both EZH2 RNA and protein were largely and specifically reduced in muscle tissue (Fig. 2A). *Ezh2* deletion did not affect the expression of other members of the PRC2 complex, Suz12 and Eed, or the PRC1 protein Bmi1 (Supplemental Fig. S2A). *Ezh2* floxed alleles were not deleted in the kidney, heart, and white fat (data not shown). *Ezh2*^{mKO} mice had no obvious feeding difficulties and were apparently healthy. At E17.5, when EZH2 is not expressed in muscle tissues (Supplemental Fig. S1A), we did not observe gross morphological changes or appreciable abnormalities in *Ezh2*^{mKO} fetal myofibers (Supplemental Fig. S1B). In addition, a comparable number of Pax7$^+$ cells in the EDL of *Ezh2*^{mKO} and littermate controls further suggested that EZH2 is not required for fetal muscle development (Supplemental Fig. S1B). However, at P8, the muscle size of *Ezh2*^{mKO} animals was obviously smaller than that of littermate controls, and myofibers with a reduced cross-sectional area (CSA) were prevalent (Supplemental Fig. S2B,C). The myofiber number was comparable with that of littermate controls. These postnatal muscle defects persisted through adulthood, and both the body mass and the total muscle mass of P60 *Ezh2*^{mKO} animals were significantly reduced (Fig. 2B,C), with a prevalence of smaller myofibers (Fig. 2D). Thus, *Ezh2* ablation in Pax7-derived skeletal muscle cells results in defects of postnatal muscle growth characterized by reduced muscle mass with smaller muscle fibers.

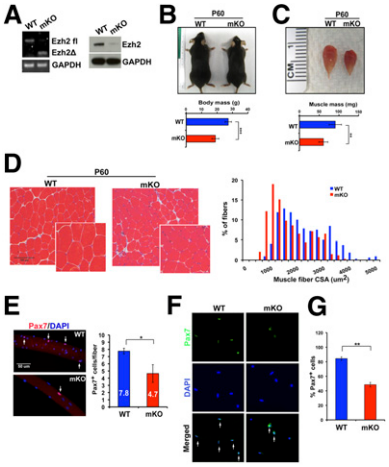

Ezh2 is required for maintenance of the adult muscle SC pool

We examined the quiescent SC population of P60 mice. Pax7$^+$ cells on freshly isolated individual myofibers were reduced by ~40% in *Ezh2*^{mKO} animals (Fig. 2E). To further substantiate these findings, we isolated the quiescent SC population from both wild-type and *Ezh2*^{mKO} animals by FACS by gating on integrin α-7$^+$ (positive selection) and Lin$^-$ (CD31$^-$,CD45$^-$,CD11$^-$, Sca1$^-$) (negative selection) cells. Although the percentage of the integrin-α7$^+$Lin$^-$ population was similar in wild type and *Ezh2*^{mKO} (Supplemental Fig. 3A), only ~50% of the purified cells were Pax7$^+$ in *Ezh2*^{mKO} compared with ~85% in wild type (Fig. 2F,G). In agreement with the results reported above, muscle cross-sections of *Ezh2*^{mKO} animals contained only ~50% of the Pax7$^+$ cells of littermate controls (Supplemental Fig. S3B). Reduced Pax7 expression in *Ezh2*^{mKO} is not the consequence of direct regulation by EZH2, since adenoviral Cre-mediated *Ezh2* excision did not affect the Pax7 level (Supplemental Fig. S3C). Together, these data suggest that EZH2 regulates establishment and/or maintenance of the adult SC pool.

Ezh2 affects SC proliferation and differentiation

We evaluated the SC population by quantifying Pax7$^+$ cells in P8 mice, when SCs are highly proliferative. Pax7$^+$ cells, located under the basal lamina, were decreased by ~40% in *Ezh2*^{mKO} animals and, consistent with *Ezh2* ablation, H3K27me3$^+$ cells were hardly detected (Fig. 3A,B; Supplemental Fig. S3D). The reduced number of Pax7$^+$ cells in *Ezh2*^{mKO} animals suggested that SC proliferation may be impaired. To test this hypothesis, individual myofibers derived from either wild-type or *Ezh2*^{mKO} EDL muscle were isolated and cultured for 3 d to allow for SC delamination and proliferation. The number of Pax7$^+$ cells derived from 3-d cultured *Ezh2*^{mKO} myofibers was significantly curtailed, when compared with that of wild-type myofibers (Fig. 3C). An equivalent number of FACS-isolated cells obtained from either wild-type or *Ezh2*^{mKO} animals was plated and cultured for 14, 48, and 96 h, respectively. Fewer *Ezh2*^{mKO} cells were present after 48 and 96 h in culture (Fig. 3D). 5-bromo-2′-deoxyuridine (BrdU) cell incorporation and immunostaining with an antibody detecting histone H3Ser10 phosphorylation—a marker of the G2/M mitotic transition—indicated that *Ezh2*^{mKO}-derived cells had reduced proliferative capacity (Fig. 3E). Apoptosis was not increased in *Ezh2*^{mKO} SCs (Supplemental Fig. S4A). The proliferation defects of *Ezh2*^{mKO} SCs are likely the consequence of derepression of the cell cycle inhibitor p16 (Cdkn2a) (Fig. 3F; Supplemental Table S1; Bracken et al. 2007; Kotake et al. 2007; Chen et al. 2009; Ezhkova et al. 2009; Pereira et al. 2010). To directly test this hypothesis, we reduced p16 in FACS-isolated and cultured SCs by siRNA (Supplemental Fig. S4B). A higher percentage of *Ezh2*^{mKO} SCs with reduced p16 scored positive for H3Ser10 phosphorylation compared with control siRNA transfected *Ezh2*^{mKO} SCs. Reducing p16 did not affect H3Ser10 phosphorylation of wild-type SCs. (Supplemental Fig. S4B). Thus, p16 up-regulation is partly responsible for the proliferative defects of *Ezh2*^{mKO} SCs. Despite the reduced number of Pax7$^+$ cells per clone (Fig. 3C), the majority of *Ezh2*^{mKO} SCs cultured for 72 h expressed myogenin (Fig. 3G), suggesting earlier differentiation potential (Juan et al. 2009). Overall, these results indicate that EZH2 plays an important role in the SC's proliferation and differentiation.

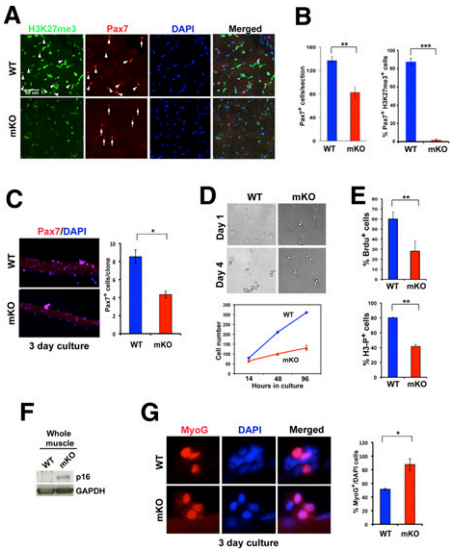

Figure 3. Skeletal muscle progenitors derived from Ezh2^{mKO} animals have proliferative defects and precociously activate myogenin. (*A*,*B*) Immunostaining of H3K27me3 and Pax7 of P8 EDL. Arrowheads indicate cells stained positive for both Pax7 and H3K27me3. Arrows indicate Pax7$^+$/H3K27me3$^-$ cells. Data are presented as mean ± SD (n = 3); (***) $P < 0.0005$; (**) $P < 0.005$. (*C*) Pax7 immunostaining of EDL single myofibers isolated from wild-type (WT) and *Ezh2*^{mKO} mice cultured for 3 d. (*) $P < 0.05$. (*D*) FACS-isolated wild-type and *Ezh2*^{mKO} SCs after 1 or 4 d in culture. Cells (1.5×10^4) of wild-type and *Ezh2* ^{mKO} SCs were seeded, and the total number obtained from counting cells present in 10 independent microscopic fields after 14, 48, and 96 h in culture was plotted in the curve graph (n = 4; $P < 0.001$ and $P < 0.003$ for 42-h and 96-h counts, respectively). (*E*) Percentage of FACS-isolated wild-type and *Ezh2*^{mKO} SCs that have incorporated BrdU or that stained positive for histone-H3 (H3-P). Data are presented as mean ± SD for BrdU (n = 3; [**] $P < 0.005$) and H3-P (n = 4; [**] $P < 0.005$). (*F*) Increased p16 protein in *Ezh2*^{mKO} muscles. GAPDH serves as a loading control. (*G*) Myogenin immunostaining of SC clones from wild-type and *Ezh2*^{mKO} myofibers. Data are presented as mean ± SD; (*) $P < 0.05$.

Muscle regeneration is compromised in Ezh2^{mKO} animals

The proliferative defects of SCs and the depletion of the quiescent SC pool observed in *Ezh2*^{mKO} mice suggested that muscle regeneration may be compromised in these animals. To test this hypothesis, muscle damage was induced by injecting the tibialis anterior (TA) muscle of adult (P60) wild-type and *Ezh2*^{mKO} animals with cardiotoxin (CTX). Three days after CTX injection, Pax7 and myogenin, which are normally undetectable by immunoblot in uninjured adult muscles (Fig. 1A), were readily seen in wild type but were reduced in *Ezh2*^{mKO} animals (Fig. 4A). Reduced myogenin expression in *Ezh2*^{mKO} animals is likely the consequence of defective SC proliferation rather than impaired differentiation, as *Ezh2*^{mKO} SCs display anticipated myogenin expression (Fig. 3G). Seven days after CTX injection, proliferation of Pax7$^+$ cells in the *Ezh2*^{mKO} regenerating muscle was severely impaired, as indicated by an almost 10-fold reduction of double-positive Pax7$^+$/phospho-H3$^+$ cells (Fig. 4B). At this stage,

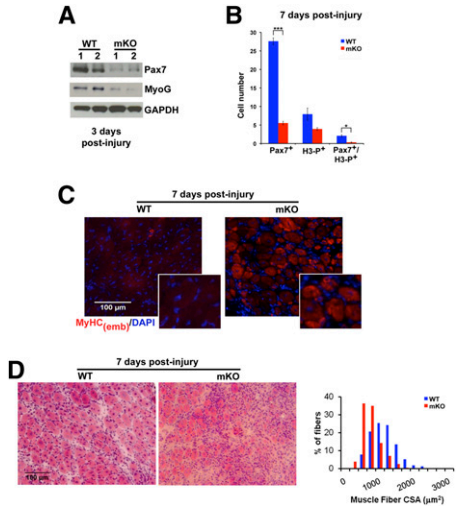

Figure 4. Impaired muscle regeneration in *Ezh2*^{mKO} animals. (*A*) Immunoblots of limb muscle extracts from wild-type (WT) or *Ezh2*^{mKO} animals (n = 2) 3 d after CTX, probed with myogenin, Pax7, and GAPDH antibodies. (*B*) Pax7 and H3-P immunostaining of TA muscles from wild-type and *Ezh2*^{mKO} animals 7 d after CTX injection. Data are presented as mean ± SD (n = 3); (***) $P < 0.0005$; (*) $P < 0.05$. (*C*) Embryonic MyHC [MyHC$_{(emb)}$] immunostaining in wild-type and *Ezh2*^{mKO} mice in 7-d regenerating myofibers. (*D*) H&E staining of transverse sections of wild-type or *Ezh2*^{mKO} regenerating TA muscles 7 d after CTX injection indicates that the CSA of centrally nucleated myofibers is reduced in *Ezh2*^{mKO} animals (n = 3). (*Right* panel) Ninety-five percent confidence intervals do not overlap.

while regenerating myofibers of littermate controls had almost extinguished expression of embryonic myosin heavy chain (eMyHC), a marker of muscle regeneration, *Ezh2*^{mKO} myofibers exhibited intense eMyHC staining and were smaller, indicating that muscle repair in *Ezh2*^{mKO} lagged behind that of control mice (Fig. 4C). Indeed, the majority of newly formed myofibers, identified by the presence of nuclei located in a central position, had a smaller CSA in *Ezh2*^{mKO} animals (Fig. 4D). Overall, these findings indicate that EZH2 is required for appropriate SC proliferation during muscle regeneration.

Ezh2 maintains the transcriptional identity of SCs

We compared transcriptional profiles of wild-type and *Ezh2*^{mKO} muscles by microarray analysis (Fig. 5A; Supplemental Table S1). Among the down-regulated transcripts in *Ezh2*^{mKO} muscle were several corresponding to developmental regulators and structural proteins (Supplemental Table S1). It is likely that reduced transcription is an indirect effect of Ezh2 ablation mediated by intermediate regulators, as H3K27me3 is not known to be directly associated with transcriptional activation. Gene ontology (GO) analysis for up-regulated genes found significant enrichment for functional classes, including those corresponding to muscle functions (Supplemental Table S2). Indeed, transcripts for muscle-expressed titin, sarcolipin, myosin Myh7, myomesin3, cardiac actin, Ankrd1, and troponin Tnni1 were increased in *Ezh2*^{mKO} (Fig. 5A; Supplemental Table S1). In addition, several developmental regulators expressed in multiple lineages that are PRC targets in ES cells were also up-regulated (Fig. 5A; Supplemental Table S1). Among those were ZIC-1 (expressed in early somites and the cerebellum), Isl1 (expressed in cardiac progenitors and the pancreas), and Tbx1 (expressed in cardiac progenitors). Transcripts of structural genes expressed in other cell lineages were also up-regulated in *Ezh2*^{mKO}. For instance, expression of the agouti-related protein homolog 1 (Agrp1), expressed in neurons of the arcuate nucleus of the hypothalamus (Hahn et al. 1998); the collagen Col22a1, specifically expressed in chondrocytes (Koch et al. 2004); and opsin1 (Opn1), encoding a retinal photopigment expressed in retinal cones (Shichida and Matsuyama 2009) was increased (Fig. 5A; Supplemental Table S1). Expression of some of the transcripts identified as up-regulated by microarray analysis was evaluated independently by quantitative PCR (qPCR) and confirmed to be increased in the limb muscles of *Ezh2*^{mKO} animals. (Fig. 5B,C). Importantly, expression of mixed cell lineage genes and p16 was increased in FACS-isolated quiescent *Ezh2*^{mKO} SCs (Fig. 5E). However, muscle-specific transcripts increased in *Ezh2*^{mKO} muscles were not augmented in *Ezh2*^{mKO} SCs (data not shown), suggesting that their misregulation occurs in myofibers.

PolII recruitment to mixed cell lineage genes and the Ink4a/Arf locus in Ezh2^{mKO} *SCs*

To mechanistically investigate how Ezh2 ablation causes gene derepression, we conducted chromatin immunoprecipitation (ChIP) assays with antibodies against

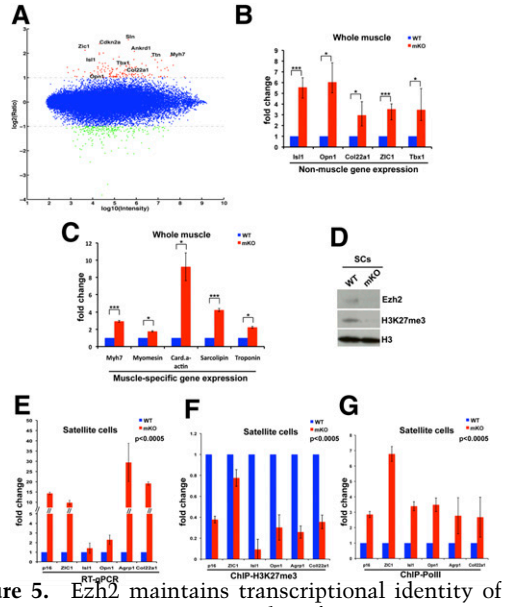

Figure 5. Ezh2 maintains transcriptional identity of SCs. (*A*) Log intensity versus ratio scatter plot of gene expression obtained from microarray data derived from muscles of wild-type (n = 2) and *Ezh2*^{mKO} (n = 2) animals. The *X*-axes represents the $\log_{10}$ of the average intensity of the data, and the *Y*-axes represents the $\log_2$ of their ratio. Each dot represents one gene. Up-regulated and down-regulated genes are color-coded red and green, respectively (fold change >2). (*B*,*C*) Expression of selected up-regulated genes identified in *A* by qPCR in muscles of wild-type or *Ezh2*^{mKO} animals. Data are presented as mean ± SD (n = 3); (***) $P < 0.0005$; (*) $P < 0.05$. (*D*) EZH2 and H3K27me3 immunoblots of FACS-isolated *Ezh2*^{mKO} SCs. Total histone H3 serves as loading control. (*E*) qPCR on selected up-regulated genes from FACS-isolated wild-type or *Ezh2*^{mKO} SCs. Data are presented as mean ± SD (n = 3); $P < 0.0005$ for all the values. (*F*,*G*) ChIP-qPCR for H3K27me3 and PolII at selected genes up-regulated in *Ezh2*^{mKO} SCs. Data are presented as mean ± SD (n = 3); $P < 0.0005$ for all the values.

H3K27me3 and PolII. ZIC-1, Ink4a/Arf (p16), Isl1, Opn1, and Coll22a1 genes were marked by H3K27me3, and PolII was undetectable in wild-type SCs. In contrast, H3K27me3 was significantly reduced and PolII was recruited at these genes in *Ezh2*^{mKO} SCs (Fig. 5D,F,G; Supplemental Fig. S4C). Overall, these results indicate that SCs are the source of mixed cell lineage and p16 gene misexpression, and that reduced H3K27me3 in *Ezh2*^{mKO} SCs allows PolII chromatin access, resulting in unwarranted gene transcription.

Conditional ablation of Ezh2 in MyoD-expressing cells recapitulates the muscle phenotypes observed in Ezh2^{mKO} mice

Pax7 expression is not limited to SCs but extends to cells located in the CNS and craniofacial tissues (Jostes et al. 1990). Indeed, some *Pax7*-Cre- *Ezh2*^{mKO} mice with CNS defects were retrieved at E15.5 and E17.5 (data not shown). To ablate *Ezh2* in committed skeletal myogenic cells (MyoD$^+$ cells), we bred *MyoD*-Cre (Chen et al. 2005) and floxed *Ezh2* mice (Supplemental Fig. S5A). Body and muscle mass were greatly reduced in *MyoD*-Cre-*Ezh2*^{mKO} mice (Supplemental Fig. S5B–E). Moreover, the number of Pax7$^+$ cells was also reduced in muscle cross-sections (Supplemental Fig. S5F). Recent studies have documented an activation of the MyoD locus in prenatal SCs (Kanisicak et al. 2009). Thus, *MyoD*-Cre-*Ezh2*^{mKO} mice may have deleted the *Ezh2*$^{fl/fl}$ alleles in SCs capable of self-renewal. While p16 derepression in *MyoD*-Cre-*Ezh2*^{mKO} was comparable with that observed in *Pax7*-Cre-*Ezh2*^{mKO} mice, expression of mixed-lineage genes ZIC-1, Agrp1, and Coll22a1 was much less pronounced (Supplemental Fig. S5G). Overall, the phenotypic similarities of *Pax7*-Cre-*Ezh2*^{mKO} and *MyoD*-Cre-*Ezh2*^{mKO} mice suggest that the observed muscle defects can be imputed to *Ezh2* ablation in skeletal myogenic cells.

Conclusions

The present study revealed that EZH2 influences several aspects of SC biology, including self-renewal, proliferation, and cell identity.

Unlike other studies in which *Ezh2* deletion was conditionally obtained in committed progenitors or differentiated cells (Chen et al. 2009; Ezhkova et al. 2009; Hirabayashi et al. 2009), we observed that Pax7-induced *Ezh2* deletion resulted in derepression of developmental regulators and structural genes physiologically not expressed in SCs. We speculate that, in committed or differentiated cells, the chromatin structure at selected genomic regions may be insensitive to epigenetic modifications caused by *Ezh2* ablation. Indeed, when Ezh2 was deleted in committed myogenic precursors (MyoD$^+$), gene misexpression was barely observed (Supplemental Fig. S5G). A more naive and plastic chromatin environment, such as that of ES cells or noncommitted Pax7$^+$/Myf5$^-$ stem cells, may react to PcG gene ablation by dysregulating gene expression (Boyer et al. 2006; Lee et al. 2006). In contrast to mixed-lineage genes, the Ink4a/Arf locus is derepressed in committed and differentiated *Ezh2*-ablated cells (*MyoD*-Cre-*Ezh2*^{mKO}) (Chen et al. 2009; Ezhkova et al. 2009; Hirabayashi et al. 2009; this study). Thus, different genomic chromatin structures may be susceptible to PcG regulation only at defined developmental windows. Interestingly, derepression of some of the mixed-lineage genes reported here has been observed in the skin of *Ezh1/Ezh2* double-knockout mice (Ezhkova et al. 2011).

EZH2 has been reported to repress Pax7 expression (Palacios et al. 2010). Specifically, EZH2 knockdown in cultured SCs results in Pax7 activation only if induced when the Pax7 level starts declining (Palacios et al. 2010). Since Cre expression in *Pax7*-Cre mice is coincident with Pax7 transcription (Keller et al. 2004), it is likely that *Ezh2* ablation in *Ezh2*^{mKO} mice occurred at the onset of Pax7 expression. In addition to the different temporal *Ezh2* inactivation strategies, cultured SCs may not experience the same physiological regulation attained in the animal, and may thus explain the different experimental outcomes.

In conclusion, the processes regulated by EZH2 are pivotal for SC homeostasis. As SCs hold therapeutic potential to treat muscle-wasting diseases (Kuang et al. 2008), PRC2 may be exploited as a target to promote ex vivo expansion and in vivo SC self-renewal.

Materials and methods

Mice and animal care

Mice were housed in a pathogen-free facility, and all experiments were performed according to the National Institutes of Health's (NIH) Animal Care and Use regulations. For a detailed animal description, see the Supplemental Material.

Myotoxic injury

The right TA muscle of 8-wk-old wild-type and *Ezh2*^{mKO} mice was surgically exposed and injected to holding capacity (~50 μL) with 10 μM CTX, as described previously (Schertzer et al. 2007). The left TA muscle was not injected and served as an uninjured control.

Histology

For a detailed histology protocol, see the Supplemental Material.

FACS sorting, myofiber isolation, BrdU labeling, immunofluorescence, and image acquisition

SC FACS sorting was performed as described previously (Joe et al. 2010). BrdU staining and immunofluorescence protocols are described in the Supplemental Material.

Transferase dUTP nick end-labeling (TUNEL) assay

FACS-sorted SCs were examined by terminal deoxynucleotidyl TUNEL assay (Roche Applied Science) according to the manufacturer's instructions.

Gene expression analyses

Total RNA from either whole-muscle or FACS-isolated SCs was reverse-transcribed using a cDNA synthesis kit (Applied Biosystems) and subjected to qPCR analysis. Gene expression analyses are detailed in the Supplemental Material.

Immunoblots

Muscles or FACS-isolated SCs were lysed, and their extracts were resolved by SDS-PAGE and transferred onto nitrocellulose filters. Specific antibodies used to perform immunoblots are described in Supplemental Table 4.

ChIP assay

Cross-linking and ChIP were performed as described (Caretti et al. 2004) with minor modifications (see the Supplemental Material).

Acknowledgments

We thank Mario Capecchi, David Goldhamer, and Alexander Tarakhovsky for sharing the *Pax7*-Cre, *MyoD*-Cre, and *Ezh2*$^{fl/fl}$ animals, respectively. Fabio Rossi provided advice with the FACS experiments, Jeffrey Lay helped with cell sorting, and Gustavo Gutierrez-Cruz assisted with animal genotyping. Members of the NIAMS Laboratory Animal Care and Use Section and NIAMS Light Imaging Section are kindly acknowledged. J.G.R. was supported by an Overseas Biomedical Research Fellowship from the NH and MRC (Australia). This work was supported in part by the Intramural Research Program of the National Institute of Arthritis, Musculoskeletal, and Skin Diseases of the National Institutes of Health.

References

Boyer LA, Plath K, Zeitlinger J, Brambrink T, Medeiros LA, Lee TI, Levine SS, Wernig M, Tajonar A, Ray MK, et al. 2006. Polycomb complexes repress developmental regulators in murine embryonic stem cells. *Nature* **441:** 349–353.

Bracken AP, Kleine-Kohlbrecher D, Dietrich N, Pasini D, Gargiulo G, Beekman C, Theilgaard-Monch K, Minucci S, Porse BT, Marine JC, et al. 2007. The Polycomb group proteins bind throughout the INK4A–ARF locus and are disassociated in senescent cells. *Genes Dev* **21:** 525–530.

Buckingham M, Relaix F. 2007. The role of Pax genes in the development of tissues and organs: Pax3 and Pax7 regulate muscle progenitor cell functions. *Annu Rev Cell Dev Biol* **23:** 645–673.

Caretti G, Di Padova M, Micales B, Lyons GE, Sartorelli V. 2004. The Polycomb Ezh2 methyltransferase regulates muscle gene expression and skeletal muscle differentiation. *Genes Dev* **18:** 2627–2638.

Chamberlain SJ, Yee D, Magnuson T. 2008. Polycomb repressive complex 2 is dispensable for maintenance of embryonic stem cell pluripotency. *Stem Cells* **26:** 1496–1505.

Chen JC, Mortimer J, Marley J, Goldhamer DJ. 2005. MyoD-cre transgenic mice: a model for conditional mutagenesis and lineage tracing of skeletal muscle. *Genesis* **41:** 116–121.

Chen H, Gu X, Su IH, Bottino R, Contreras JL, Tarakhovsky A, Kim SK. 2009. Polycomb protein Ezh2 regulates pancreatic β-cell Ink4a/Arf expression and regeneration in diabetes mellitus. *Genes Dev* **23:** 975–985.

Collins CA, Olsen I, Zammit PS, Heslop L, Petrie A, Partridge TA, Morgan JE. 2005. Stem cell function, self-renewal, and behavioral heterogeneity of cells from the adult muscle satellite cell niche. *Cell* **122:** 289–301.

Conboy MJ, Karasov AO, Rando TA. 2007. High incidence of non-random template strand segregation and asymmetric fate determination in dividing stem cells and their progeny. *PLoS Biol* **5:** e102. doi: 10.1371/journal.pbio.0050102.

Ezhkova E, Pasolli HA, Parker JS, Stokes N, Su IH, Hannon G, Tarakhovsky A, Fuchs E. 2009. Ezh2 orchestrates gene expression for the stepwise differentiation of tissue-specific stem cells. *Cell* **136:** 1122–1135.

Ezhkova E, Lien WH, Stokes N, Pasolli HA, Silva JM, Fuchs E. 2011. EZH1 and EZH2 cogovern histone H3K27 trimethylation and are essential for hair follicle homeostasis and wound repair. *Genes Dev* **25:** 485–498.

Hahn TM, Breininger JF, Baskin DG, Schwartz MW. 1998. Coexpression of Agrp and NPY in fasting-activated hypothalamic neurons. *Nat Neurosci* **1:** 271–272.

Hirabayashi Y, Suzki N, Tsuboi M, Endo TA, Toyoda T, Shinga J, Koseki H, Vidal M, Gotoh Y. 2009. Polycomb limits the neurogenic competence of neural precursor cells to promote astrogenic fate transition. *Neuron* **63:** 600–613.

Joe AW, Yi L, Natarajan A, Le Grand F, So L, Wang J, Rudnicki MA, Rossi FM. 2010. Muscle injury activates resident fibro/adipogenic progenitors that facilitate myogenesis. *Nat Cell Biol* **12:** 153–163.

Jostes B, Walther C, Gruss P. 1990. The murine paired box gene, Pax7, is expressed specifically during the development of the nervous and muscular system. *Mech Dev* **33:** 27–37.

Juan AH, Kumar RM, Marx JG, Young RA, Sartorelli V. 2009. mir-214-dependent regulation of the Polycomb protein Ezh2 in skeletal muscle and embryonic stem cells. *Mol Cell* **36:** 61–74.

Kanisicak O, Mendez JJ, Yamamoto S, Yamamoto M, Goldhamer DJ. 2009. Progenitors of skeletal muscle satellite cells express the muscle determination gene, MyoD. *Dev Biol* **332:** 131–141.

Keller C, Hansen MS, Coffin CM, Capecchi MR. 2004. Pax3:Fkhr interferes with embryonic Pax3 and Pax7 function: implications for alveolar rhabdomyosarcoma cell of origin. *Genes Dev* **18:** 2608–2613.

Koch M, Schulze J, Hansen U, Ashwodt T, Keene DR, Brunken WJ, Burgeson RE, Bruckner P, Bruckner-Tuderman L. 2004. A novel marker of tissue junctions, collagen XXII. *J Biol Chem* **279:** 22514–22521.

Kotake Y, Cao R, Viatour P, Sage J, Zhang Y, Xiong Y. 2007. pRB family proteins are required for H3K27 trimethylation and Polycomb repression complexes binding to and silencing p16INK4α tumor suppressor gene. *Genes Dev* **21:** 49–54.

Kuang S, Kuroda K, Le Grand F, Rudnicki MA. 2007. Asymmetric self-renewal and commitment of satellite stem cells in muscle. *Cell* **129:** 999–1010.

Kuang S, Gillespie MA, Rudnicki MA. 2008. Niche regulation of muscle satellite cell self-renewal and differentiation. *Cell Stem Cell* **2:** 22–31.

Lee TI, Jenner RG, Boyer LA, Guenther MG, Levine SS, Kumar RM, Chevalier B, Johnstone SE, Cole MF, Isono K, et al. 2006. Control of developmental regulators by Polycomb in human embryonic stem cells. *Cell* **125:** 301–313.

Montarras D, Morgan J, Collins C, Relaix F, Zaffran S, Cumano A, Partridge T, Buckingham M. 2005. Direct isolation of satellite cells for skeletal muscle regeneration. *Science* **309:** 2064–2067.

Palacios D, Mozzetta C, Consalvi S, Caretti G, Saccone V, Proserpio V, Marquez VE, Valente S, Mai A, Forcales SV, et al. 2010. TNF/p38α/Polycomb signaling to Pax7 locus in satellite cells links inflammation to the epigenetic control of muscle regeneration. *Cell Stem Cell* **7:** 455–469.

Pasini D, Bracken AP, Hansen JB, Capillo M, Helin K. 2007. The polycomb group protein Suz12 is required for embryonic stem cell differentiation. *Mol Cell Biol* **27:** 3769–3779.

Pereira JD, Sansom SN, Smith J, Dobenecker MW, Tarakhovsky A, Livesey FJ. 2010. Ezh2, the histone methyltransferase of PRC2, regulates the balance between self-renewal and differentiation in the cerebral cortex. *Proc Natl Acad Sci* **107:** 15957–15962.

Sauvageau M, Sauvageau G. 2010. Polycomb group proteins: multi-faceted regulators of somatic stem cells and cancer. *Cell Stem Cell* **7:** 299–313.

Schertzer JD, Gehrig SM, Ryall JG, Lynch GS. 2007. Modulation of insulin-like growth factor (IGF)-I and IGF-binding protein interactions enhances skeletal muscle regeneration and ameliorates the dystrophic pathology in mdx mice. *Am J Pathol* **171:** 1180–1188.

Shea KL, Xiang W, LaPorta VS, Licht JD, Keller C, Basson MA, Brack AS. 2010. Sprouty1 regulates reversible quiescence of a self-renewing adult muscle stem cell pool during regeneration. *Cell Stem Cell* **6:** 117–129.

Shen X, Liu Y, Hsu YJ, Fujiwara Y, Kim J, Mao X, Yuan GC, Orkin SH. 2008. EZH1 mediates methylation on histone H3 lysine 27 and complements EZH2 in maintaining stem cell identity and executing pluripotency. *Mol Cell* **32:** 491–502.

Sherwood RI, Christensen JL, Conboy IM, Conboy MJ, Rando TA, Weissman IL, Wagers AJ. 2004. Isolation of adult mouse myogenic progenitors: functional heterogeneity of cells within and engrafting skeletal muscle. *Cell* **119:** 543–554.

Shichida Y, Matsuyama T. 2009. Evolution of opsins and phototransduction. *Philos Trans R Soc Lond B Biol Sci* **364:** 2881–2895.

Shinin V, Gayraud-Morel B, Gomes D, Tajbakhsh S. 2006. Asymmetric division and cosegregation of template DNA strands in adult muscle satellite cells. *Nat Cell Biol* **8:** 677–687.

Su IH, Basavaraj A, Krutchinsky AN, Hobert O, Ullrich A, Chait BT, Tarakhovsky A. 2003. Ezh2 controls B cell development through histone H3 methylation and Igh rearrangement. *Nat Immunol* **4:** 124–131.

JOHN WILEY AND SONS LICENSE TERMS AND CONDITIONS

Sep 01, 2014

This is a License Agreement between Alessandra Pasut ("You") and John Wiley and Sons ("John Wiley and Sons") provided by Copyright Clearance Center ("CCC"). The license consists of your order details, the terms and conditions provided by John Wiley and Sons, and the payment terms and conditions.

All payments must be made in full to CCC. For payment instructions, please see information listed at the bottom of this form.

License Number	3460540164998
License date	Sep 01, 2014
Licensed content publisher	John Wiley and Sons
Licensed content publication	Journal of Anatomy
Licensed content title	The formation of skeletal muscle: from somite to limb
Licensed copyright line	Copyright © 2003, John Wiley and Sons
Licensed content author	Margaret Buckingham,Lola Bajard,Ted Chang,Philippe Daubas,Juliette Hadchouel, Sigolène Meilhac,Didier Montarras,Didier Rocancourt,Frédéric Relaix
Licensed content date	Jan 24, 2003
Start page	59
End page	68
Type of use	Dissertation/Thesis
Requestor type	University/Academic
Format	Print and electronic
Portion	Figure/table
Number of figures/tables	1
Original Wiley figure/table number(s)	one figure
Will you be translating?	No
Title of your thesis / dissertation	Characterization of muscle stem cell function by the transcprtion factor pax7
Expected completion date	Oct 2014
Expected size (number of pages)	200
Total	0.00 USD
Terms and Conditions	

TERMS AND CONDITIONS

This copyrighted material is owned by or exclusively licensed to John Wiley & Sons, Inc. or

ELSEVIER LICENSE
TERMS AND CONDITIONS

Sep 01, 2014

This is a License Agreement between Alessandra Pasut ("You") and Elsevier ("Elsevier") provided by Copyright Clearance Center ("CCC"). The license consists of your order details, the terms and conditions provided by Elsevier, and the payment terms and conditions.

All payments must be made in full to CCC. For payment instructions, please see information listed at the bottom of this form.

Supplier	Elsevier Limited The Boulevard,Langford Lane Kidlington,Oxford,OX5 1GB,UK
Registered Company Number	1982084
Customer name	[redacted]
Customer address	
License number	3460530605070
License date	Sep 01, 2014
Licensed content publisher	Elsevier
Licensed content publication	Cell
Licensed content title	The Canonical Notch Signaling Pathway: Unfolding the Activation Mechanism
Licensed content author	Raphael Kopan,Ma. Xenia G. Ilagan
Licensed content date	17 April 2009
Licensed content volume number	137
Licensed content issue number	2
Number of pages	18
Start Page	216
End Page	233
Type of Use	reuse in a thesis/dissertation
Portion	figures/tables/illustrations
Number of figures/tables/illustrations	1
Format	both print and electronic
Are you the author of this Elsevier article?	No
Will you be translating?	No